



UNIVERSITY OF
BIRMINGHAM

**ELUCIDATING PATHWAYS OF
BROMINATED FLAME RETARDANT
MIGRATION INTO INDOOR DUST**

by

CASSANDRA BREA RAUERT

B.Sc (Hons)

A thesis submitted to the University of Birmingham for the degree of:

DOCTOR OF PHILOSOPHY (Ph.D)

Division of Environmental Health and Risk Management

School of Geography, Earth and Environmental Sciences

College of Life and Environmental Sciences

University of Birmingham

United Kingdom

July 2014

UNIVERSITY OF
BIRMINGHAM

University of Birmingham Research Archive

e-theses repository

This unpublished thesis/dissertation is copyright of the author and/or third parties. The intellectual property rights of the author or third parties in respect of this work are as defined by The Copyright Designs and Patents Act 1988 or as modified by any successor legislation.

Any use made of information contained in this thesis/dissertation must be in accordance with that legislation and must be properly acknowledged. Further distribution or reproduction in any format is prohibited without the permission of the copyright holder.

ABSTRACT

Brominated flame retardants (BFRs) are ubiquitous in indoor air and dust, leading to human exposure and resultant concerns about its adverse impact on health. Despite observations of their presence at elevated concentrations in indoor dust, relatively little is known about how BFRs transfer to dust from goods within which they are incorporated. A test chamber was therefore constructed to investigate the pathways via which BFRs migrate from source materials to indoor dust. The BFRs studied were: polybrominated diphenyl ethers (PBDEs) and hexabromocyclododecanes (HBCDs). Experimental methods were optimised to mimic experimentally three such migration pathways. These were: (1) BFRs volatilise from treated products and subsequently partition to dust, (2) particles or fibres of the source material abrade from products and transfer to dust directly, and (3) BFRs transfer as a result of direct source-dust contact. Two different products were tested: a textile curtain treated with HBCDs, and a plastic TV casing treated with BDE-209 and lower levels of other PBDEs. Volatilisation with subsequent partitioning to dust was shown to be a less effective transfer mechanism than abrasion of the treated product. Direct source-dust contact was also shown to result in effective and rapid transfer, with the majority of transfer via this pathway seen in the first 24 hours of contact. Both highly contaminated “real world” indoor dust samples, and chamber generated dust samples artificially contaminated via abrasion of a known source, were further investigated with forensic microscopy techniques. Polymer particles containing BDE-209 were identified in two “real world” dust samples. These were shown to likely originate from a BFR treated polymeric material; consistent with the hypothesis that abrasion of source materials can generate highly elevated concentrations of BFRs in dust. The hypothesis that bioaccessibility of BFRs in dust will be lower from samples containing abraded particles with which BFRs are more strongly associated, than from particles contaminated with BFRs via atmospheric deposition, was investigated using an *in vitro* colon extended physiologically based extraction test. Results suggest that current estimates of human exposure via ingestion of dust that assume 100% uptake, are likely overestimates. Moreover, there are indications that bioaccessibility may be less efficient from samples containing elevated concentrations of BFRs, and from dusts contaminated primarily via source material abrasion. More detailed research is essential to confirm these indicative findings.

ACKNOWLEDGMENTS

Firstly I would like to say a big thank you to my supervisor and the INFLAME project coordinator Professor Stuart Harrad for all your hard work and support of me and for this project. The INFLAME project has provided many opportunities for networking and travel and I am very grateful for the opportunity to work in this program and thank you to the Marie Curie Initial Training Network program for allowing these opportunities. From this I also would like to say thank you to all the other ESRs and ERs in the INFLAME project for your constant support, the laughs and the friendship. I look forward to collaborating with everyone in the not too distant future.

Thank you to the organisations who allowed me the opportunity to undertake secondments with them, providing opportunities to learn from and work with some amazing researchers. Particular thanks to Dr Marianne Stranger at the Flemish Institute for Vision on Technology (Belgium); Dr Anna Palm-Cousins at the Swedish Environmental Research Institute (Sweden); and Dr Go Suzuki and Professor Hidetaka Takigami at the National Institute for Environmental Studies (Japan).

To all the other students in room 216 who have come and gone over the years, thank you for the discussions, ideas, and for making my time at the University of Birmingham so much more enjoyable. Special thank you to Dr Congqiao Yang for the constant friendship and laughs and to Dr Sandra Brommer for all your support, friendship, many laughs and for always being up for wearing a vampire cape.

A big thank you to Dr Alan Yates for being my cross-cultural advisor during my stay in England and for all your supportive emails. And to all my friends in Birmingham who have made my stay here “such fun”. To Jacqui, Gill and Allan – thank you for all your contributions to the 50 shades of dust and to Bev for so many laughs and fantastic travels.

Lastly a huge thank you goes to my amazing family for their unwavering support for my decision to move to the other side of the world and their constant encouragement; especially to Mum who has kept me sane, I could not have done this without you. ☺

TABLE OF CONTENTS

LIST OF TABLES	viii
LIST OF FIGURES	xii
ABBREVIATIONS	xvi
CHAPTER 1 INTRODUCTION.....	1
1.1 Brominated flame retardants (BFRs)	1
1.1.1 Polybrominated diphenyl ethers (PBDEs)	3
1.1.1.1 Production.....	3
1.1.1.2 Regulatory aspects.....	4
1.1.1.3 Physicochemical properties.....	5
1.1.2 Hexabromocyclododecane (HBCDs)	10
1.1.2.1 Production.....	11
1.1.2.2 Regulatory aspects.....	11
1.1.2.3 Physicochemical properties.....	11
1.2 Environmental, pathways, fate and behaviour of BFRs	13
1.3 Human Exposure to BFRs	17
1.4 BFR Toxicology and Health Effects	20
1.5 BFRs in Indoor Environments	24
1.6 Migration of BFRs to air and dust.....	32
1.6.1 The Influence of Dust Particle Size Distribution on BFR Concentrations in Settled Dust and Implications for Human Exposure.....	33
1.6.2 Bioaccessibility	35
1.6.3 Linking Putative Sources with Indoor Contamination with BFRs.....	36
1.6.3.1 Source attribution insights from correlations between matched indoor air and dust samples.....	38
1.6.4 Influence of Microenvironment on BFR Contamination.....	39
1.6.5 Within-building and within-room spatial and temporal trends in BFR concentrations in indoor dust	41
1.6.6 Modelling studies.....	44
1.7 Quantifying BFR emissions from Source Materials.....	47
1.7.1 Measurement of specific emission rates (SERs) to air	47
1.7.2 Measurements of migration to indoor dust	53
1.7.3 Sink Effects	54
1.8 Forensic Microscopy	56
1.9 Summary.....	58
1.10 Aims	59
CHAPTER 2 TEST CHAMBER CONFIGURATION, ANALYTICAL METHODOLOGY AND FORENSIC MICROSCOPY METHODOLOGY	60
2.1 Test chamber experimental design	60
2.1.1 Test chamber experimental design.....	60
2.1.2 Commercially available Emission Chamber at Flemish Institute for Technological Research (VITO)	62
2.1.3 Experimental Design for investigating BFR partitioning to dust after volatilisation.....	63
2.1.4 Experimental design for investigating BFR direct partitioning via abrasion...	64
2.1.5 Experimental design for investigating BFR partitioning via direct contact of BFR source to dust.....	65
2.1.6 BFR treated products	66
2.1.6.1 HBCD treated fabric curtains	66
2.1.6.2 BDE-209 treated plastic TV casings (InterLab sample)	66
2.1.7 Low level dust procurement.....	66

2.1.7.1	Dust sampling procedure and indigenous BFR concentrations.....	67
2.2	Forensic Microscopy Investigations.....	67
2.2.1	Energy dispersive Micro X-ray fluorescence spectroscopy (Micro XRFS).....	68
2.2.2	Laser Microscopy.....	68
2.2.3	Scanning Electron Microscopy with Energy Dispersive Spectroscopy (SEM/EDS).....	69
2.2.4	Fourier Transform Infrared spectroscopy (FTIR) analysis.....	69
2.2.5	Analysis of isolated particles for BFR content.....	69
2.3	Sample Extraction and purification.....	70
2.3.1	Chemicals.....	70
2.3.2	Sample preparation and extraction.....	70
2.3.3	Sample clean up.....	70
2.4	Analysis.....	71
2.4.1	Justification for choice of high performance liquid chromatography (HPLC) tandem mass spectrometry (MS/MS) analysis.....	71
2.4.2	HBCD Analysis.....	72
2.4.3	PBDE Analysis.....	74
2.4.4	Calibration Standards.....	76
2.4.5	Internal Standards.....	80
2.4.5.1	Quantification of analytes.....	80
2.4.5.2	Internal standard recoveries.....	81
2.5	QA/QC criteria.....	83
2.5.1	Accuracy and Precision.....	83
2.5.2	Preparation of an in-house reference dust material.....	84
2.5.3	Analysis of Blanks, calculation of LODs and LOQs.....	85
2.6	Statistical Analysis.....	87
CHAPTER 3 TEST CHAMBER STUDIES OF BFR VOLATILISATION FROM SOURCES AND SUBSEQUENT PARTITIONING TO DUST.....		88
3.1	Summary.....	88
3.2	Experimental Design development.....	88
3.2.1	Initial experimental design and measurements.....	88
3.2.2	PUF Breakthrough.....	92
3.2.3	Minimising analyte loss during post experiment disassembly.....	93
3.2.4	Influence of exit air sampling train length.....	93
3.3	Sink Effects.....	97
3.3.1	Glass test cell and PTFE chamber coating.....	100
3.3.2	Post-experiment chamber heating.....	102
3.3.3	Chamber solvent rinse vs chamber wipe and different chamber air flows.....	102
3.4	Partitioning to dust using a spiked GFF as the source.....	105
3.4.1	Chamber heated experiments with emission sampling every 24 hours.....	111
3.5	HBCD partitioning to dust using HBCD treated curtains as the source.....	118
3.6	Summary/Conclusions.....	123
CHAPTER 4 SIMULATING MIGRATION OF BFRs TO DUST VIA ABRASION AND VIA DIRECT CONTACT WITH BFR SOURCES.....		124
4.1	Summary.....	124
4.2	Test chamber abrasion experiments.....	124
4.2.1	Fibre abrasion to dust from HBCD treated curtain.....	124
4.2.2	Interpreting abrasion results in terms of a 'real world' scenario.....	128
4.3	Migration of HBCDs via direct contact between source and dust.....	132
4.4	Comparison of HBCD transfer from treated textiles via three different migration pathways.....	141
4.5	Summary/Conclusions.....	143

CHAPTER 5 FORENSIC MICROSCOPY INVESTIGATION OF DUSTs OF ELEVATED BFR CONCENTRATIONS	144
5.1 Summary.....	144
5.2 Forensic Microscopy analysis of chamber generated dust sample.....	145
5.2.1 Sample preparation	145
5.2.2 Micro X-ray Fluorescence Spectroscopy.....	146
5.2.3 3D Laser Microscopy.....	149
5.2.4 Scanning Emission Microscopy/Energy Dispersive Spectroscopy	150
5.2.5 Fourier Transform Infrared Spectroscopy	155
5.3 Forensic microscopy analysis of archive dust samples	157
5.3.1 Micro X-ray Fluorescence Spectroscopy.....	158
5.3.2 3D Laser Microscopy.....	162
5.3.3 Scanning Emission Microscopy/Energy Dispersive Spectroscopy	166
5.3.4 Fourier Transform Infrared Spectroscopy	177
5.3.4.1 Calcium Carbonate.....	185
5.3.4.2 FTIR Mapping.....	187
5.4 Analysis of BFR content in isolated particles	190
5.5 Limitations of the forensic microscopy methods employed.....	191
5.6 Summary/Conclusions.....	192
CHAPTER 6 MIGRATION OF PBDEs FROM PLASTIC TV CASING TO DUST VIA THREE DIFFERENT MIGRATION PATHWAYS.....	194
6.1 Summary.....	194
6.2 InterLab Sample Waste TV backplate Lot No. 01-02.....	194
6.3 Migration via volatilisation with subsequent partitioning to dust.....	195
6.4 Migration via abrasion of particles directly to dust.....	199
6.5 Migration via direct contact between source and dust.....	207
6.6 Summary/Conclusions.....	212
CHAPTER 7 BIOACCESSIBILITY STUDY OF HBCDs FROM DUST CONTAMINATED VIA DIFFERENT MIGRATION PATHWAYS	214
7.1 Summary.....	214
7.2 Dust Characterisation	215
7.2.1 Particle size distribution	216
7.2.2 Fraction of organic carbon.....	219
7.3 Chamber generation of dust samples	219
7.3.1 Volatilisation with partitioning to dust particles.....	220
7.3.2 Abrasion of textile fibres to dust.....	220
7.3.3 Concentration in generated dust samples	221
7.4 Bioaccessibility method	224
7.4.1 Method description.....	224
7.4.2 Chemicals	224
7.4.3 Methodology	224
7.4.4 Stomach/small intestine.....	226
7.4.5 Colon and Residue.....	227
7.4.6 Extraction and Clean up.....	227
7.4.7 Bioaccessibility calculation	228
7.5 Results	229
7.5.1 Method Blanks	229
7.5.2 HBCD concentrations in compartments of bioaccessibility assay using SRM 2585 dust as the test sample.....	229
7.5.3 HBCD concentrations in compartments of bioaccessibility assay for a low-HBCD dust sample	232

7.5.4	HBCD concentrations in compartments of bioaccessibility assay of generated dusts and calculated bioaccessibility for each dust analysis.....	233
7.5.5	Bioaccessibility comparison between generated dust samples.....	243
7.5.6	Influence of HBCD concentration in dust on bioaccessibility.....	246
7.6	Summary/Conclusions.....	251
CHAPTER 8	SUMMARY AND CONCLUSIONS	253
8.1	Development of a test chamber and experimental designs to simulate migration of BFRs to dust	254
8.2	Migration of BFRs to dust via three migration pathways from treated consumer products	255
8.2.1	Partitioning to dust post volatilisation.....	255
8.2.2	Abrasion of particles or fibres to dust.....	256
8.2.3	Uptake to dust via direct contact between source and dust.....	257
8.3	Forensic Microscopy investigation of BFR containing dust samples	258
8.4	<i>In vitro</i> bioaccessibility study.....	259
8.5	Research gaps and future areas of research.....	259
REFERENCES		249
APPENDIX A: LIST OF PUBLICATIONS AND CONFERENCE PRESENTATIONS		265

LIST OF TABLES

CHAPTER 1 INTRODUCTION	1
<i>Table 1.1: Physicochemical properties of PBDE technical mixtures</i>	5
<i>Table 1.2: Physicochemical properties of individual PBDE congeners</i>	6
<i>Table 1.3: Physicochemical properties of the HBCD technical formulation</i>	12
<i>Table 1.4: Physicochemical properties of α-, β- and γ-HBCD</i>	12
<i>Table 1.5: Summary of Arithmetic Mean or Median concentrations (with range) reported in Indoor and Outdoor air (pg.m^{-3})</i>	23
<i>Table 1.6: Summary of Arithmetic Mean or Median concentrations (with range) reported in Indoor dust and Outdoor soil (ng.g^{-1})</i>	25
<i>Table 1.7: ΣPBDE calculations comparing emissions to air/dust in different microenvironments</i>	41
<i>Table 1.8: Summary of reported specific emission rates of BFRs determined from various chamber studies</i>	44
CHAPTER 2 TEST CHAMBER CONFIGURATION, ANALYTICAL METHODOLOGY AND FORENSIC MICROSCOPY METHODOLOGY	57
<i>Table 2.1: Mean and %RSD BFR concentrations (ng g^{-1}) in bulk dust samples used for chamber experiments</i>	63
<i>Table 2.2: BFR concentrations (ng g^{-1}) in archived dust samples</i>	64
<i>Table 2.3: Gradient program for HPLC elution of HBCD diastereomers</i>	69
<i>Table 2.4: Optimised MS/MS parameters for the analysis of HBCDs on LC-MS/MS</i>	70
<i>Table 2.5: Parent to product ion m/z transitions monitored for native HBCD diastereomers, IS and RDS</i>	70
<i>Table 2.6: Gradient program for HPLC elution of PBDE congeners</i>	71
<i>Table 2.7: Optimised MS/MS parameters for the analysis of PBDEs on LC-MS/MS</i>	72
<i>Table 2.8: Parent to product ion m/z transitions monitored for native PBDE congeners, IS and RDS</i>	72
<i>Table 2.9: Concentrations of analyte, IS and RDS compounds in the five HBCD calibration standards</i>	73
<i>Table 2.10: Concentrations of analyte, IS and RDS compounds in the five PBDE calibration standards</i>	73
<i>Table 2.11: Calculated mean RRFs for analyts and %RSD</i>	77
<i>Table 2.12: Mean, range, standard deviation and %RSD of IS recoveries from analysed samples</i>	78
<i>Table 2.13: Mean \pm standard deviation of BFRs in SRM 2585, %RSD and Certified and Indicative values</i>	79
<i>Table 2.14: Volume of each native standard solution added to dust, mean concentration, SD and %RSD of replicate analyses of the dust reference material</i>	80
<i>Table 2.15: Calculated LODs (ng on column) and method LOQs for HBCD diastereomers and PBDE congeners in this study</i>	81

CHAPTER 3 TEST CHAMBER STUDIES OF BFR VOLATILISATION FROM SOURCES AND SUBSEQUENT PARTITIONING TO DUST	83
<i>Table 3.1: Recoveries (%) of BFRs recovered from the GFF, PUFs and chamber inner surface rinses in initial trial experiments at 22 °C for 1 week and 60 °C for 24 hours</i>	85
<i>Table 3.2: Recoveries (%) of BFRs from PUF breakthrough experiments</i>	86
<i>Table 3.3: Total BFR recoveries (%) and BFR proportion recovered from PUFs (%) from experiments at 60 °C for 24 hours for (a) initial trial chamber experiments, (b) cooling the chamber before disassembling and (c) trialling shorter sample air train length</i>	88
<i>Table 3.4: Literature reported BFR vapour pressures at 25 °C, literature reported enthalpy of vaporisation and calculated vapour pressure at 60 °C</i>	90
<i>Table 3.5: BFR recoveries (%) of PBDEs and HBCDs from various compartments during experiments testing sink effects from the UoB and micro chambers</i>	93
<i>Table 3.6: BFR proportion (%) recovered from rinsing chamber inner surfaces with various solvents after UoB sink effects experiment</i>	94
<i>Table 3.7: Mean (min, max) BFR analyte recovery (%) of heated chamber experiments from the UoB chamber, the glass test cell, the PTFE coated test cell and the glass test cell at 22 °C</i>	95
<i>Table 3.8: Mean (min, max) BFR analyte recovery (%) from post experiment chamber heating</i>	96
<i>Table 3.9: Mean BFR recoveries (%) from chamber solvent rinses and chamber wipes</i>	97
<i>Table 3.10: Mean (min, max) BFR recoveries (%) from micro chamber experiments with different air flows</i>	98
<i>Table 3.11: Mean BFR recoveries (%), proportions recovered in various chamber compartments and dust concentrations (ng g⁻¹) for deposition to dust experiments in the UoB and micro chamber</i>	100
<i>Table 3.12: Mean (min, max) BFR concentrations in dust (ng g⁻¹) and BFR mass on PUFs, GFF and chamber solvent rinse from extended chamber experiment at 60 °C</i>	105
<i>Table 3.13: HBCD mass (ng) in different compartments and dust concentrations (ng g⁻¹) of UoB heated experiment (60 °C) for 24 hours</i>	112
<i>Table 3.14: HBCD mass (ng) in different compartments and dust concentrations (ng g⁻¹) of UoB room temperature experiment, 22 ± 1 °C, for 1 week (n=3)</i>	112
<i>Table 3.15: HBC D mass (ng) in different compartments and dust concentrations (ng g⁻¹) of Micro chamber heated experiment (60 °C) for 24 hours (n=6)</i>	112
CHAPTER 4 SIMULATING MIGRATION OF BFRs TO DUST VIA ABRASION AND VIA DIRECT CONTACT WITH BFR SOURCES	116
<i>Table 4.1: Concentrations (ng g⁻¹) of HBCD diastereomers in dust pre and post abrasion experiments and HBCD mass (ng) collected on PUFs and in chamber rinses for four experiment durations</i>	120
<i>Table 4.2: Estimated ‘real world’ curtain abrasion and subsequent dust contamination scenarios, extrapolated from abrasion experiment results, and other treated fabric scenarios</i>	124
<i>Table 4.3: Mean and (min, max) concentrations (ng g⁻¹) of HBCDs in dust from direct contact experiments conducted for 24 hours and 1 week</i>	126

<i>Table 4.4: Literature parameters and calculated fugacity capacities (Z) for the HBCD technical formulation in different media</i>	130
<i>Table 4.5: Mean concentrations (ng.g⁻¹) of HBCDs in the same starting bulk dust, post experiment, from chamber experiments investigating three different migration pathways using HBCD treated curtains</i>	133
CHAPTER 5 FORENSIC MICROSCOPY INVESTIGATION OF DUSTs OF ELEVATED BFR CONCENTRATIONS	135
<i>Table 5.1: Concentration (ng.g⁻¹) of HBCDs and BDE-209 in archived dust samples</i>	148
<i>Table 5.2: Properties and calculation of estimated BDE-209 concentration in particles isolated from Dust 1 and Dust 2</i>	181
CHAPTER 6 MIGRATION OF PBDEs FROM PLASTIC TV CASING TO DUST VIA THREE DIFFERENT MIGRATION PATHWAYS	184
<i>Table 6.1: PBDE concentrations (µg g⁻¹) and %RSD of 4 analyses of interlab sample Lot No. 01-02 (Plastic TV back casing), as provided by NIES</i>	185
<i>Table 6.2: Concentrations of PBDEs (ng g⁻¹) in dust pre and post volatilisation experiments and mass of PBDEs (ng) collected on PUFs and in chamber solvent rinses, from two temperature scenarios</i>	187
<i>Table 6.3: Concentrations (ng g⁻¹) in dust pre experiment and post experiment for four different abrasion experimental durations</i>	190
<i>Table 6.4: Calculated BDE-183 abrasion mass (mg), relation to abrasion test standards and estimated 'real world' TV casing abrasion</i>	196
<i>Table 6.5: Calculated BDE-209 abrasion mass (mg), relation to abrasion test standards and estimated 'real world' TV casing abrasion</i>	196
<i>Table 6.6: Mean concentrations (ng g⁻¹) of PBDEs in dust pre experiment and maximum and minimum concentrations (ng g⁻¹) in dust post direct contact experiment for 24 hours and 1 week exposure</i>	199
CHAPTER 7 BIOACCESSIBILITY STUDY OF HBCDs FROM DUST CONTAMINATED VIA DIFFERENT MIGRATION PATHWAYS	203
<i>Table 7.1: Mean, standard deviation and RSD of %N and %C contents in instrument QC samples and Belgian dust</i>	207
<i>Table 7.2: Concentration of HBCDs (ng g⁻¹) in replicate analyses of dust samples contaminated via migration of HBCDs via volatilisation with subsequent partitioning to dust</i>	209
<i>Table 7.3: Concentration of HBCDs (ng g⁻¹) in the initial dust samples contaminated via abrasion of textile fibres and replicate analyses of the final dust sample after dilution with low level dust</i>	210
<i>Table 7.4: Results of Independent Samples T-test for comparison of HBCD concentrations determined in volatilisation generated and abrasion generated dusts</i>	211
<i>Table 7.5: Ingredients in each solution media to model the different compartments of the gastrointestinal tract</i>	213
<i>Table 7.6: HBCD concentrations (ng g⁻¹) in method compartments from three replicates of bioaccessibility test of laboratory sand, used as a method blank</i>	217

<i>Table 7.7: Indicative concentrations (ng g⁻¹) of HBCDs in SRM 2585 and HBCD concentrations in each compartment from the bioaccessibility study for three replicate analyses of the SRM</i>	218
<i>Table 7.8: Concentrations (ng g⁻¹) of HBCDs in SRM 2585 used at (a) the University of Reading and (b) the University of Birmingham</i>	219
<i>Table 7.9: HBCD concentrations (ng g⁻¹) in each compartment from the experiment repeat of the bioaccessibility study for three SRM replicate analyses</i>	219
<i>Table 7.10: Indicative concentrations (ng g⁻¹) of HBCD in low level Belgian dust and HBCD concentrations in each compartment from the bioaccessibility study for three replicate analyses</i>	220
<i>Table 7.11: HBCD concentrations (ng g⁻¹) in each compartment from experiment repeat of bioaccessibility test of Belgian dust analyses</i>	221
<i>Tables 7.12: Concentrations (ng g⁻¹) previously determined in the generated dust samples and concentrations (ng g⁻¹) and calculated bioaccessibilities for dust samples generated via volatilisation with partitioning of HBCDs</i>	223
<i>Tables 7.13: Concentrations (ng g⁻¹) and calculated bioaccessibility for extraction of generated dust samples contaminated via the abrasion of HBCD treated textile fibres</i>	227
<i>Table 7.14: Results of Independent Samples T-test for comparison of total HBCD concentration determined in each bioaccessibility assay, from volatilisation generated and abrasion generated dusts</i>	231
<i>Table 7.15: Calculated values from an Independent Samples T-test of bioaccessibilities determined in dust contaminated post volatilisation of HBCDs and via abrasion of textile fibres</i>	232

LIST OF FIGURES

CHAPTER 1 INTRODUCTION

<i>Figure 1.1: General chemical structure of PBDEs and HBCDs</i>	1
<i>Figure 1.2: Hypothesised migration pathways of FRs from treated products into indoor air and dust</i>	2

30

CHAPTER 2 TEST CHAMBER CONFIGURATION, ANALYTICAL METHODOLOGY AND FORENSIC MICROSCOPY METHODOLOGY

57

<i>Figure 2.1: UoB Chamber configuration</i>	58
<i>Figure 2.2: Photograph of micro chamber configuration</i>	59
<i>Figure 2.3: Schematic of test chamber experiment for generating volatilisation of BFRs with subsequent partitioning to dust.</i>	60
<i>Figure 2.4: Schematic of test chamber experiment for generating abrasion of a BFR treated product</i>	61
<i>Figure 2.5: Schematic of test chamber experiment for generating migration to dust via direct contact between BFR source and dust particles</i>	62
<i>Figure 2.6: Mobile phase gradient program used for HBCD analysis</i>	69
<i>Figure 2.7: Mobile phase gradient program for PBDE analysis</i>	71
<i>Figure 2.8: LC-MS/MS Chromatograms of (a) IS, (b) RDS and (c) HBCD analytes in calibration standard C</i>	74
<i>Figure 2.9: LC-MS/MS Chromatograms of Internal Standards (b),(d),(f),(i), Recovery Determination Standard (d) and PBDE analytes (a),(c),(e),(g),(h) in calibration standard C</i>	75

CHAPTER 3 TEST CHAMBER STUDIES OF BFR VOLATILISATION FROM SOURCES AND SUBSEQUENT PARTITIONING TO DUST

83

<i>Figure 3.1: Output from the LogTag thermocouple showing temperature profiles inside the test chamber during 2 days at room temperature, and 24 hours at 60 °C</i>	85
<i>Figure 3.2: Mass of BFR (ng) collected on PUF plugs sampling chamber exit air for different exit air sampling train lengths</i>	89
<i>Figure 3.3: Plot of vapour pressure (60 °C) vs BFR mass on PUF in mass balance experiments using optimised chamber configuration</i>	91
<i>Figure 3.4: Concentrations (ng g⁻¹) of PBDEs in dust, pre and post partitioning experiment in the UoB chamber and micro chamber using a spiked GFF as the source</i>	100
<i>Figure 3.5: Mean recovery (%) of PBDEs in various components in the UoB chamber and the micro chamber using a spiked GFF as the source</i>	101
<i>Figure 3.6: Graph of vapour pressure (60 °C) vs BFR mass on PUF for UoB and micro chambers during partitioning to dust experiments</i>	102
<i>Figure 3.7: Graph of K_{OA} vs PBDE mass collected on PUF for UoB chamber and Micro chamber during partitioning to dust</i>	103
<i>Figure 3.8: BFR mass (ng) collected on PUFs at 24 hour time intervals</i>	107
<i>Figure 3.9: Plotted vapour pressure vs total BFR mass collected on PUFs</i>	108
<i>Figure 3.10: PBDE mass collected on PUF plug (ng) over the entire experimental collection period vs literature K_{OA} values</i>	110

<i>Figure 3.11: Concentrations of HBCDs in dust (ng g⁻¹) pre- and post-experiment using a HBCD-treated curtain as the source after 24 hours at 60 °C in the UoB chamber; 1 week at room temperature in the UoB chamber, and 24 hours at 60 °C in the micro chamber</i>	113
<i>Figure 3.12: Image of a chamber dust sample post volatilisation experiment with HBCD treated curtains in the Micro chamber</i>	114
CHAPTER 4 SIMULATING MIGRATION OF BFRs TO DUST VIA ABRASION AND VIA DIRECT CONTACT WITH BFR SOURCES	116
<i>Figure 4.1: Experimental configuration for chamber experiments evaluating abrasion of HBCD treated curtains</i>	117
<i>Figure 4.2: (a) Concentration (ng g⁻¹) of HBCDs in dust both pre and post abrasion experiments (b) Concentration (ng.g⁻¹) vs abrasion time period for each HBCD diastereomer and ΣHBCDs</i>	118
<i>Figure 4.3: Chamber experimental configuration for studying direct contact of HBCDs from a treated curtain to dust</i>	119
<i>Figure 4.4: Mean concentrations (ng g⁻¹) of HBCDs in dust, pre and post direct contact experiments for 24 hours and 1 week exposure</i>	125
CHAPTER 5 FORENSIC MICROSCOPY INVESTIGATION OF DUSTs OF ELEVATED BFR CONCENTRATIONS	135
<i>Figure 5.1: Photographs of sample preparation for Micro XRFS of generated abraded curtain fibre experiments showing (a) fibres in dust for the original sample (b) abraded fibres on the clean GFF and (c) removed GFF area attached to the glass sample plate</i>	136
<i>Figure 5.2: Sample areas analysed by Micro XRFS.</i>	138
<i>Figure 5.3: Micro XRFS optical image of a small fibre on the sample GFF and the corresponding sample Br mapping image</i>	134
<i>Figure 5.4: Optical and 3D laser images of GFF containing abraded textile fibres on its surface</i>	140
<i>Figure 5.5: SEM images of single and intertwined fibres in the analysed sample before platinum coating the sample surface, showing the effect of charging on image resolution and after platinum coating the sample surface</i>	141
<i>Figure 5.6: SEM backscattering image of a mass of intertwined fibres and corresponding EDS elemental profile from (a) the fibre surface and (b), (c) impurity particles present on the fibre surface</i>	143
<i>Figure 5.7: Diamond compression cell used for %Transmission FTIR analysis and captured image of the collected fibre</i>	145
<i>Figure 5.8: Returned database spectral searches of entire sample spectrum, highlighted peaks of interest and HBCD reference spectra</i>	146
<i>Figure 5.9: An example of the Micro XRFS analysis of Dust 2 to identify the location of one high Br content area showing the optical images and corresponding bromine mapping images</i>	149
<i>Figure 5.10: Micro XRFS analysis of three archived dust samples, with optical images and corresponding Br mapped images</i>	150

<i>Figure 5.11: Pictures of microscope used for removing 2 x 2 mm areas of interest from sample to aluminium stub, LEXT 3D laser microscope with sample stub and 25 x 25 mm sample with removed region placed on stub</i>	151
<i>Figure 5.12: Colour optical, 3D laser images and measured lengths of suspect particles in 8 identified areas of high Br-content</i>	154
<i>Figure 5.13: Secondary electron SEM image and backscattering image, showing the dark and light patches that indicate the presence of lighter and heavier elements respectively</i>	156
<i>Figure 5.14: Backscattering electron images and corresponding EDS elemental profile from suspect Br-rich fragments identified in the 7 sample areas from the first 1 mg analysis of Dust 1 and Dust 2</i>	158
<i>Figure 5.15: Backscattering electron image and corresponding EDS point analysis of light and dark regions over the surface of a particle isolated from Dust 2</i>	163
<i>Figure 5.16: Backscattering image and corresponding EDS elemental profile of a small fragment in Dust 3, (a) without coating (b) with Pt coating (c) of contamination particle present on fragment surface and (d) large organic material</i>	165
<i>Figure 5.17: FTIR sample spectra from 8 particles isolated from Dust 1 and 9 particles isolated from Dust 2</i>	169
<i>Figure 5.18: Software library database matches for the entire sample spectrum and peaks of interest for Br-rich fragments from Dust 1</i>	170
<i>Figure 5.19: Comparison of spectra from a fragment isolated from Dust 1 and reference spectra for BDE-209, antimony trioxide, and ABS copolymer</i>	172
<i>Figure 5.20: Software library database matches for the entire sample spectrum and for peaks of interest for Br-rich fragments from Dust 2</i>	173
<i>Figure 5.21: Comparison of spectra from a fragment isolated from Dust 2 and reference spectra for BDE-209, antimony trioxide, ABS copolymer and calcium carbonate</i>	175
<i>Figure 5.22: FTIR spectra of fragmented particle and reference calcium carbonate, SEM backscattering electron image and corresponding EDS elemental profile obtained post FTIR analysis</i>	176
<i>Figures 5.23: (a) Image of particle from Dust 1 in the diamond compression cell, and mapping images of (b) BDE-209 distribution, (c) antimony trioxide distribution and (d) the polymer distribution with the corresponding sample spectra and peak of interest highlighted.</i>	177
CHAPTER 6 MIGRATION OF PBDEs FROM PLASTIC TV CASING TO DUST VIA THREE DIFFERENT MIGRATION PATHWAYS	184
<i>Figure 6.1: Internal test chamber experiment configuration for investigating migration of PBDEs from TV casing to dust via volatilisation and deposition to dust</i>	186
<i>Figure 6.2: Internal test chamber configuration for investigating migration of PBDEs from plastic to dust via abrasion of particles</i>	189
<i>Figure 6.3: Concentrations (ng g⁻¹) in dust pre and post abrasion experiments for four experimental durations of (a)BDE-209 (b)BDE-183 (c)BDE-153 (d)BDE-154</i>	191

<i>Figure 6.4: (a) Relative contributions (%) of BDE-209 and 183 in the four chamber generated abrasion dust samples, the original TV casing and the low level dust pre-experiment, derived from log-normalised concentrations (b) Relative contributions (%) of BDE-153, 154, 183 and 209 in the 2 hour and 24 hour chamber generated abrasion dust samples, the original TV casing and the low level dust</i>	193
<i>Figure 6.5: Experimental configuration used to investigate migration of PBDEs from plastic to dust via direct contact between source and dust showing the positioned pieces and dust layered on the top surface</i>	194
<i>Figure 6.6: Concentrations (ng g⁻¹) of (a) BDE-209, (b) BDE-183 and (c) BDE-153 in dust pre and post partitioning via direct contact experiments</i>	197
<i>Figure 6.7: Relative contributions (%) of BDE-153, 183 and 209 in three chamber generated abrasion dust samples, the original TV casing and the low level dust, derived from log-normalised concentrations</i>	199
CHAPTER 7 BIOACCESSIBILITY STUDY OF HBCDs FROM DUST CONTAMINATED VIA DIFFERENT MIGRATION PATHWAYS	203
<i>Figure 7.1: Particle size distribution analysis results and plot for low level Belgian dust</i>	206
<i>Figure 7.2: Illustration of the bioaccessibility methodology</i>	214
<i>Figure 7.3: Concentration vs bioaccessibility (%) for α- and β-HBCDs in dusts contaminated via volatilisation with subsequent partitioning to dust and associated correlation p-values, and γ-HBCD with and without the data point at 3700 ng.g⁻¹</i>	237
<i>Figure 7.4: Concentration vs bioaccessibility (%) for α- and β-HBCDs in dusts contaminated via abrasion of fibres to dust and associated correlation p-values, and γ-HBCD with and without the data points above 2000 ng.g⁻¹</i>	238

ABBREVIATIONS

ABS	Acrylonitrile-Butadiene-Styrene
APCI	Atmospheric Pressure Chemical Ionisation
APPI	Atmospheric Pressure Photoionisation
ASE	Accelerated Solvent Extractor
BFR	Brominated Flame Retardant
CE-PBET	Colon Extended Physiologically Based Extraction Test
DEHP	Di(2-ethylhexyl) phthalate
DnBP	Di- <i>n</i> -butylphthalate
ECNI	Electron Capture Negative Ionisation
EF	Emission Factor
EI	Electron Ionisation
ESI	Electrospray Ionisation
f_{OC}	Fraction of organic carbon
FR	Flame Retardant
FTIR	Fourier Transform Infrared
GC-MS	Gas Chromatography Mass Spectrometry
GC-HR/MS	Gas Chromatography-High Resolution Mass Spectrometry
GFF	Glass Fibre Filter
GIT	Gastrointestinal Tract
HBCD	Hexabromocyclododecane
HIPS	High Impact Polystyrene
HPLC	High Performance Liquid Chromatography
IS	Internal Standard
K_{AW}	Air:water partition coefficient
K_{OA}	Octanol:air partition coefficient
K_{OW}	Octanol:water partition coefficient
K_{OC}	Organic carbon:water partition coefficient
LC-MS/MS	Liquid Chromatography tandem Mass Spectrometry
LOD	Limit of Detection
LOQ	Limit of Quantification
MRM	Multiple Reaction Monitoring

MRL	Minimum Risk Level
PBDE	Polybrominated Diphenyl Ether
PBT	Persistent Bioaccumulative Toxic
POP	Persistent Organic Pollutant
PTFE	Polytetrafluoroethylene
PUF	Polyurethane Foam
PVC	Polyvinyl Chloride
QA	Quality Assurance
QC	Quality Control
RDS	Recovery Determination Standard
RfD	Reference dose
RRF	Relative Response Factor
RSD	Relative Standard Deviation
SD	Standard Deviation
SEM/EDS	Scanning Electron Microscopy / Energy Dispersive Spectroscopy
SER	Specific Emission Rate
SPE	Solid Phase Extraction
SRM	Standard Reference Material
SVOC	Semi-volatile Organic Chemical
TBBP-A	Tetrabromobisphenol-A
UV	Ultraviolet
V _P	Vapour Pressure
VDU	Video Display Unit
VOC	Volatile Organic Chemical
vPvB	very Persistent very Bioaccumulative
XRFS	X-Ray Fluorescence Spectroscopy
Z	Fugacity Capacity

CHAPTER 1

INTRODUCTION

Residential and occupational fires can present a very serious risk to life, with the potential for great economic cost. In Europe alone, there are approximately 12 fire related deaths every day with 120 people suffering fire related injuries. The estimated annual global fire related death toll is approximately 300,000 people (WHO, 2011) with at least 94% of reported fire deaths occurring in residential homes and buildings (EFRA, 2014). Added onto this is the direct and indirect economic fire related cost, estimated at around 1% GDP in the developed world (ISO/TC92, 2014). In the USA, losses due to fires totalled US \$12.4 billion during 2012 (NFPA, 2013). Attempts to reduce fire cost and damage have been reported as far back as in Egypt, 450 BC, and the Roman empire with the fire-proofing of wood with alum. Today there are myriad inorganic and organic chemicals used as flame retardants and they have been credited with saving many lives and reducing property damage. The introduction of the United Kingdom Furniture and Furnishings (Fire Safety) Regulations in 1988 is estimated to have saved over 230 lives and 4200 injuries up to 2002 (BSEF, 2012). The flame retardants (FRs) that have been/are in use fall under 6 main categories, the halogenated FRs (containing bromine and/or chlorine), phosphorous, nitrogen, intumescent systems (e.g. expanded foam), mineral (containing aluminium or magnesium) and others (including antimony trioxide and nanocomposites) (EFRA, 2007). The brominated flame retardants (BFRs) are one of the most widely produced flame retardants that have found increasing use in consumer products since the 1970s (ATSDR, 2004a).

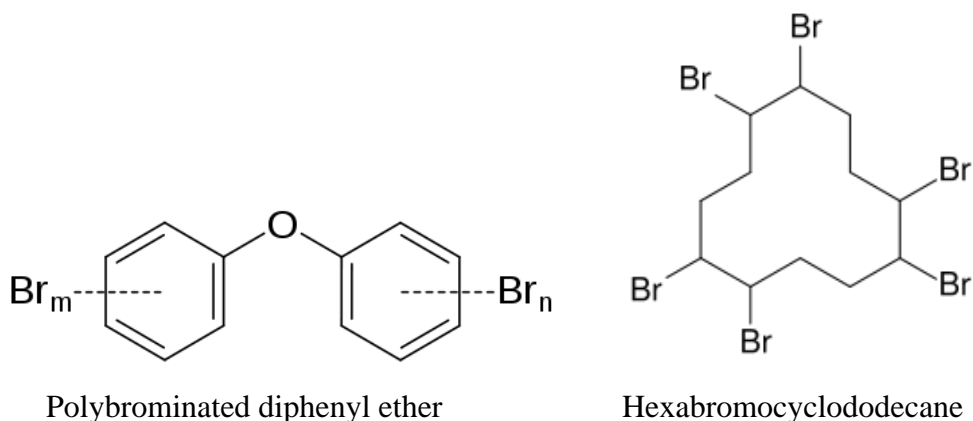
1.1 Brominated flame retardants (BFRs)

BFRs inhibit or slow down the growth of a fire through the release of free radical bromine atoms into the gas phase, before the material can reach its ignition temperature. This quenches the chemical reactions in the flame, reducing heat

generation and slowing the burning process, preventing the fire cycle from establishing and sustaining itself. Hydrogen bromide is produced through dehydrogenation of the product polymer and enhances charring of the polymer, contributing to the flame retardancy of the product. Often metal containing compounds, such as antimony trioxide, are added to enhance the efficiency of a BFR through formation of metal oxohalides which deposit in a protective layer, as metal oxides (EFRA, 2014). There are currently around 75 different commercial BFRs available with electronics and electrical equipment (e.g. TV casings and computer monitors) accounting for more than 50% of their usage (EFRA, 2007). BFRs are added to the product either through an additive (mixed into the polymer during production) or reactive (covalently bonded to the matrix polymer) process, depending on the chemical and intended use.

Two commonly used BFRs are the polybrominated diphenyl ethers (PBDEs) and hexabromocyclododecanes (HBCDs), depicted in Figure 1.1.

Figure 1.1: General chemical structure of PBDEs and HBCDs



Commercial production of PBDEs first began in the 1970s (ATSDR, 2004a) and the presence of PBDEs was first reported in the environment in 1981 with detectable concentrations reported in fish samples from Sweden (Andersson and Blomkvist, 1981). Currently, products containing PBDEs and HBCDs are ubiquitous in indoor environments with measurable concentrations reported in indoor air and dust (Harrad et al., 2010a) from different microenvironments.

1.1.1 Polybrominated diphenyl ethers (PBDEs)

There are three PBDE formulations that have been produced and used commercially as flame retardant treatments, containing congeners of different bromination levels. All three formulations are incorporated into products via the additive process. The Penta-BDE formulation consists primarily of BDE-47 (a tetra-BDE) and BDE-99 (a penta-BDE), with other tri- to hepta-BDEs present. It is used to flame retard polyurethane foam (PUF) in carpets, vehicle interiors, furniture, and bedding, as well as in printed circuit boards and microprocessor packaging in computers. The Octa-BDE formulation is a mixture of hexa- to deca-BDEs and used to treat thermoplastics, such as high impact polystyrene (HIPS) and acrylonitrile-butadiene-styrene (ABS) copolymers. The Deca-BDE formulation consists primarily of BDE-209 (deca-BDE) with trace levels of nona- and octa-BDEs and is used in HIPS and ABS applied primarily in plastic housings for electrical goods, as well as in textiles (La Guardia et al., 2006, Harrad et al., 2008b).

The primary constituents of the three formulations are: BDE-47 (tetra-BDE), BDEs-85, -99, -100 (hexa-BDEs), BDEs-153, -154 (hepta-BDEs), BDE-183 (octa-BDE) and BDE-209 (deca-BDE) (La Guardia et al., 2006). These congeners are thus the predominant PBDEs found in the indoor environment, and therefore are those monitored in this thesis.

1.1.1.1 Production

Limited information is available on production volumes of BFRs. The USEPA has estimated that worldwide production of PBDEs between 1992 and 2003 ranged from 40,000 to 67,000 metric tons per year (USEPA, 2010a). Further estimates of the three technical formulations put PentaBDE at 8,500, OctaBDE at 3,800 and DecaBDE at 54,800 metric tons per year during 1999 (Boon et al., 2002). 2001 saw a total market demand of 67,000 metric tons of PBDEs with DecaBDE consisting of 83% of production at 56,000 metric tons, and Octa and PentaBDE consisting of 6 and 11% at 4,000 and 7,500 metric tons respectively. Approximately 98% of global demand for PentaBDEs was in North America in 2004 (ATSDR, 2004b). More up-to-date production figures are not available.

1.1.1.2 Regulatory aspects

PBDEs can enter the environment during their manufacture or as release from products treated with PBDEs, which raises concerns about potential environmental or human health effects due to exposure. As such, measures have been implemented to stop or reduce the manufacture of these chemicals. The PentaBDE and OctaBDE formulations are listed as persistent organic pollutants (POPs) under the Stockholm Convention, decision SC-4/14 and SC-4/18, (UNEP, 2009). The tetra, penta, hexa and heptaBDEs are all listed under Annex A of the convention and parties that sign to ratify the Stockholm Convention are required to take measures to eliminate production or prohibit the use of the chemicals listed under this Annex (USEPA, 2009). Products containing Penta and OctaBDE, with a content of greater than 0.1%, have been prohibited from the EU market since August 2004 (ATSDR, 2004b) and the Penta and OctaBDE formulations are no longer produced or imported into the United States.

The use of DecaBDE has been banned in Europe in use in electronics and electrical applications since 2008, including both manufacture and import of such items. A phase out of manufacture, import and sales of DecaBDE in the United States started in 2010 with ordinary production, import and sales ceased on December 31, 2012 (USEPA, 2009). Recently, DecaBDE has been listed as "a substance of very high concern because of its persistent, bioaccumulative and toxic/very persistent and very bioaccumulative (PBT/vPvB) properties" by the EU (ECHA, 2012). However, large uncertainty exists in the understanding of the bioaccumulative potential of DecaBDE, primarily due to the wide range of reported values for the octanol:water partition coefficient ($\log K_{OW}$: 6.27 to 10.2, Table 1.1). The very low water solubility of DecaBDE is expected to contribute to the uncertainty, hence variation, in measured K_{OW} data and the age of the reported values (some reported over a decade ago) provides further uncertainty. Even the two studies from 2012 reported $\log K_{OA}$ values ranging between 9.4 to 10.2. Moreover, the biotransformation to other, more toxic, lower brominated PBDEs is likely of greater concern than the bioaccumulation of DecaBDE itself.

1.1.1.3 Physicochemical properties

Information on the physicochemical properties of PBDEs facilitates understanding of their persistence in the environment, bioaccumulation and other aspects of their environmental fate, further discussed in Section 1.2. A summary of reported physicochemical properties of the three PBDE formulations and of individual PBDE congeners are listed in Tables 1.1 and 1.2.

Table 1.1: Physicochemical properties of PBDE technical mixtures (ATSDR, 2004b), (Environment Canada, 2006)^A, (Dinn et al., 2012)^B, (Kelly et al., 2007)^C, (Tian et al., 2012)^D

	PentaBDE	OctaBDE	DecaBDE
CAS Number	32534-81-9	32536-52-1	1163-19-5
Physical state at 25 °C	Viscous liquid	Powder	Powder
Melting point	-7 to -3 °C	85 to 89 °C	290 to 306 °C
Boiling point	Above 300 °C (decomposition 200 °C)	Decomposition above 330 °C	Decomposition above 320 °C
Density at 25 °C (g mL ⁻¹)	2.28	2.76, 2.8	3.0, 3.25
Log K _{ow}	6.57 to 6.97	6.29	6.27 (measured) ^A 9.4 ^B 9.9 ^C 9.97 (calculated) ^A 10.2 ^D
Vapour pressure (Pa at 25 °C)	2.92 x 10 ⁻⁵ to 7.32 x 10 ⁻⁵	1.20 x 10 ⁻⁸ to 2.26 x 10 ⁻⁷	4.26 x 10 ⁻⁶ to 4.62 x 10 ⁻⁶
Henry's Law Constant (Pa.m ³ mol ⁻¹ at 25 °C)	1.2, 0.12, 0.35	7.6 x 10 ⁻³ , 2.6 x 10 ⁻²	0.162, 1.96 x 10 ⁻³ , 1.2 x 10 ⁻³ , 4.5 x 10 ⁻³

Table 1.2: Physicochemical properties of individual PBDE congeners (ATSDR, 2004b)^A (Palm et al., 2002)^B (Kuramochi et al., 2004)^C (Tittlemier et al., 2002)^D (Hardy, 2004)^E (Cetin and Odabasi, 2005)^F (Hardy, 2002)^G (Harner and Shoeib, 2002)^H (Wania et al., 2002)^I (Webster et al., 2006)^J (USEPA, 2012c)^K (Fu and Suuberg, 2011)^L (USEPA, 2008a)^M (Braekevelt et al., 2003)^N (Wania and Dugani, 2003)^O

Congener	IUPAC name	Formula	Molecular Weight (g mol ⁻¹)	Water solubility (µg L ⁻¹ at 25 °C) ^D	Log K _{OW}	Vapour pressure (Pa at 25 °C) ^D	Log K _{OA}	Henry's Law constant (Pa.m ³ mol ⁻¹ at 25 °C)
BDE-47	2,2',4,4'-tetra-bromodiphenyl ether	C ₁₂ H ₆ Br ₄ O	485.8	15	6.81 ^M 6.01-6.77 ^B 6.48 ^C 6.55 ^D	1.9 x 10 ⁻⁴	10.53 ^H 10.34 ^I	1.50 ^A 0.85 ^F
BDE-85	2,2',3,4,4'-penta-bromodiphenyl ether	C ₁₂ H ₅ Br ₅ O	564.7	6	6.57-7.66 ^B 7.03 ^D 7.37 ^M	9.9 x 10 ⁻⁶	11.66 ^H	0.11 ^A
BDE-99	2,2',4,4',5-penta-bromodiphenyl ether	C ₁₂ H ₅ Br ₅ O	564.7	9	7.32 ^M 6.53-7.66 ^B 7.21 ^C 7.13 ^D 7.66 ^E	1.76 x 10 ⁻⁵	11.31 ^H 11.28 ^I	0.23 ^A 0.60 ^F
BDE-100	2,2',4,4',6-penta-bromodiphenyl	C ₁₂ H ₅ Br ₅ O	564.7	40	7.24 ^M 6.86 ^D	2.86 x 10 ⁻⁵	11.13 ^H	6.9 x 10 ⁻² ^A 0.24 ^F

	ether							
BDE-153	2,2',4,4',5,5'- hexa- bromodiphenyl ether	C ₁₂ H ₄ Br ₆ O	643.6	1	7.90 ^M 7.83 ^C 7.62 ^D	2.1 x 10 ⁻⁶	11.82 ^H 12.15 ^I	6.70 x 10 ^{-2A} 0.04 ^F
BDE-154	2,2',4,4',5,6'- hexa- bromodiphenyl ether	C ₁₂ H ₄ Br ₆ O	643.6	1	7.82 ^M 7.39 ^D	3.79 x 10 ⁻⁶	11.92 ^H	0.24 ^A 8.0 x 10 ^{-2F}
BDE-183	2,2',3,4,4',5',6- hepta- bromodiphenyl ether	C ₁₂ H ₃ Br ₇ O	722.5	2	8.27 ^M	4.68 x 10 ⁻⁷	11.96 ^H	7.40 x 10 ^{-3A}
BDE-209	2,2',3,3',4,4',5,5', 6,6'-deca- bromodiphenyl ether	C ₁₂ Br ₁₀ O	959.17	< 0.1 ^M	6.2-12.6 ^G 6.27 ^A 8.70 ^O	1.2 x 10 ^{-7K} 1.2 x 10 ^{-10L}	13.21 ^J	4.0 x 10 ^{-2F}

The reported $\log K_{OW}$, $\log K_{OA}$ and vapour pressure (V_p) values of the different PBDE congeners vary between different studies, and a selection of the reported values are listed in Table 1.2. This variation in the reported literature values provides evidence of the difficulty in measuring physicochemical properties of these compounds and results in associated uncertainty in predicting their volatilisation from products and their subsequent fate and behaviour in the environment. Despite uncertainty about the exact values of many physicochemical properties, it is clear that the low water solubility and high K_{OA} values of PBDEs will lead to substantial partitioning to suspended and surficial sediments and soil (ATSDR, 2004b), as well as to airborne particulates (ATSDR, 2004b). The reaction with hydroxyl radicals in the atmosphere causes PBDE degradation, which has been experimentally observed in reaction chambers (Raff and Hites, 2006) where bromophenols and Br_2 byproducts are produced from hydroxyl reactions with di to hexaBDEs.

The V_p of PBDEs, generally decreases with degree of bromination and is greater for isomers containing bromine in the ortho position to the ether bond (de Wit, 2002). Due to their semi-volatile nature, airborne PBDEs exist in both the gaseous and particulate phases, with gas to particulate partitioning varying widely between individual congeners, governed by the vapour pressure (Mandalakis et al., 2009). Tetra and penta PBDEs exist predominantly in the vapour phase, whereas hexa to octa PBDEs are primarily located in the particulate phase, with decaBDE suggested to be present exclusively in the particulate phase (USEPA, 2009). This hypothesised enhanced partitioning to airborne particulates with increasing bromination level is supported by experimental evidence, as the percentages measured in the vapour phase of indoor air are: 66-86% for BDE-47, 54-65% for BDE-99, 63-74% for BDE-100, <20-48% for BDE-153 and 37-48% for BDE-154 (Harrad et al., 2004). Similar partitioning has been reported in outdoor air (at a similar temperature, 20 ± 3 °C) in North America and China (Strandberg et al., 2001, Yang et al., 2013) with gas phase fractions of 80% for BDE-47, 55-65% for BDEs-99 and 100, and 30-50% for BDEs-153 and 154. These partitioning ratios indicate similar factors influence PBDE phase partitioning in both indoor and outdoor air. However, variable atmospheric phase partitioning has been reported in urban air, with Mandalakis et al. (2009) observing a gas phase fraction of 24-29% for a number of PBDEs in the centre of Athens

compared to 69-92% in a suburban region of Heraklion city. The difference is likely due in part to the lower ambient temperatures in the Athens sampling area and substantially higher concentrations of particulate matter that were also observed in central Athens (total suspended particulate mass of 110 and 56 $\mu\text{g m}^{-3}$ in Athens and the suburban region respectively).

BDE-209, thought to be exclusively attached to particulates in air, has been observed at low concentrations in the gaseous phase of UK urban air (Wilford et al., 2008). The authors acknowledge the concentrations on the PUF may also be due to very fine particulates (containing BDE-209) that are not trapped on the GFF and are thus extracted with the PUF. PBDEs have shown increased partitioning to smaller particle sizes, with greater than 60% of particulate phase Σ PBDEs partitioning to particles with an aerodynamic diameter of $<1.8 \mu\text{m}$ (Zhang et al., 2012) and 87% of Σ PBDEs associated with particles of diameter $<1.66 \mu\text{m}$ elsewhere (Mandalakis et al., 2009). This enhanced partitioning to smaller particle sizes suggests increased potential for long-range atmospheric transport of PBDEs, as fine particles experience greater atmospheric residence times due to lower efficiency of scavenger mechanisms, such as wet deposition (Mandalakis et al., 2009). However, particulate bound PBDEs have also been shown to be removed from the atmosphere by wet and dry deposition with dry particle, dry gas and wet deposition inputs to soil calculated to contribute 60, 32 and 8% respectively to the annual PBDE flux to suburban soil in Turkey (Cetin and Odabasi, 2007).

An enrichment in PBDE concentrations in the boundary layer between the atmosphere and ocean surface (typically 40-100 μm thick), as compared to that determined in bulk seawater of Hong Kong coastal regions, has also been reported (Wurl et al., 2006). Between 2 to 6 times higher concentrations were observed in the boundary layer, suggesting this boundary layer serves as an important interface facilitating exchange of PBDEs between the atmosphere and oceans, particularly for the more volatile congeners.

Partitioning between 'freely dissolved' (in the water phase) and suspended particulate phases in aquatic systems has also been investigated, with studies generally reporting

much higher proportions associated with suspended particulates, consistent with the higher K_{ow} values of PBDEs. Between 78-93% of Σ PBDE in a San Francisco estuarine system was observed to be associated with suspended particulate matter (Oros et al., 2004), with a significant positive relationship between the total suspended solids and Σ PBDE concentrations determined at the sampling location. A smaller fraction of PBDEs in suspended particulate matter as compared to that freely dissolved was seen in Hong Kong, with fractions ranging from 26 to 79% for BDE-209, and from 30 to 44% for BDE-47 (Wurl et al., 2006). The range in values determined over different sampling sites may be due to different concentrations of suspended particulates, the organic matter content or temperature fluctuations over sampling sites. The partitioning to particulates from water is an important phase change in terms of assessing transport and migration to biota from digestion of suspended particulates, which may lead to bioaccumulation through the food chain, and will be largely reliant on the organic compound's physicochemical properties such as K_{ow} , water solubility and vapour pressure (Wurl et al., 2006, Oros et al., 2004).

1.1.2 Hexabromocyclododecane (HBCDs)

The HBCD production process results in the formation of 16 stereoisomers, due to varying orientations of the bromine-carbon bonds, and includes six pairs of enantiomers and four *meso* configurations. The commercially available HBCD technical formulation consists primarily of three diastereomers α -, β - and γ -HBCD (each a racemic mixture of the (+) and (-) enantiomers), present at 11.8, 5.8, and 81.6% respectively, with very small contributions from other stereoisomers present (Heeb et al., 2008). Like PBDEs, the HBCD formulation is also incorporated into treated products in an additive fashion. It is used widely to flame retard polystyrene foams for thermal insulation of buildings, back coating of fabrics for furniture, and HIPS used in enclosures for electronic equipment, such as TVs (Harrad et al., 2010a, Weil and Levchik, 2007). HBCDs are effective at low concentrations and typically are present in expanded polystyrene foams at 0.5% weight HBCD, however they can be present in fabrics, textiles, rubber and plastics from 1 to 30% weight HBCD (USEPA, 2010b).

As the α -, β - and γ -HBCDs are the primary constituents of the technical formulation (Heeb et al., 2008), and hence are the predominant stereoisomers found in the indoor environment, they are monitored in this thesis.

1.1.2.1 Production

Little information is available on historical production of HBCDs, however HBCDs have been on the world market since the late 1960s (Marvin et al., 2012). In 2001, worldwide production was estimated at 16,700 metric tons per year, 8% of the global BFR market (EC, 2011), and 22,000 metric tons per year in 2003 (Covaci et al., 2011). Worldwide annual production was estimated at 23,000 tonnes per year in 2009 (UNEP, 2011). The European Chemicals Association estimates that the UK alone produced 1,000 to 5,000 metric tonnes per year during 1996 to 2003 (ECHA, 2008). More up-to-date production figures are not available.

1.1.2.2 Regulatory aspects

As with PBDEs, HBCDs can enter the environment during their manufacture or by release from products treated with HBCDs and as such, measures have been implemented to reduce their production/use. In 2008, HBCD was proposed for listing as a possible Persistent Organic Pollutant under the Stockholm Convention and was added to Appendix E of the convention in 2010 (UNEP 2010, UNEP 2011). Recently, HBCDs have been listed in Annex A of the convention, decision SC-6/13 (UNEP, 2013), with specific exemptions for use in expanded polystyrene and extruded polystyrene in buildings. In 2011, HBCD was included in the ECHA list of substances subject to authorisation under REACH, with HBCD use not permitted without authorisation after 2015 (UNEP, 2011).

1.1.2.3 Physicochemical properties

Similar to PBDEs, information on the physicochemical properties of HBCDs aids understanding of their persistence, bioaccumulation and other aspects of their fate in the environment, further discussed in Section 1.2. Reported physicochemical properties of the HBCD formulation are listed in Table 1.3 and properties of the α -, β - and γ -HBCDs are listed in Table 1.4.

Table 1.3: Physicochemical properties of the HBCD technical formulation (USEPA 2010b, EC 2011, USEPA 2008a)

	HBCD formulation
IUPAC designation	1,2,5,6,9,10-HBCD
CAS No.	3194-55-6
Formula	C ₁₂ H ₁₈ Br ₆
Molecular Weight	641.69
Physical State (25 °C)	Solid
Melting Point	180-185 °C
Boiling Point	Decomposes above 445 °C
Density (g/mL)	2.3 to 2.37
Log K _{OW} (25 °C)	5.625 to 5.81
V _P (21 °C)	8.34 x 10 ⁻³ Pa
P _S - Solid phase V _P (25 °C)	7.47 x 10 ⁻⁷ Pa
Henrys Law Constant	4.7 Pa m ³ .mol ⁻¹
Water Solubility (25 °C)	8.6 µg.L ⁻¹

Table 1.4: Physicochemical properties of α -, β - and γ -HBCD (EC, 2011)^A
(Kuramochi and Sakai, 2013)^B (Goss et al., 2008)^C
(Weschler and Nazaroff, 2010)^D K_{OA} calculated as K_{OW}/K_{AW}

	Log K _{OW} (25 °C)	Log K _{AW} (25 °C)	Log K _{OA} (Calculated from K _{OW} /K _{AW} ^C)	Vapour Pressure (Pa at 25 °C)	Water solubility (µg L ⁻¹)
α -HBCD	5.07 ± 0.09 ^A 5.59 ^C	-8.84 ^C	14.43	1.05 x 10 ⁻⁸ ^B	48.8 ^A
β -HBCD	5.12 ± 0.09 ^A 5.44 ^C	-9.20 ^C	14.64	5.82 x 10 ⁻⁹ ^B	14.7 ^A
γ -HBCD	5.47 ± 0.10 ^A 5.53 ^C	-8.64 ^C	14.17	8.39 x 10 ⁻¹¹ ^B	2.1 ^A

Similar to PBDEs, HBCDs are semi volatile compounds due to their lower vapour pressures and thus will exist in both gaseous and airborne particulate phases. HBCDs in the gaseous phase are likely to degrade through reactions with photochemically produced hydroxyl radicals, and the expected reaction half life in air is 1-3 days (Tomko and McDonald, 2013). However, sorption to airborne particulates increases the resistance to degradation and oxidation of HBCD, enhancing its potential for long range transport (USEPA, 2010b).

Fewer studies are available that study the partitioning of HBCDs to particulates than exist for PBDEs, however they display a similar propensity for binding to particulates. In indoor air, HBCDs have been shown to exist at 35% present in the particulate phase as compared to the vapour phase (Harrad and Abdallah, 2008). Again, few studies are available on atmospheric deposition, however evidence of wet deposition of HBCDs has been reported with 110 kg of HBCDs calculated to have been deposited into Lake Ontario from 2004-2009 via this method (Robson et al., 2013). The low water solubility of HBCD encourages partitioning to suspended particulates in aquatic environments (Marvin et al., 2012). Partitioning between particulate and freely dissolved phases in aquatic systems has been reported at similar fractions to PBDEs with between 22 and 47% of HBCDs present in the freely dissolved phase (Harrad et al., 2009b, He et al., 2013).

1.2 Environmental, pathways, fate and behaviour of BFRs

BFRs can be released into the environment through wastewater effluents, airborne emissions from manufacturing facilities, industrial use (e.g. incorporation into finished materials), and the use and disposal of BFR containing products (EC, 2011). Once in the environment, they have the potential to bioaccumulate in the fatty tissues of organisms, a result of their high hydrophobicity, and biomagnify along the food chain (Santín et al., 2013), thus posing a potential human health risk via exposure through dietary intake.

Contamination of soil with PBDEs has been suggested as a key entry point for PBDEs into terrestrial food chains. This contamination has been suggested to occur from a variety of pathways, including: volatilisation of PBDE congeners from a treated

product with subsequent partitioning to soil; deterioration of a treated product polymer leading to polymer fragments entering the soil; and as a consequence of land application of contaminated sewage sludge-derived biosolids (Gaylor et al., 2013). Gaylor et al., (2013) investigated transfer to organisms of PBDEs from contaminated soil via direct uptake by earthworms; reporting that PBDEs accumulated in organisms ingesting both soil containing PBDE contaminated biosolids, and soil containing fragments of PBDE treated waste plastic. Ingestion of polymer micro-particles containing percentage levels of PBDE additives was shown to be an important PBDE exposure route for organisms. These organisms may subsequently transfer their body burdens to predators and facilitate the transport of PBDE mass to other locations, leading to contamination of other species.

E-waste recycling sites and surrounding areas have been of particular concern recently, with an increasing number of studies reporting highly elevated PBDE concentrations in soil in these areas (Luo et al., 2009, Luo et al., 2013, Tang et al., 2014, Zhang et al., 2013a). The processes used in such recycling sites, such as burning components of the treated products to recover scrap metal, facilitates the release of high concentrations of PBDEs to air and soil which then have the potential for accumulation in the food chain. Soil surrounding e-waste sites has also displayed elevated PBDE concentrations. As concentrations tend to decrease with distance from sites carrying out such activity (Luo et al., 2013) the soil contamination is thought to arise from atmospheric transport of combustion residues from e-waste burning.

PBDEs can persist in aquatic environments for many years leading to bioaccumulation in organisms. Uptake of PBDEs by an organism is driven by a combination of direct partitioning between the organism and the abiotic environment and dietary uptake; with dietary exposure suggested to be more relevant for more hydrophobic compounds ($\log K_{ow} > 5$) (Van Ael et al., 2013). A positive correlation between contamination of PBDEs in aquatic organisms and the lipid content of the organism has been shown in several studies, with Law et al. (2006) reporting a significant positive correlation ($p < 0.05$) between Σ PBDE concentrations and lipid content in fish. Significant correlations ($r^2 > 0.2$, $0.0006 < p < 0.035$) have also been reported in the Scheldt estuary between PBDE tissue concentrations in aquatic biota

and lipid content (Van Ael et al., 2013). In this study, PBDE concentrations were reported to increase with increasing body size for some fish species; however, other factors such as position in the food chain and lipid content exerted a greater overall influence (Van Ael et al., 2013).

The biomagnification of PBDEs in various food webs has also been observed. Biomagnification occurs if a chemical's concentration in an organism exceeds the concentration in its diet and if the absorption rate exceeds the elimination rate from the organism. Biomagnification is related to a chemical's persistence and has been shown for BDE-47 and BDE-209 in the Lake Winnipeg food web (Law et al., 2006). PBDEs biomagnification as a function of trophic level is also observed in the arctic marine food chain (Sørmo et al., 2006) with BDE-47 displaying clear biomagnification in zooplankton, polar cod and ringed seal, however only BDE-153 was found to biomagnify in polar bears, suggesting polar bears can metabolise and biodegrade other PBDEs.

The majority of studies have shown a predominance of the lower brominated PBDEs detected in organisms, however interspecies differences in PBDE congener patterns have also been reported. Higher concentrations of the lower brominated PBDEs, particularly BDE-47 are generally observed in fish (Ilyas et al., 2013, Santín et al., 2013). The greater hydrophobicity of the higher brominated congeners renders them less available for fish uptake, as they will bind strongly to both suspended and surficial sediments. It has also been suggested that metabolic debromination of higher brominated PBDEs is responsible for the predominance of the lower brominated congeners (Ilyas et al., 2013, Santín et al., 2013). Varying PBDE profiles have been seen in different fish species, possibly an indication of species-specific metabolic debromination of PBDEs occurring in aquatic organisms (Zeng et al., 2013). Interspecies differences of PBDE congeners are also detected in avian species, with kestrels having a predominance of the higher brominated congeners and owls a predominance of the lower brominated congeners; likely due to greater biotransformation of the higher brominated congeners in owls (Yu et al., 2013a).

The majority of studies have focused on the bioaccumulation of PBDEs in predator species; however, recent studies have investigated bioaccumulation of PBDEs in

plants and herbivores. Plants constitute a significant fraction of planetary biomass and are known to contain PBDEs; therefore, they likely play an important role in transfer of these chemicals through the food chain (She et al., 2013). The study of an e-waste recycling area in south China revealed BDE-209 as the dominant PBDE congener in paddy soils, rice plants and apple snails at 55%, 40%, 43% of Σ PBDEs respectively; consistent with the likely predominance of this congener in the electronic items dismantled at the site (She et al., 2013). A significant negative correlation was seen between the ratio of concentrations of individual PBDEs in plant foliage:soil and the log K_{OW} of the congener ($r^2 = 0.65$, $p = 0.002$). The lower water solubility and larger molecular size of PBDEs with higher K_{OW} values, contribute to lower plant foliage:soil concentration ratios through molecular steric hindrance restricting migration from plant roots to foliage, and via stronger retention of the more hydrophobic compounds by soil organic carbon. However, foliar uptake of PBDEs volatilised from soil was also suggested as an effective pathway of soil-to-plant transfer.

Similarly to PBDEs, HBCDs have shown to persist in aquatic environments and Law et al., (2006) reported a significant positive correlation between Σ HBCD concentrations and lipid content in fish ($p < 0.0001$). Of the HBCDs, α -HBCD is the predominant diastereomer detected in fish (Ilyas et al., 2013, He et al., 2013) which may indicate a higher bioavailability of this isomer in the aquatic environment or possible isomerisation from the other diastereoisomers. Despite α -HBCD dominating the isomer profile in fish samples, in a Chinese river study γ -HBCD predominated in the surface layer sediment of the sampled areas (He et al., 2013). However, α -HBCD again dominated the isomer pattern over γ -HBCD in deeper sediment layers, indicating γ -HBCD degrades more rapidly than α -HBCD under anaerobic conditions. A predominance of α -HBCD is also observed in predator and prey species in both aquatic (Yu et al., 2013a, Tomy et al., 2004) and terrestrial (Yu et al., 2013a) food webs. The diastereomer profile shift towards α -HBCD is suggested to result from a combination of factors including: differing solubility and partitioning preferences and hence bioavailability of the diastereomers; differing uptakes and hence biotransformation; and preferential bioisomerisation of the α -HBCD (Marvin et al., 2012).

The biomagnification of HBCDs has been reported in the Lake Ontario food web (Tomy et al., 2004), with a significant positive relationship between Σ HBCDs (α -HBCD and γ -HBCD) and trophic level ($p < 0.0001$) reported. HBCDs were also shown to biomagnify with trophic level in the arctic marine food chain (Sørmo et al., 2006) from polar cod to ringed seal and α -HBCD has been reported to increase significantly ($p < 0.001$) with increasing trophic level in the Norwegian coastal food web (Haukås et al., 2010).

HBCD presence in vegetables and vegetable oil is likely to occur from use of contaminated sewage sludge as fertiliser (Kupper et al., 2008) and HBCD uptake by plants has been reported with the highest HBCD concentrations in the plant observed in foliage, followed by plant roots and soil (Zhang et al., 2013b). In line with other studies, the transfer from soil to plants, which contain a high water content, was suggested as less facile for highly hydrophobic compounds with $\log K_{OW} > 5$, but foliar uptake of HBCDs following volatilisation from soil was highlighted as a likely transfer pathway.

In conclusion, both PBDEs and HBCDs display persistence in the environment and biota. This, coupled with their hydrophobicity, leads to their biomagnification in various food chains, including predator to prey and plant to herbivore species. Most environmental studies report the prevalence of the lower brominated PBDEs and the α -HBCD isomer in biota, suggesting these BFRs are more relevant in the context of dietary exposure.

1.3 Human Exposure to BFRs

Humans can be exposed to BFRs in the workplace, via use of consumer products containing BFRs, and indirectly from the environment via dermal, oral and respiratory contact with contaminated food, soil, water, air and dust (ECHA, 2008). Due to the hydrophobicity and resistance to rapid metabolism of BFRs, they are retained in fatty tissues with half-lives estimated to be of the order of years. As such fatty foods, in particular fish, are suggested to be a substantial dietary exposure route (ATSDR, 2004b). The inhalation of air/particles is another important exposure route that leads

to BFRs entering the body through the lungs and stomach and passing into the blood stream (ATSDR, 2004b).

Adult exposure to PBDEs in Japan was assessed by Kakimoto et al. (2014) who explored exposure via inhalation and diet. Air (gas and particle phase), and food samples from a market basket survey (based on official food consumption figures from the National Nutrition Survey) were analysed for PBDEs. The mean daily Σ PBDE inhalation intake was calculated at 0.24 ng day^{-1} and dietary intake at 62 ng day^{-1} . From these calculations, PBDE exposure occurred primarily via diet, however the calculations assumed that similar concentrations of PBDEs are present in indoor and outdoor air. This is not the case, as PBDE emission sources (e.g. the products treated with PBDEs) are primarily located in indoor environments and indoor air/dust concentrations are often magnitudes of order higher than outdoor air/soil concentrations, as summarised in Tables 1.5 and 1.6. Previous studies have also shown dust ingestion/dermal absorption to be an important human exposure pathway, which was omitted in this study.

Children are exposed to PBDEs in generally the same way as adults but because of their lower weight, their intake of PBDEs/kilogram of body weight is greater (ATSDR, 2004b). Lower brominated PBDEs have shown to accumulate in breast milk (ATSDR, 2004b), ingestion of which is thus an important exposure pathway for nursing infants. Infant exposure to PBDEs via breast milk from nursing UK mothers has been calculated at an average exposure of Σ PBDEs of $37 \text{ ng.kg bw}^{-1} \text{ day}^{-1}$ (Abdallah and Harrad, 2014), exceeding upper bound dietary intake estimates from the diet for toddlers ($13 \text{ ng.kg bw}^{-1} \text{ day}^{-1}$ (FSA, 2006)) and also for adults ($5.9 \text{ ng.kg bw}^{-1} \text{ day}^{-1}$ (FSA, 2006)). However, the daily intake of BDE-47 at $19 \text{ ng.kg bw}^{-1} \text{ day}^{-1}$ and of BDE-99 at $4.2 \text{ ng.kg bw}^{-1} \text{ day}^{-1}$ was lower than the USEPA reference dose (RfD) for BDE-47 of $100 \text{ ng.kg bw}^{-1} \text{ day}$ for a neurodevelopmental effect toxicology endpoint (USEPA, 2007).

Dust ingestion and dermal uptake (by handling surfaces coated with dust (EC, 2011)) is an important pathway of exposure to PBDEs for toddlers (ATSDR 2004b, Jones-Otazo et al., 2005). This was indicated in an assessment of exposure of the US

population to PBDEs via food, water, inhalation and via ingestion and dermal contact with house dust. It was estimated that children (1-5 years) had a higher Σ PBDE intake ($49 \text{ ng.kg bw}^{-1} \text{ day}^{-1}$) than adults ($7.7 \text{ ng.kg bw}^{-1} \text{ day}^{-1}$) due to an estimated two-fold higher dust ingestion rate for this age group (100 compared to 50 mg day^{-1}) (Lorber, 2008). Moreover, it was concluded that exposure to Σ PBDEs in house dust from a combination of ingestion and dermal contact contributed 82% of overall total adult exposure to Σ tri to deca PBDEs.

Positive, statistically significant associations have been reported between Σ PBDE concentrations in breast milk in first time mothers and dust ($r = 0.76$, $p = 0.003$) and also with consumption of dairy produce ($r = 0.41$, $p = 0.005$) and meat ($r = 0.37$, $p = 0.01$); implying that both diet and the indoor environment are important contributors to human exposure of PBDEs (Wu et al., 2007). Moreover, a positive correlation has been observed between Σ di-hexaBDE concentrations in dust and plasma (Karlsson et al., 2007) and a significant positive correlation seen between BDE-47 in house dust and placental tissue ($p = 0.048$, $r = 0.29$) (Frederiksen et al., 2009).

Exposure to nursing infants of HBCDs through breast milk has also been reported. A Canadian exposure estimate model determined the most highly exposed sector of the Canadian population to HBCDs is breast-fed infants (0-6 months), with an upper bound exposure estimated at $90 \text{ ng.kg bw}^{-1} \text{ day}^{-1}$ based on combined intake from breast milk, dust and other environmental media (EC, 2011). Consumer product exposure estimates for 6-24 month old infants from mouthing of HBCD treated textiles and upholstered furniture were also highlighted as smaller yet still important contributors to overall exposure at 1.2 and $4 \text{ ng.kg bw}^{-1} \text{ day}^{-1}$ respectively (EC, 2011). Foetal exposure through the placenta in utero (ATSDR, 2004b) is a potential concern, and measurable concentrations of HBCDs have been determined in human foetuses from as early as 6.5 weeks gestation (Rawn et al., 2014). Mouthing of textiles treated with HBCDs or toys containing HBCDs is another important exposure pathway for toddlers. A simulation study of leaching of HBCDs from toys, saw the release of 0.9% of the original HBCD content present, over a 30 minute mouthing duration (EC, 2011).

Again the importance of dust as an exposure pathway to HBCDs has been reported in exposure estimate studies. The study by Abdallah et al. (2008a) compared exposure to Σ HBCDs via dust, diet and inhalation in the UK. Dust ingestion was estimated to contribute 24% of total exposure for adults and 63% for children. A study of workers at a Norwegian expandable polystyrene processing plant by Thomsen et al. (2007) found elevated concentrations of HBCDs in serum samples of 10 workers (6 to 856 ng g⁻¹ lipid) and airborne dust (0.2 to 150 μ g m⁻³) sampled from the 'breathing zone' of the workers during a shift. Although a correlation was not seen between air and serum concentrations, serum concentrations were highly elevated to that in the control group (<1 ng g⁻¹ lipid) suggesting an important inhalation exposure source. A significant correlation ($p < 0.01$) between dust ingestion and Σ HBCD concentrations in serum of Belgian adults was reported by Roosens et al. (2009), however in the same study, a correlation was not seen with dietary exposure ($p > 0.1$). Exposure to HBCDs via dermal absorption has been investigated further in an *in vitro* study with human skin. Total dermal absorption of Σ HBCDs was estimated at 4% from application of 640 μ g of ¹⁴C Σ HBCD to the skin matrix (ECHA, 2008).

1.4 BFR Toxicology and Health Effects

Very little information is available on the toxicological effects of BFRs in humans and the few epidemiological studies that exist mostly study small population groups, making any conclusions about health effects from exposure to BFRs difficult to establish.

As discussed previously, the lower brominated PBDE congeners display greater retention in lipid-rich tissues in the body and lower rates of metabolism and elimination. As such, the PentaBDE and OctaBDE formulations are thought to display greater toxicity than the DecaBDE formulation. Despite this, DecaBDE has been classified as an EPA Group C compound, a possible human carcinogen (ATSDR, 2004b). PentaBDE and OctaBDEs are both listed as non-classifiable, however this is due to the lack of available toxicological data on all these compounds (USEPA 2012a, USEPA 2012b). As DecaBDE can undergo photolytic and possible microbial debromination in certain environmental conditions, resulting in the formation of tri to

nonaBDEs (USEPA, 2009), the lower brominated congeners are likely more relevant for assessing potential health risk from exposure.

Estimated minimum risk levels (MRLs) have been derived for PBDEs by the Agency for Toxic Substances and Disease Registry (ATSDR) from the limited toxicological information available. The MRL is an estimate of daily human exposure to a substance over a specified duration period, below which adverse effects will not occur. To calculate MRLs, three exposure periods are widely used: acute (14 days), intermediate (15 to 364 days), and chronic (365 days or more), which are estimated from toxicological studies with specified toxicity end points, for both oral and inhalation exposure. The reported MRLs for PBDEs have been calculated from studies investigating liver, nasal and thyroid effect end points. However, as stated by ATSDR (2004b), inconsistencies between studies and the lack of other sufficiently sensitive end points at the time of derivation, decreases confidence in derived MRLs and acute dose MRLs could not be derived for inhalation exposure. For the tri to hepta PBDEs, an MRL of $0.03 \text{ mg.kg}^{-1} \text{ day}^{-1}$ for acute-duration *oral* exposure and $0.007 \text{ mg.kg}^{-1} \text{ day}^{-1}$ for intermediate-duration *oral* exposure have been derived. A MRL of 0.006 mg m^{-3} has also been derived for intermediate-duration *inhalation* exposure of the lower brominated PBDEs. For decaBDE a higher MRL of $10 \text{ mg.kg}^{-1} \text{ day}^{-1}$ has been derived for intermediate-duration *oral* exposure, however this was derived from very limited data. No acute or chronic-duration *oral* MRLs were derived for decaBDE due to insufficient data (ATSDR, 2004b).

More recent studies have investigated neurobehavioural/developmental effects from oral exposure to PBDEs as a more sensitive toxicological end point than that used for the previous MRL derivation. From these studies, the USEPA has derived reference doses (RfDs) for oral exposure to BFRs, where RfDs represent the maximum acceptable oral dose of a toxic substance. The reported RfD for BDE-47 of $0.1 \text{ } \mu\text{g kg}^{-1} \text{ day}^{-1}$ was derived from a benchmark dose of $0.35 \text{ mg kg}^{-1} \text{ day}^{-1}$, for neurodevelopmental effects, using an uncertainty factor of 3000 (USEPA, 2008b). Calculated RfDs of BDEs-99 and 153 have also been reported at 0.1 and $0.2 \text{ } \mu\text{g kg}^{-1} \text{ day}^{-1}$ respectively, again using a neurodevelopmental effects end point, from benchmark doses of 0.29 and $0.45 \text{ mg kg}^{-1} \text{ day}^{-1}$ respectively and an uncertainty factor

of 3000 (USEPA, 2008c, USEPA, 2008d). The calculated RfD for BDE-209 for neurobehavioural/developmental effects was reported at $7 \mu\text{g kg}^{-1} \text{day}^{-1}$ (USEPA, 2008e), calculated from a No Observable Adverse Effects Level (NOAEL) of $2.22 \text{ mg kg}^{-1} \text{day}^{-1}$ with an uncertainty factor of 300. Inhalation reference concentrations (RfC) for PBDEs have not been derived due to insufficient data on inhalation toxicity of these compounds.

The few toxicological studies that exist and limitations of the current studies provide lower confidence levels in the calculated RfDs. The limitations are clearly highlighted when comparing current RfDs with the previously calculated RfDs for the PentaBDE formulation by the USEPA from 1990 (as summarised in USEPA, 2008c). For this earlier study the less sensitive end point of induction of liver enzymes was used with a NOAEL level of $1.8 \text{ mg kg}^{-1} \text{day}^{-1}$ (and uncertainty factor of 1000) to determine the RfD of $2 \mu\text{g kg}^{-1} \text{day}^{-1}$, an order of magnitude higher than the current BDE-99 estimate. The investigation of liver enzyme induction is not the best choice of toxicological end point however, as other negative liver effects have not been shown. Therefore, the choice of neurodevelopmental effects as the end point, increases confidence in the more recently reported RfD value.

An RfD for oral exposure to the HBCD formulation, using liver effects as the endpoint has been calculated at $0.2 \text{ mg kg}^{-1} \text{day}^{-1}$ (NRC, 2000). However, the calculation of the RfD used a NOAEL of $450 \text{ mg kg}^{-1} \text{day}^{-1}$ from a study that was over 30 years old and confidence in this RfD value is low due to a lack of other available studies. Further investigation with a more sensitive end point (such as neurobehavioural effects, as with the PBDEs) will likely provide a RfD value of higher confidence. Again, inhalation reference concentrations (RfC) for HBCDs have not been derived due to insufficient data on their inhalation toxicity.

Knowledge of human body burdens and any relationships to potential health effects is obtained from population biomonitoring studies; although in general, health effects of BFRs are not adequately studied and more epidemiological studies of human populations are needed. Limited evidence exists for PBDE exposure effects on

thyroid hormone production; however, more recent studies have reported associations with behavioural and developmental effects in children.

In vitro oestrogen receptor and thyroid hormone transport protein binding assays have suggested the potential for PBDEs to disrupt thyroid and other endocrine system functions in humans. BDE-47 has a structural similarity to thyroid hormone T4, hence may interfere with thyroid hormone transport through competitive binding with the thyroid hormone-binding transport protein, TTR, in plasma (USEPA, 2007). If this is correct, it is reasonable to hypothesise an association between BDE-47 exposure and higher free T4 hormone levels will exist; and a positive relationship between PBDE serum concentrations and free T4 hormone was observed in a study of 24 men in the US (Meeker et al., 2009). However, the more recent study by Chevrier et al. (2010) did not find a clear association between PBDE concentrations and serum T4 levels in 270 pregnant women from California. A correlation was also not determined between PBDE levels in the plasma of Swedish workers in an electronic recycling facility and changes in thyroid hormone levels (Julander et al., 2005), although only a small study population was monitored (11 participants). Effects on thyroid hormone homeostasis and the critical role that the thyroid plays in development of the central nervous system, suggests that neurobehavioural development is another potential effect of concern (ATSDR, 2004b).

In more recent studies, associations have been reported between PBDE concentrations and behavioural effects. Increased PBDE concentrations in breast milk of 222 North Carolina mothers were associated with increased activity/impulsive behaviour in infants and toddlers, who were followed and observed for 3 years (Hoffman et al., 2012). Behavioural influences have also been reported in the study by Gascon et al. (2011) with a significant association observed between BDE-47 concentrations in 224 toddlers and the occurrence of attention deficit hyperactivity disorder and reduced social competence. The larger study by Eskenazi et al. (2013) conducted a follow up investigation of 310 five year old and 323 seven year old children, determining negative associations with attention, fine motor skills and cognition in children exposed to PBDEs *in utero* or as children. The study of Herbstman et al. (2008) followed 210 children in New York for 6 years, reporting significant associations between higher concentrations of BDE-47, 99 and 100 in cord blood and lower

mental and physical developmental scores. The correlations and associations reported in the above studies, provide clear support for using neurobehavioural/developmental effects, as a more relevant toxicological end point in risk assessments and in the determination of RfDs.

Similar to PBDEs, health effects of HBCDs have been inadequately studied to date and limited data is available on the effects of human exposure to HBCDs (ECHA, 2008). HBCDs are thought to affect the thyroid system via hepatic enzyme induction, and in cell cultures, HBCDs have been observed to exert antagonistic effects on progesterone, androgen, and oestrogen receptors. The *in vitro* cell culture assay of Yamada-Okabe et al. (2005) indicated that HBCDs bind to thyroid receptors effecting thyroid function. These factors are thought to contribute to effects on thyroid hormone homeostasis. Disturbances in thyroid function may lead to altered energy metabolism and abnormal development (ECHA, 2008). Overall, the limited data available on HBCD and PBDE toxicity, suggests that while more research is needed to clarify their adverse effects on humans; there is limited evidence of thyroid effects arising from exposure to both PBDEs and HBCDs and more recently adverse effects on behavioural and development in children.

1.5 BFRs in Indoor Environments

It is estimated that people spend up to 95% of their time in indoor microenvironments (Palm Cousins, 2012), hence indoor contamination with BFRs can provide a substantial source of exposure to these compounds. PBDEs and HBCDs are additive flame retardants in that they are blended physically (rather than chemically bonded) into the polymeric product, and thus have the potential to migrate into the indoor environment with concomitant potential for human exposure (Harrad et al., 2010a). Numerous studies have reported elevated concentrations in indoor air and dust, in many world-wide locations, showing the ubiquity of these compounds. Dust contamination is of particular interest as lower volatility compounds have been detected at elevated concentrations in this compartment (Batterman et al., 2009, Harrad et al., 2008a, Webster et al., 2009). This is of concern, as exposure from indoor dust via its inhalation, ingestion or dermal contact is an important exposure pathway for toddlers in particular (Jones-Otazo et al., 2005, Stapleton et al., 2012).

Table 1.5 summarises concentrations of BFRs in indoor and outdoor air reported in the literature; while Table 1.6 summarises concentrations detected in indoor dust and soil, showing the general trend of higher indoor concentrations of BFRs, in some cases orders of magnitude higher.

Table 1.5: Summary of Arithmetic Mean or Median concentrations (with range) reported in Indoor and Outdoor air ($\mu\text{g m}^{-3}$)

Location	BFR	Houses		Offices	Day Care	Public Areas	Cars	Outdoor Air	Reference
UK (vapour phase) n=33,25,4 for homes, offices, public areas n=5 for outdoor air	Σ HBCDs <i>Median (range)</i>	180 (70-1300)		170 (70-460)		900 (820-960)		37 (34-40)	(Abdallah et al., 2008a)
UK (vapour phase) n=17 or 31,33,3,25 for homes, office, public areas, cars, n=6 outdoor air	Σ tri-hexaBDEs <i>Mean (range)</i> <i>Median</i>	50 (4-245) 130		170 (10-1420) 1080		110 (30-160)	710 (10-8180)	21	(Harrad et al., 2006) (Harrad et al., 2004)
UK (Particulate phase) n=28	Σ tri-decaBDEs <i>Median (range)</i>							18 (<0.5-400)	(Wilford et al., 2008)
Sweden (vapour phase) n=10 for houses, day care, offices n=24 for cars	Σ tri-decaBDEs Σ HBCDs <i>Median (range)</i>	Houses 330 (70-1400) 2.0 (<1.6-30)	Apartments 60 (1.3-990) 0 (<1.6-15)	4000 (140-7300) 0 (<1.6)	1400 (70-5400) 0 (<1.6-35)		510 (250-2800) 0 (<1.6)		(de Wit et al., 2012)
Greece (vapour phase) n=5 for homes, offices; n=7 for public areas; n=2 furniture store; n=8,9 outdoor air	Σ di-heptaBDEs <i>Mean (range)</i> Σ tri-hexaBDEs <i>Mean (range)</i>	8 (3-15)		205 (20-10850)		130 (50-590)	Vapour phase Particulate	18 (7-128) 9.7 (3-40) 11 (1-23)	(Mandalakis et al., 2008) (Mandalakis et al., 2009)
Izmir, Turkey n=13	Σ tri-decaBDEs Vapour phase					Suburban Outdoor Air 12 \pm 12	Urban Outdoor Air	Industrial Outdoor Air	(Cetin and Odabasi, 2007)

	Particulate <i>Mean</i> \pm <i>SD</i>					12 \pm 6.6	8.6 \pm 5.3 27 \pm 17	29 \pm 15 62 \pm 29	
US Indoor n=12 US/Great Lakes Outdoor (vapour phase) n=48	Σ tri-decaBDEs Vapour phase Particulates <i>Mean</i> \pm <i>SD</i>	Houses 4500 1200	Garages 2500 720				710 480	Urban 52 \pm 30 Rural 7.2 \pm 13	(Batterman et al., 2009) (Strandberg et al., 2001)
Boston, US n=20	<i>Mean (range)</i> Σ tri-decaBDEs	Personal air 770 (230-2680)		Bedroom 460 (175-1530)					(Allen et al., 2007)
Canada/Ottawa (vapour phase) n=74 n=7 outdoor air	Σ tri-hexaBDEs <i>Mean (range)</i>	260 (2.0-3600)						2.2 (<0.5 - 4.4)	(Wilford et al., 2004)
Kuwait (vapour phase) n=70	Σ tri-heptaBDEs <i>Mean</i> \pm <i>SD</i>	15 \pm 23		32 \pm 79					(Gevao et al., 2006)
China (vapour phase) n=14, 5 for houses and offices	Σ tri-heptaBDEs BDE-209 <i>Median (range)</i>	630 (125-2880) 250 (40-11470)		520 (180-8315) 170 (80-13730)					(Chen et al., 2008)
Northeast China n=49 China Urban Guangzhou n=32	Σ tri-decaBDEs Vapour phase Particulate <i>Mean (range)</i>							15 (6.4-21) 93 (29-141) 745 (400-1300) 22 (13-35)	(Yang et al., 2012) (Zhang et al., 2012)

Table 1.6: Summary of Arithmetic Mean or Median concentrations (with range) reported in Indoor dust and Outdoor soil (ng g^{-1})

Location No samples	BFR	Houses	Offices	Cars	Child Day Care Centres	Soil	Reference
UK n=31,6 for homes, offices	Σ HBCDs <i>Median (range)</i>	730 (140-110000)	650 (90-3600)				(Abdallah et al., 2008a)
UK n=8	Σ 9 PBDEs <i>Mean (range)</i>	215 (16-625)					(Harrad et al., 2006)
UK n=30,18,20 for homes, offices and cars	Σ tri-hexaBDEs BDE-209 <i>Median (range)</i>	46 (7.1-250) 8100 (<dl- 2,200,000)	100 (16-1100) 6200 (620-280,000)	190 (54-22,000) 100,000 (12,000- 2,600,000)			(Harrad et al., 2008a),
UK n=28 Canada n=10 New Zealand n=20 US (Texas) n=20 UK Soil n=11	Σ tri-decaBDEs Σ tri-decaBDEs Σ tri-hexaBDEs Σ tri-decaBDEs Σ tri-hexaBDEs <i>Median (range)</i>	2900 (360-520,000) 950 (750-3500) 96 (13-680) 3500 (920-17000)				0.7 (0.073- 3.89)	(Harrad et al., 2008b) (Harrad and Hunter, 2006)
UK n=112, sampled from 2 houses	Σ tri-hexaBDEs <i>Median (range)</i>	House 1 62 (21-280)	House 2 368 (20-1000)				(Muenhor and Harrad, 2012)
Australia Soil near large automotive	Σ tetra- decaBDEs <i>Mean (range)</i>					270 (29- 726)	(Hearn et al., 2013)

shredding facility							
Belgium n=43,10 for houses, offices	Σtri-nonaBDEs BDE209 ΣHBCDs <i>Median (range)</i>	27 (4-1210) 313 (<5-5300) 130 (5-42690)	140 (59-10880) 440 (69-11570) 370 (256-1150)				(D'Hollander et al., 2010)
Sweden n=10,44,10,10,24 for houses, apartments, offices, day care centres, cars	Σtri-decaBDEs ΣHBCDs <i>Median (range)</i>	Houses 510 (53-4000) 100 (15-990)	Apartments 1400 (13-100,000) 45 (<3-2400)	1200 (800-13,000) 300 (190-5700)	1400 (54- 30,000) 54 (6.8-170)	1200 (420- 3900) 340 (190- 1600)	(de Wit et al., 2012) (Thuresson et al., 2012)
Izmir, Turkey n=13	Σtri-decaBDEs <i>Mean (range)</i>					245 (0.90 – 2840)	(Cetin and Odabasi, 2007)
US n=19 US n=11	ΣHBCDs Σtri-decaBDEs <i>Median (range)</i>	230 (<4.5-130,200) 1910 (590-34 400)					(Stapleton et al., 2008) (Wu et al., 2007)
US n=31 for offices and living areas; n=29,20 for bedroom and cars	Σtri-hexaBDEs <i>Mean (range)</i>	Living area 1690 (9.0-91000)	Bedroom 1380 (252-20900)	2170 (141-61300)	2610 (110- 44300)		(Watkins et al., 2011)
US n=12	Σtri-decaBDEs <i>Mean (maximum)</i>	Houses 49,000 (290,000)	Garages 210,000 (4,100,000)		15,000,000 (210,000,000)		(Batterman et al., 2009)
US Cars n=60	Σtri-decaBDEs <i>Median (range)</i>				50,780 (4800-		(Lagalante et al., 2009)

					3,635,400)		
US n=108	<i>Mean (range)</i> Σ_{12} PentaBDEs Σ_4 OctaBDEs Σ_4 DecaBDEs Σ PBDEs	Living area 5460 (975-52300) 50 (6.2-420) 4700 (810-185,600) 13,700 (30200-192,100)	Bedroom 2610 (140-47,600) 55 (0.4-3030) 1870 (41-37,900) 6260 (200-48100)				(Allen et al., 2008a)
South Africa	Σ tri-decaBDEs <i>Medium (range)</i>		160 (22-580)				(Kefeni and Okonkwo, 2012)
Japan Hotel n=8	Σ tri-decaBDEs Σ HBCDs <i>Mean (range)</i>	1030 (10-1700) 630 (72-1300)					(Takigami et al., 2009)
Hong Kong n=25,55 for Homes, workplaces	Σ tri-decaBDEs <i>Mean (range)</i>	Homes 4200 (685-18,400)	Workplaces 6490 (400-40,200)				(Kang et al., 2011)
Singapore n=31 Philipines University n=8	Σ tri-decaBDEs BDE-209 <i>Median (range)</i> BDE-209 <i>Mean (range)</i>	98 (11-12000) 1000 (68-13000)	2170 (<dl-4120)				(Tan et al., 2007) (Fulong and Espino, 2013)
Indonesia (industrial, urban, rural, dumping site & agricultural areas) n=23	Σ mono-decaBDEs Σ HBCDs <i>Mean (range)</i>					7.4 (0.07 – 24) 0.48 (<dl – 1.8)	(Ilyas et al., 2011)
South China	Σ HBCDs			E-waste recycling	Surrounding	Industrial	(Gao et al., 2011)

n=8,50,33 for e-waste site, surrounding soil, industrial	<i>Mean (range)</i>			Soil 106 (30 – 28) 2.3 (0.4 – 4.1)	area Soil 0.79 (0.01 – 5.8) 0.22 (0.01 – 1.5)	area Soil 1.1 (0.05 – 3.7) 0.31 (0.05 – 1.3)	
Cambodia (municipal waste dumping site) n=45 Tibet n=40	Σ tri-decaBDEs Σ HBCDs <i>Mean (range)</i> Σ tetra-heptaBDEs					32 (0.5 - 90) 0.2 (<0.005 - 0.4) <dl - 0.03	(Eguchi et al., 2013) (Wang et al., 2012)
Northern China Soil from plastic waste recycling area n= 62	Σ tri-decaBDEs <i>Mean (range)</i>					600 (1.25-5500)	(Tang et al., 2014)
Beijing China n=42	Σ mono-decaBDEs <i>Mean (range)</i>					8.5 (0.24-120)	(Zhang et al., 2013a)
UK n=14 cars	Σ tri-nonaBDEs Σ HBCDs		Cabin 284200 (29600-846800) 9070 (1240-23700)	Trunk 4030 (210-11700) 1460 (200-3100)			(Harrad and Abdallah, 2011)
Airplane dust n=40 <i>Median (range)</i>	Σ HBCDs Σ tri-decaBDEs	Floor 7600 (180-1100000) 498700	Vent 10000 (370-97000) 483500				(Allen et al., 2013)

1.6 Migration of BFRs to air and dust

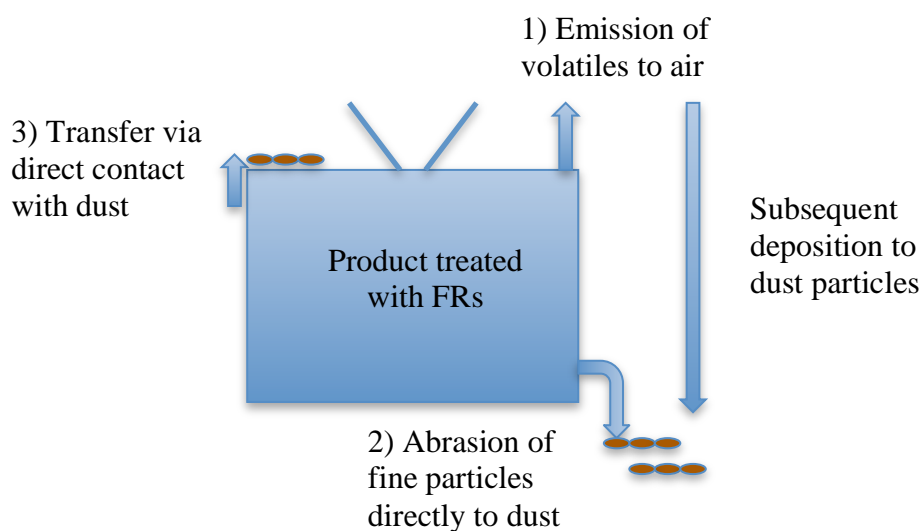
Measurement of emissions of chemicals from treated products is an essential first step in the assessment of the potential for exposure and ultimately the risk to human health. Moreover, emission measurements can be used to develop models to predict indoor concentrations under different environmental conditions and use scenarios, and to compare specific emission rates for different material and product use scenarios.

One pathway via which BFRs enter the indoor environment is via volatilisation from source materials. This is particularly facile from electronics that heat during operation, or from fabrics heated by exposure to direct sunlight e.g. curtains. Such volatile emissions have been measured and used to calculate specific emission rates (SERs) of BFRs in a small number of emission chamber experiments. More limited information is available on the mechanisms via which BFRs migrate from products into dust. Proposed hypotheses are depicted in Figure 1.2. They comprise: (1) deposition to dust after volatilisation of BFRs from products, (2) physical transfer of BFRs via abrasion of products, whereby BFRs associated with abraded particles/fibres are transferred directly to dust, and (3) transfer of BFRs from products via direct contact with dust on the surface of the product.

While all of these mechanisms may apply in varying degrees to all BFRs, regardless of their volatility, it is hypothesised that mechanism (1) is likely to be less important for the less volatile BFRs, such as BDE-209. While such low volatility BFRs partition preferentially to dust from the vapour phase, their low vapour pressures render them far less capable of volatilisation from products into the vapour phase in the first place. Conversely, while partitioning of BFRs from the vapour phase to dust via mechanism (1) will be less facile for BFRs with higher vapour pressures, this is counterbalanced by the fact that such BFRs will volatilise from products more readily. Mechanism (2) has been proposed as a likely explanation for the highly elevated concentrations of the very low volatility BFR, BDE-209, in some indoor dust samples (210 mg g^{-1} (Batterman et al., 2009) and 2.6 mg g^{-1} (Harrad et al., 2008a)). The high concentrations in such samples are hypothesised to arise from the presence of a small number of particles/fibres of products containing BDE-209, overlaid onto a relatively

low-level of background contamination arising from mechanisms (1) and (3). Finally, migration via mechanism (3) is likely to be a complex integral of direct partitioning of BFRs between the product, dust, and the vapour phase in the product/dust boundary layer. Such partitioning will be governed by factors such as: the physicochemical properties of the BFR, the process via which the BFR is incorporated into the product (e.g. covalently bound or not), properties of the dust (e.g. organic carbon content), and the duration of contact time between the product and dust.

Figure 1.2: Hypothesised migration pathways of FRs from treated products into indoor air and dust



1.6.1 The Influence of Dust Particle Size Distribution on BFR Concentrations in Settled Dust and Implications for Human Exposure

The distribution of BFRs over different particle size ranges is an important parameter as it will influence estimated exposure to BFRs from dust and particulates. Exposure to particulate bound BFRs via inhalation will occur primarily from smaller, lighter particles that are airborne, as larger, heavier particles will preferentially partition to settled dust. The smaller particle sizes also have the potential for further transport into the respiratory system. Particles of diameter $< 10 \mu\text{m}$ are able to pass the throat and nose to enter the lungs, with particles $< 2.5 \mu\text{m}$ of higher concern due to their potential for deeper lung penetration (USEPA, 2014). Zhang et al. (2012) observed that more than 60% of ΣPBDEs present in the particulate phase of urban outdoor air

were associated with particles with an aerodynamic diameter $< 1.8 \mu\text{m}$. Similarly, Mandalakis et al. (2009) determined that greater than 46% of Σ PBDEs were associated with particles $< 0.57 \mu\text{m}$ in diameter and 87% in particles of diameter $< 1.66 \mu\text{m}$ in urban air. These studies indicate the majority of particulate bound PBDEs are associated with smaller particles, which have the potential to travel further into the lungs and respiratory system and hence are likely more important in the context of human exposure assessment.

Exposure via contact with dust is widely thought to occur primarily through hand to mouth contact leading to ingestion, as well as dermal uptake. As a result, identifying which particle size range adheres most strongly to hands and other exposed skin surfaces is relevant. There are limited studies on the adherence of dust particles to hands with most studies investigating adherence of soil particles. The USEPA's Integrated Exposure Uptake Biokinetic (IEUBK) model specifies that it is "critical to sieve soil samples to $< 250 \mu\text{m}$ to more closely represent the size of soil particles that would be expected to adhere to children's hands" (USEPA, 1999). Duggan and Inskip (1985) observed that using a $200 \mu\text{m}$ particle size limit allowed analysis of 95% of the mass adhering to hands, whereas Yamamoto et al. (2006) found soil particle sizes up to $300 \mu\text{m}$ in diameter on children's hands (mean 4 years). Combined, the data from these studies suggests that dust particles greater than $300 \mu\text{m}$ in diameter are of questionable relevance for assessing exposure via ingestion or dermal uptake.

Clearly therefore, if the majority of BFRs in dust are associated with particles exceeding $300 \mu\text{m}$ in diameter, then the potential exposure via ingestion of and dermal uptake from dust is likely minimal. This is especially pertinent when considering dust contaminated via the abrasion migration pathway, as larger particles consisting of fragments of BFR-treated source materials will have much higher BFR concentrations but will be of limited relevance for human exposure if their diameter exceeds the range considered to adhere efficiently to skin. The concentration distribution of BFRs between different dust particle size ranges is thus an important topic. Cao et al. (2012) reviewed the available literature in this area for PBDEs. In general, PBDE concentrations in dust increase as particle size decreases; with particles $< 100 \mu\text{m}$ containing higher concentrations than larger particles. As

highlighted above, particles < 100 µm will likely adhere to skin, confirming the relevance of ingestion of and dermal contact with dust as pathways of human exposure to BFRs.

1.6.2 Bioaccessibility

The bioavailability of a compound refers to the fraction of a chemical ingested that reaches the central (blood) compartment of the gastrointestinal tract. By way of distinction, bioaccessibility refers to the fraction that dissolves in the gastrointestinal tract and is thereby available for absorption into the body (Cave et al., 2010). The bioaccessibility of BFRs can be assessed in *in vitro* studies that model the gastrointestinal tract to determine the percentage of ingested BFR that will pose a possible risk to health and hence provide an indication of a chemical's bioavailability. Data from the few such studies conducted to date, indicate that BFRs have a reasonably low bioaccessibility, thereby reducing the effective exposure.

Abdallah et al. (2012) investigated the bioaccessibility of PBDEs and HBCDs in dust using a colon-enhanced physiologically based extraction test, where dust was added to gastrointestinal tract (GIT) media before incubation. After extraction of the supernatant and residue, the bioaccessibility was determined as the ratio of the BFR mass in the supernatant compared to that determined in the original dust. The bioaccessibility of the tri to hepta-BDEs ranged from 32-58% that of BDE-209 was 14%, while the bioaccessibility of ΣHBCDs was 77%. The γ-HBCD diastereomer displayed lower bioaccessibility (72%) than either α- or β-HBCDs. The lower water solubilities of both γ-HBCD and BDE-209 relative to other HBCDs and PBDEs respectively, was considered one likely explanation for their lower bioaccessibilities. It was also hypothesised that BDE-209 may have been present associated with particles or fibres abraded from source materials, from which bioaccessibility would be less facile. However, forensic microscopic examination of the dust sample subjected to bioaccessibility testing with scanning electron microscopy (SEM) did not identify likely abraded particles in the sample.

Yu et al. (2012) also used a GIT model to determine the bioaccessibility of PBDEs. Bioaccessibility of individual PBDE congeners ranged from 14 to 66%. The lower

bioaccessibility of BDE-209 in this study (14%) was suggested to be due at least partly to its presence within abraded plastic particles in the dust, from which bioaccessibility was hypothesised to be lower. A negative correlation was determined between the average bioaccessibility of 13 PBDE congeners and the organic matter content of the dust. The hydrophobic nature of PBDEs means they likely bind strongly to organic matter, hence bioaccessibility is hypothesised to diminish as dust organic matter increases. Lepom et al. (2010) investigated the oral bioaccessibility of PBDEs from dust using a previously developed *in vitro* gastrointestinal model (German Standard DIN 19738) which used artificial saliva, synthetic gastric and intestinal juices to determine the fraction of ingested chemical that is solubilised in the gastrointestinal tract. The NIST reference material SRM 2585 (organics in dust) was used as the dust sample (1 g) with 3 series of replicates (n=8 in total) extracted with the bioaccessibility assay. The average bioaccessibility from each series of analyses for tri- heptaBDEs ranged 27 to 42% whilst BDE-209 was lower at 7 to 14%, again showing a lower bioaccessibility for this congener which is in line with the studies by Yu et al. (2012) and Abdallah et al. (2012).

All three studies by Abdallah et al. (2012), Lepom et al. (2010) and Yu et al. (2012) reported BFR bioaccessibilities of substantially less than 100%, suggesting default assumptions of 100% uptake of PBDEs associated with ingested dust are overestimates and should be reconsidered.

1.6.3 Linking Putative Sources with Indoor Contamination with BFRs

Given the ubiquitous nature of BFR contamination of indoor environments and its potential health implications; establishing the relationship between the level of contamination and the presence of putative sources has been the subject of numerous studies. However, most such studies to date, have failed to report statistically significant relationships (Allen et al., 2007, Wu et al., 2007, Gevao et al., 2006) and this absence of such relationships is likely due to misclassification of putative sources.

The lack of a statistical correlation between putative sources and PBDE concentrations in air from Kuwait homes by Gevao et al. (2006) was suggested to be due to insufficient information on the presence of PBDEs (as opposed to alternative

FRs) in different materials. Likewise, Kang et al. (2011) did not find significant correlations between PBDE concentrations in Hong Kong house dust and house characteristics; including numbers of foam furniture and electronic appliances present, age of the house, floor area, and carpet coverage. Furthermore, Tan et al. (2007) did not detect significant correlations between PBDE concentrations in indoor dust and microenvironment characteristics in Singapore, such as number of TVs/computers, flooring material and floor area.

Hazrati and Harrad (2006) reported statistically significant differences in the atmospheric concentrations of PBDEs in two office rooms in the same building. The observed differences in concentrations were attributed to disparities in room usage patterns (e.g. computer usage, and room ventilation rates), and the numbers of putative sources in the two rooms. The office with higher air concentrations contained seven PUF containing chairs and six PCs, while the less contaminated office contained one PC and four chairs. Similarly, an earlier UK study by Harrad et al. (2004), reported a statistically significant positive relationship between concentrations of all monitored PBDEs in indoor air, and the number of electrical appliances and PUF-containing chairs in sampled locations. The highest PBDE levels occurred in rooms containing numerous computers and PUF containing chairs, whereas the lowest concentrations were seen in rooms with no PUF-containing furniture. Two rooms containing either fume hoods or a mechanical ventilation system had very low concentrations suggesting ventilation systems are an important factor in reducing indoor air levels. Even clearer evidence of a link between indoor contamination and putative sources was provided by the study of de Wit et al. (2012). A statistically significant correlation was reported between PBDE and HBCD concentrations in indoor air and dust and microenvironment characteristics, including numbers of different putative sources in the sampled area, such as numbers of mattresses, electronics etc.

The correct identification of BFR containing products to minimise source misclassification (Harrad et al., 2010a) is a key issue to overcome. Product (source) misclassification was investigated by Allen et al. (2008b) using an X-ray fluorescence (XRF) analyser. No significant associations were found between concentrations of

PBDEs in indoor dust and an initial estimated count of putative sources in the room. However, using XRF to identify products that contain bromine and thus likely PBDEs, yielded significant associations between counts of products containing measurable bromine levels and PBDE concentrations in the corresponding dust samples. Significant variations in bromine concentrations were seen between similar products (television concentrations ranged from < 5 to 190 000 ppm) showing the ease with which putative sources may be misclassified.

The ever increasing range of BFRs present in goods and materials used indoors can easily lead to source misclassification as identification of bromine content does not identify the presence of e.g. PBDEs. Many BFRs including PBDEs, HBCDs, tetrabromobisphenol-A (TBBP-A) and novel BFRs (NBFRs), as well as other brominated compounds may be present in the product matrix. As identification of bromine will only suggest the presence of a BFR is possible, and often essential information about the product such as which FR is present or its age is not available; classification and hence an association with microenvironment contamination is very difficult. Determining correlations between putative sources containing BFRs and BFR concentrations in the immediate environment is important to provide information on how BFRs are entering the indoor environment and to help develop relevant exposure estimates, yet this is still an area of research that needs considerable attention.

1.6.3.1 Source attribution insights from correlations between matched indoor air and dust samples

The relationship between concentrations of PBDEs in air and dust sampled from the same room has also been studied for source attribution purposes. The study by Wilford et al. (2004) of homes in Ottawa, Canada, reported a positive significant correlation between concentrations of lower brominated PBDEs in indoor air and dust sampled from the same locations. This suggested a common source to air and dust for these congeners. No correlation was seen for BDE-183 and BDE-209. Some light is shed on the different behaviour of BDE-183 and BDE-209 to that of the lower brominated congeners in a later study by Zhang et al. (2011). In this, a positive correlation was observed between concentrations of individual PBDE congeners in

corresponding air and dust samples in homes from Toronto. However, a correlation was not seen for Σ PBDE. To examine this further, the relationship between the air to dust partitioning of PBDEs and the octanol to air partitioning coefficient (K_{OA}) was evaluated. A linear relationship between $\log(\text{Conc}_{\text{Air}}/\text{Conc}_{\text{Dust}})$ and $\log(K_{OA})$ for a given PBDE was hypothesised as indicating its presence in dust was a result of air to dust partitioning (Zhang et al., 2011). For compounds with less than 5 bromine atoms this relationship was shown, but was absent for the heavier congeners. This distinct behaviour for the higher brominated congeners was suggested as being either due to a failure to reach air:dust equilibrium; that airborne particulates (and associated PBDEs) deposited to PUF disks, thereby overestimating vapour phase concentrations; or because source material abrasion was the principal pathway via which the heavier congeners entered dust. However, the authors noted that if abrasion was the only contributing pathway, the $\log(\text{Conc}_{\text{Air}}/\text{Conc}_{\text{Dust}})$ would exceed the $\log(K_{OA})$, which was not observed in their study, suggesting that many factors could be at play in the transfer pathways of these PBDEs.

1.6.4 Influence of Microenvironment on BFR Contamination

Various studies have compared concentrations of BFRs in indoor air and dust originating from different microenvironments, including homes, offices and vehicles, with a general trend of higher concentrations in microenvironments like offices, that contained greater numbers of putative sources.

In a study by Harrad et al. (2008a), concentrations in dust were consistent between the three above mentioned microenvironments for PBDE congeners found primarily in the OctaBDE and DecaBDE formulations. Concentrations of PBDEs associated with the PentaBDE formulation varied however; with average values in dust from houses, offices, and vehicles of 80 ng g^{-1} , 250 ng g^{-1} , and 2300 ng g^{-1} respectively. Fulong and Espino (2013) investigated PBDEs in dust from eight different university microenvironments in the Philippines with the highest BDE-209 concentrations (4000 ng g^{-1}) occurring in a small computer centre containing a mix of old and new computers ($n=4$). The lowest levels (1000 ng g^{-1}) were present in an office lounge containing only one TV set as a putative source. Concentrations of Σ PBDEs in dust from Hong Kong workplaces exceeded those in homes by 2 to 60 times (Kang et al.,

2011). In the same study, electronics factories displayed the highest concentrations of Σ PBDEs (2000 to 40 000 ng g⁻¹), which likely originated from the electrical equipment (particularly computers) assembled in the factories. Chen et al. (2008) investigated atmospheric Σ PBDE concentrations in Chinese houses, offices and other workplaces. Concentrations were generally higher in workplaces than houses, but not significantly so. The office with the highest air concentration of Σ PBDEs (8000 pg m⁻³) contained 28 computers and 31 PUF-containing chairs, whereas the office with the lowest reported concentration (200 pg m⁻³) contained only 15 computers. Perhaps more importantly, the computers in the second office were not in use and the ambient temperature was lower (8 °C), possibly also resulting in lower emissions.

A study of different microenvironments in Greece by Mandalakis et al. (2008) found higher levels of PBDEs in offices and stores compared to homes. One office, reporting elevated Σ PBDEs at 11 000 pg m⁻³, accommodated the network servers and other telecommunications infrastructure of a public utility. This suggests that electrical equipment may be a significant source of BFRs, due to enhanced volatilisation driven by the higher temperatures generated during their operation. In a similar vein, Gevao et al. (2006) reported higher average airborne concentrations of PentaBDE congeners in Kuwaiti offices (19 pg m⁻³) than homes (9.1 pg m⁻³). Moreover, Kefeni and Okonkwo (2012) reported the highest dust concentrations of BDE-209 (600 ng g⁻¹) in their study in a South African office containing the highest number of old computers, sofas, foam chairs and electronics. Zhang et al. (2011) reported the results of a principal component analysis of congener profiles, which suggested electrical equipment was the main contamination source of PBDEs in rooms (usually offices) containing higher concentrations. Study areas with lower concentrations (usually homes) had PUF furniture and carpets as the likely PBDE sources.

A Flemish study by D'Hollander et al. (2010) compared concentrations of BFRs in dust from homes and offices, with offices containing higher mean HBCD and PBDE concentrations. The median Σ PBDE concentrations in homes were 27 ng g⁻¹ and 310 ng g⁻¹ for BDE-209 with median office concentrations of 140 ng g⁻¹ for Σ PBDE and 440 ng g⁻¹ for BDE-209. Higher HBCD concentrations were also reported in

offices, with median Σ HBCD concentrations at 370 ng g^{-1} exceeding the 130 ng g^{-1} detected in homes. A Mann–Whitney U test showed office dust was significantly more contaminated than house dust for both Σ PBDEs and Σ HBCDs ($p = 0.01$ and $p < 0.01$ respectively). A study of HBCDs in indoor air Abdallah et al. (2008a) found higher mean Σ HBCD concentrations in public environments e.g. pubs and restaurants (900 pg m^{-3}) than in homes and offices at 250 and 180 pg m^{-3} respectively. Thuresson et al. (2012) analysed dust from offices, houses and apartments, day care centres, and cars in Sweden. They reported significantly higher concentrations of PBDEs and HBCDs in dust from offices (mean Σ PBDEs = 1200 and Σ HBCDs = 300 ng g^{-1}) compared to houses (mean Σ PBDEs = 510 and Σ HBCDs = 100 ng g^{-1}). However, the microenvironments with the highest Σ PentaBDE concentrations were child day care centres, with a mean concentration of 240 ng g^{-1} suggested to be due to the number of foam mattresses present.

Watkins et al. (2011) compared PBDE concentrations in blood serum with those in dust from offices, living areas, bedrooms and vehicles. Higher mean concentrations of Σ PentaBDE were found in office and vehicle dust than in homes, but PBDE concentrations in bedroom and main living area dust were the strongest predictors of Σ PBDEs in serum. Correlations between Σ PentaBDE concentrations in serum and dust were seen in living areas ($r = 0.42$, $p = 0.02$) and bedrooms ($r = 0.49$, $p = 0.008$). This suggests exposure in the home is the most important contributor to body burden and will be strongly influenced by different behaviours and time spent in the home microenvironment, such as percentage of time spent in areas containing putative sources, extent of movement around the room leading to dust disturbance and cleaning habits such as frequency of vacuuming.

1.6.5 Within-building and within-room spatial and temporal trends in BFR concentrations in indoor dust

Spatial and temporal variability of BFR contamination of dust within microenvironments has provided information on the influence of putative sources on sampled areas.

Within-room and within-house spatial variability in concentrations of PBDEs in UK dust was studied by Muenhor and Harrad (2012). Two of the studied rooms showed within-room differences in PBDE dust concentrations. In one case, concentrations close to putative sources (TV, laptop, chair and sofa) exceeded those in dust sampled more than two metres away from the source (Σ PBDEs 540 and 290 ng g⁻¹ respectively). The study also investigated temporal variability, analysing samples every month for eight months and noting insertion and removal of putative sources. Concentrations of Σ PBDEs increased substantially with the addition of a TV to one room, while a decrease in Σ PBDE concentrations was observed following the removal of an old bed. Another room saw a marked increase in concentrations of BDEs-153 and 154 when two laptops were introduced. Similarly, another study by Harrad et al. (2008a) reported temporal trends of PBDEs in dust from three rooms, over an 8 to 10 month sampling period. Substantial increases in BDE-209 concentrations were noted in one room after the insertion of a fabric padded bed cover and polyester fabric window blinds (from 17 000 to 42 000 ng g⁻¹). Another room in the study saw an order of magnitude increase in BDE-209 concentrations (1300 to 36 000 ng g⁻¹), coinciding with the addition of a new mattress and curtains to the room. The authors suggested these results show fabrics treated with BDE-209 can be a substantial source of contamination for indoor environments.

Within-room spatial variability in concentrations of HBCDs in dust have also been investigated in homes and offices (Harrad et al., 2009a). This study reported increased concentrations of HBCDs in dust sampled closer to the source. One office saw the dust sampled closest to a PC and related electronic equipment containing 4 to 5 times higher concentrations than other samples from the same room. Similarly, sampling in another room revealed dust samples closest to a TV set to contain higher concentrations. A shift in the diastereomer ratio was also seen in this sample with a predominantly γ -diastereomer pattern closest to the TV, contrasting with a shift towards to the α -diastereomer with increasing distance from the TV (Harrad et al., 2009a). The diastereomer shift observed in many studies from a predominantly γ -HBCD content in the commercial formulation towards an α -HBCD dominance in dust, is thought to be due to a thermal isomerisation during the production process, combined with post-emission thermal and/or photolytic γ - to α -HBCD isomerisation

in the dust (Harrad et al., 2009a, Koppen et al., 2008). Similarly, a study by Stapleton et al. (2008) reported intra-house variations in concentrations of Σ HBCD in dust samples from 19 homes in Boston. Concentrations in the main living area were significantly higher ($p < 0.05$) than concentrations determined in the bedroom with levels in the main living area, ranging from < 5 to $130\ 200\ \text{ng g}^{-1}$, and bedrooms varying between < 5 and $9\ 710\ \text{ng g}^{-1}$.

A further study into spatial distribution by Harrad and Abdallah (2011) of BFRs in dust within vehicles, found higher concentrations of HBCDs, PBDEs, and tetrabromobisphenol-A (TBBP-A) in the cabin as opposed to the boot. This is consistent with the use of these compounds in fabrics and printed circuit boards used in cabins. Within building variations were investigated by Takigami et al. (2009) with dust from different floors of the same hotel (one combined sample for each floor) varying in concentration by up to two orders of magnitude for both HBCDs and PBDEs.

Such within-room and within-building spatial trends suggest a risk that sampling by vacuuming the whole floor of one room or combining dust from a number of rooms (Wu et al., 2007) - as when using householder-provided vacuum cleaner dust bag contents; will create an average concentration that is unlikely to reflect individual sources of contamination (TV, foam chairs etc). Such combined samples will not reflect the varying levels of contamination between sampling areas due to within-room variations in BFR concentrations in dust (Harrad et al., 2010a). Conversely, sampling one specific area within a room will not necessarily provide better correlation between putative sources and BFR contamination of dust if the sampling area is too small and not impacted significantly by those sources.

The evidence of higher concentrations in areas closest to putative sources, combined with statistically significant relationships between putative sources and contamination levels in the environments within which the sources are located, show the importance of accurate source classification. As technology becomes increasingly embedded in our lifestyles, the number of flame-retarded products used in indoor environments e.g. electronics is likely to increase, with correspondingly enhanced potential for

contamination with FRs. Particular needs exist for better information about specific emission rates and mass transfer from products and/or air to particulates, to help predict contamination of indoor microenvironments and resultant human exposure.

1.6.6 Modelling studies

Mathematical modelling of the indoor environment may be used to calculate emission factors (EFs) which are a representative value that relates the quantity of a pollutant released to the atmosphere with an activity associated with the release of that pollutant; specific emission rates (SERs) and potential exposure via various indoor pathways (Schripp et al., 2010). Providing data on the emissions of BFRs from products gives an indication of contamination from sources into the microenvironments they are contained in, i.e. indoor contamination. Knowing the emission behaviour from treated products in indoor environments also increases knowledge of sources and mechanisms of outdoor environmental contamination.

Most models have assessed chemical movement in urban environments but have not considered the indoor environment as a contributing compartment (Palm Cousins, 2012). As generally people spend up to 95% of their time indoors (Palm Cousins, 2012), such chemicals in indoor environments will have a greater contribution to human exposure than when in outdoor environments. The proportion of time spent indoors is likely to vary between countries/regions and a survey by the USEPA calculated that an average adult in the US would spend 80% of their day in indoor environments and 20% in the outdoors (USEPA, 2011). The variable extent of indoor occupation will influence exposure as indoor environments generally contain elevated BFR concentrations in air and dust to outdoor microenvironments, hence increasing the time spent indoors increases potential exposure.

Palm Cousins (2012) adapted their previously published model which investigated the urban fate of emitted chemicals, including BDE-209, from Stockholm (Palm, 2001) to assess the effect of the indoor environment on urban fate. The model predicts a relationship between the log K_{OA} of a chemical and the impact of the ventilation rate of the indoor environment and outdoor environmental concentrations of BDE-209. Additional partitioning to indoor surfaces due to greater removal pathways of dust

and indoor films, leading to loss of the chemical from the system has a greater influence on final emissions of BDE-209. In the model, indoor parameters such as air temperature, ventilation rate, particle deposition rate and K_{OW} will influence contaminant concentrations in outdoor air (Palm Cousins, 2012). Hence it is important to understand indoor fate of these chemicals to gain an understanding of urban and global fate.

Wilford et al. (2003), who measured PBDE emissions from commercially treated PUF products, concluded that volatilisation of PBDEs from treated PUFs is a significant source to indoor air, providing an explanation for why indoor air PBDE levels are on average 20 times higher than outdoor air. Elevated concentrations reported in urban areas were suggested to be due to higher concentrations of treated PUF and other consumer goods.

The multimedia mass balance model by Batterman et al. (2009) calculated emission rates of PBDEs from in-use building materials and the contents of USA residences. In this study, measured concentrations of air and dust along with air exchange rates from 12 houses and garages were used to model average emissions. By using a mass balance approach based on measured concentrations, these houses were used as a “natural” test chamber for calculating emission rates. Using these data, the area predicted emission rate for the USA was calculated at $20 \text{ ng m}^{-2} \text{ h}^{-1}$. However, the authors reported large uncertainties due to underestimates and assumptions with this model, that included assuming the air is well mixed in each compartment and that the concentrations are at steady state. Batterman et al. (2009) did not consider emissions from offices in their national estimates, where elevated concentrations of congeners present in the PentaBDE formulation have been seen (Mandalakis et al., 2008, Gevaio et al., 2006, Chen et al., 2008).

The Batterman et al. (2009) study also investigated the contributions to overall emissions arising from emissions from houses to outdoor air, houses to indoor dust, garages to outdoor air and garages to dust. This revealed greater contributions from houses than garages to both air and dust; perhaps expected as houses likely contain more putative sources, with substantially higher levels estimated to migrate to house

dust. Table 1.7 lists the estimated emission rates from the model and the relative USA national estimated emission.

Table 1.7: Σ PBDE calculations from the Batterman et al. (2009) study comparing emissions to air/dust in different microenvironments

Emission	Michigan levels (mg year⁻¹ house⁻¹)	USA national estimate (kg year⁻¹)
House to outside air	4.6	585
House to dust	21	2715
Garage to outside air	1.9	137
Garage to dust	4.1	292

Zhang et al. (2009) studied a UK office environment for which PBDE concentrations in air were reported previously by Hazrati and Harrad (2006), supplemented by additional measurements of PBDE concentrations in the PUF containing chairs and carpet in the office. A multimedia fugacity model was developed and applied to the office using these data and EFs for scenarios based on emissions from two different computers in the office. Emissions were calculated at 5.4 and 35 ng Σ PBDE h⁻¹ respectively, equating to 0.05-0.3 kg year⁻¹. The estimated range of emissions from the 180 million computers in use in North America at 9-55 kg year⁻¹ is within an order of magnitude of the calculated emissions from the computers used in the Zhang et al. (2009) study. Moreover, SERs from the office studied by Zhang et al. (2009) (5.4-35 ng unit⁻¹ h⁻¹ or 25-175 ng m⁻² h⁻¹) are broadly in line with those for TV housing and printed circuit boards derived from chamber studies by Kemmlein et al. (2003) of 11 ng m⁻² h⁻¹ and 21 ng unit⁻¹ h⁻¹ respectively.

To fill knowledge gaps about emissions of BFRs from treated products; improved knowledge of the physicochemical properties of BFRs, combined with direct determination of EFs and SERs from chamber studies is recommended. The mass transfer of BFRs to dust also needs further investigation to better understand these processes. Dust to air partitioning coefficients may be used to predict equilibrium

concentrations in air and dust, thereby predicting the mass transfer to dust (Schripp et al., 2010). But as these partitioning coefficients are also directly related to available K_{OA} values, the uncertainty of any model is again reliant on the accuracy of available data. Moreover, such equilibrium phase partitioning approaches fail to account for transfer mechanisms like abrasion and direct source:dust contact.

1.7 Quantifying BFR emissions from Source Materials

The direct determination of chemicals emitted from treated products is typically carried out in environmental test chambers, where emissions are studied under controlled conditions. Emissions are collected in the chamber exit airline, and the calculated emitted mass is normalised to the quantity of the test material present in the chamber, the air exchange rate and the duration of the experiment to calculate a specific emission rate (SER) for each analyte.

The influence of test conditions on emission rates, is related to the physicochemical properties of the investigated chemicals and the type and use of the product under test. Assessment of emissions of SVOCs like PBDEs and HBCDs in environmental chambers is more complex than for VOCs. Challenges arise with sampling and analysis of gas-phase SVOCs due to their physicochemical properties such as lower vapour pressures, resulting in reduced gas-phase concentrations. Moreover, the slow emission and higher sorption affinity to chamber walls of SVOCs (sink effects) may increase the time to reach steady state conditions inside the chamber environment.

1.7.1 Measurement of specific emission rates (SERs) to air

There are only a few chamber studies focusing on emissions of BFRs from indoor materials published in peer-reviewed journals (Bakó-Biró et al., 2004, Kemmlein et al., 2003, Wilford et al., 2003). Given the tremendous interest in environmental contamination with BFRs, this appears at first sight somewhat surprising. However, the scarcity of such studies to date is likely due to the difficulties of determining low concentrations and the need for longer studies in order to reach steady state conditions in the chamber. In fact, there are few cases where a limited number of days (e.g. less than 50 days) is sufficient to measure time-release behaviour of SVOCs at room

temperature (Clausen and Kofoed-Sørensen, 2009) and longer experimental durations are often impractical. Investigations at elevated temperatures are useful as the experimental time needed to reach steady state conditions are reduced and in some cases loss to sink effects is reduced (Clausen et al., 2012). Increasing the temperature however may decrease the relevance of chamber experiments to ‘real world’ scenarios. A summary of the reported specific emission rates of BFRs from the Kemmlein et al. (2003) study is given in Table 1.8 as well as calculated release rates of PBDEs from PUF pieces treated with the PentaBDE formulation, as measured by Wilford et al. (2003) and release rates of HBCDs and PBDEs from textiles treated with the HBCD and DecaBDE formulations as measured by Kajiwara and Takigami (2013).

Table 1.8: Summary of reported specific emission rates of BFRs determined using chamber studies by Kemmlein et al. (2003) and calculated release rate of PBDEs from PentaBDE treated PUF in the chamber study by Wilford et al. (2003) and treated textile in the Kajiwara and Takigami (2013) study.

Product	Analyte	SERa* ng m⁻² h⁻¹ (Kemmlein et al., 2003)			
Insulation board 23 °C	HBCD	4.0 – 29			
TV set housing 23 °C	BDE-28	0.2			
	BDE-47	6.6			
	BDE-66	0.5			
	BDE-99	1.7			
	BDE-100	0.5			
	BDE-153	1.0			
	BDE-154	0.2			
	ΣHeptaBDE	4.5			
	ΣNonaBDE	0.8			
		ΣOctaBDE 1.5			
		SERu* ng unit⁻¹ h⁻¹			
Printed circuit board 60 °C	BDE-17	0.6			
	BDE-28	1.9			
	BDE-47	14.2			
	BDE-66	0.6			
	BDE-85	0.1			
	BDE-99	2.6			
	BDE-100	1.3			
	BDE-153	0.04			
	BDE-154	0.1			
*SERa = Area specific emission rate *SERu = Unit specific emission rate					
Product	BFR	Release Rate (Wilford et al., 2003)			
PUF foam 30 °C		ng (g foam)⁻¹ m⁻³	ng (g foam)⁻¹ h⁻¹		
	BDE-47	360	3380		
	BDE-99	85	800		
	BDE-100	30	280		
Product	BFR	Emission Rate ng m⁻² h⁻¹ (Kajiwara and Takigami, 2013)			
Textile curtain		20 °C	40 °C	60 °C	80 °C
	HBCD Sample (1)	250	1600	300	5700
	HBCD Sample (2)	160	190	400	7500
	tetraBDEs	0.04	0.17	1.3	11
	pentaBDEs	n.d.	0.04	0.26	2.4
	decaBDE	1.9	5.2	1.9	7.9

n.d. = non detect

Kemmlin et al. (2003) measured emissions of a broad range of FRs (PBDEs, HBCDs, TBBP-A and organophosphorus flame retardants) from different types of building materials and consumer goods (e.g. computers, TVs, printed circuit boards). All products, with the exception of a TV housing unit and a PC housing, were obtained directly from the manufacture and tested immediately. The experiments were conducted in three types of emission test chambers: two glass cells (0.001 m³ and 0.02 m³) and a standard volatile organic compound (VOC) emission stainless steel test chamber (1 m³). Emission chamber conditions were controlled at 23 ± 0.1 °C (50 ± 3% relative humidity (RH)) for building materials and consumer goods, and at 60 ± 0.1 °C (8 ± 3% RH) to simulate operational conditions of printed circuit boards. Active air sampling was conducted using a glass tube equipped with pre-cleaned PUF plugs. Emissions of HBCD from polystyrene insulating boards were investigated with emissions not detected in air after a test period of more than 100 days. This may have been due to high experimental LODs (between 0.09 and 1.8 ng m⁻³), combined with low sampling volumes (5-40 m³), with this latter issue also reported by Bakó-Biró et al. (2004) for SVOCs. Also, the test conditions may be of relevance as SERs or SVOCs have shown to be strongly dependent on the air exchange rate in the chamber and air velocity over the test material surface (Clausen et al., 2010). However, after rinsing the chamber walls with solvent, 21 µg.m⁻² (0.02 m³ chamber) and 0.33 µg m⁻² (0.001 m³ chamber) were recovered for ΣHBCDs. The reported SERa of ΣHBCD from polystyrene insulating boards, calculated from these recovered concentrations, varied between 0.1 ng m⁻² h⁻¹ and 29 ng m⁻² h⁻¹.

The Kemmlin et al. (2003) study also measured emissions of PBDEs from electronic goods, including TV sets, PCs and TV housings. The PC and TV housings were post-consumer products and hence had had the opportunity for substantial release of the more volatile FRs during their life cycle before testing. The unit specific emission rates (SERu) determined were 0.6 -14.2 ng unit⁻¹ h⁻¹ for PBDEs. Initial printed circuit board emission measurements were conducted at 23 °C with only concentrations of BDE-28 and 47 detected, at 0.9 to 3.4 ng m⁻³ over a period of 30 days. The temperature was then raised to 60 °C and concentrations of BDE-28 and BDE-47 increased significantly with BDE-17, 99, 66, 100, 154, and 153 also detected. The

calculated SERu of the PBDEs were thus only calculated from measured emissions from the board at 60 °C and ranged from 0.04 to 14.2 ng unit⁻¹ h⁻¹.

Bakó-Biró et al. (2004) measured the emissions from a personal computer system in a 1 m³ glass test chamber. Samples from the exhaust airflow of the chamber were collected on Tenax TA for VOCs and XAD-II for SVOCs. Although the presence of BFRs was expected in the tested PC systems, no emissions were detected in the air samples. It was presumed this result was due to the poor sensitivity of the analytical method (LOD 20 µg m⁻³). The test temperature increased from 24 °C at the start of the experiment to 32 °C during the experiment due to heat released from the working computer system. Carlsson et al. (2000) also reported increased temperatures of up to 50 °C on the top outlet cover of video display units (VDUs) during operational conditions.

Wilford et al. (2003) conducted a survey of PUF products in use in the UK and North America to screen for high PBDE concentrations (> 0.1% by weight). Significant differences were detected in the PBDE content of foam procured in the UK compared to that from North America. Only low or non-detectable traces of ΣPBDEs (~0.001% w/w) were found in the UK samples, whereas the North American samples contained ~5% w/w of ΣPBDEs. Subsequent chamber emission studies were conducted on the identified products to investigate the rate of release of PBDEs with a standard high volume air sampling module adapted for use as the chamber. The chamber study consisted of an air sampling module containing 3 PUF plugs: a pre-extracted PUF to pre-clean passing air, the test PUF sample, and a pre-extracted PUF plug to measure emissions. The calculated average ΣPBDE levels released in the chamber experiments was 500 ng m⁻³ g⁻¹ of foam. BDE-47, -99 and -100 were released at rates determined by their K_{OA} values (360, 85 and 30 ng m⁻³ g⁻¹ respectively). The authors concluded from this study that volatilisation of PBDEs to air from treated PUFs is a significant source to indoor and subsequently outdoor air. An attempt was made to convert the reported emissions to comparable release rates (ng (g foam)⁻¹ h⁻¹) to the SERs reported in the Kemmlein et al. (2003) study from the information provided in the Wilford et al. (2003) manuscript, values listed in Table 1.8. The calculated release rate of PBDEs from treated PUF pieces at 30 °C was much higher than the PBDE release from TV casings at 23 °C or printed circuit boards at 60 °C. Although it is

difficult to compare the chamber experiments due to the different conditions used (different size chambers, air change rates etc) it does appear the lower brominated PBDEs are more easily released from treated PUF than from treated plastic matrices.

Kajiwara and Takigami (2013) conducted similar preliminary chamber experiments to measure emission via volatilisation of BFRs from textile curtains treated with (a) HBCDs and (b) PBDEs. The test chamber consisted of a small stainless steel cylindrical container of 210 cm³ volume. Air flow was not attached to the chamber, rather emissions were collected by means of a PUF plug connected to the inner surface of the chamber lid. The piece of textile (5 x 5 cm) to be tested was placed on the chamber floor before the chamber was sealed and placed in a temperature controlled environment for 120 hours. Experiments were conducted at 20, 40, 60 and 80 °C. Post experiment the sampling PUFs and chamber inner surface solvent rinses (acetone) were extracted, combined for each experiment and analysed. The calculated emission rates at each temperature are listed in Table 1.8 and range from 160 to 7500 ng m⁻² h⁻¹ for HBCDs and 0.04 to 7.9 ng m⁻² h⁻¹ for the tetra, penta and decaBDEs.

The calculated HBCD emission rate was at least an order of magnitude greater than that calculated by Kemmlein et al. (2003) from insulation boards, however the Kemmlein et al. (2003) study calculated SERs from HBCD concentrations recovered from chamber solvent rinses only as no emissions were detected on collection PUFs. Again it is difficult to compare these very different chamber experiments, particularly as the Kajiwara and Takigami (2013) study is an enclosed chamber experiment with no air exchange. However, the results indicate release of HBCDs from the textile is more facile than from a plastic matrix, likely due to how the HBCDs are incorporated into the respective product types during manufacture. Emissions of the tetra and pentaBDEs from the treated textile, although smaller than for the HBCDs, still increase with increasing temperature; however only minor increases in emissions of decaBDE were observed over the temperature range examined. The observation of decaBDE emissions is surprising and the authors suggest that decaBDE has sufficient volatility at room temperature to produce the observed emissions.

1.7.2 *Measurements of migration to indoor dust*

Alongside emissions to indoor air, migration of BFRs from treated products to indoor dust is another (and frequently more) important pathway of relevance to human exposure. To date, no published articles have focused on simulating the migration pathways of BFRs into dust. Two studies have used modified chambers/test cells to investigate deposition and transfer via direct contact to house dust of phthalates (another class of SVOC). Issues encountered with studying emissions of SVOCs in this way, such as sink effects and long times to reach steady state conditions inside the chamber, were highlighted and can be extrapolated to underline how these experiments can be performed to investigate BFRs.

Schripp et al. (2010) investigated the mass transfer of the SVOCs di(2-ethylhexyl) phthalate (DEHP) and di-*n*-butylphthalate (DnBP) to different samples of house dust, soil and sand from emission sources. Deposition of volatilised phthalates was investigated in 0.5 m³ stainless steel chambers using different air velocities. Glass plates, coated with pure phthalate or with plasticised wall paint containing 1% w/w of phthalate, were placed inside the chamber along with 3 g of house dust, soil or sand. Significant increases of DHEP were not seen in any of the solid matrices, potentially due to non-attainment of equilibrium inside the chamber. Significant increases in concentrations detected in all the different dust or soil matrices were reported for DnBP with higher concentrations (>10 times higher) seen in dust and soil than in sand. The authors suggested this was due to the different organic carbon contents of the solid matrices influencing the level of deposition, and a weak correlation was reported between phthalate uptake and the organic carbon content of the receiving matrix. Greater concentrations in dust/soil were also associated with higher air velocities inside the chamber, due to different emission behaviours in each scenario. Higher air velocities facilitate vapourisation of analytes and increase subsequent mass transfer to dust.

Schripp et al. (2010) also investigated migration *via* direct contact, using a 3 L glass flask with 130 mg of pre-extracted dust placed directly on top of plasticised PVC (containing DEHP). Another portion of dust (130 mg) was placed on a shelf above the foil to investigate deposition from volatiles. There was no significant uptake of DEHP

in the dust separated from the source, but higher mass transfer was reported in the dust in direct contact with the source. Clausen et al. (2004) also investigated the uptake of DEHP via direct contact from PVC flooring into indoor dust. A “chamber for laboratory investigations of materials, pollution and air quality” (CLIMPAQ) emission test chamber contained five pieces of PVC with the upper side of the top pieces layered with 0.5 g of homogenised house dust. After specified time periods, the dust was sampled. Transfer of DEHP to the dust was four-fold greater compared to that emitted to the air. Air emissions were also similar in chamber scenarios containing dust compared with those without, suggesting direct uptake via dust:source contact represents an additional pathway of release from the PVC.

Proposed mechanisms for mass transfer to dust include phthalate uptake via capillary forces (Schripp et al., 2010) or that the dust in direct contact acts as a sorbent of phthalates from the source (Clausen et al., 2004). Moreover, abrasion (physical breakdown of the PVC caused by the vacuuming process) may also be responsible for the high levels observed in dust. In conclusion, Clausen et al. (2004) suggested that since particles and dust can increase total contamination of indoor environments, the migration of contaminants from sources to dust is of importance when evaluating the potential for human exposure. Similar experiments have yet to be conducted with BFR sources.

1.7.3 Sink Effects

The lower vapour pressure of SVOCs affects their study in test chambers as it can lead to preferential sorption, following their volatilisation, to chamber surfaces rather than collection in gas phase emissions. The loss of analytes via sorption to chamber wall surfaces is referred to as sink effects and has been previously reported in chamber studies of SVOCs (Katsumata et al., 2008, Kemmlein et al., 2003, Uhde and Salthammer, 2006, Xu et al., 2012). Methods suggested to reduce this loss include lining the chamber with a Teflon coating and electroplating stainless steel wall surfaces (Destailats et al., 2008), or using hand polished surfaces such as in the Field and Laboratory Emission Cell (FLEC), for a greater reduction of active sites (Clausen et al., 2004). Reducing contact time through increased air exchange rates and decreasing chamber surface to volume ratios, and using new approaches such as

passive flux samplers (Ni et al., 2007) may help reduce these effects. A novel chamber system designed by Xu et al. (2012), that minimises the surface area of internal chamber surfaces and maximises surface area of the source, has been shown to reduce the time required for the plasticiser DEHP to reach steady state conditions compared to the CLIMPAQ and FLEC chambers. This chamber has potential for reducing sink effects as well as the time required to reach steady state conditions for measurements of BFRs from polymeric materials.

A variety of methods to minimise losses to sink effects by recovering analytes reversibly-sorbed to internal chamber surfaces have been reported and include: heating the chamber post-experiment to elevated temperatures and collecting subsequent air emissions; as well as rinsing the chamber walls with solvent (Katsumata et al., 2008, Kemmlein et al., 2003). Such methods have met with some (though not complete) success. For example, heating an emission chamber to 80 °C post-experiment recovered detectable concentrations of BDE-47, BDE-99 and BDE-100 (Kemmlein et al., 2003). Placing convex glass pieces inside the emission chamber throughout experiments and rinsing with toluene, post experiment, returned detectable concentrations of TBBPA (64-116 ng m⁻³) and rinsing test chamber walls, was also shown to return 21 µg m⁻² (from a 0.02 m³ chamber) and 0.33 µg m⁻² (from a 0.001 m³ chamber) of ΣHBCDs (Kemmlein et al., 2003).

Repeated mass balance experiments may provide information on the magnitude of sink effect losses (Destailats et al., 2008) for different BFRs, through measurements of BFR mass entering a chamber and mass recovered post-experiment. A reproducible concentration loss (as evidenced e.g. by RSD values for a number of experiments falling within an acceptable range) can be incorporated into calculated emissions and subsequent SERs, and calculations of mass transferred to dust. As sorption of SVOCs to chamber walls is often not a linear process (Clausen et al., 2004), this method assumes that chamber conditions reach steady state to allow a reproducible calculated loss. However, as the emission is slow for SVOCs and partitioning to chamber walls may be strong, a long time can be required to reach steady state (Xu et al., 2012), making this method unsuitable for many BFRs.

Even with an accurate measure of sink effects, limitations exist for chamber experiments when extrapolating information to indoor models as the isolated chamber conditions differ from those in the environment being simulated. Indoor environments themselves provide other surfaces that act as BFR sinks, such as thin films on glass windows (Butt et al., 2004). Typically, sink effects within an indoor environment are unknown and as test chambers do not easily mimic “real-world” fluctuating environmental conditions (Schripp et al., 2010), there is difficulty in extrapolating results from emission chamber tests to indoor microenvironments. The lack of a thorough investigation into sink effects, especially for BFRs, highlights the need to determine the extent of such sorptive losses for BFRs. Such knowledge is essential if accurate measurements of EFs and SERs of BFRs from treated products are to be obtained, as well as their subsequent deposition to dust.

1.8 Forensic Microscopy

Common forensic microscopy techniques, such as Micro X-Ray Fluorescence Spectroscopy (Micro XRFS) or Scanning Electron Microscopy with Energy Dispersive Spectroscopy (SEM/EDS), provide information on elemental (e.g. Br) distribution throughout a sample and hence may provide information on migration pathways of BFRs to dust. A dust sample contaminated *via* volatilisation with subsequent partitioning to particles is hypothesised to have a uniform distribution of BFRs, exemplified by a homogenous distribution of bromine through the sample. In contrast, a dust contaminated *via* small particles or fibres generated by abrasion of treated products, is hypothesised to display a non-uniform distribution of BFRs and a heterogeneous bromine distribution throughout the sample. When used in conjunction with other analytical techniques (such as GC-MS or LC-MS/MS) microscopy may be a useful tool for obtaining a greater understanding of these mechanistic pathways.

X-ray fluorescence spectroscopy (XRFS) has been employed as a preliminary indicative method of possible BFR presence in putative sources (Webster et al., 2009, Suzuki et al., 2009, Allen et al., 2008b). XRFS bombards a sample with high-energy photons, generated by an X-ray source. Measurement of released X-rays (unique to the particular element present) can estimate density and calculate elemental

concentrations in the product (Allen et al., 2008b). Working along the same principles is SEM/EDS. From viewing secondary electrons, produced by inelastic scattering of the electron beam, high resolution images of the material are provided (Webster et al., 2009). Also, backscatter electrons, produced by elastic collisions, show locations of atoms with higher atomic numbers (e.g. bromine). These atoms scatter the electrons more strongly, thus appearing brighter in the images. X-rays, produced when outer shell electrons fill vacancies in inner shells after collisions with the electron beam, provide elemental spectra.

Suzuki et al. (2009) used micro XRFS, in conjunction with GC-HR/MS, to investigate the existence of bromine as an indicator of the presence of BFRs in dust. After micro XRFS, fragments containing high bromine levels were imaged with a digital optical microscope. The fragments containing high levels of bromine were small and unevenly distributed, although the micro XRFS was only able to detect concentrations above ~0.1% bromine. The particles analysed under the digital microscope were larger than 0.5 μm , introducing a possible selection bias. There was poor correlation between the micro XRFS measurement and PBDE concentrations of the sample, with the latter much lower, suggesting that other brominated compounds were present in the sample. A fragment in which bromine was not detected was also analysed on the GC-HR/MS, and was shown to contain levels of BDE-209 comparable with a sample positively identified with the micro XRFS. This shows the major limitations of the XRFS method, are its high detection limit and inability to distinguish between different bromine containing compounds.

Webster et al. (2009) utilised Micro XRFS for identification of areas of high bromine content in dust samples containing high concentrations of BDE-209 (260 to 2600 $\mu\text{g g}^{-1}$), followed by SEM/EDS to provide compositional and morphological information. The presence of bromine was confirmed on SEM/EDS and showed a heterogeneous distribution through the sample. These preliminary results are consistent with the abrasion hypothesis but do not rule out highly localised sorption of BDE-209 or non-detectable concentrations of bromine in smaller particles. A limitation with this method is that smaller bromine containing particles may not be detected unless operating conditions (e.g. dwell time) are adjusted (Webster et al., 2009). The

bromine was embedded in the organic material and associated with calcium-rich particles (polymeric/organic matrix). Subsequent FTIR analysis showed flakes consistent with a plastic material, suggesting that the BDE-209 in this dust sample occurred as inclusions in plastic flakes.

However, the XRFS and SEM/EDS techniques used in these preliminary studies can only confirm the existence of bromine, so additional confirmation is required of the presence of BFRs. Using GC-MS, Suzuki et al. (2009) were able to identify and quantify the content of PBDEs (pg per bromine rich fragment) contained within individual bromine rich particles isolated from dust samples, with BDE-209 quantified in each isolated fragment. However, due to the uncertainty associated with the gravimetric determination, the mass of the particles themselves could not be measured. Subsequent studies by Ghosal and Wagner (2013) and Wagner et al. (2013) reported the use of Raman micro-spectroscopy to study bromine rich particles, after identification with SEM/EDS, for non-destructive confirmation of the presence of PBDEs. Collectively, studies applying various combinations of forensic microscopic techniques to date, have all identified in some dust samples, the presence of particles or fibres originating from a product treated with BFRs, suspected to migrate via the abrasion migration pathway.

1.9 Summary

Various information gaps in the literature have been highlighted that are important for understanding how BFRs enter the indoor environment from the products they are used in. BFRs are found ubiquitously in indoor and outdoor environments hence humans are continuously exposed to BFRs via different exposure pathways. Little is known about the toxic effects of BFRs; however, as extremely high levels have been reported in homes, this exposure is of concern. Very limited knowledge is available on emission of these compounds with no studies to date investigating migration to dust. Dust has been shown to be an important exposure pathway to humans, especially young children. Hence understanding of how dust is contaminated and the relevance of this contamination for human health is an important knowledge gap that needs to be filled.

1.10 Aims

The above discussion of the literature has identified a number of gaps in current knowledge about how and to what extent BFRs transfer from treated products into indoor dust. Consequently, the aims of this study are to:

- 1) Test the hypothesis that BFRs are transferred from treated products to dust via three different pathways:
 - a. volatilisation with subsequent partitioning to dust;
 - b. abrasion of particles and fibres from treated products that transfer directly to dust;
 - c. direct contact between treated products and dust settled on the product surface.
- 2) Test the hypothesis that the volatilisation pathway will be the least effective of these transfer pathways, and
- 3) Test the hypothesis that BFRs in dust contaminated via the abrasion pathway will have a lower bioaccessibility than BFRs that enter dust via volatilisation and partitioning, as the BFRs will be more strongly retained within the product polymer pieces.

To achieve these aims, this study will:

- 1) Design, develop, and validate a test chamber to facilitate simulation of the different hypothesised pathways via which PBDEs and HBCDs transfer from source materials to indoor dust.
- 2) Apply the test chamber to study the transfer to indoor dust of PBDEs and HBCDs from treated products *via* these different pathways and assess their relative importance.
- 3) Apply forensic microscopy techniques to test chamber-generated dust samples to provide further information on pathways of BFR transfer from source to dust; and
- 4) Employ *in vitro* bioaccessibility tests to assess the bioaccessibility of HBCDs from dust contaminated via abrasion of a source item, with that from dust contaminated via atmospheric deposition from the vapour phase.

CHAPTER 2

TEST CHAMBER CONFIGURATION, ANALYTICAL METHODOLOGY AND FORENSIC MICROSCOPY METHODOLOGY

In-house designed test chamber apparatus were utilised to simulate the three main hypothesised migration pathways of PBDEs and HBCDs to dust, as described in Chapter 1. The use of forensic microscopy techniques provided alternative insights into the origins of these BFRs present in dust samples generated in test chamber experiments, as well as in indoor dust sampled from real-world microenvironments. A commercially available industry standardised emission chamber, located at the Flemish Institute for Technological Research, VITO, (Mol, Belgium) was utilised in experiments as a comparison with the in-house test chamber. This commercial emission chamber had previously been validated for measurement of VOC emissions to air, but not for the measurement of SVOC emissions to air, nor for their subsequent deposition to settled dust. Extraction and analysis methods used for the determination of all target analytes were adaptations of previously published methods (Abdallah et al., 2009, Abdallah et al., 2008b). The test chamber configuration, validation and application, coupled with the forensic microscopy investigations, and the extraction, clean up and analysis steps of BFRs in air and dust samples are discussed in this chapter, as well as the quality control/quality assurance measures employed.

2.1 Test chamber experimental design

2.1.1 Test chamber experimental design

A cylindrical in-house designed and built test chamber (UoB chamber) was utilised for these investigations. Constructed from stainless steel with dimensions of 10 cm diameter and 20 cm height, the total chamber volume was 1570 cm³, with an internal surface area of 785 cm². Attachment of a Capex L2 Diaphragm Pump (Charles Austen Pumps Ltd, Surrey, UK) provided a constant air flow of 10 L min⁻¹ through

the chamber, equivalent to 400 air changes per hour. Air flow was measured and maintained using a Sensidyne Gilibrator-2 air flow calibrator (ShawCity, Oxfordshire, UK). Emissions in both the gas and airborne particulate phases were collected on polyurethane foam (PUF) plugs (140 mm diameter, 12 mm thickness, 360.6 cm² surface area, 0.07 g cm⁻³ density, PACS, Leicester, UK), attached to the exit air vent. A separate PUF plug was attached between the pump and entry air vent, to remove any contaminants (airborne or particulate) in the air prior to chamber entry. Both PUF holders were wrapped in aluminium foil to minimise any analyte degradation from UV radiation exposure. All PUF plugs were cleaned before use by pressurised liquid extraction (ASE 350, Dionex Europe, UK) using hexane:dichloromethane (1:1 v/v).

A removable, aluminium mesh shelf was placed either halfway down the chamber or 3 cm above the chamber floor, depending on the experimental design, to allow separation of the BFR 'source' and an aliquot of dust. Experimental details of the different BFR migration to dust experiments are provided later in this chapter. The BFR partitioning to the chamber wall surfaces was assessed through rinsing all chamber inner wall surfaces, post experiment, with 200 mL of hexane:dichloromethane (1:1 v/v). The chamber was maintained at the desired temperature by immersion in a hot water bath with the chamber internal temperature monitored using a LogTag TRIX-8 temperature data logger (LoggerShop Technology, Dorset, UK). Three extra test chambers, of identical dimensions and materials, were later commissioned and used for replicate experiments. Figure 2.1 shows a photograph of the test chamber experimental configuration.

Figure 2.1: UoB chamber configuration showing the stainless steel test chamber with connected air pump and collection PUFs



2.1.2 Commercially available Emission Chamber at Flemish Institute for Technological Research (VITO)

A Micro-Chamber/Thermal ExtractorTM (Markes International) located at the Flemish Institute for Technological Research, VITO, (micro chamber) consisting of 6 linked chambers was used for comparison with the UoB chamber. Each linked chamber had internal surfaces constructed of electropolished stainless steel, and dimensions of 4.5 cm diameter and 2.8 cm height to give a total chamber volume of 44 cm³, and an internal surface area of 71 cm². A uniform heating system (20-120°C) surrounded each chamber and adjustable airflow provided to the chamber was set at 0.5 L min⁻¹ (equating to 682 air changes per hour) for these experiments. The addition of a PUF plug (140 mm diameter, 12 mm thickness, 360.6 cm² surface area, 0.07 g cm⁻³ density, PACS, Leicester, UK) to the exit air line, facilitated collection of emitted analytes. The micro-chambers were also fitted with a shelf mid-way to facilitate separation of the BFR source from the dust placed in the chamber. Figure 2.2 portrays the six-chamber set-up with attached collection PUFs.

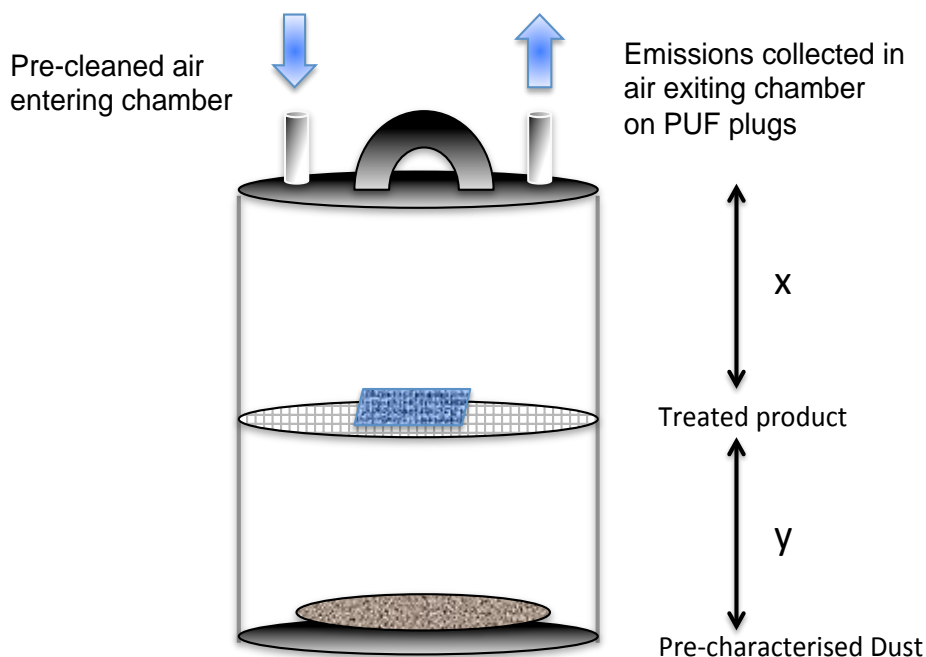
Figure 2.2: Photograph of micro chamber configuration, showing 6 linked chambers



2.1.3 Experimental Design for investigating BFR partitioning to dust after volatilisation

The chamber experimental design for generating the volatilisation of BFRs with subsequent partitioning to dust consisted of a mass of pre-characterised dust (200 mg), weighed onto a glass fibre filter (GFF) and placed on the chamber floor. A product treated with BFRs (the BFR source) was placed on the mesh shelf located half way down the chamber. Initial validation experiments were conducted with a small GFF (4.25 cm diameter), fortified with 100 ng of each target BFR, placed on the chamber shelf as the BFR source. A schematic of these experiments is illustrated in Figure 2.3. The chamber was heated in a hot water bath for the duration of the experiment. Post-experiment, the chamber was cooled and maintained at room temperature for 5 hours (with the pump maintaining air flow) to minimise loss of volatiles with chamber lid removal. The dust, PUFs, GFFs and chamber solvent washes were extracted and analysed separately.

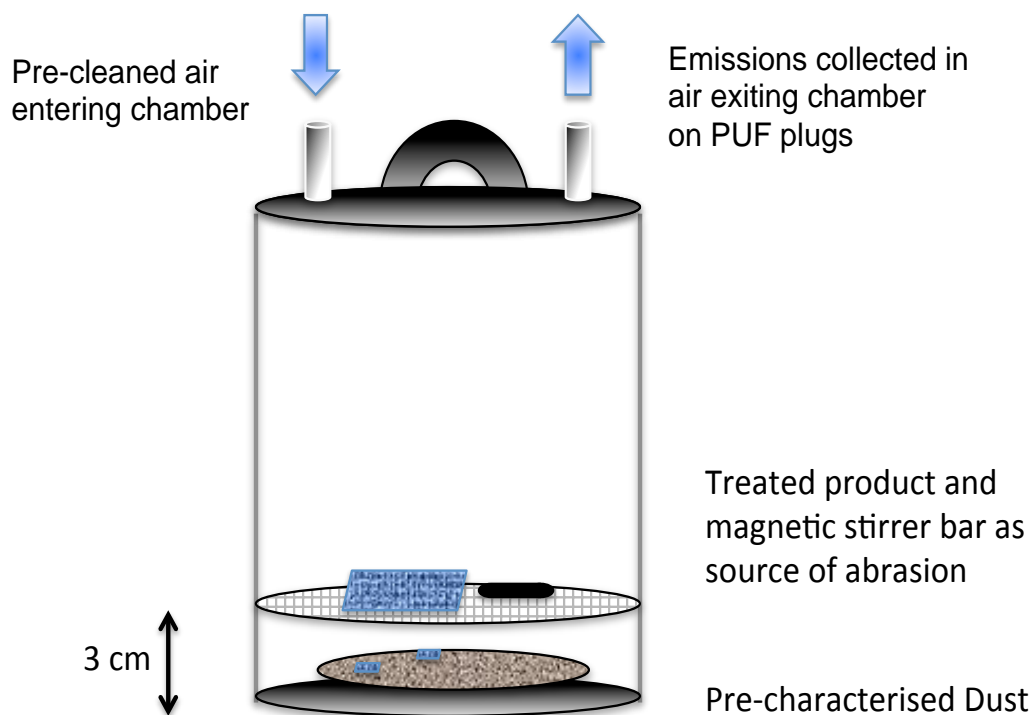
Figure 2.3: Schematic of test chamber experiment for generating volatilisation of BFRs with subsequent partitioning to dust.



2.1.4 Experimental design for investigating BFR direct partitioning via abrasion

The test chamber experiments were further modified to generate abrasion of a BFR source in the chamber. The experiments again consisted of a mass of pre-characterised dust (200 mg), weighed onto a GFF, and placed on the chamber floor. The shelf was lowered to 3 cm above the chamber floor and a piece of product treated with BFRs (the BFR source) was placed on the shelf. A magnetic stirrer bar, 40 mm x 8 mm, (Fisher Scientific, Leicestershire, UK) was also placed on the mesh shelf to generate abrasion. The chamber was placed on a magnetic stirrer plate, set at 200 rotations per minute, and the rotating stirrer bar in direct contact with the piece of treated product encouraged the loosening of fibres and particles to then fall into the dust mass. The abrasion was conducted for various time intervals, and at room temperature to discourage volatilisation of the BFRs of interest. Attachment of a pump to the chamber allowed collection of airborne analytes on PUF plugs to monitor emissions of BFRs. At the end of each experiment the dust, PUFs, GFFs and chamber surface solvent rinses were extracted and analysed separately. The chamber experimental design for these experiments is illustrated in Figure 2.4.

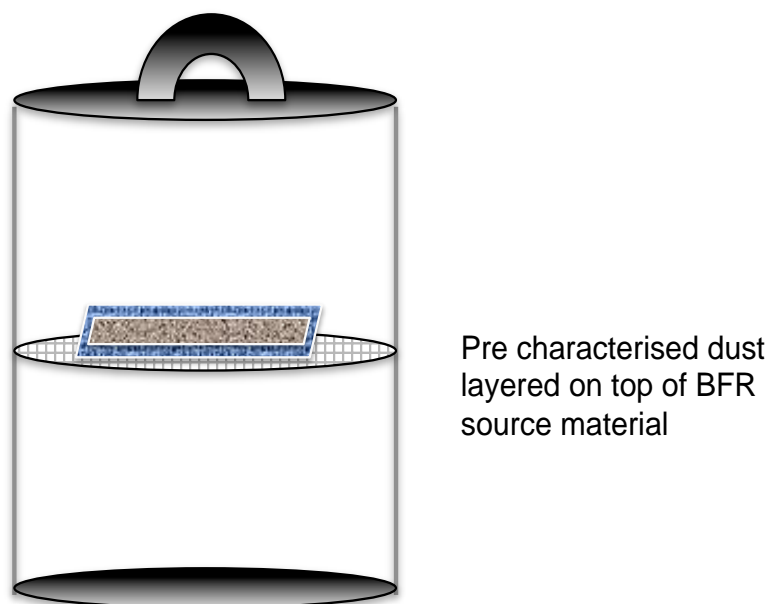
Figure 2.4: Schematic of test chamber experiment for generating abrasion of a BFR treated product, with loosened particles/fibres entering the dust aliquot



2.1.5 Experimental design for investigating BFR partitioning via direct contact of BFR source to dust

To generate migration *via* direct contact between a BFR source and dust sample the chamber was completely enclosed, disconnecting the pump and thus eliminating air flow. A piece of product treated with BFRs (the BFR source) was placed on a GFF, situated on the mesh shelf, in the middle of the chamber. A thin layer of pre-characterised dust (150 to 500 mg) was placed directly on and covering the top surface of the BFR source, using a pair of tweezers. The chamber was kept at room temperature and after a specified time period, the dust was gently brushed off the source and collected for extraction and analysis. Figure 2.5 illustrates the experimental design.

Figure 2.5: Schematic of test chamber experiment for generating migration to dust via direct contact between BFR source and dust particles



2.1.6 BFR treated products

2.1.6.1 HBCD treated fabric curtains

Fabric curtains treated with the HBCD technical formulation were obtained from the National Institute for Environmental Studies (NIES), Tsukuba, Japan. Concentrations of HBCDs in these curtains were previously reported at 18,000 mg kg⁻¹ for α -HBCD, 7,500 mg kg⁻¹ for β -HBCD and 17,000 mg kg⁻¹ for γ -HBCD (Kajiwara et al., 2013).

2.1.6.2 BDE-209 treated plastic TV casings (InterLab sample)

The InterLab sample 'Waste TV backplate Lot No. 01-02' was obtained from the National Institute for Environmental Studies (NIES), Tsukuba, Japan. The sample consisted of remoulded TV cathode ray tube back casings, and was certified to contain a BDE-209 concentration of 90,000 $\mu\text{g g}^{-1}$ (9% BDE-209 content).

2.1.7 Low level dust procurement

Initial source-air-dust partitioning experiments were conducted using a bulk house dust sample obtained from a private residence in Birmingham. In common with many UK dust samples, this dust contained moderately elevated concentrations of HBCDs and BDE-209, rendering it unsuitable for experiments studying these analytes. A

further bulk dust sample containing lower concentrations of PBDEs and HBCDs was collected from a private residence in Belgium and used in all further studies.

2.1.7.1 Dust sampling procedure and indigenous BFR concentrations

Bulk dust samples were collected with resident owned vacuum cleaners. The contents of the vacuum cleaner bag were emptied and sieved with a 500 µm mesh size hand held sieve. The dust sample was thoroughly homogenised before 100-200 mg subsamples were extracted and analysed to determine indigenous BFR concentrations. Mean concentrations in both dust bulks (n=6 for the Birmingham dust and n=9 for the Belgian dust) and standard deviations (SD) are listed in Table 2.1.

Table 2.1: Mean ± standard deviation and %RSD of BFR concentrations (ng g⁻¹) in bulk dust samples used for chamber experiments

Analyte	Birmingham dust (n=6)	%RSD	Belgian dust (n=9)	%RSD
α-HBCD	390 ± 110	27	46 ± 18	39
β-HBCD	180 ± 45	25	13 ± 10	77
γ-HBCD	2600 ± 3200	120	50 ± 39	78
BDE-47	5 ± 8	200	10 ± 11	110
BDE-85	1 ± 1	100	2 ± 2	100
BDE-99	18 ± 4	22	27 ± 31	115
BDE-100	4 ± 2	50	5 ± 5	100
BDE-153	7 ± 5	71	6 ± 6	100
BDE-154	2 ± 5	250	3 ± 3	100
BDE-183	11 ± 7	64	2 ± 2	100
BDE-209	2000 ± 550	27	230 ± 180	77

2.2 Forensic Microscopy Investigations

Test chamber generated dust samples, as well as three samples taken from the University of Birmingham dust archive (previously characterised to contain elevated BFR concentrations, Table 2.2) were analysed further using various forensic

microscopy techniques at the National Institute for Environmental Studies (NIES), Tsukuba, Japan. The following describes the general procedure used for the analysis of each dust with selected forensic microscopy techniques.

Table 2.2: BFR concentrations (ng g⁻¹) in archived dust samples

	Concentration in bulk dust (ng g ⁻¹)			
	α -HBCD	β -HBCD	γ -HBCD	BDE-209
Dust #1	380	340	2 800	1 440 000
Dust #2	280	70	140	280 000
Dust #3	9 900	6 700	72 000	24 000

2.2.1 Energy dispersive Micro X-ray fluorescence spectroscopy (Micro XRFS)

A subsample of the dust (1 mg) was sprinkled over a 25 x 25 mm area of double sided carbon tab, attached to a glass sample stage, using a pair of tweezers. The 1 mg dust sample was mapped for location of areas of high bromine content with a Micro XRFS (' μ Ray' μ EDX-1200, Shimadzu Co), equipped with a Rhodium X-ray tube and Nickel filter as the X-ray filter. The instrument was operated with a tube voltage of 50 kV, tube current of 1000 μ A, and beam diameter of 50 μ m as described previously Suzuki et. al. (2009). Initial high speed bromine mapping was performed using a 0.5 sec dwell time with step sizes of 50 μ m in the x and y-directions. Mapping of the entire 1 mg sample was conducted over the 25 x 25 mm sample area for 76 hours. Identified areas of interest were remapped at 4 x 3 mm for 4.5 hours and again at a further refined area of 2 x 1.5 mm for 11 minutes for more specific identification of areas and possible fragments of high bromine content. Further, more sensitive mapping of suspected abraded fibres was performed with 10 sec mapping mode over these same sample areas. This improved the instrument detection limit and facilitated identification of fibres containing elevated bromine concentrations.

2.2.2 Laser Microscopy

The high bromine content locations, identified via Micro XRFS analysis, were removed from the dust sample by cutting out a 2 x 2 mm square with a scalpel, and positioning the square on an aluminium stub. These areas were imaged with an

Olympus, LEXT, 3D Laser Microscope – OLS 4100. Optical and 3D laser images were taken of particles in each isolated sample area suspected of containing high bromine content. The particle length was also recorded.

2.2.3 Scanning Electron Microscopy with Energy Dispersive Spectroscopy (SEM/EDS)

The suspect particles were analysed on SEM/EDS for determination of elemental composition and confirmation of bromine presence. SEM/EDS was performed with a JSM-7600F Field emission SEM (JEOL, Japan) with a retractable backscattering electron detector and energy dispersive X-ray spectrometer (EDS) analyser with silicon drift X-ray detector, and analysis was performed at an accelerating voltage of 20 kV. As the bromine $L\alpha$ (1.480 keV) and aluminium $K\alpha$ (1.486 keV) lines almost overlap, bromine was confirmed by the presence of the $K\alpha$ line at 11.907 keV. The bromine $L\alpha$ peak counts were ~1000 times higher than the background aluminium peak count, measured from the aluminium stub, hence interference from aluminium was considered negligible. SEM/EDS identified the particles containing bromine in these selected sample areas, allowing these particles to be investigated further.

2.2.4 Fourier Transform Infrared spectroscopy (FTIR) analysis

The identified particles of high bromine content were removed from the sample area with tweezers and analysed with a Nicolet Continuum Microscope connected to a Nicolet 6700 Fourier transform infrared spectrometer, FTIR, (Thermo Scientific, Waltham, USA) using a diamond compression cell. Sample spectra searches were conducted with the spectral library database provided with the software package (OMNIC Software, Thermo Scientific) to determine closest chemical match and hence provide information on composition of the identified particle. This procedure is described further in Chapter 5 – Forensic Microscopy.

2.2.5 Analysis of isolated particles for BFR content

Particles identified with spectral matches to BFRs, were collected from each dust for LC-MS/MS analysis of BFR content. The procedure is described later in this chapter.

2.3 Sample Extraction and purification

2.3.1 Chemicals

All solvents used for extraction and analysis were of HPLC grade quality (Fisher Scientific, Loughborough, UK). Standards of individual PBDEs (BDEs 47, 85, 99, 100, 153, 154, 183, 209), HBCDs (α -HBCD, β -HBCD, γ -HBCD), labelled ^{13}C HBCDs (α -, β -, γ -), d_{18} γ -HBCD and labelled ^{13}C PBDEs (BDEs 47, 99, 100, 153, 209) were purchased from Wellington Laboratories (Guelph, ON, Canada). Florisil (60-100 mesh) and silica gel (60Å, 60-100 mesh) were purchased from Sigma Aldrich (Dorset, UK) with concentrated sulfuric acid purchased from Merck (Darmstadt, Germany). Glass fibre filters (GFF, 12.5cm diameter, 1 μm pore size, Whatman, UK) were purchased from Agilent (UK), and oxygen-free nitrogen gas from BOC Gases (UK).

2.3.2 Sample preparation and extraction

Sample extraction and purification was performed using slight modifications of in-house published methods (Abdallah et al., 2009, Abdallah et al., 2008b). Dust, PUFs, GFFs and isolated plastic particles (from the forensic microscopy investigation) were extracted with pressurised liquid extraction (ASE 350, Dionex Europe, UK). PUFs and GFFs were packed into precleaned 66 mL cells using precleaned Hydromatrix (Varian Inc., UK) to fill the void. Dust samples were loaded into 66 mL cells containing 1.5 g of Florisil and Hydromatrix. Each cell was fortified with 4 ng each of ^{13}C -labelled α -, β -, and γ -HBCD; 40 ng of ^{13}C -PBDE 47; 10 ng each of ^{13}C -labelled PBDE-99 and PBDE-153; and 20 ng of ^{13}C -PBDE 209 as internal (surrogate) standards prior to extraction with hexane:dichloromethane (1:1 v/v) at 90°C and 1500 psi. The cell was heated for 5 min, held static for 4 min and purged for 90 s, with a flush volume of 50%, for 3 cycles.

2.3.3 Sample clean up

The collected ASE extracts and (where appropriate) chamber inner surface solvent rinses were concentrated to 0.5 mL using a Zymark Turbovap II (Hopkinton, MA, USA) before purification. Clean-up was conducted by loading onto SPE cartridges filled with 4 g of precleaned acidified silica (44% concentrated sulfuric acid w/w).

The analytes were eluted with 30 mL of hexane:dichloromethane (1:1, v/v), with the eluate evaporated to dryness under a gentle stream of nitrogen. Samples were reconstituted to 100 μ L with 2 ng of d_{18} - γ -HBCD and 20 ng of 13 C-PBDE 100 in HPLC grade methanol, used as recovery standards for internal standard recovery determination.

2.4 Analysis

2.4.1 *Justification for choice of high performance liquid chromatography (HPLC) tandem mass spectrometry (MS/MS) analysis*

Traditionally gas chromatography mass spectrometry (GC-MS) methods have been used for the analysis of both HBCDs and PBDEs. However the thermal sensitivity of some analytes can cause issues with this method. GC-MS is unsuitable for resolution of the HBCD diastereomers as they will degrade at temperatures above 240°C and in a dirty GC injection port (Covaci et al., 2007). The higher temperatures associated with GC-MS also cause thermal rearrangement of the HBCD diastereomers so subsequent elution is as a broad, unresolved peak, with only total HBCD contribution calculable (Law et al., 2005). Electron-capture negative ionisation (ECNI) mode is commonly used with GC and typically the bromide ions (m/z 79 and 81) are monitored as larger fragment ions do not form in ECNI mode (Law et al., 2005). As only the bromide ions are monitored with this method, isotopically labelled internal (surrogate) standards are indistinguishable, hence unusable, reducing the accuracy of this method (Law et al., 2005). LC-MS/MS removes the issues associated with high temperatures such as degradation and rearrangement and as such, resolved baseline separation of the diastereomers have been reported (Budakowski and Tomy, 2003, Abdallah et al., 2008b).

PBDEs have historically been analysed using GC-MS techniques with an ECNI source, monitoring the bromine ions fragments (m/z 79 and 81) (Covaci et al., 2007). Again, as only the bromine ions are monitored, labelled analogues are indistinguishable, with the exception of 13 C-BDE 209 which produces $[C_6Br_5O]^-$ ions from cleavage of the ether bond (Björklund et al., 2003). While other ionisation methods such as electron ionisation (EI) are also widely used and permit the use of

isotopically labelled internal standards, EI lacks sensitivity for congeners containing greater than six bromine atoms. More generally, BDE-209 suffers thermal degradation on GC, requiring a scrupulously clean injection port and shorter GC columns (Abdallah et al., 2009), as well as injection techniques that minimise time spent in the heated injection zone (Covaci et al., 2007).

Given this potential for BDE-209 degradation during GC analysis, PBDEs have recently been measured via LC-MS/MS using an atmospheric pressure photoionisation (APPI) source (Riu et al., 2006, Lagalante and Oswald, 2008, Debrauwer et al., 2005, Abdallah et al., 2009). The UV source within the APPI source initiates ionisation of the molecules of a doping agent, and the subsequent radical cation formation allows nonpolar molecules (e.g. PBDEs) to be ionised that otherwise cannot be analysed by electrospray ionisation (ESI) or atmospheric pressure chemical ionisation (APCI) methods (Abdallah et al., 2009) on the LC-MS/MS. Negative ionisation mode is more sensitive for the higher brominated compounds, so is more suited for the analysis of BDE-209, as the high electron affinity of the bromine ion means the more brominated the compound, the easier the electron capture and greater sensitivity (Debrauwer et al., 2005). As reported in the study by Debrauwer et al. (2005) often a signal in negative ionisation mode is not seen for the di to tri PBDEs and only a low signal for the tetra-BDEs. This method is only suitable for the tetra to deca PBDE congeners but importantly eliminates the degradation of BDE-209 seen in the GC/MS methods.

In view of the above, LC-MS/MS was the method of choice for all target analytes in this study.

2.4.2 HBCD Analysis

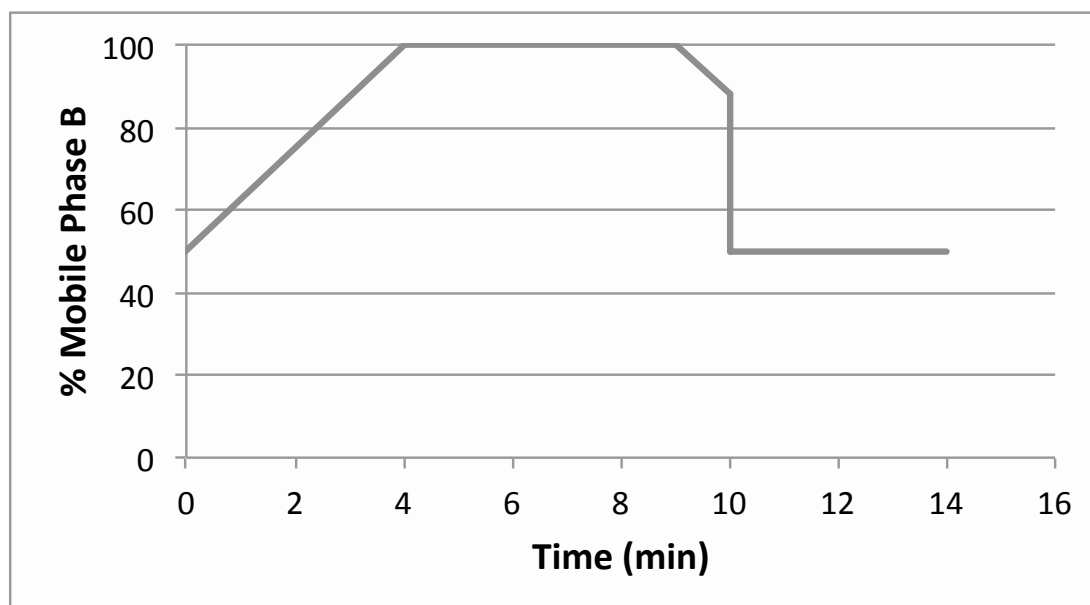
Target HBCDs were separated with a dual pump Shimadzu LC-20AB Prominence liquid chromatograph (Shimadzu, Kyoto, Japan) equipped with a SIL-20A autosampler, and a DGU-20A3 vacuum degasser. A Varian Pursuit XRS3 C18 reversed phase analytical column (150 mm x 4.6 mm i.d., 3 μ m particle size) was used for separation of target HBCDs (α -, β -, γ -). A mobile phase program based upon (mobile phase A) 1:1 methanol/water and (mobile phase B) methanol at a flow rate of

0.18 mL min⁻¹ was applied for elution of the target compounds, as described in Table 2.3 and Figure 2.6.

Table 2.3: Gradient program for HPLC elution of HBCD diastereomers

Time (min)	% Mobile Phase A	% Mobile Phase B
0.00	50	50
4.00	0	100
9.00	0	100
10.00	12	88
10.01	50	50
14.00	50	50

Figure 2.6: Mobile phase gradient program used for HBCD analysis



Mass spectrometric analysis was performed using a Sciex API 2000 triple quadrupole mass spectrometer (Applied Biosystems, Foster City, CA) equipped with an ESI ion source operated in negative ion mode. MS/MS detection, operated in multiple reaction monitoring (MRM) mode, was used for quantitative determination of the HBCD diastereomers, ¹³C-, and d₁₈- labelled analogues. Table 2.4 lists the optimised MS/MS parameters and Table 2.5 lists the ion transitions monitored for the HBCD diastereomers, labelled internal standards (IS) and recovery determination standard (RDS).

Table 2.4: Optimised MS/MS parameters for the analysis of HBCDs on LC-MS/MS

Parameter (units)	Value	Parameter (units)	Value
Curtain Gas (a.u)	30	Declustering Potential (V)	-12
Collision Gas (a.u)	5	Focussing Potential (V)	-250
IonSpray Voltage (V)	-4500	Entrance Potential (V)	-10
Temperature (°C)	450	Collision Energy (eV)	-40
Ion Source Gas 1 (a.u)	55	Collision Cell Exit Potential (V)	-6
Ion Source Gas 2 (a.u)	60	Dwell Time (msec)	200

* a.u = arbitrary units

Table 2.5: Parent to product ion m/z transitions monitored for native HBCD diastereomers, IS and RDS

Diastereomer	Ion transition (m/z)
α -, β -, γ -HBCD	640.6 \rightarrow 78.9
^{13}C α -, β -, γ -HBCD (IS)	652.4 \rightarrow 79.0
d_{18} γ -HBCD (RDS)	657.6 \rightarrow 78.9

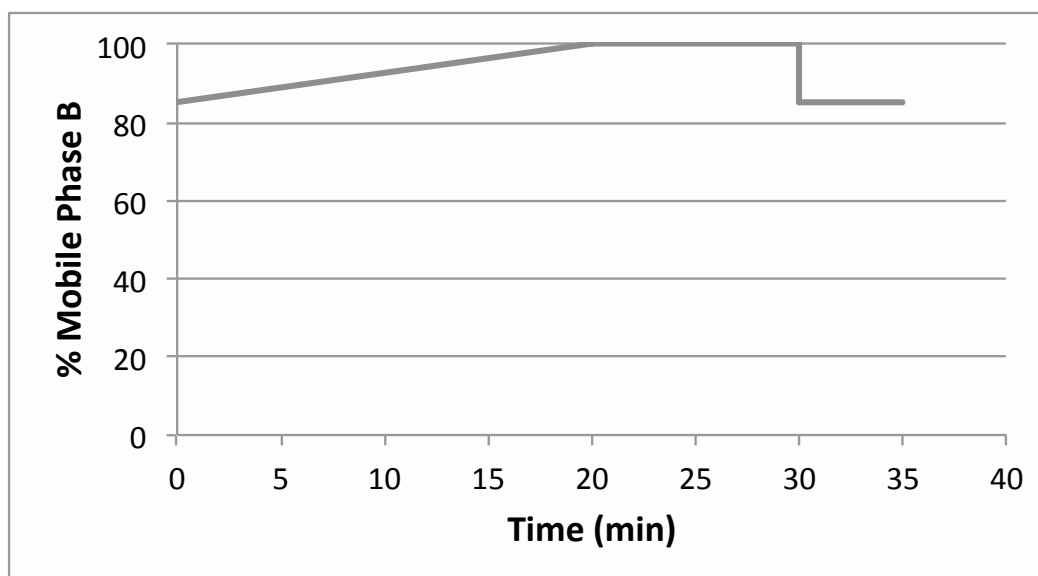
2.4.3 PBDE Analysis

Target PBDEs were separated with a dual pump Shimadzu LC-20AB Prominence liquid chromatograph (Shimadzu, Kyoto, Japan) equipped with a SIL-20A autosampler, and a DGU-20A3 vacuum degasser. A Varian Pursuit XRS3 (Varian, Inc., Palo Alto, CA) C18 reversed phase analytical column (250 mm x 4.6 mm i.d., 3 μm particle size) was used for separation of target PBDEs (47, 85, 99, 100, 153, 154, 183 and 209). A mobile phase program based upon (mobile phase A) 1:1 methanol/water and (mobile phase B) 1:4 toluene/methanol at a flow rate of 0.4 mL min⁻¹ was applied for elution of the target compounds, as described in Table 2.6 and Figure 2.7.

Table 2.6: Gradient program for HPLC elution of PBDE congeners

Time (min)	% Mobile Phase A	% Mobile Phase B
0.00	15	85
20.00	0	100
30.00	0	100
30.01	15	85
35.00	15	85

Figure 2.7: Mobile phase gradient program for PBDE analysis



Mass spectrometric analysis was performed using a Sciex API 2000 triple quadrupole mass spectrometer (Applied Biosystems, Foster City, CA) equipped with an APPI ion source operated in negative ion mode. MS/MS detection, operated in MRM mode, was used for quantitative determination of the native and labelled ^{13}C -PBDE congeners. Table 2.7 lists the optimised MS/MS parameters and Table 2.8 lists the ion transitions monitored for the PBDE congeners, labelled internal standards (IS) and recovery determination standard (RDS).

Table 2.7: Optimised MS/MS parameters for the analysis of PBDEs on LC-MS/MS

Parameter (units)	Value	Parameter (units)	Value
Curtain Gas (a.u)	25	Declustering Potential (V)	-5
Collision Gas (a.u)	11	Focussing Potential (V)	-250
Ion Spray Voltage (V)	-1250	Entrance Potential (V)	-12
Temperature (°C)	400	Collision Energy (eV)	-75
Ion Source Gas 1 (a.u)	60	Collision Cell Exit Potential (V)	-8
Ion Source Gas 2 (a.u)	55	Dwell Time (msec)	100

* a.u = arbitrary units

Table 2.8: Parent to product ion m/z transitions monitored for native PBDE congeners, IS and RDS

Congener	Ion transition (m/z)
BDE-47	420.9 → 78.6
¹³ C BDE-47 (IS)	432.9 → 78.8
BDE-85, -99, -100	500.8 → 78.6
¹³ C BDE-99 (IS); 100 (RDS)	512.9 → 80.6
BDE-153, -154	578.8 → 78.6
¹³ C BDE-153 (IS)	590.7 → 78.8
BDE-183	658.6 → 78.6
BDE-209	486.6 → 78.8
¹³ C BDE-209 (IS)	494.7 → 80.6

2.4.4 Calibration Standards

Calibration standard sets were prepared for both HBCDs and PBDEs, containing native analytes, labelled internal standards (IS) and labelled recovery determination standards (RDS), to prepare a five point calibration curve for assessment of MS linearity. Concentrations of the five HBCD and PBDE calibration standards are listed in Tables 2.9 and 2.10. The calibration standards were run on the LC-MS/MS with every batch of samples before and after the list of samples for a short sample run list, or after every 20 samples for a longer sample list, to assess any instrumental drift throughout the analysis. The same IS and RDS standard solutions used for fortification of samples were used for preparation of the calibration standards and

when a new IS or RDS standard was prepared, new calibration standards prepared with it, to minimise any inter-standard concentration variation. The calibration standards were also prepared on a regular basis (monthly to trimonthly, depending on instrument use) in amber vials, and kept in the refrigerator (4 °C) when not in use, to reduce any analyte degradation or rearrangement caused by UV light or age of the solution.

Often in trace analysis the extent to which matrix effects (a signal enhancement or suppression due to interfering compounds in the sample matrix) influence a sample MS signal is assessed. A sample matrix, containing concentrations below method LOQs of the analytes of interest, is solvent extracted then fortified with standard solutions of the analytes. The MS signal of this sample is compared to that of a prepared solvent solution fortified with standard solutions of the analytes, to provide an indication of signal enhancement or suppression. Unfortunately, due to the ubiquity of both HBCDs and PBDEs in indoor dust, a dust matrix sample with analyte concentrations <LOQs was not available; hence the influence of matrix effects in the dust sample could not be investigated in this manner.

Table 2.9: Concentrations of analyte, IS and RDS compounds in the five HBCD calibration standards

	<i>HBCD Native</i> <i>(ng g⁻¹)</i>	<i>¹³C- HBCD (IS)</i> <i>(ng g⁻¹)</i>	<i>d₁₈ γ-HBCD (RDS)</i> <i>(ng g⁻¹)</i>
<i>Std A</i>	2	20	20
<i>Std B</i>	5	20	20
<i>Std C</i>	20	20	20
<i>Std D</i>	50	20	20
<i>Std E</i>	100	20	20

Table 2.10: Concentrations of analyte, IS and RDS compounds in the five PBDE calibration standards

	PBDE Native (ng g ⁻¹)	¹³ C BDE-47 (IS) (ng g ⁻¹)	¹³ C BDE-99, -153 (IS) (ng g ⁻¹)	¹³ C BDE-209 (IS) (ng g ⁻¹)	¹³ C BDE-100 (RDS) (ng g ⁻¹)
Std A	20	1000	250	500	200
Std B	50	1000	250	500	200
Std C	200	1000	250	500	200
Std D	500	1000	250	500	200
Std E	900	1000	250	500	200

The BDE-47, ¹³C BDE-47, BDE-209, and ¹³C BDE-209 congeners have a higher limit of detection on the LC-MS/MS. All samples and calibration standards were thus fortified with higher concentrations of labelled ¹³C BDE-47 and ¹³C BDE-209, and final concentrations of the PBDE IS were in the ratio 4:1:2 for ¹³C BDE-47: -99, -153: -209 respectively. Typical chromatograms of calibration Standard C, showing the resolution of the three HBCD diastereomers is presented in Figure 2.8 and Figure 2.9 for calibration Standard C of the PBDE congeners.

Figure 2.8: LC-MS/MS Chromatograms of (a) IS, (b) RDS and (c) HBCD analytes in calibration standard C

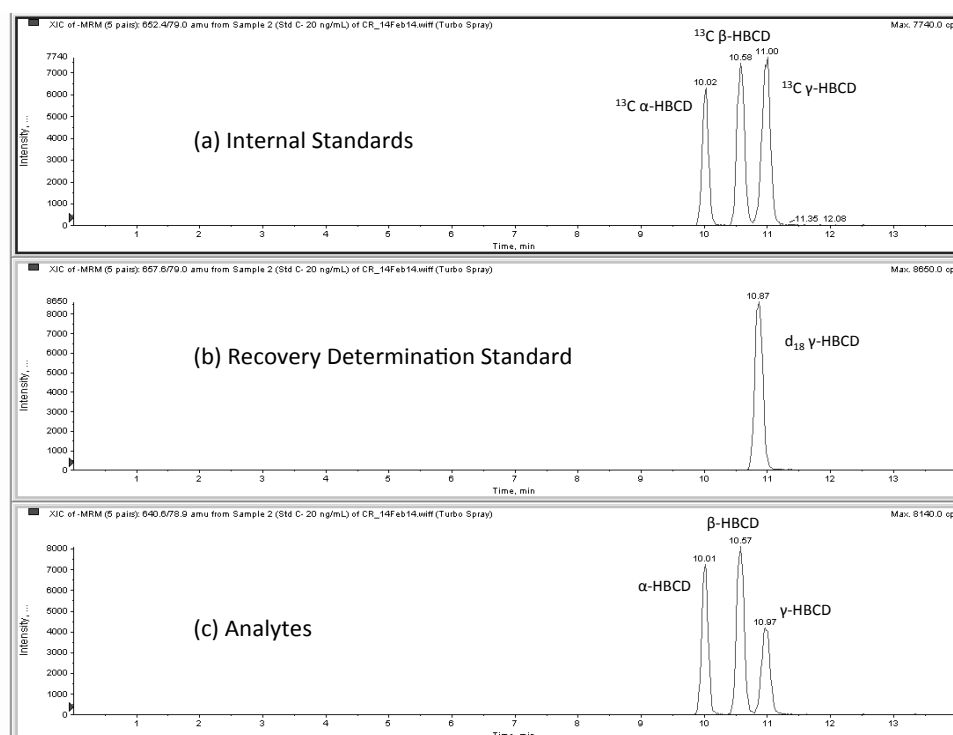
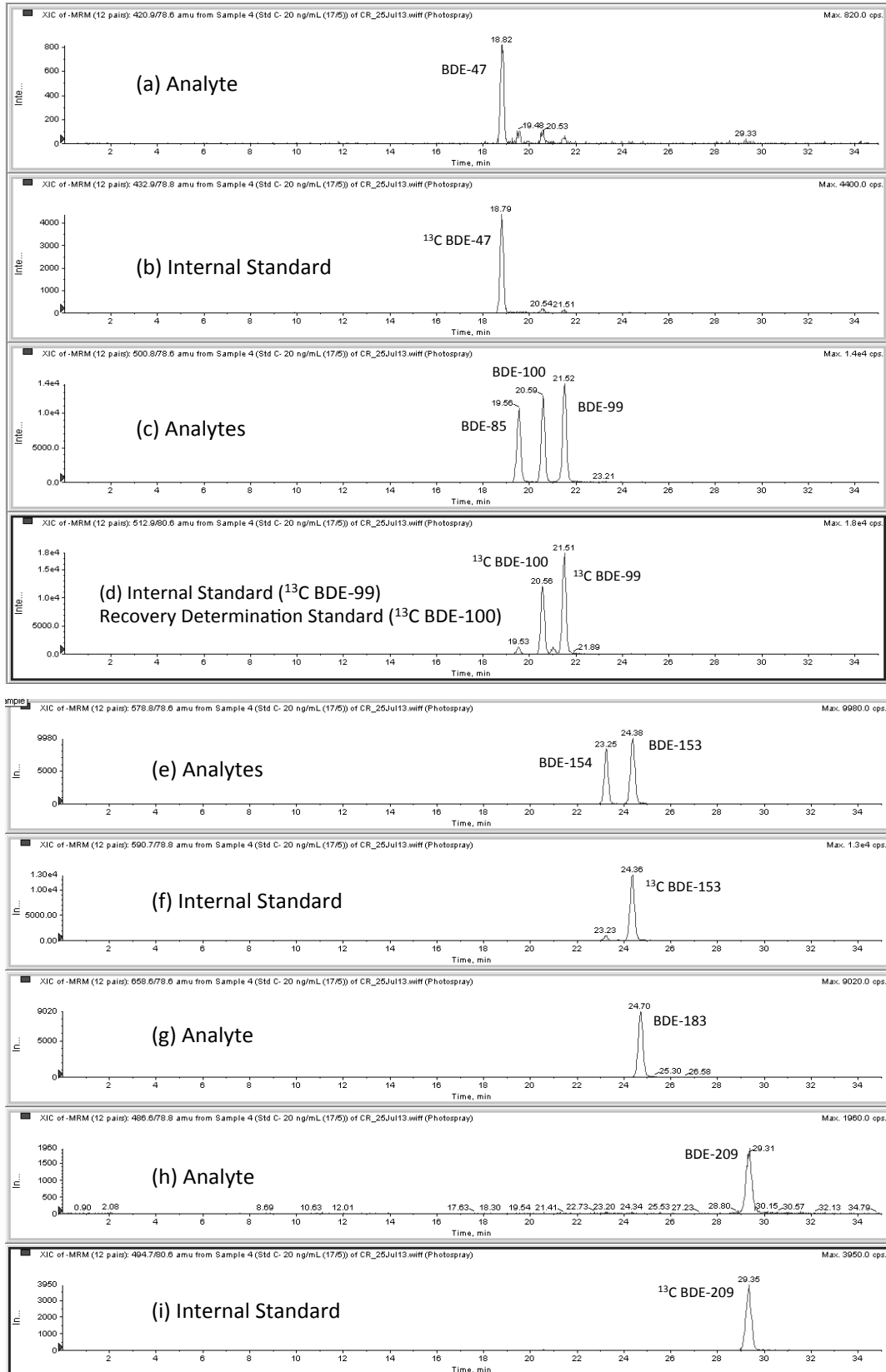


Figure 2.9: LC-MS/MS Chromatograms of Internal Standards (b),(d),(f),(i), Recovery Determination Standard (d) and PBDE analytes (a),(c),(e),(g),(h) in calibration standard C



2.4.5 Internal Standards

Labelled analogues (^{13}C) of the BFR analytes were obtained for use as internal (surrogate) standards. Internal standards were utilised to correct for analyte loss due to the extraction and purification procedure, matrix effects (a signal enhancement or suppression due to other components present in the sample matrix), or instrumental biases. As the labelled analogues closely match the analyte in chemical nature, size and shape, they are expected to suffer the same influence from any of these effects. Thus a ratio of the response of the analyte with respect to the IS remains the same and negates any effect. From this ratio the sample analyte concentration can be calculated with greater confidence. An acceptable IS recovery falls between the range of 30 to 150%. An above 100% recovery is possible due to matrix effects causing a signal enhancement, or an instrumental bias for that sample, creating an enhanced response in the detector. The signal to noise ratio for IS should be 20:1 for the peak area to be classed as acceptable (Ambidge et al., 1990). This was the case for all IS used in this method.

2.4.5.1 Quantification of analytes

Analyte concentrations were manually calculated from peak areas, determined with Analyst version 1.4.2 software, as provided with the AbSciex MS/MS, and using Excel (Microsoft Office 2011) for subsequent calculations. The relative response factor (RRF) was calculated, using equation (2.1) for each calibration standard and for each analyte.

$$RRF_N = \left(\frac{A_{NAT}}{A_{IS}} \right) \times \left(\frac{M_{IS}}{M_{NAT}} \right) \quad (2.1)$$

RRF_N refers to the relative response factor of the native analyte, A_{NAT} is the peak area of the native in the calibration standard, A_{IS} is the peak area of the IS in the calibration standard, M_{IS} is the mass (ng) of IS added to the calibration standard and M_{NAT} is the mass (ng) of native analyte added to the calibration standard. An average of the calculated RRF_N of the five calibration standards was taken for the final RRF value of each analyte. Table 2.11 lists mean RRFs, including %RSDs for the HBCD and PBDE calibration standards. The %RSD should not exceed 15% (Ambidge et al., 1990), as is the case here.

Table 2.11: Calculated mean RRFs for each analyte and %RSD

Analyte	Mean RRF	%RSD
α -HBCD	1.16	5.8
β -HBCD	1.01	7.2
γ -HBCD	0.52	7.1
BDE-47	0.51	10
BDE-85	0.81	7.4
BDE-99	1.04	4.6
BDE-100	0.83	4.9
BDE-153	0.98	8.8
BDE-154	0.77	9.7
BDE-183	0.87	7.6
BDE-209	1.29	9.0

The calculated RRFs were then used in equation (2.2) to calculate the concentration of the analyte (ng g^{-1}) in the sample.

$$C_N = \left(\frac{A_{NAT}}{A_{IS}} \right) \times \left(\frac{M_{IS}}{SM} \right) \times \left(\frac{1}{RRF_N} \right) \quad (2.2)$$

C_N refers to the analyte concentration (ng g^{-1}) in the sample, A_{NAT} is the peak area of the native in the sample, A_{IS} is the peak area of the IS in the sample, M_{IS} is the mass (ng) of IS added to the sample and SM is the sample mass extracted (g).

2.4.5.2 Internal standard recoveries

Calculation of the recoveries of internal standards (IS) added prior to extraction are facilitated by the addition of a recovery determination standard (RDS) to the final sample extract just before injection on the LC-MS/MS. Calculation of the recoveries of IS helps to assess the performance of the extraction and clean up methods. The RRF for each IS was calculated from the calibration standards using equation (2.3).

$$RRF_{IS} = \left(\frac{A_{IS}}{A_{RDS}} \right) \times \left(\frac{M_{RDS}}{M_{IS}} \right) \quad (2.3)$$

A_{RDS} is the peak area of the recovery determination standard (RDS) in the calibration standard and M_{RDS} is the mass of RDS added to the calibration standard (ng). Again an average of the RRF_{IS} from all five calibration standards was calculated for the final, average RRF value of each IS used in equation (2.4) to calculate the % recovery of the IS.

$$\% \text{ IS Recovery} = \left[\left(\frac{A_{IS}}{A_{RDS}} \right) \times \left(\frac{M_{RDS}}{RRF_{IS}} \right) \times \left(\frac{1}{M_{IS}} \right) \right] \times 100 \quad (2.4)$$

A_{IS} is the peak area of the IS in the sample, A_{RDS} is the peak area of the RDS in the sample, M_{RDS} is the mass of RDS added to the sample (ng) and M_{IS} is the actual mass of IS added to the sample (ng). For ^{13}C α -, β -, and γ -HBCDs, average recoveries ranged from 71 to 85% while for ^{13}C -PBDE 47, 99, 153, and 209, average recoveries ranged from 83 to 85%. Table 2.12 lists the mean recoveries and standard deviation for each IS.

Table 2.12: Mean, range, standard deviation and %RSD of IS recoveries from analysed samples

IS	Number of samples	Mean (%)	Range	SD	%RSD
^{13}C PBDE-47	84	84	50-117	14	17
^{13}C PBDE-99	84	85	51-119	14	17
^{13}C PBDE-153	84	83	51-121	14	17
^{13}C PBDE-209	84	84	40-124	20	24
^{13}C α -HBCD	94	71	44-119	20	28
^{13}C β -HBCD	94	84	48-121	18	21
^{13}C γ -HBCD	94	85	48-120	16	19

2.5 QA/QC criteria

2.5.1 Chromatographic Selectivity

For a given chromatographic peak to be identified as a target compound, the following criteria were required to be met. Firstly, the relative retention time (the ratio of the retention time of the analyte to that of its corresponding internal standard) of the analyte in the sample solution had to match that present in the calibration standard within a specified tolerance of $\pm 2.5\%$ (EC Directive 2002/657/EC). Secondly, for analytes with the same monitored ion transitions, i.e. PBDE isomers and HBCD diastereomers, appropriate separation between eluting analyte peaks had to be achieved. Specifically, the peak 'valley' between eluting peaks had to be $< 20\%$ of the smallest peak height.

2.5.2 Accuracy and Precision

As a measure of accuracy and precision of the method, the NIST dust standard reference material (SRM) 2585 was analysed on a regular basis. Certified PBDE concentrations are published for this SRM; however, only indicative HBCD concentrations are published. Due to the lack of an appropriate reference material for HBCDs, this SRM was analysed with concentrations compared to the indicative values. The SRM was analysed with every 20 samples as an ongoing method performance check. The mean concentration \pm standard deviation (SD), %RSD, certified PBDE and indicative HBCD values are listed in Table 2.13. As the %RSDs are below 20%, the repeatability of the method is acceptable (EC Directive 2002/657/EC). The measured concentration value (within the limit of the standard deviation) falls within the indicative/certified values for all analytes except β -HBCD. The difference in the β -HBCD value range is within $\pm 10\%$ of the limit of the indicative value hence falls within suitable precision criteria (EC Directive 2002/657/EC) and the measurements of the SRM show the method has suitable trueness, precision, and accuracy i.e. is fit for purpose.

Table 2.13: Mean \pm standard deviation of BFRs in SRM 2585, %RSD and Certified and Indicative values

Analyte	Measured mean \pm Standard Deviation (n = 15)	% RSD	Indicative Value (Keller et al., 2007)
α -HBCD	22 \pm 3.8	17.6	19 \pm 3.7
β -HBCD	6.8 \pm 1.3	18.9	4.3 \pm 1.1
γ -HBCD	129 \pm 26	12.0	120 \pm 22
Analyte	Measured mean \pm Standard Deviation (n = 15)	% RSD	Certified Value (Stapleton et al., 2006)
BDE-47	438 \pm 59	13.6	498 \pm 46
BDE-85	37.7 \pm 5.0	13.3	43.8 \pm 1.6
BDE-99	817 \pm 61	7.4	892 \pm 53
BDE-100	140 \pm 12	8.6	145 \pm 11
BDE-153	124 \pm 15	12.0	119 \pm 1
BDE-154	76.7 \pm 10	13.6	83.5 \pm 2.0
BDE-183	42.4 \pm 5.9	14.0	43.0 \pm 3.5
BDE-209	2410 \pm 300	12.3	2510 \pm 190

2.5.3 Preparation of an in-house reference dust material

An in-house dust reference material was produced as an extra quality control check for the dust extraction analysis procedure. 25 g of the Birmingham low level, pre-characterised house dust (described previously in 2.1.7.1) was fortified with concentrated standards of the native HBCD diastereomers and PBDE congeners. Standard solutions (50 $\mu\text{g mL}^{-1}$) of each analyte were added to the dust sample in volumes (μL) listed in Table 2.13 as are the indigenous BFR concentrations.

The dust sample was mixed thoroughly by vortexing for 5 minutes before placement in a mechanical shaker for 24 hours, to achieve homogeneous distribution of analytes in the dust sample. After homogenisation, six aliquots of the dust were analysed to determine the dust concentration and homogeneity of the dust bulk. Two subsamples were taken from the top of the dust bulk, two from the middle and two from the

bottom. Samples of the dust were analysed on a regular basis and mean concentrations in the dust and standard deviations from these samples (n=9) are listed in Table 2.14. As the Birmingham dust already contained elevated concentrations of HBCDs and BDE-209 the added mass from fortification of these congeners had little effect on the total concentration of these congeners and hence the results are consistent with that previously determined in the dust bulk. The high standard deviation and %RSD (>15%) for γ -HBCD, and BDE-209 suggests heterogeneity through this dust for these analytes and this was seen previously in the original analysis of the low level Birmingham dust, before fortification. The acceptable %RSD for PBDEs 47 to 183 suggest an acceptable level of homogeneity of these analytes through the prepared dust and that this material is acceptable as an additional measure of method performance.

Table 2.14: Volume of each native standard solution added to dust, mean concentration, SD and %RSD of replicate analyses of the dust reference material

Analyte	Birmingham dust bulk concentration (ng g⁻¹) (n=6)	Volume of 50 ng μL⁻¹ standard added (μL)	Mean concentration in prepared dust (ng g⁻¹) (n=9)	Standard Deviation	%RSD
α -HBCD	390 \pm 110	10	290	44	15
β -HBCD	180 \pm 45	2.5	130	14	11
γ -HBCD	2600 \pm 3200	30	1500	870	57
<i>BDE-47</i>	5 \pm 8	50	120	18	16
<i>BDE-85</i>	1 \pm 1	20	45	6	14
<i>BDE-99</i>	18 \pm 4	25	70	7	11
<i>BDE-100</i>	4 \pm 2	40	94	9	10
<i>BDE-153</i>	7 \pm 5	45	100	7	7
<i>BDE-154</i>	2 \pm 5	20	46	4	9
<i>BDE-183</i>	11 \pm 7	20	48	5	9
BDE-209	2000 \pm 550	100	2100	600	28

2.5.4 Analysis of Blanks, calculation of LODs and LOQs

The limit of detection of the instrument (LOD) for each analyte was calculated as the concentration (ng on the column) responsible for a signal to noise ratio of 3:1 on the

instrument and the calculated values are listed in Table 2.14. The tetra to hepta PBDEs were not detected in the dust method blanks (extracting an ASE cell filled with pre-cleaned hydromatrix), PUF or GFF method blanks (extraction of a pre-cleaned GFF and PUF respectively). The limit of quantification (LOQ) of these analytes was therefore calculated as the concentration (ng g^{-1} or ng) relating to a 10:1 signal to noise ratio. Very low concentrations of the HBCD diastereomers and BDE-209 were detected in dust method blanks (typically 0.5 to 1.3 ng g^{-1} of HBCDs and 2.2 ng g^{-1} of BDE-209) hence LOQs for these analytes were calculated as the mean + 3 times the standard deviation. GFF and PUF method blanks also had very low concentrations of HBCDs (0.1 to 0.7 ng) and BDE-209 (0.3 to 2.2 ng) present hence the LOQs for these congeners was again calculated the mean + 3 times the standard deviation. Calculated method LOQs for each analyte in dust, PUF and GFFs are listed in Table 2.15.

Table 2.15: Calculated LODs (ng on column) and method LOQs for HBCD diastereomers and PBDE congeners in this study

Analyte	LOD (ng on column)	Method LOQs		
		Dust (ng g^{-1}) Assuming 0.2 g of dust	PUF (ng per PUF)	GFF (ng per GFF)
α -HBCD	0.029	2.19	0.39	0.56
β -HBCD	0.030	1.92	0.27	0.23
γ -HBCD	0.028	4.20	1.23	1.60
BDE-47	1.30	4.49	4.49	4.49
BDE-85	0.24	0.80	0.80	0.80
BDE-99	0.23	0.78	0.78	0.78
BDE-100	0.22	0.72	0.72	0.72
BDE-153	0.39	1.29	1.29	1.29
BDE-154	0.55	1.84	1.84	1.84
BDE-183	0.29	0.96	0.96	0.96
BDE-209	2.35	6.88	1.16	6.30

2.6 Statistical Analysis

Statistical analysis was conducted using Microsoft Excel (Microsoft Office 2011) and SPSS version 22 for Independent Sample t-tests and Pearson correlations. Confidence intervals in SPSS were preset at 95% and significance levels were set at 0.05.

CHAPTER 3

TEST CHAMBER STUDIES OF BFR VOLATILISATION FROM SOURCES AND SUBSEQUENT PARTITIONING TO DUST

3.1 Summary

The following chapter describes the optimisation of the test chamber experimental design for the measurement of BFR migration to air via volatilisation from source materials and the measurement of subsequent BFR partitioning to dust. Investigations to evaluate the optimum configuration for this experimental design are described and the performance of the chamber for such experiments was evaluated against that of a commercially available emission chamber. An investigation into sources of analyte loss during chamber studies was conducted, particularly loss from sink effects (preferential partitioning to inner chamber surfaces) with methods to minimise this loss evaluated. Following the chamber comparison study, the in-house chamber was used to study the transfer of HBCDs from curtains treated with the HBCD technical formulation to air and dust.

3.2 Experimental Design development

3.2.1 *Initial experimental design and measurements*

Initially, mass balance experiments were conducted to gain a measure of BFR transfer to key compartments of the chamber. These were the PUFs fitted to the chamber exit line to collect BFR emissions and the chamber wall surfaces. The trial experiments used as the BFR “source” standards of native PBDEs and HBCDs spiked onto a small GFF (100 ng/analyte). The GFF was placed on the chamber shelf (situated half way down the chamber) and air flow was attached to the chamber as described previously (Section 2.1). The chamber was maintained at the desired temperature in a hot water

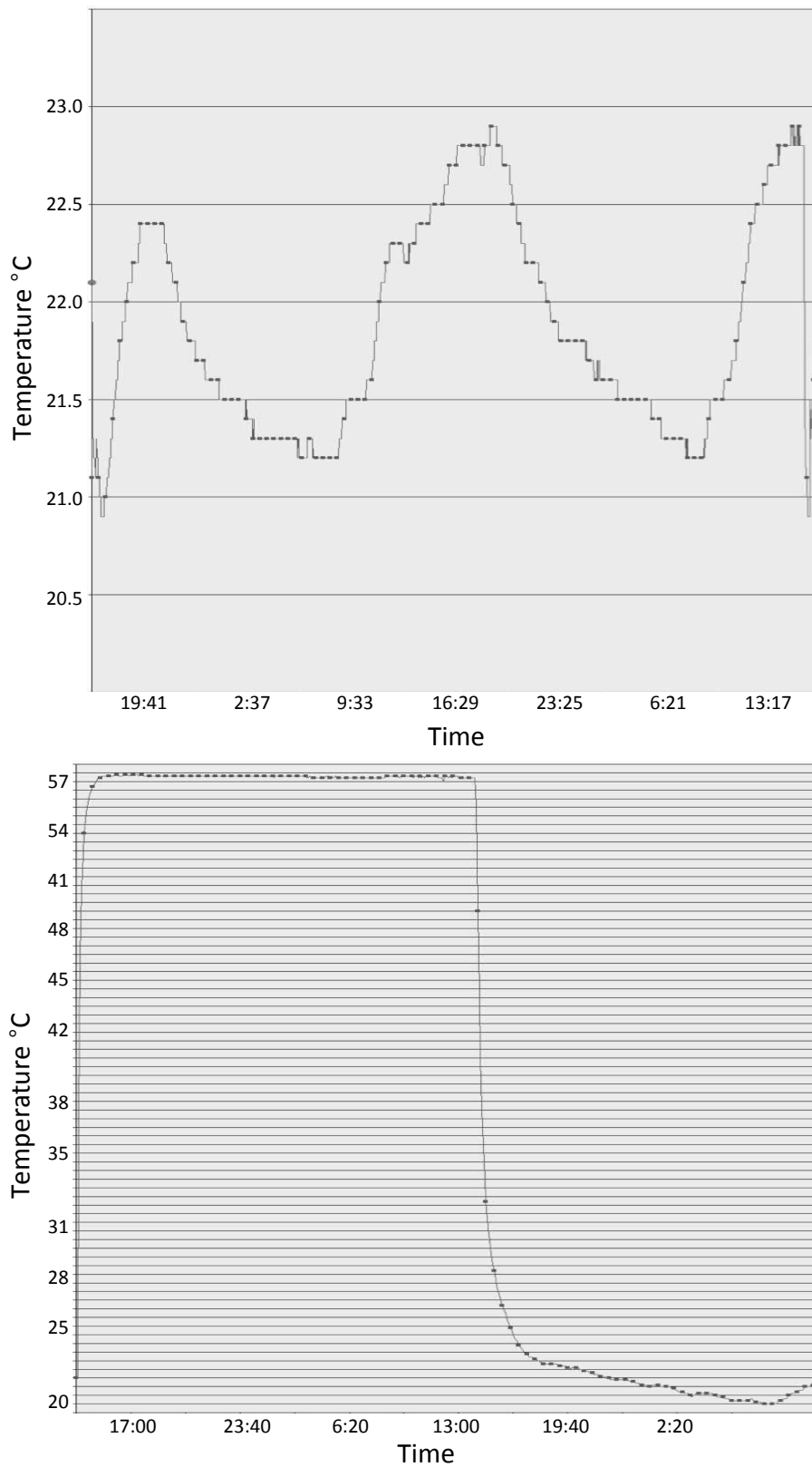
bath for a specified time period. Post experiment, the GFF, exit line PUFs and solvent rinses of the chamber inner surfaces, were analysed separately. This experiment was repeated at both 60 °C and room temperature. The internal chamber temperature was monitored with a LogTag thermocouple for the duration of the experiment, with temperatures maintained at 22 ± 1 °C for the room temperature experiments, and a constant 57 °C in the heated water bath, when set at 60 °C, Figure 3.1.

Addition of the BFR concentrations extracted from the GFF, PUFs and solvent rinses revealed that 100% recovery was not obtained for any analyte. Percentage analyte recoveries from each compartment and total BFR recovery (%) are listed in Table 3.1. The substantial analyte loss from these initial mass balance experiments prompted a series of investigations into: (1) the fate of the missing analyte mass and (2) designing experimental strategies to minimise analyte loss. The following sections describe these investigations.

Table 3.1: Recoveries (%) \pm SD (where applicable) of BFRs recovered from the GFF, PUFs and chamber inner surface rinses in initial trial experiments at 22 ± 1 °C for 1 week (n=1) and 60 °C for 24 hours (n=3)

Analyte	22 °C \pm 1 for 10 days (n=1)				60 °C for 24 hours (n=3)			
	GFF	PUF	Chamber Rinse	Total %Recovery	GFF	PUF	Chamber Rinse	Total %Recovery
α-HBCD	93	0.8	1.6	95	94 \pm 0.4	0.7 \pm 0.4	2.7 \pm 0.5	98 \pm 5.3
β-HBCD	85	0.6	<LOQ	86	51 \pm 0.2	0.5 \pm 0.2	1.4 \pm 0.9	53 \pm 12
γ-HBCD	90	<LOQ	1.5	92	47 \pm 10	<LOQ	1.2 \pm 0.8	49 \pm 10
BDE-47	30	<LOQ	45	75	15 \pm 2.7	10 \pm 3.4	13 \pm 7.1	39 \pm 7.3
BDE-85	91	<LOQ	2.2	93	61 \pm 6.0	1.1 \pm 0.5	12 \pm 3.2	74 \pm 7.6
BDE-99	85	<LOQ	4.1	89	45 \pm 3.7	2.8 \pm 1.2	19 \pm 3.1	67 \pm 4.5
BDE-100	74	<LOQ	8.2	82	32 \pm 3.0	5.7 \pm 1.9	21 \pm 1.9	59 \pm 2.6
BDE-153	86	<LOQ	<LOQ	86	73 \pm 7.6	<LOQ	6.8 \pm 1.7	80 \pm 6.3
BDE-154	76	<LOQ	<LOQ	76	68 \pm 9.9	<LOQ	12 \pm 2.9	81 \pm 8.4
BDE-183	89	<LOQ	<LOQ	89	84 \pm 2.1	<LOQ	2.4 \pm 0.6	87 \pm 1.5
BDE-209	93	<LOQ	<LOQ	93	80 \pm 4.0	7.3 \pm 10	5.6 \pm 2.4	92 \pm 13

Figure 3.1: Output from the LogTag thermocouple showing temperature profiles inside the test chamber during an experiment conducted for: (Top) 2 days at room temperature, and (Bottom) 24 hours at 60 °C



3.2.2 PUF Breakthrough

As summarised in Table 3.1, only a minimal proportion of each target BFR was recovered from the PUF plugs and this prompted an investigation to test the sampling efficiency of the PUFs used to collect BFRs in chamber exit air. Two PUFs were placed sequentially in a glass holder with the chamber-side end of the first collection PUF spiked with standards of native PBDEs and HBCDs (100 ng/analyte) before attachment to the chamber. The empty chamber was maintained at 60 °C to replicate an experimental scenario in which substantial losses might be expected (warm air passing through the system configuration), and air was pumped through the system for 24 hours. Post experiment, both PUFs were extracted separately and analysed. Analyte concentrations were below LOQs on the second “air-side” PUF while recoveries of analytes on the chamber-side PUF were 99 ± 7 %. These data provide clear evidence that there are no significant analyte losses via PUF breakthrough when using the UoB chamber. Similar experiments were conducted with the micro chamber utilised at the Flemish Institute for Technological Research (VITO), as described in Section 2.1.2, and also revealed satisfactory analyte recoveries from the chamber-side PUF of 90 ± 11 %. Percentage recoveries of individual analytes are listed in Table 3.2.

Table 3.2: Recoveries (%) of BFRs from PUF breakthrough experiments

Analyte	UoB chamber (n=1)	Micro chamber (n=1)
α-HBCD	92	102
β-HBCD	93	80
γ-HBCD	100	94
BDE-47	93	92
BDE-85	106	88
BDE-99	105	89
BDE-100	106	82
BDE-153	101	92
BDE-154	100	82
BDE-183	92	87
BDE-209	107	83

3.2.3 Minimising analyte loss during post experiment disassembly

After concluding that PUF breakthrough was not contributing to analyte loss in these experiments, other pathways of BFR loss were investigated. Table 3.1 reveals that greater analyte loss is experienced during the heated chamber experiments. Hence, it was hypothesised that opening the chamber lid post-experiment, whilst the temperature of the chamber is still above room temperature, may result in release of volatilised BFRs that are not captured by the exit PUF. Trials were conducted under similar conditions (24 hours at 60 °C), and the chamber was cooled to room temperature for 5 hours post experiment, with air flow still attached before opening the chamber. This was deemed a sufficient time period for any remaining volatilised analytes to be collected on the exit PUF. Again the spiked GFF, PUF and chamber inner surface solvent rinses were analysed separately post experiment. There was a slight increase in the total BFR proportion (%) recovered from the exit PUF for all BFRs except for the less volatile BDE-183 and BDE-209. While this did not lead to a substantial increase in overall analyte recoveries, this extended post-experiment cooling period was employed in future experiments. Table 3.3 lists the total BFR recoveries (%) and BFR proportion (%) collected on the PUF for these experiments. The remaining unaccounted for proportion of analyte, suggests that there are substantial loss mechanisms occurring within the chamber itself.

3.2.4 Influence of exit air sampling train length

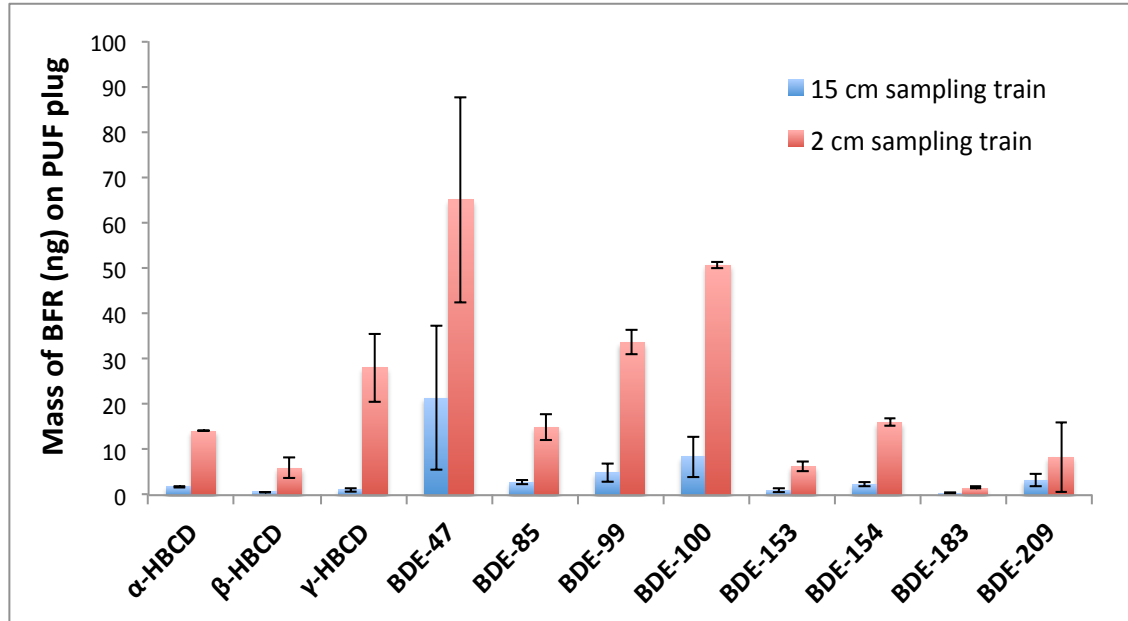
The influence of the length of polypropylene tubing carrying air exiting the chamber to the collection PUF was investigated as a potential source for analyte loss. In this scenario, chamber experiments were conducted at 60 °C for 24 hours (to promote volatilisation) and again a small GFF spiked with PBDE and HBCD standards (100 ng/analyte) was used as the BFR source. The PUF, GFF and chamber solvent rinses were analysed post experiment and reducing the tubing length from 15 cm to 2 cm increased the proportion of all BFRs collected on the PUFs by up to 7 times. There was a statistically significant ($p < 0.05$) higher mass collection for all analytes except BDE-183 and 209. Table 3.3 and Figure 3.2 compare the BFR proportion (%) collected on the PUF for both tubing lengths as well as listing total BFR recoveries (%). The substantially higher BFR masses detected on the PUF with shorter tubing length, suggests the analytes sorb strongly to the inner tubing surfaces before being

collected on the PUF. Hence, using the longer 15 cm tubing length underestimates volatile emissions, which is particularly relevant for chamber experiments conducted at above-ambient temperatures that encourage volatilisation. Consistent with our data, Xu et. al. (2012) reported that reducing the length of the stainless steel tube connecting their chamber to the sampling sorbent tube, increased apparent volatilisation of di(2-ethylhexyl)phthalate (DEHP) from vinyl flooring. As a result of reducing the length of the connecting tube, Xu et al. (2012) found gas-phase concentrations reached steady state conditions in 20 rather than 40 days. Therefore the length of the connection between the chamber exit and the sampling sorbent should be kept to a minimum for studies of SVOCs like BFRs. The results from this investigation show that BFRs can partition irreversibly to certain surfaces that act as sinks and this effect was investigated further in the stainless steel chamber.

Table 3.3: Total BFR recoveries (%) ± SD and BFR proportion recovered from PUFs (%) ± SD for experiments at 60 °C for 24 hours: (a) initial trial chamber experiments, (b) cooling the chamber before disassembling (c) shorter sample air train length

Analyte	Initial trial experiment (n=3)		Chamber ‘cool down’ (n=3)		Proportion on PUF (%) (2 cm air train length) (n=2)
	Total recovery (%)	Proportion on PUF (%)	Total recovery (%)	Proportion on PUF (%) (15 cm air train length)	
α-HBCD	98 ± 5.3	0.7 ± 0.4	82 ± 16	1.9 ± 0.2	14 (14, 14)
β-HBCD	53 ± 12	0.5 ± 0.2	49 ± 6.3	0.7 ± 0.1	5.9 (4.3, 7.5)
γ-HBCD	49 ± 10	<LOQ	38 ± 6.6	1.2 ± 0.4	28 (23, 33)
BDE-47	39 ± 7.3	10 ± 3.4	43 ± 22	21 ± 16	65 (49, 81)
BDE-85	74 ± 7.6	1.1 ± 0.5	83 ± 8.9	2.8 ± 0.6	15 (13, 17)
BDE-99	67 ± 4.5	2.8 ± 1.2	67 ± 1.7	4.9 ± 1.9	34 (32, 35)
BDE-100	59 ± 2.6	5.7 ± 1.9	55 ± 8.1	8.4 ± 4.5	51 (50, 51)
BDE-153	80 ± 6.3	<LOQ	63 ± 7.0	1.0 ± 0.3	6.3 (5.6, 6.9)
BDE-154	81 ± 8.4	<LOQ	53 ± 3.1	2.3 ± 0.5	16 (16, 17)
BDE-183	87 ± 1.5	<LOQ	80 ± 7.8	<LOQ	1.5 (1.4, 1.7)
BDE-209	92 ± 13	7.3 ± 10	110 ± 10	<LOQ	8.4 (3.0, 14)

Figure 3.2: Mass of BFR (ng) collected on PUF plugs sampling chamber exit air for different exit air sampling train lengths



A comparison of the mass collected from the chamber exit air and reported physicochemical properties of the analytes was conducted to determine if the behaviour of the BFRs can be described by e.g. their vapour pressures. The literature reported vapour pressures of BFRs at 25 °C (Tittlemier et al., 2002, USEPA 2012c, Kuramochi and Sakai, 2013) were converted to calculated vapour pressures at 60 °C using Equation 3.1 and the literature and calculated vapour pressure values are listed in Table 3.4.

$$\ln\left(\frac{V_{P2}}{V_{P1}}\right) = \frac{\Delta H_{VAP}}{R} \left(\frac{1}{T_1} - \frac{1}{T_2}\right) \quad (3.1)$$

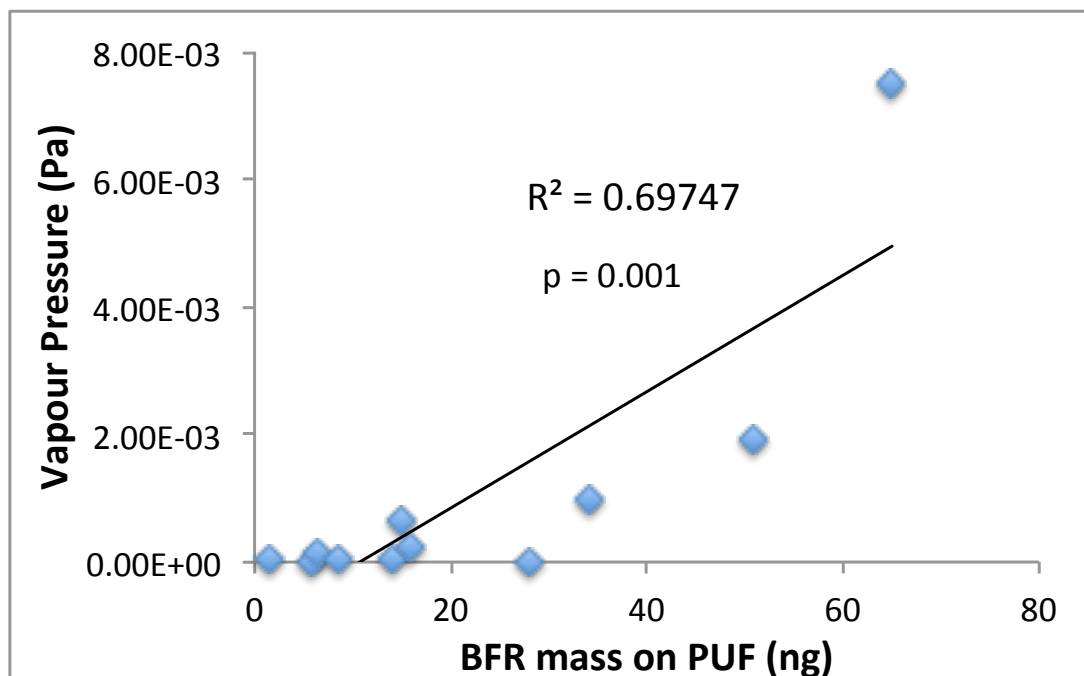
V_{P1} is the reported vapour pressure (Pa) at 25 °C (or 298.15 K), ΔH_{VAP} is the enthalpy of vaporisation for the BFR (J mol^{-1}), R is the gas constant i.e. $8.3145 \text{ J mol}^{-1} \text{ K}^{-1}$, T_1 is 298.15 K and T_2 is the temperature (K) corresponding to the calculated vapour pressure (V_{P2}), and in this case is 333.15 K.

Table 3.4: Literature reported BFR vapour pressures at 25 °C, literature reported enthalpy of vaporisation (Bläuenstein, 2007, ChemSpider, 2014) and calculated vapour pressure at 60 °C.

Analyte	V _P at 25 °C (Pa)	ΔH _{VAP} (J mol ⁻¹)	V _P at 60 °C (Pa)
α-HBCD	1.40 x 10 ⁻⁶	74550	3.30 x 10 ⁻⁵
β-HBCD	7.74 x 10 ⁻⁷	74550	1.82 x 10 ⁻⁵
γ-HBCD	1.12 x 10 ⁻⁸	74550	2.64 x 10 ⁻⁷
BDE-47	1.90 x 10 ⁻⁴	86730	7.50 x 10 ⁻³
BDE-85	9.90 x 10 ⁻⁶	99521	6.72 x 10 ⁻⁴
BDE-99	1.76 x 10 ⁻⁵	94768	9.77 x 10 ⁻⁴
BDE-100	2.86 x 10 ⁻⁵	99521	1.94 x 10 ⁻³
BDE-153	2.10 x 10 ⁻⁶	97242	1.29 x 10 ⁻⁴
BDE-154	3.79 x 10 ⁻⁶	97242	2.34 x 10 ⁻⁴
BDE-183	4.68 x 10 ⁻⁷	115521	6.26 x 10 ⁻⁵
BDE-209	1.20 x 10 ⁻⁷	145022	5.60 x 10 ⁻⁵

The vapour pressure at 60 °C was plotted against the BFR mass collected on the PUF for the optimised chamber experiment (short sampling train length). Figure 3.3 presents the plot of the data for all target PBDEs and HBCDs and shows the fitted trend line. A significant positive linear correlation was seen ($r = 0.835$, $p < 0.01$) between the vapour pressure and BFR mass collected from the air. The significant correlation illustrates that the reported vapour pressures of these analytes can dictate their chamber emission pattern.

Figure 3.3: Plot of vapour pressure (60 °C) vs BFR mass on PUF in mass balance experiments using optimised chamber configuration.



3.3 Sink Effects

Another possible explanation for the observed analyte loss is due to “sink effects” i.e. sorption of BFRs to the internal chamber surfaces. Following volatilisation, the lower vapour pressures of SVOCs can lead to preferential sorption to chamber surfaces rather than collection in gas phase emissions. The loss of analyte to chamber wall surfaces is referred to as sink effects and has been previously reported in chamber studies of SVOCs (Katsumata et al., 2008, Kemmlein et al., 2003, Uhde and Salthammer, 2006, Xu et al., 2012). The loss to sink effects in both the UoB test chamber and the micro chamber configurations were investigated in enclosed chamber experiments (no air flow) to gain a measure of a worst case scenario of analyte loss. Small GFFs were spiked with standards of PBDEs and HBCDs (100 ng/analyte) and placed inside the sealed chambers, which were then heated to 60 °C for 24 hours. Post experiment, whilst still sealed, both the UoB chamber and the micro chamber were cooled to room temperature for 5 hours. The inner chamber surfaces were then solvent rinsed to assess the proportion of analytes reversibly deposited to inner surfaces, and the GFF analysed to determine the non-volatilised

proportion. The total recovered proportion of individual BFRs was calculated as the sum of that recovered in the chamber solvent rinses plus proportion remaining on the GFF; with the percentage unaccounted for assumed to be due to loss to unrecovered sorption to internal chamber surfaces.

Considerable quantities of the more volatile analytes were recovered in the solvent washes of the chamber walls but 100% recovery was not obtained for any of the analytes. Table 3.5 lists the total BFR recoveries (%) in both the UoB and micro chambers, as well as the proportion (%) recovered from the chamber inner surface rinses and that remaining on the GFF. Liu et al. (2013) listed measures that can be undertaken to reduce such sink effects and minimise time for steady-state to be reached. These comprise: increasing the source surface area, decreasing the sink (i.e. chamber) surface area per volume ratio, using materials for chamber surfaces with lower sorptive capacity, and increasing the chamber air change rate.

As the same size GFF was used in both chambers, no differences exist in the source area of the two chamber configurations compared in this study. In contrast, the lower surface area-to-volume ratio for the UoB chamber (50 m^{-1}) compared to the micro chamber (160 m^{-1}) should reduce losses due to sink effects. The sink effects experiments were enclosed (no air flow) hence the air exchange rate is not a contributing factor in this particular scenario. The data from the chamber experiments generally agrees with the suggested influential properties by Liu et al (2013), as larger losses were observed with the micro chamber. However, the similar losses of BDEs-47, 85, 99, and 100 suggest other factors likely play a role. Other efforts were made to minimise sink effects for the UoB chamber and these are described below.

Table 3.5: BFR recoveries (%) \pm SD (where applicable) of PBDEs and HBCDs from various compartments during experiments testing sink effects from the UoB (n=1) and micro chambers (n=6)

Analyte	UoB Chamber (n=1)			Micro Chamber (n=6)		
	GFF	Chamber Rinse	Total recovery	GFF	Chamber Rinse	Total recovery
α-HBCD	86	2.6	89	45 \pm 21	10 \pm 3.1	55 \pm 22
β-HBCD	69	1.0	70	32 \pm 20	4.4 \pm 1.5	36 \pm 21
γ-HBCD	63	1.8	65	20 \pm 23	5.1 \pm 2.9	25 \pm 26
BDE-47	5.3	38	43	6.2 \pm 5.9	41 \pm 9.8	47 \pm 14
BDE-85	21	32	52	13 \pm 6.0	37 \pm 4.0	50 \pm 6.1
BDE-99	13	41	54	10 \pm 5.4	39 \pm 5.5	49 \pm 8.9
BDE-100	10	41	51	8.0 \pm 5.2	38 \pm 8.5	46 \pm 13
BDE-153	59	30	89	25 \pm 14	28 \pm 5.7	53 \pm 9.1
BDE-154	35	43	78	15 \pm 13	36 \pm 5.0	51 \pm 12
BDE-183	71	5.6	76	45 \pm 11	15 \pm 5.3	60 \pm 6.0
BDE-209	85	4.3	90	96 \pm 14	1.4 \pm 0.8	97 \pm 14

Rinsing the UoB chamber with different solvents, following the experiments to investigate sink effects, was also examined in an attempt to improve recoveries, with 100 mL of hexane:DCM (1:1 v/v), 100 mL toluene, then 100 mL methanol used to rinse the chamber. The toluene and methanol washes only returned minor proportions (%) of BFRs and a large proportion of analytes again remained unaccounted for. As the majority of analytes recovered from solvent rinses were found in the hexane:DCM wash, 200 mL of this solvent was employed for the chamber inner surface solvent rinse step in the remaining experiments. The BFR proportion (%) recovered from the solvent rinses are listed in Table 3.6.

Table 3.6: BFR proportion (%) recovered from rinsing chamber inner surfaces with various solvents after UoB sink effects experiment.

Analyte	Hexane:DCM (1:1)	Toluene	Methanol
α-HBCD	2.6	1.0	1.0
β-HBCD	1.0	0.3	0.5
γ-HBCD	1.8	<LOQ	<LOQ
BDE-47	38	<LOQ	<LOQ
BDE-85	32	6.3	2.2
BDE-99	41	5.8	2.5
BDE-100	41	5.1	2.4
BDE-153	30	5.9	2.5
BDE-154	43	9.6	4.8
BDE-183	5.6	<LOQ	<LOQ
BDE-209	4.3	<LOQ	<LOQ

3.3.1 Glass test cell and PTFE chamber coating

The mass balance experiments were repeated in a blown glass tube (20 cm length, 3 cm diameter, 140 cm³ cell volume) to compare loss to different material surfaces (stainless steel vs glass). The glass cell was set up the same way as the mass balance experiment in the UoB chamber, with a spiked GFF placed at the beginning of the cell and a PUF plug inserted at the end of the cell. Air was pumped through the cell with the Capex pump (10 L min⁻¹) and the cell heated in a hot water bath at 60 °C for 24 hours. Post experiment, the cell was cooled for 5 hours and the GFF, PUF and solvent rinses of the glass test cell were analysed. Similar losses were experienced with both the stainless steel chamber and glass test cell and the mean BFR recovery (%) from both the UoB chamber and glass test cell are listed in Table 3.6. Similar to the micro chamber, the surface area-to-volume ratio for the glass cell (1.4 m⁻¹) is higher than the UoB chamber (0.5 m⁻¹) so greater sink effect loss is expected. However, again this may be partially offset by the higher air change rate for this cell (4200 h⁻¹ c.f. 400 h⁻¹ for the stainless steel chamber). These factors combined with the different sorptive capacities of the two materials result in a similar percentage analyte loss between the two chambers and hence changing the chamber construction material to glass did not

reduce losses to sink effects. The glass test cell experiment was repeated at room temperature, 22 ± 1 °C, for 1 week with very similar losses observed to the heated test cell experiment and under both temperature scenarios the glass cell material did not improve BFR recoveries.

Coating the test cell inner surfaces with a polytetrafluoroethylene (PTFE) spray was explored in the glass cell, with the aim of removing active sites on inner surfaces and hence reducing absorption of BFRs to active sites. A common store purchased PTFE spray coating (WD40 PTFE High Performance Lubricant) was used to coat the inner surfaces of the glass test cell. The above mass balance experiment was repeated in the PTFE-coated chamber and post experiment, the GFF, PUF and chamber rinses were extracted and analysed. Again there was no improvement in analyte recovery from chamber walls, showing that coating the chamber inner surfaces with PTFE did not reduce the surface sorptive capacity. Mean BFR recoveries (%) are listed in Table 3.7.

Table 3.7: Mean (min, max) BFR analyte recovery (%) of heated chamber experiments from the UoB chamber (n=2), the glass test cell (n=2), the PTFE coated test cell (n=2) and the glass test cell at 22 °C (n=1)

Analyte	UoB chamber @ 60 ° C for 24h (n=2)	Glass test cell @ 60 ° C for 24h (n=2)	PTFE coated test cell @ 60 ° C for 24h (n=2)	Glass test cell @ 22 ± 1 ° C for 1 week (n=1)
α-HBCD	91 (86, 96)	82 (79, 84)	95 (93, 96)	82
β-HBCD	47 (42, 53)	35 (29, 41)	57 (53, 62)	63
γ-HBCD	36 (31, 41)	31 (23, 36)	54 (52, 56)	51
BDE-47	43 (27, 58)	27 (25, 28)	23 (12, 35)	42
BDE-85	83 (77, 90)	78 (77, 79)	63 (53, 73)	77
BDE-99	67 (66, 68)	62 (61, 62)	46 (37, 55)	72
BDE-100	55 (50, 61)	46 (45, 48)	36 (24, 48)	67
BDE-153	63 (58, 68)	92 (86, 97)	66 (62, 70)	96
BDE-154	53 (51, 55)	76 (70, 81)	49 (49, 49)	89
BDE-183	80 (74, 85)	92 (84, 100)	77 (76, 78)	92
BDE-209	110 (107, 120)	110 (87, 130)	85 (71, 98)	80

3.3.2 Post-experiment chamber heating

The study by Kemmlein et al. (2003) measured the emission of flame retardants from treated products in emission chambers, while noting analyte losses to sink effects in the chambers. In an attempt to recover the analytes lost to sink effects, the test chambers were heated to 80 °C, post experiment, and concentrations of BDE-47, 99 and 100 were detected on collection PUFs as a result of this heating step. In an attempt to improve analyte recovery from sink effects in the UoB chamber, this method was trialled post volatilisation experiment. New, pre-cleaned, PUF plugs were attached to the now empty chamber and the chamber was heated to 80 °C for 8 hours. Only low concentrations of BFRs were detected on the exit PUF, listed in Table 3.8, and still a large concentration remained unaccounted for. Higher post-experiment temperatures were avoided to prevent analyte degradation or thermal stereoisomerisation of HBCDs (Heeb et al., 2008).

Table 3.8: Mean (min, max) BFR analyte recovery (%) from post experiment chamber heating (n=2).

Analyte	80 °C heating (n=2)
α-HBCD	14 (9.6, 18)
β-HBCD	4.6 (1.6, 7.5)
γ-HBCD	16 (9.8, 22)
BDE-47	2.7 (1.3, 4.0)
BDE-85	12 (11, 12)
BDE-99	12 (12, 12)
BDE-100	7.5 (6.6, 8.2)
BDE-153	5.4 (4.7, 6.1)
BDE-154	8.8 (7.5, 10)
BDE-183	2.2 (1.3, 2.5)
BDE-209	<LOQ

3.3.3 Chamber solvent rinse vs chamber wipe and different chamber air flows

Different methods for recovering BFRs from the chamber inner surfaces were tested in the micro chamber. The BFR mass recovered from solvent rinses with

hexane:DCM (1:1 v/v) and from wiping all inner surfaces with solvent dampened tissue (hexane:DCM 1:1 v/v) were compared. Mean BFR recoveries (%) are listed in Table 3.9. There was no substantial difference in recoveries from the two methods and as solvent rinsing is easier in the much larger UoB chamber, this method was continued for further experiments.

Table 3.9: Mean BFR recoveries (%) ± SD from chamber solvent rinses and chamber wipes for n=3 replicates for HBCDs and n=1 for PBDEs

Analyte	Chamber solvent rinse	Tissue chamber wipe
α-HBCD	1.3 ± 0.9	2.0 ± 0.5
β-HBCD	0.3 ± 0.1	0.8 ± 0.2
γ-HBCD	<LOQ	<LOQ
BDE-47	<LOQ	<LOQ
BDE-85	3.2	3.2
BDE-99	3.9	2.8
BDE-100	3.8	3.1
BDE-153	3.6	3.3
BDE-154	4.5	3.9
BDE-183	3.0	3.0
BDE-209	<LOQ	3.2

The influence of varying air flow on analyte loss was also explored in the micro chamber, with experiments repeated at an air flow of 0.5 mL min⁻¹ (682 air changes per hour) and 0.25 mL min⁻¹ (341 air changes per hour). The volatilisation experiment was set up as previously described and the chambers heated to 60 °C for 24 hours, before GFFs, PUFs and chamber solvent rinses were extracted and analysed post experiment. There were very low total recoveries of the HBCDs, which may be due to sink effects in the longer polypropylene tubing of the chamber air exit line used for these trial experiments. As shown previously with the air train pathway length investigation in the UoB chamber, the polypropylene tubing can act as an effective sink for volatilised analytes. HBCD recoveries were slightly higher for the 0.5 mL min⁻¹ air flow with no discernible difference in PBDE recoveries, so experiments

were continued with 0.5 mL min⁻¹ air flow. The mean BFR recoveries (%) are listed in Table 3.10.

Table 3.10: Mean (min, max) BFR recoveries (%) from micro chamber experiments with different air flows (n=2)

Analyte	0.5 mL min ⁻¹ air flow (n=2)	0.25 mL min ⁻¹ air flow (n=2)
α-HBCD	37 (36, 38)	17 (15, 18)
β-HBCD	16 (15, 16)	5.7 (5.4, 6.1)
γ-HBCD	14 (12, 16)	5.4 (4.0, 6.8)
BDE-47	93 (92, 93)	60 (52, 68)
BDE-85	70 (64, 76)	60 (57, 63)
BDE-99	72 (71, 74)	65 (60, 70)
BDE-100	77 (75, 79)	60 (54, 66)
BDE-153	73 (69, 76)	69 (65, 73)
BDE-154	69 (69, 70)	70 (66, 74)
BDE-183	73 (71, 75)	72 (67, 77)
BDE-209	74 (74, 75)	81 (77, 86)

The experiments listed above that aim to recover analytes lost to sink effects, such as rinsing the chamber with various solvents, ‘wiping’ the chamber with dampened tissue, and heating the chamber post experiment, yielded minimal (if any) improvement in analyte recovery. The inability to recover the BFRs sorbed to chamber inner surfaces illustrates this effect is highly relevant when investigating emissions of SVOCs. To ascertain the full extent of sink effects of the stainless steel surfaces of the chamber, longer experiments (possible of the order of months) are required for attainment of steady state conditions inside the chamber, due to the slow emission rates and strong partitioning to chamber surfaces associated with SVOCs like BFRs (Xu et al., 2012). If steady state conditions are not reached, then gas phase emissions and the rate of partitioning to dust may be underestimated. Our investigations suggest that the UoB chamber is not constructed of low sorptive material and that over the experimental durations employed in this study, it is likely

that steady state conditions are not attained. Therefore, the results presented here are an indicator of the importance of sink effects when determining SERs of BFRs and studying their migration to dust, and of the factors influencing sink effects; rather than a detailed study of partitioning to chamber interior surfaces.

3.4 Partitioning to dust using a spiked GFF as the source

Initial experiments evaluating the partitioning of BFRs to dust following their emission to air were conducted in both the UoB and the micro chamber. In these experiments, a known mass of house dust (100-200 mg) was placed on a GFF on the chamber floor. Another GFF was spiked with standards of PBDEs (100 ng/analyte) and placed on the mesh shelf, separated from the dust (by 5 cm in the UoB chamber and 1 cm in the micro chamber), as the BFR ‘source’. To mimic operating conditions of electronic devices like PCs (Kemmlin et al., 2003), the chamber was operated at 60 °C for 24 hours; with the dust, GFF, and chamber surface rinses analysed post experiment. BFR partitioning to dust was observed in both chambers and Figure 3.4 shows the post experiment increase in PBDE concentrations in the dust. Data for the HBCDs and BDE-209 is not included as the UK house dust used in these initial experiments contained substantial concentrations of these analytes pre-experiment.

The incremental concentration detected post experiment in the dust is significantly greater ($p < 0.05$) than pre-experiment in the UoB chamber for all PBDEs except BDE-183. Conversely a significant difference ($p < 0.05$) was only seen for BDE-47, 85, and 100 in the micro chamber. The higher concentrations partitioned to dust in the UoB chamber is likely due to the lower air change rate resulting in increased contact time compared to the micro chamber. Conversely, in the micro chamber, a greater proportion of the target analytes appear on the PUF with a lower proportion remaining on the GFF, leading to the more consistent total recovery (%) between congeners than in the UoB chamber. The micro chamber appeared to be more efficient at promoting volatilisation of BFRs which were subsequently collected on the PUF, rather than partitioning to dust, due to the micro chamber’s comparatively higher air change rate (60% higher) and smaller volume. This also results in a shorter distance between the “source” and air outlet leading to greater analyte capture by the PUF. Table 3.11 lists

the mean BFR recoveries (%) from various compartments in the chamber experiment and Figure 3.5 plots the proportion of the BFRs recovered in the various components of each experiment, including the solvent chamber interior surface rinses.

Figure 3.4: Concentrations (ng g^{-1}) of PBDEs in dust, pre and post partitioning experiment in the UoB chamber ($n=3$) and micro chamber ($n=5$) using a spiked GFF as the source

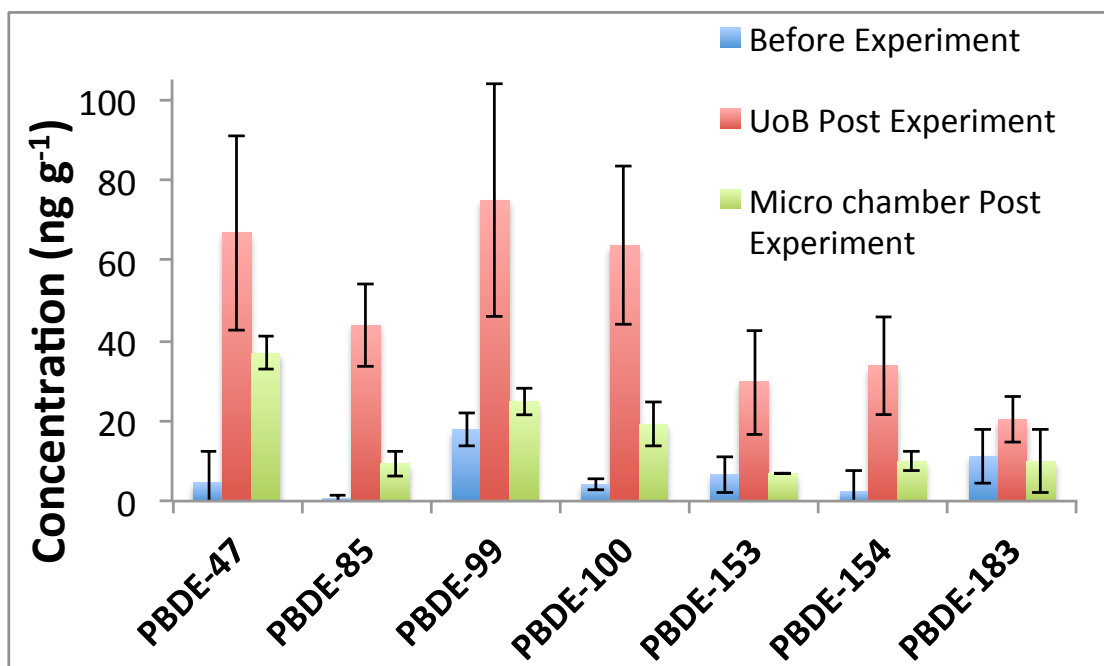
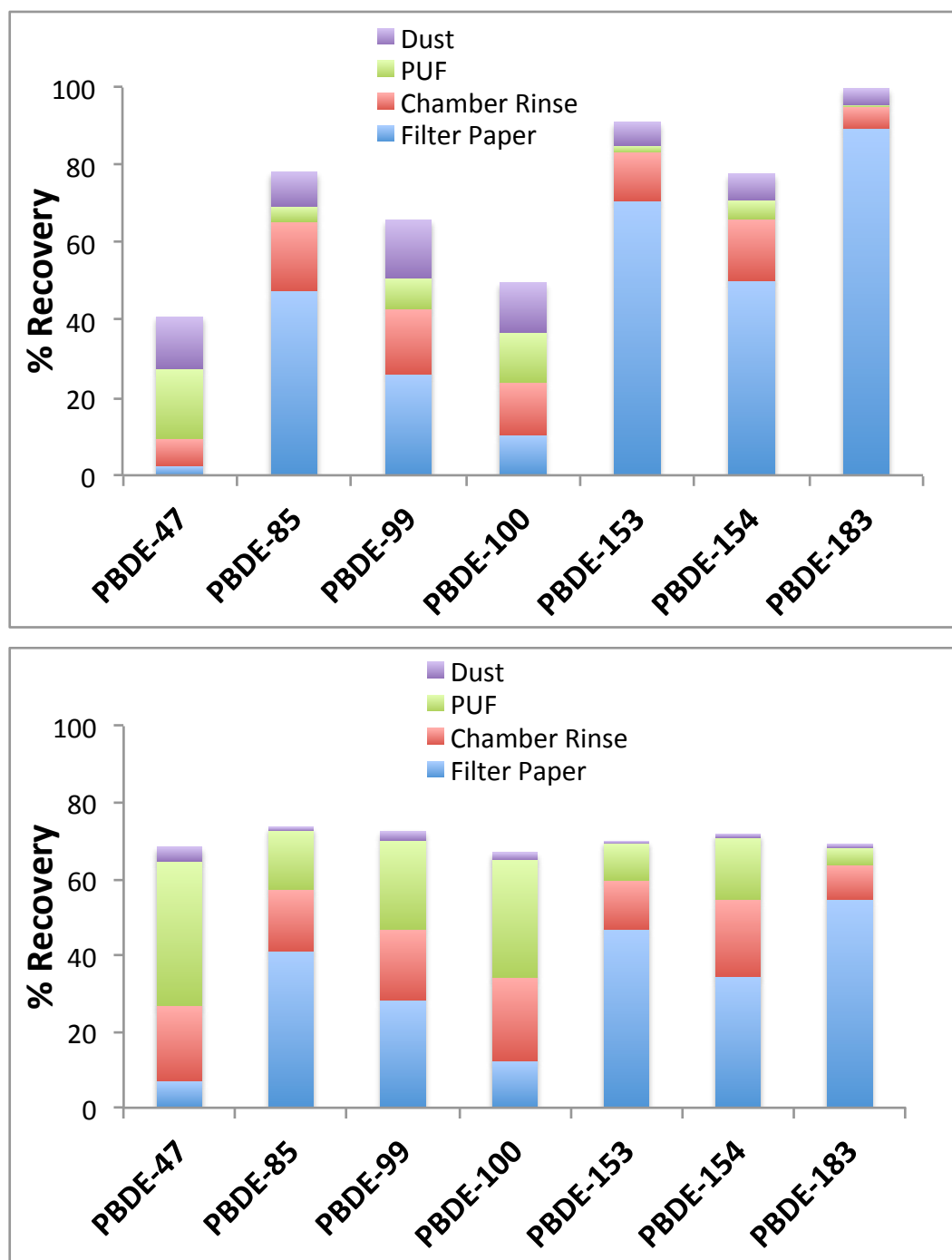


Table 3.11: Mean BFR recoveries (%) \pm SD, proportions recovered in various chamber compartments and dust concentrations (ng g^{-1}) for deposition to dust experiments in the UoB ($n=3$) and micro chamber ($n=5$)

Analyte	UoB Chamber (n=3)				Micro Chamber (n=5)			
	Chamber Rinse	GFF	PUFs	Dust (ng g^{-1})	Chamber Rinse	GFF	PUFs	Dust (ng g^{-1})
BDE-47	7.5 \pm 0.8	2.2 \pm 1.4	14 \pm 9.9	67 \pm 24	16 \pm 11	6.0 \pm 3.8	35 \pm 3.4	25 \pm 6.3
BDE-85	18 \pm 0.5	44 \pm 7.2	2.9 \pm 2.0	44 \pm 11	14 \pm 6.5	38 \pm 10	15 \pm 2.0	6.3 \pm 1.6
BDE-99	16 \pm 1.7	23 \pm 5.1	5.5 \pm 4.1	75 \pm 29	16 \pm 8.4	24 \pm 7.9	22 \pm 3.2	20 \pm 3.1
BDE-100	13 \pm 0.9	9.6 \pm 3.0	9.1 \pm 6.6	64 \pm 20	18 \pm 10	11 \pm 5.2	28 \pm 2.9	13 \pm 3.7
BDE-153	13 \pm 0.7	65 \pm 11	1.3 \pm 1.0	30 \pm 13	11 \pm 4.4	43 \pm 6.5	9.9 \pm 1.4	6.3 \pm 2.4
BDE-154	15 \pm 3.4	45 \pm 8.7	3.3 \pm 2.7	34 \pm 12	18 \pm 7.6	30 \pm 7.2	18 \pm 2.2	7.1 \pm 2.0
BDE-183	6.4 \pm 1.4	83 \pm 13	0.4 \pm 0.3	20 \pm 5.6	7.7 \pm 2.8	56 \pm 4.2	5.0 \pm 0.7	15 \pm 11

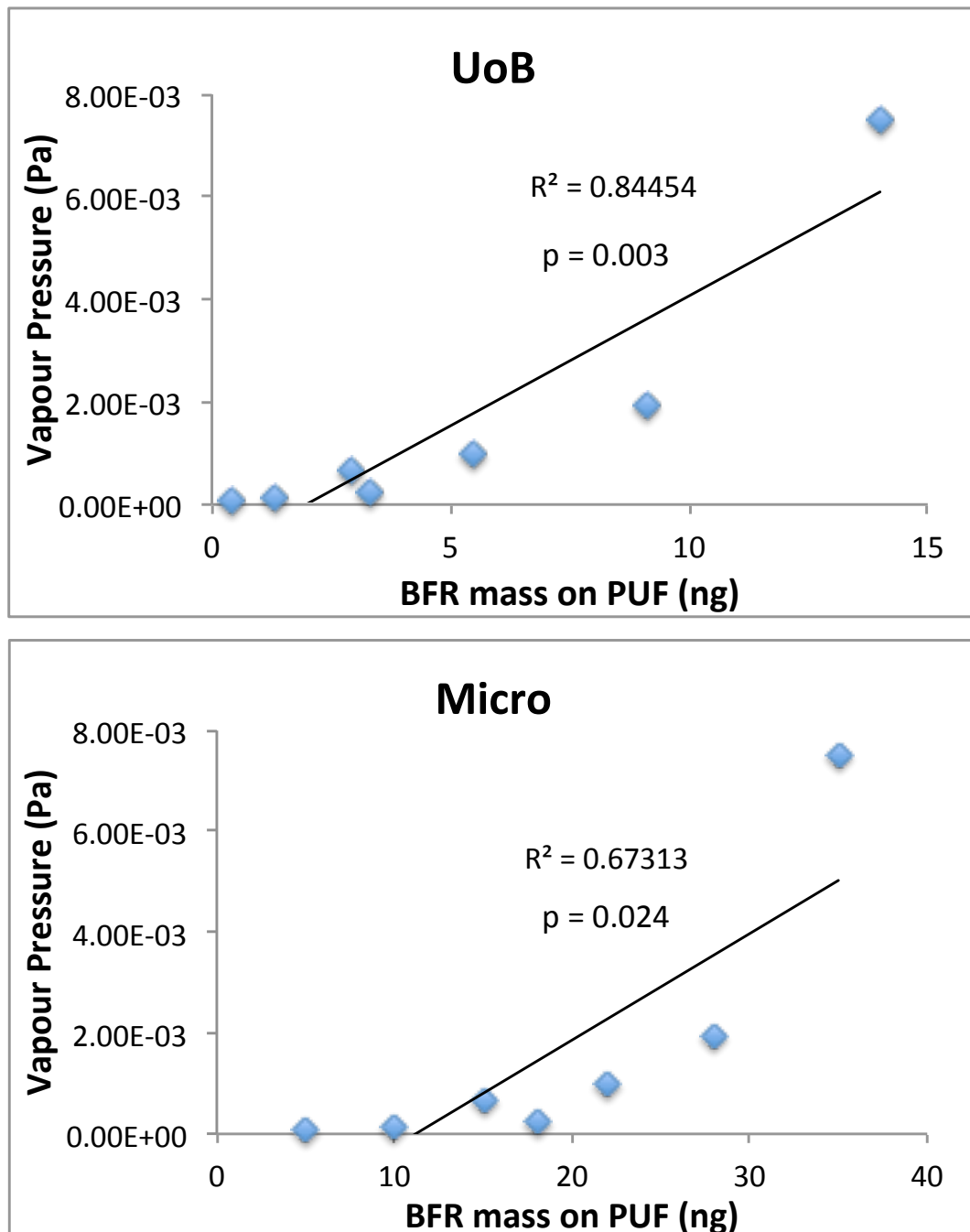
Figure 3.5: Mean recovery (%) of PBDEs in various components in (top) the UoB chamber (n=3) and (bottom) the micro chamber (n=6) using a spiked GFF as the source



Again the calculated vapour pressures at 60 °C for the PBDE congeners were plotted against the mass collected on the PUF plug. Figure 3.6 presents the data for BDE-47 to 183, from both the UoB and micro chambers showing the fitted trend line. A

significant positive correlation was again seen, for both chamber, with $r = 0.919$, $p = 0.003$ for the UoB chamber and $r = 0.820$, $p = 0.024$ for the micro chamber.

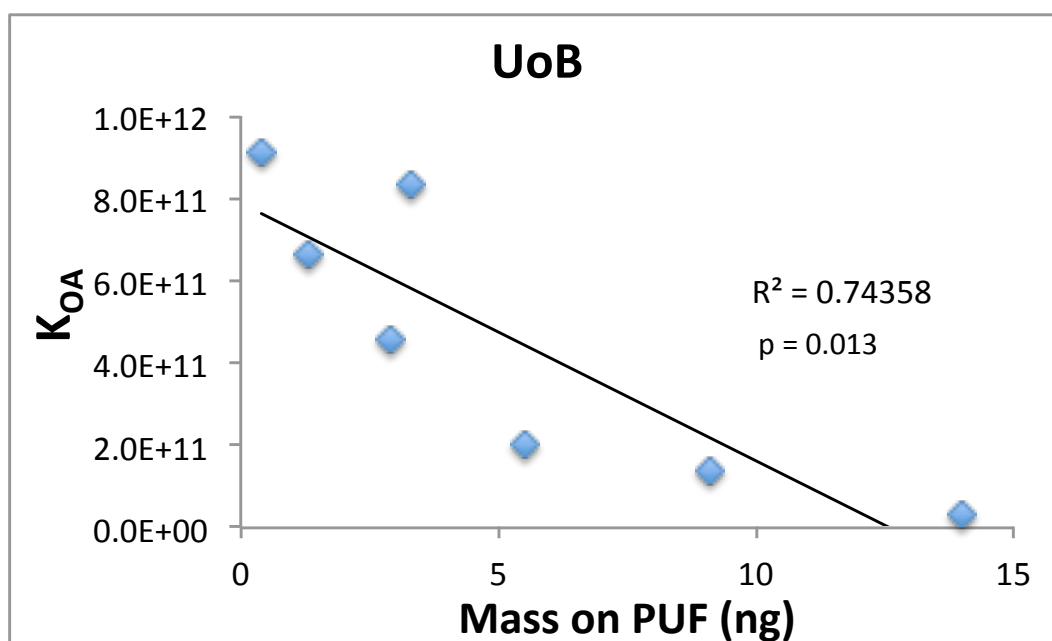
Figure 3.6: Graph of vapour pressure (60 °C) vs BFR mass on PUF for (Top) UoB chamber and (Bottom) micro chamber during partitioning to dust experiments

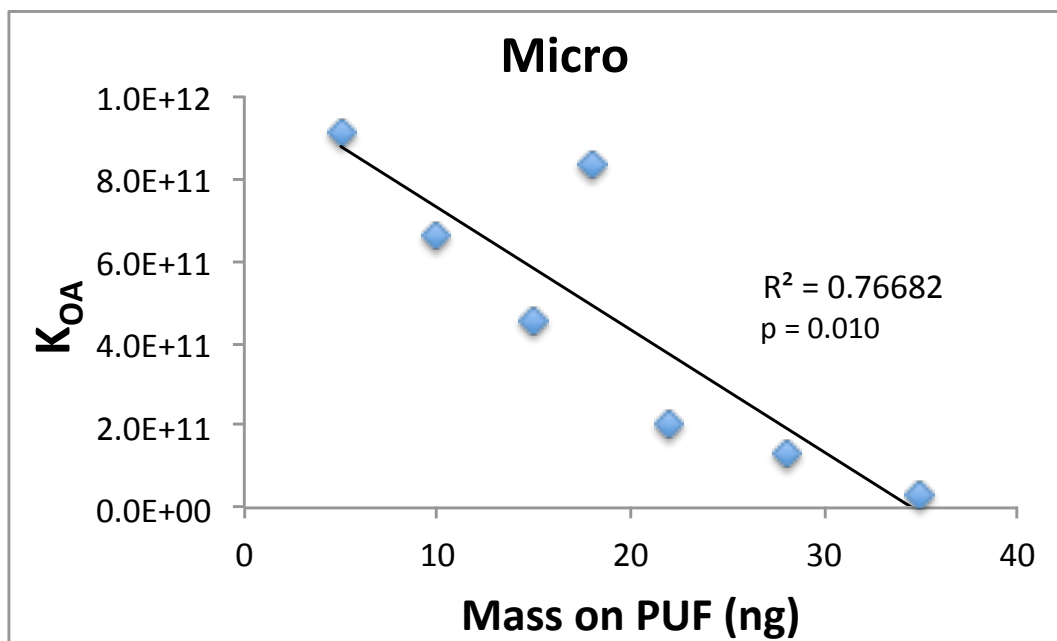


The PBDE mass on the PUF was also compared to the octanol:air partition coefficients (K_{OA}) for each congener (Harner and Shoeib, 2002) and a significant

negative correlation was seen for both chambers ($r = -0.862$, $p = 0.013$ for the UoB chamber data and $r = -0.876$, $p = 0.010$ for the micro chamber data). This trend shows that congeners with a higher K_{OA} (and higher level of bromination) have a reduced tendency to volatilise from the source and are thus present at lower concentrations in the air, and on the PUF. The correlation in both chambers illustrates that the behaviour of PBDEs in the chamber environment is strongly dictated by their physicochemical properties. Figure 3.7 plots the data for BDE-47 to 183 for both the UoB and micro chambers.

Figure 3.7: Graph of K_{OA} vs PBDE mass collected on PUF for (Top) UoB chamber and (Bottom) Micro chamber during partitioning to dust experiments





3.4.1 Chamber heated experiments with emission sampling every 24 hours

An elevated temperature chamber experiment was conducted over a longer experimental duration to assess the rate of collected emissions from a spiked GFF and to gain a measure of the chamber approaching steady state conditions in the chamber. The chamber experiment was set up as before, with a small GFF spiked with standards of PBDEs (100 ng/analyte) and 200 mg of dust placed on the chamber floor, before the chamber was heated to 60 °C. The PUF plugs were changed every 24 hours and retained for separate extraction and analysis. After 4 days, the chamber was cooled for 5 hours and the GFF, dust, all PUFs, and chamber inner surface solvent rinses were extracted and analysed. Mean BFR recoveries (%) in various chamber compartments, the PUFs sampled every 24 hours and concentrations in dust post experiment (ng g^{-1}) are listed in Table 3.12.

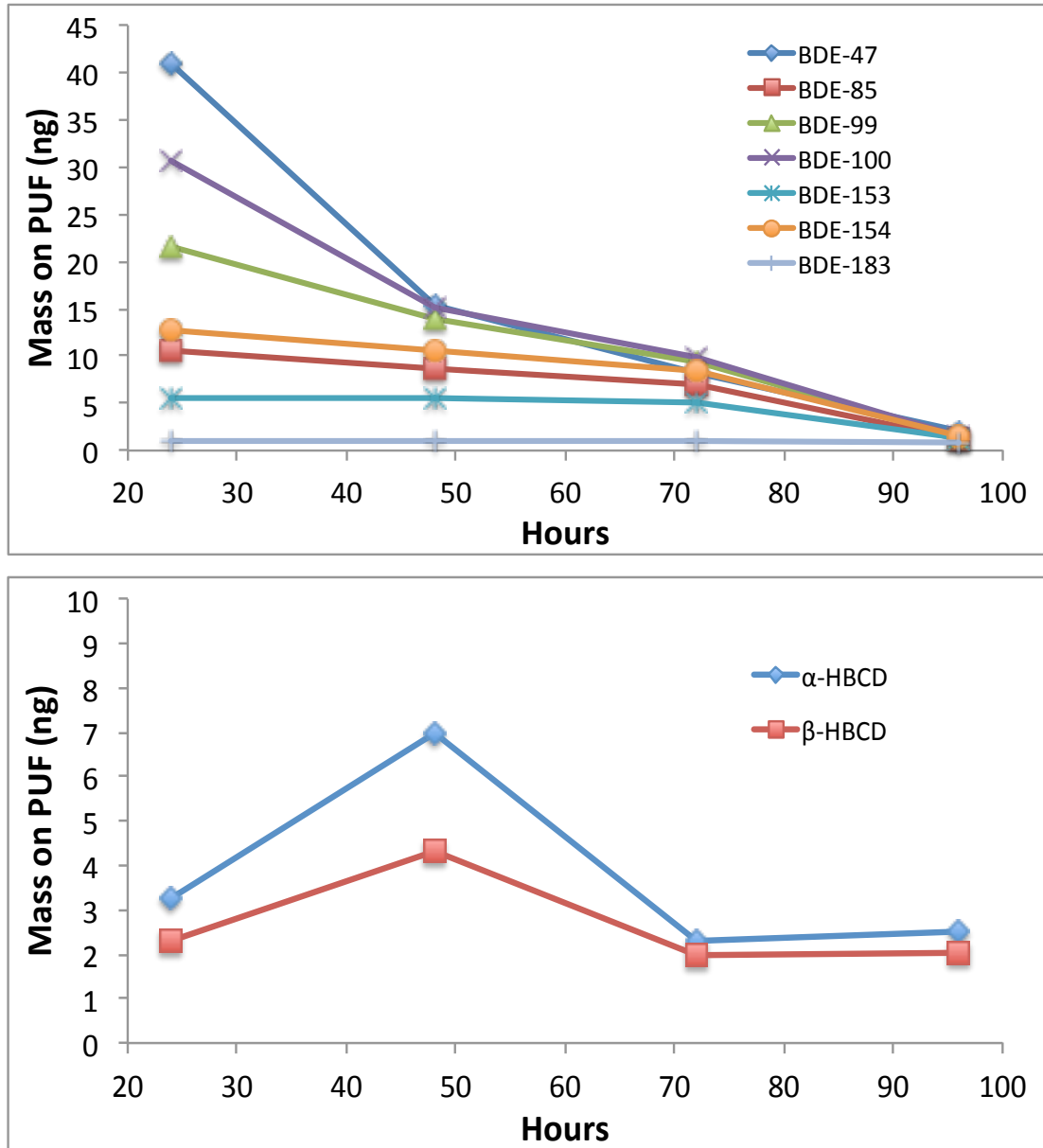
Table 3.12: Mean (min, max) BFR concentrations in dust (ng g⁻¹) and BFR mass (ng) on PUFs, GFF and chamber solvent rinse from extended chamber experiment at 60 °C (n=2)

Analyte	GFF (ng)	Dust (ng g ⁻¹)	Chamber Rinse (ng)	PUF 24 h (ng)	PUF 48 h (ng)	PUF 72 h (ng)	PUF 96 h (ng)
α-HBCD	81 (80, 82)	10.2 (8.5, 12)	<LOQ	3.3 (2.7, 3.8)	7.0 (6.7, 7.2)	2.3 (0.8, 3.8)	2.5 (1.4, 3.6)
β-HBCD	24 (21, 27)	2.3 (1.6, 3.0)	<LOQ	2.3 (1.3, 3.3)	4.3 (3.1, 5.6)	2.0 (0.3, 3.6)	2.0 (1.0, 3.0)
γ-HBCD	35 (18, 44)	16 (9.4, 23)	<LOQ	<LOQ	<LOQ	<LOQ	<LOQ
BDE-47	1.3 (1.2, 1.4)	4.2 (3.6, 4.7)	10 (9.5, 11)	41 (38, 44)	15 (12, 19)	8.2 (7.4, 9.0)	<LOQ
BDE-85	13 (6.0, 20)	3.2 (3.1, 3.2)	23 (19, 27)	11 (7.5, 14)	8.6 (7.3, 10)	6.9 (6.1, 7.7)	1.2 (1.1, 1.3)
BDE-99	5.7 (2.6, 8.7)	4.2 (3.5, 5.0)	22 (17, 27)	22 (15, 28)	14 (13, 15)	9.4 (9.3, 9.5)	1.5 (1.2, 1.7)
BDE-100	2.4 (1.4, 3.4)	3.5 (2.6, 4.5)	17 (14, 21)	31 (23, 38)	15 (15, 16)	9.9 (9.1, 11)	1.5 (1.1, 1.9)
BDE-153	31 (21, 40)	2.8 (2.4, 3.1)	23 (23, 24)	5.5 (4.1, 7.0)	5.6 (4.3, 6.8)	5.1 (4.1, 6.2)	1.3 (1.2, 1.4)
BDE-154	13 (7.0, 20)	2.9 (3.0, 3.2)	23 (23, 27)	13 (9.3, 16)	11 (8.9, 12)	8.4 (7.6, 9.2)	<LOQ
BDE-183	67 (59, 72)	2.3 (1.7, 2.9)	11 (7.6, 14)	1.0 (0.9, 1.1)	1.0 (0.7, 1.2)	1.0 (0.7, 1.3)	<LOQ
BDE-209	110 (90, 130)	<LOQ	<LOQ	<LOQ	<LOQ	<LOQ	<LOQ

Emissions of PBDEs reduce gradually over the experimental duration until at the experiment end, emissions are close to the method LOQs, and have either ceased or steady-state conditions are attained. Analysis of the GFF returned a measurable mass of “unemitted” PBDEs still present so the BFR ‘source’ remained throughout the experiment. This may suggest the chamber experiment is close to or at steady state. The less volatile congeners (BDE-153 and BDE-183) show a very low but steady release of the congeners with the majority still remaining on the GFF post experiment, and BDE-209 was not collected on the PUF, as expected. A constant release of the HBCD diastereomers was also observed, which is in line with the lower vapour pressures of these isomers, a similar range to BDE-153 and BDE-183.

According to literature reported vapour pressure (V_p) values, volatile emissions of PBDEs should be in the order BDE-47, 99, 100, 153, 154, 85, 183, 209 (Tittlemier et al., 2002, USEPA 2012c) however in this experiment, 100 shows greater emission than 99 and 154 greater emission than 153. This is consistent with all the chamber volatilisation experiments conducted, with greater mass of 100 than 99 and 154 than 153 collected on the PUFs. This observation again suggests there are limitations and uncertainty with calculated values of vapour pressure reported in the literature. For the HBCDs, only α - and β -HBCD were measured on the PUFs as γ -HBCD concentrations were below method LOQs. The α - and β -HBCD emissions show a similar slow yet steady release as BDE-153 and BDE-183, which is consistent with the similar reported vapour pressures in the literature of all four of these analytes. Figure 3.8 plots the PUF masses collected every 24 hours over the four day period for (a) PBDEs and (b) HBCDs, providing an estimate of BFR emissions over this time period.

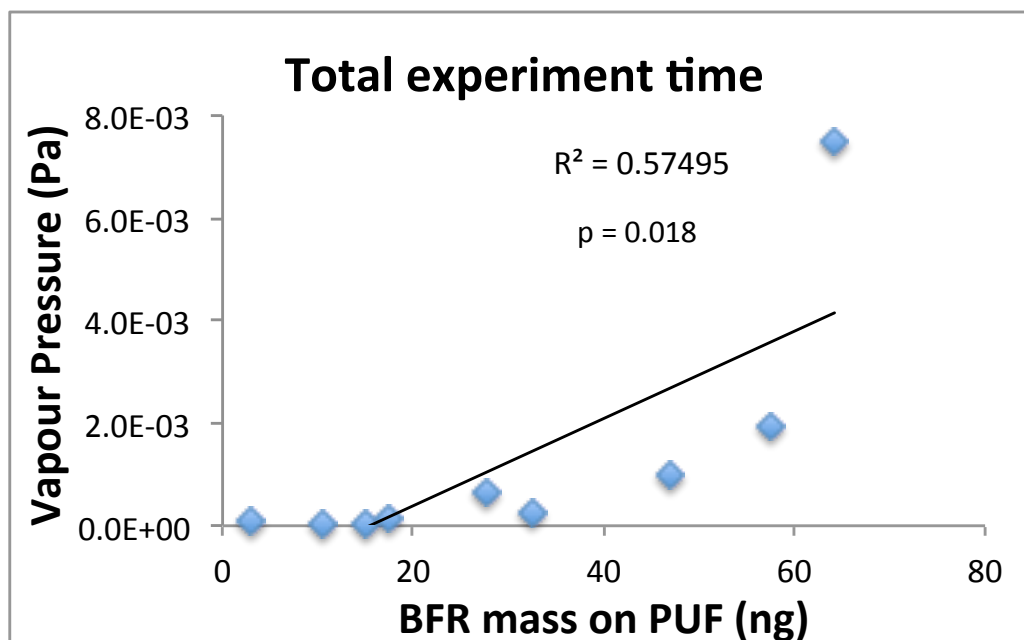
Figure 3.8: BFR mass (ng) collected on PUFs at 24 hour time intervals

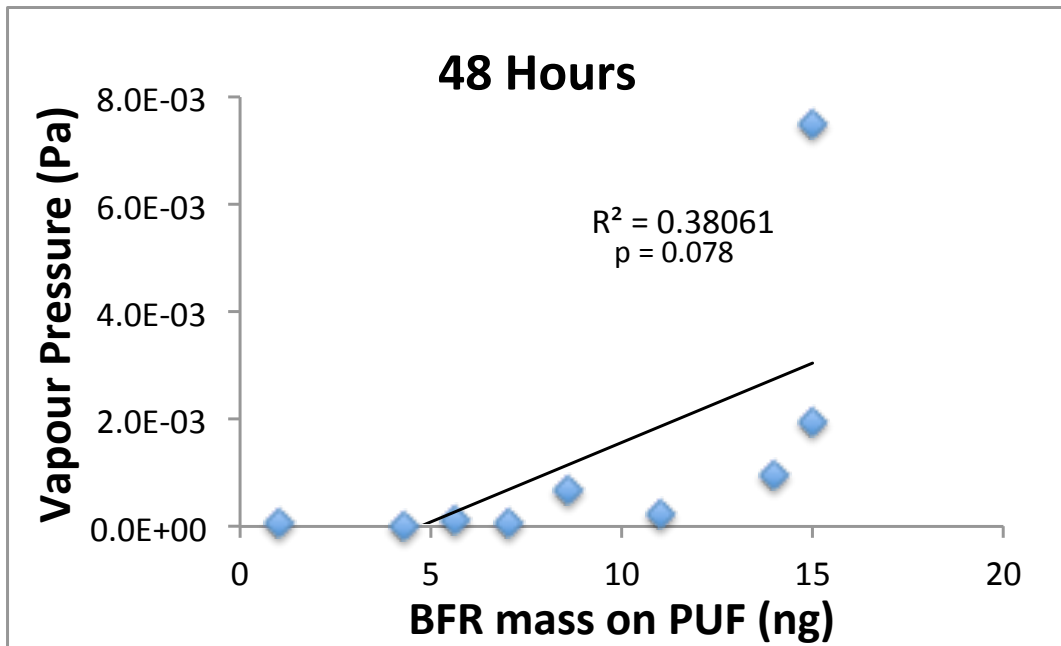
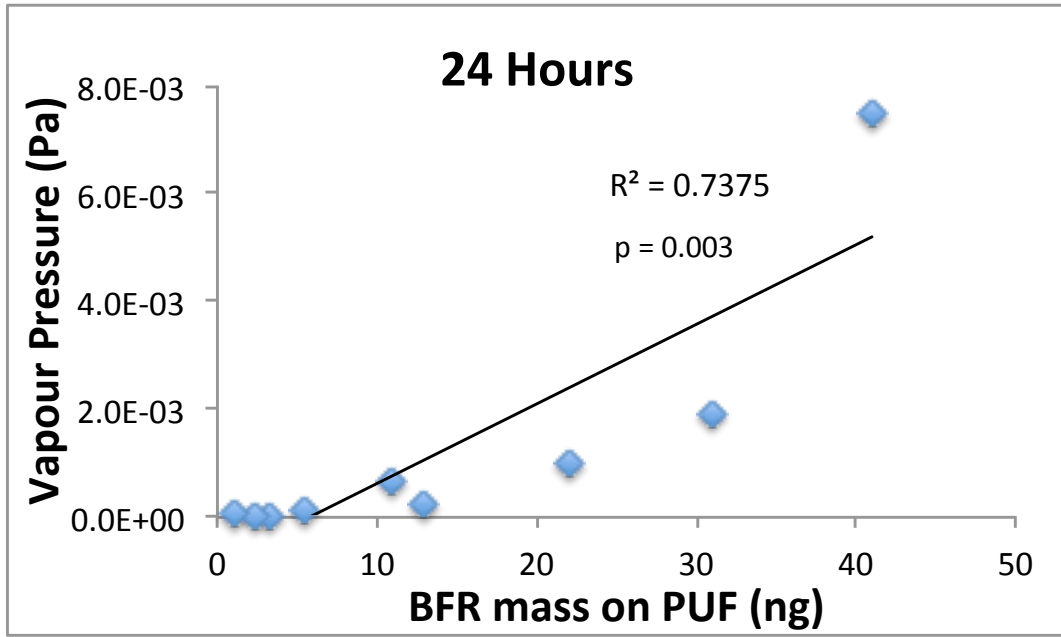


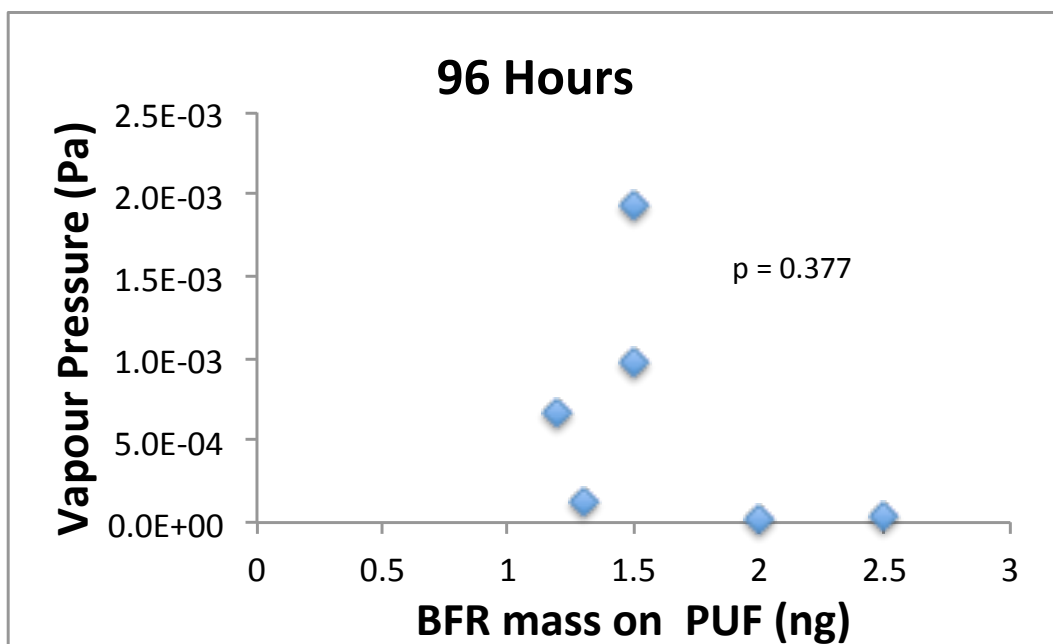
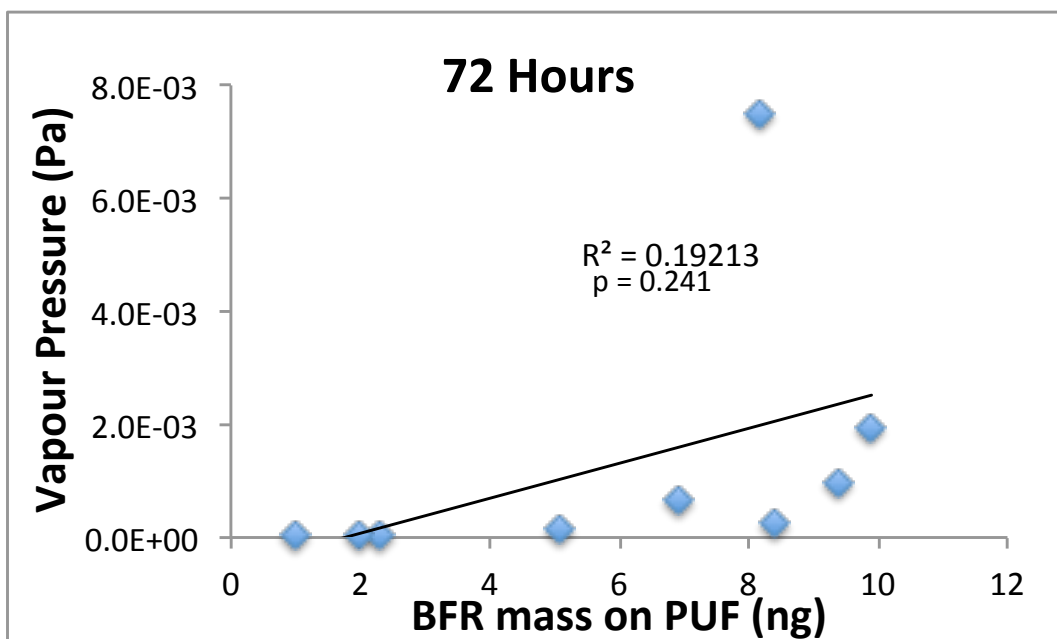
The vapour pressures at 60 °C were plotted against the BFR mass collected on the PUF at each 24 hour time period and for the total mass collected over the experiment. There was no trend line for the emission collected between 72 and 96 hours and the mass collected was either below or close to method LOQs due to lower emissions after this time period, lending greater uncertainties to these values. Figure 3.9 shows a plot of vapour pressure vs mass collected on the PUF for the total collected emission and at each 24 hour time period. The collection at 24 hours saw a significant correlation with vapour pressure ($r = 0.857$, $p = 0.003$) however the correlation

weakens over the duration of the experiment and a significant correlation was not seen for measurements at 48, 72 and 96 hours ($p = 0.078, 0.241$ and 0.377 respectively). As the experiment progresses the BDE-47 data point (the outlier above the line of best fit on each graph) is increasingly removed from the line of best fit, contributing to the decreasing significance of the correlation, and suggests the literature vapour pressure values for BDE-47 may have a large uncertainty associated with them.

Figure 3.9: Plotted vapour pressure vs total BFR mass collected on PUFs both over entire experiment and at various time intervals

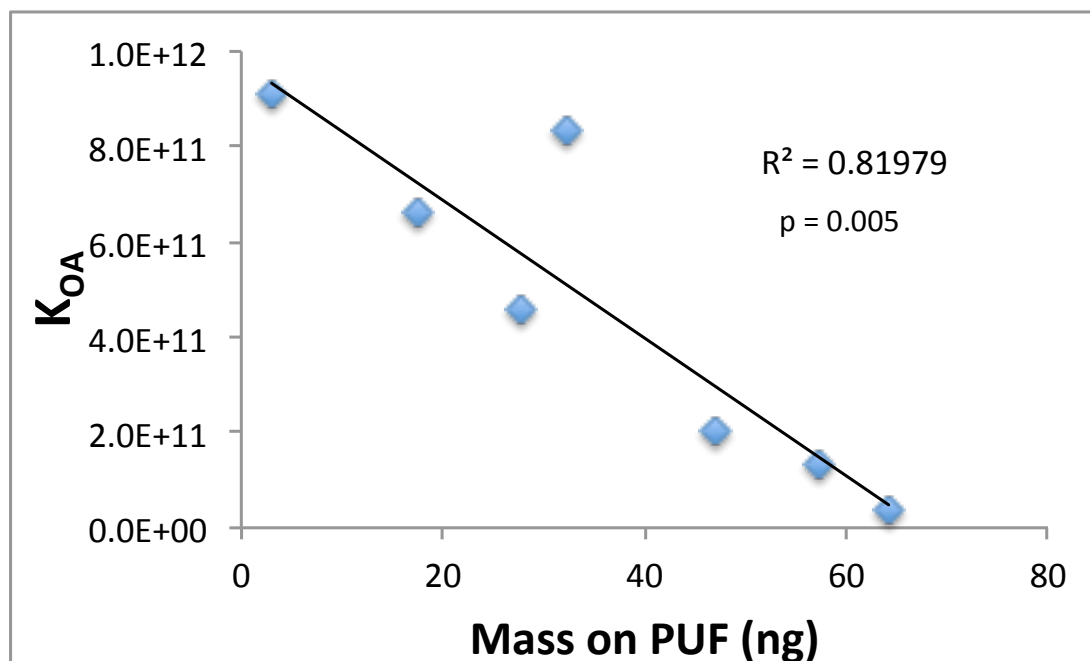






The mass collected on the PUF (from the entire experiment period) was compared to the literature K_{OA} values of PBDEs and a strong negative correlation was observed ($r = -0.906$ $p < 0.01$). Again the higher brominated congeners, with higher K_{OA} values, saw a smaller mass collected on the PUF suggesting lower volatile emissions from the source. The strong correlation illustrates that the behaviour of PBDEs in the chamber experiment is dictated by their physicochemical properties. Figure 3.10 plots the PBDE mass on the PUF against literature K_{OA} values.

Figure 3.10: PBDE mass collected on PUF plug (ng) over the entire experimental collection period vs literature K_{OA} values



3.5 HBCD partitioning to dust using HBCD treated curtains as the source

Following the initial experiments using spiked GFFs as the BFR “source”, partitioning to dust of HBCDs was investigated using a 2 x 2 cm square piece of HBCD treated curtain placed on the chamber shelf as the source. Initial experiments with the treated curtains were conducted in the UoB and micro chambers for 24 hours at 60 °C to promote volatilisation of the analytes. Further experiments in the UoB chamber were conducted at room temperature for 1 week, to better simulate ‘real-world’ conditions.

Tables 3.13, 3.14 and 3.15 list HBCD mass (ng) collected in the chamber solvent rinse, on the PUF and HBCD concentrations (ng g^{-1}) in the dust, for the UoB heated chamber, UoB room temperature and micro chamber heated experiments respectively. Substantial increases in HBCD concentrations in dust were observed in both scenarios, providing clear evidence of HBCD migration from the curtain to dust *via* volatilisation and subsequent partitioning, however only the 60 °C UoB chamber

experiment saw a statistically significant ($p < 0.05$) increase in dust concentrations post experiment. Figure 3.11 shows the pre and post experiment concentrations of HBCDs in dust for both temperature scenarios in both the UoB and micro chambers. Far greater variations in post experiment concentrations were observed in the micro chamber than those obtained under the same conditions using the UoB chamber. This may be due to the shelf location in the micro-chamber, as it is placed a short distance (1 cm) from the entering airflow. Also, the air change rate in the micro chamber is 60% higher resulting in a higher air velocity than in the UoB chamber. The resulting greater airflow turbulence to which the curtain sample was exposed in the micro chamber, is hypothesised to have caused abrasion of the curtain. This is supported by the detection post experiment of visible small fibres in the dust, highlighted in the image in Figure 3.12. Such abrasion was not reproducible and likely accounts for the more variable concentrations of HBCDs in the post experiment dust samples. The importance of an appropriate experimental configuration is clearly shown by these results with the UoB chamber being more fit-for-purpose for these highly specific experiments. It is also of note that the curtains tested were not obtained 'new' from the manufacturer, but had been stored at $-18\text{ }^{\circ}\text{C}$ for 2-3 years prior to testing. Other studies have reported that the age of the product tested can influence emissions of SVOCs, with emissions reducing significantly over time (Carlsson et al., 2000, Ni et al., 2007, Salthammer et al., 2003). Thus emissions from this small sub-sample may not be representative of this and similar materials generally.

Table 3.13: HBCD mass (ng) in different compartments and dust concentrations (ng g⁻¹) of UoB heated experiment (60 °C) for 24 hours (n=4)

	Chamber Rinse (ng)	PUF (ng)	Dust (ng g⁻¹)
α-HBCD	35 ± 17	34 ± 33	180 ± 52
β-HBCD	13 ± 7.3	7.0 ± 2.7	63 ± 3.8
γ-HBCD	46 ± 24	29 ± 22	370 ± 85

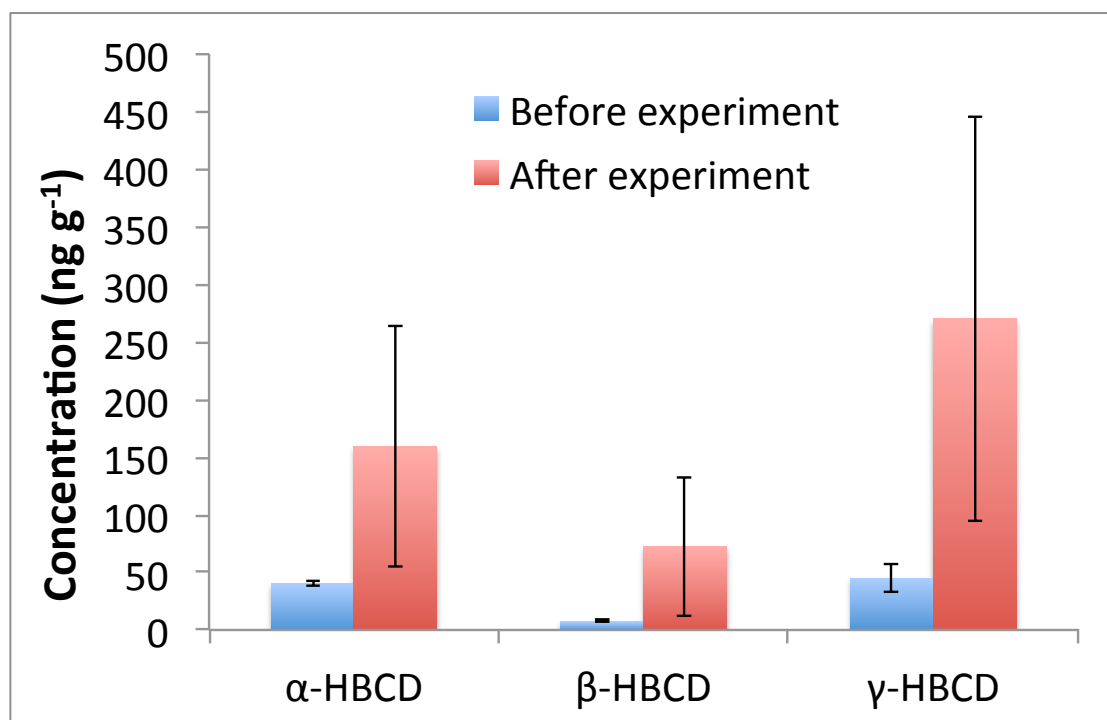
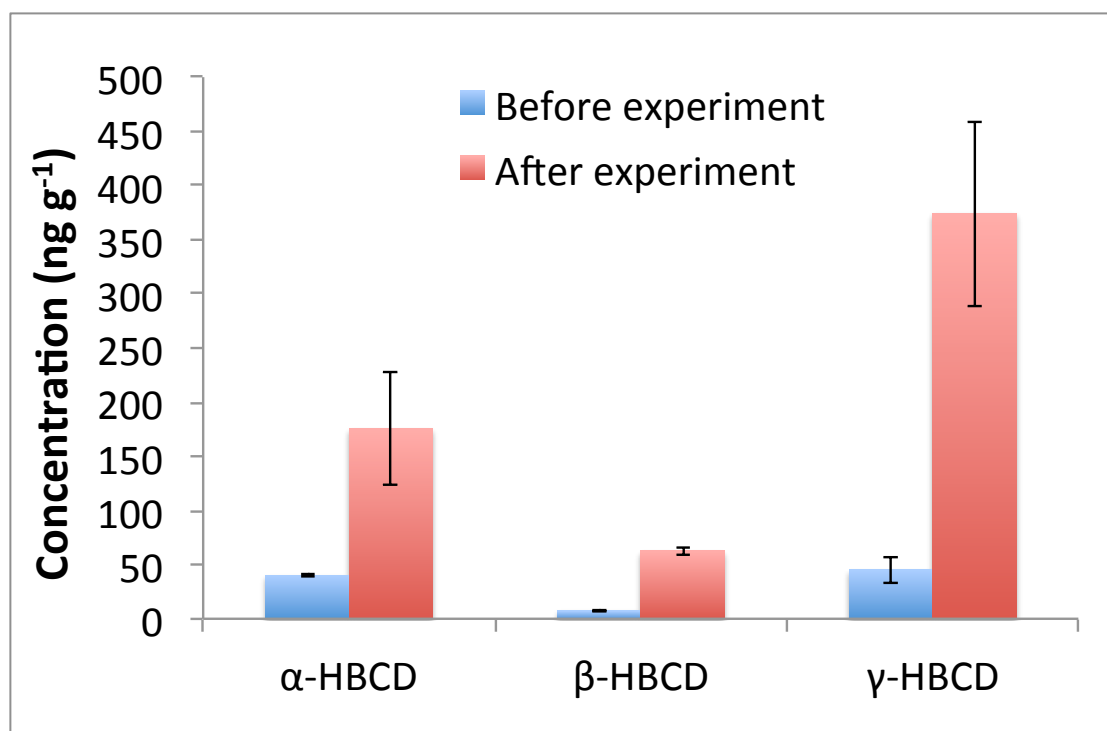
Table 3.14: HBCD mass (ng) in different compartments and dust concentrations (ng g⁻¹) of UoB room temperature experiment, 22 ± 1 °C, for 1 week (n=3)

	Chamber Rinse (ng)	PUF (ng)	Dust (ng g⁻¹)
α-HBCD	41 ± 31	43 ± 33	160 ± 100
β-HBCD	20 ± 18	19 ± 17	72 ± 60
γ-HBCD	83 ± 66	78 ± 69	270 ± 180

Table 3.15: HBCD mass (ng) in different compartments and dust concentrations (ng g⁻¹) of Micro chamber heated experiment (60 °C) for 24 hours (n=6)

	Chamber Rinse (ng)	PUF (ng)	Dust (ng g⁻¹)
α-HBCD	36 ± 8.1	10 ± 1.7	400 ± 380
β-HBCD	4.7 ± 1.0	0.6 ± 0.2	120 ± 120
γ-HBCD	7.6 ± 2.2	1.4 ± 0.2	240 ± 230

Figure 3.11: Concentrations of HBCDs in dust (ng g^{-1}) pre- and post-experiment using a HBCD-treated curtain as the source after: (top) 24 hours at 60 °C in the UoB chamber ($n=4$); (middle) 1 week at room temperature, 22 ± 1 °C, in the UoB chamber ($n=3$), and (overleaf) 24 hours at 60 °C in the micro chamber ($n=6$)



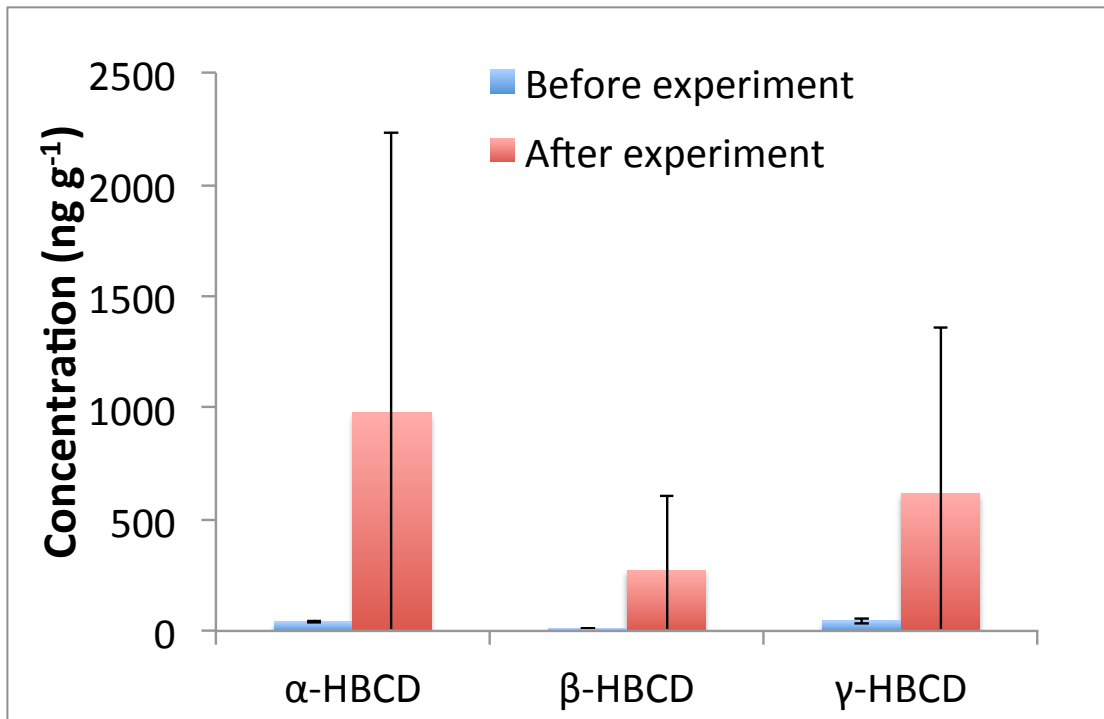


Figure 3.12: Image of a chamber dust sample post volatilisation experiment with HBCD treated curtains in the Micro chamber. Visible fibres present in the dust sample are circled.



3.6 Summary/Conclusions

Migration of HBCDs and PBDEs from source materials to dust *via* volatilisation and subsequent deposition was demonstrated for the first time in these test chamber experiments, confirming that this pathway is an important contributor to the concentrations of BFRs widely observed in indoor dust. Experimental evidence is provided that confirms sink effects are an important issue associated with chamber studies of BFRs. Moreover, this study demonstrates that chamber configuration, dimensions, and operating conditions can have a substantial influence on experimental outcomes, and that a thorough understanding of such factors is essential to facilitate correct interpretation of data generated by chamber studies. Notwithstanding these issues, the ease with which volatilisation from a source followed by deposition to dust can be reproduced in test chambers, both underlines the validity of this migration pathway, and the potential for similar chamber experiments to study the migration to dust of BFRs and other SVOCs from a range of source materials via this pathway.

CHAPTER 4

SIMULATING MIGRATION OF BFRs TO DUST VIA ABRASION AND VIA DIRECT CONTACT WITH BFR SOURCES

4.1 Summary

The different migration pathways responsible for BFR transfer from source to dust may provide one explanation of why studies report a large variation (over several orders of magnitude) in concentrations in indoor dust. The transfer of BFRs to dust via abrasion of particles or fibres from treated products has been suggested as one explanation for elevated concentrations (up to 210 mg g⁻¹, (Batterman et. al., 2009)) of low volatility BFRs such as BDE-209 detected in dust. In contrast, migration via direct contact between BFR containing sources and dust has attracted less attention in the literature. The UoB test chamber, already shown to successfully simulate migration of BFRs *via* volatilisation with subsequent partitioning to dust particles, was utilised to investigate migration via abrasion of particles/fibres and migration via direct transfer of BFRs between source and dust using modified experimental designs. Again migration of HBCDs from curtains treated with the HBCD formulation was investigated and HBCD migration to dust via both these pathways was successfully simulated resulting in highly elevated post-experiment concentrations of HBCDs in dust. The following chapter describes these experiments and their outcomes. An attempt to relate these experiments to ‘real world’ scenarios is provided as is an evaluation of the relative significance of HBCD migration to dust from fabrics via all three migration pathways.

4.2 Test chamber abrasion experiments

4.2.1 *Fibre abrasion to dust from HBCD treated curtain*

The test chamber was configured as described previously (Chapter 2, Section 2.1.4), with an aliquot of dust placed on the chamber floor and the mesh shelf positioned

3 cm above the dust. Abrasion of the HBCD treated textile curtain was induced using a stirrer bar as the abradant at room temperature, 22 ± 1 °C. A picture of the chamber configuration is shown in Figure 4.1.

Figure 4.1: Experimental configuration for chamber experiments evaluating abrasion of HBCD treated curtains

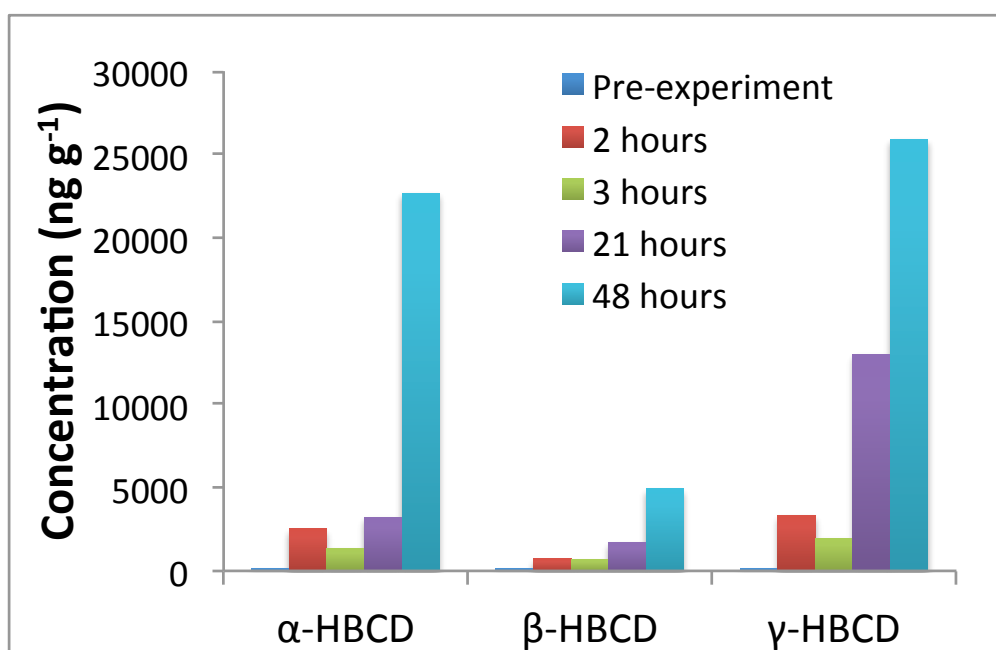


This induced abrasion in the test chamber was successful, with loosened fibres observed post experiment on the tested textile and in the dust on the chamber floor. The entire dust sample, including all abraded fibres, was extracted and analysed to determine concentrations of HBCDs in the dust. Air flow was applied to this chamber configuration for the duration of the experiment with HBCD emissions collected on PUFs. The PUFs, chamber solvent rinse and dust mass were analysed post experiment. The experiment was repeated for four different time periods (abrasion for 2, 3, 21 and 48 hours) for comparison. Figure 4.2 (a) shows the pre and post experimental concentrations of HBCD diastereomers in the dust for the four abrasion experiments, and (b) a scatter plot showing the linearity between concentration and experimental time period. In all experiments, there is a one to almost three orders of magnitude increase in concentrations of HBCDs in the dust post experiment, consistent with textile fibres (of high HBCD concentration) being incorporated into the dust.

An investigation of the relationship between abrasion time and concentration transferred to dust saw a linear relationship (r values ranging 0.93 to 0.99) with significant positive correlations for the β -HBCD and γ -HBCD diastereomers and Σ HBCDs ($p < 0.05$, $p < 0.01$ and $p < 0.05$ respectively), however a significant correlation was not determined for the α -HBCD diastereomer ($p = 0.065$). It was surprising to see a correlation between the HBCD concentrations and abrasion time frame as the abrasion was not thought to be a consistent process. However conclusions on a positive relationship should be treated with caution due to the small sample size (four experiments) and more experiments are required to increase confidence in this result. The lack of correlation for the α -HBCD diastereomer may be suggestive of a heterogeneous diastereomer distribution through the curtain, and combined with the variable nature of the abrasion process has provided a lack of significant correlation.

In a ‘real world’ scenario of abrasion of treated products in indoor microenvironments, ‘wear and tear’ of a product will not occur in a linear fashion and will depend on factors such as: the product material (e.g. plastic or textile), how and how often the product is used, its age and extent to which it is exposed directly to UV light or microbial contamination and consequent weathering.

Figure 4.2: (a) Concentration (ng g^{-1}) of HBCDs in dust pre and post abrasion



(b) Concentration ($\text{ng}\cdot\text{g}^{-1}$) vs abrasion time period for each HBCD diastereomer and Σ HBCDs with line of best fit for each data set

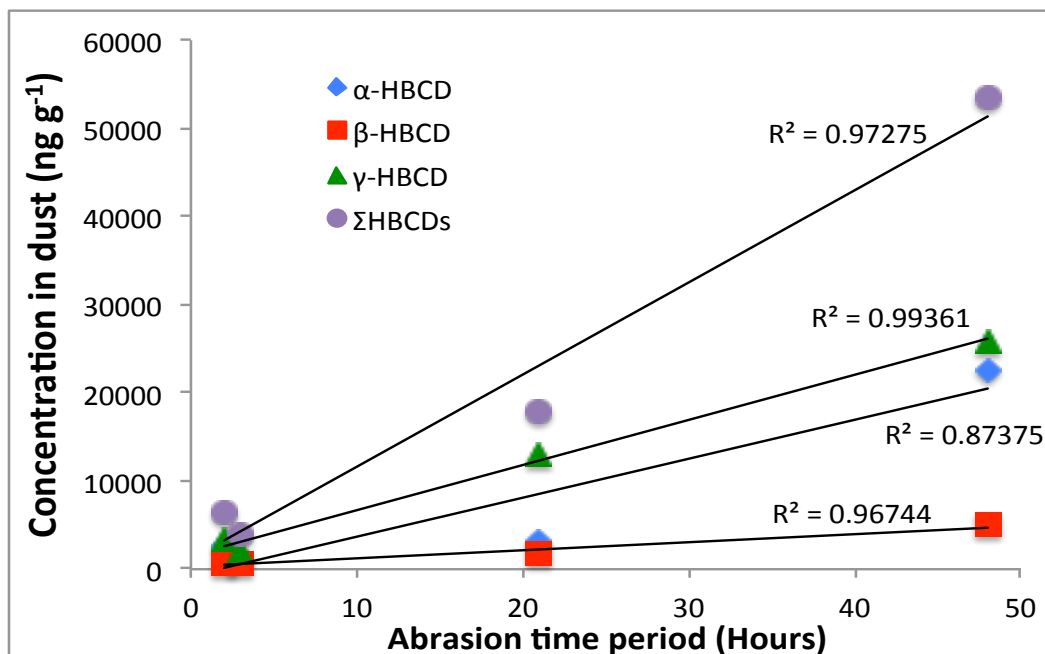


Table 4.1 lists the HBCD dust concentrations pre and post abrasion experiments as well as HBCD mass (ng) collected on the PUF plug and in chamber solvent rinses. A small mass of HBCDs was detected on PUF plugs in all four experiments, suggesting that even over the limited duration of these experiments (2 to 48 hours) volatilisation of HBCDs may still occur. The mass of HBCDs collected on the PUF during the 21 hour abrasion experiment at room temperature (178 ng Σ HBCDs) was in fact higher than that collected during the volatilisation experiment conducted for 1 week at room temperature (140 ng Σ HBCDs) or even for 24 hours at 60 °C (70 ng Σ HBCDs), Section 3.5, indicating volatilisation may be enhanced by the abrasion process. Abrasion of the textile (loosening and breaking textile fibres) increases the total source surface area, facilitating volatile emissions of the HBCDs from the source matrix, to be collected on the PUF. The presence of HBCDs on the exit PUFs may suggest that migration *via* volatilisation is still occurring in this scenario, albeit to a much smaller extent than *via* abrasion, also implying that in a ‘real world’ scenario, dust contamination is likely a result of a combination of different migration pathways. In addition, the exit PUFs may also collect fine fibres abraded from the textile source in this chamber set up, contributing to HBCD concentrations recovered on the PUF.

Larger, and less consistent, HBCD mass was detected in chamber rinses and this is likely due to very fine fibres, abraded from the curtain, attaching to chamber surfaces instead of falling into the dust mass and which are instead collected in the chamber solvent rinses. The ease with which abrasion can be replicated in these chamber experiments suggests this is a feasible migration pathway for the transfer of high concentrations of BFRs to dust.

Table 4.1: Concentrations (ng g⁻¹) of HBCD diastereomers in dust pre and post abrasion experiments and HBCD mass (ng) collected on PUFs and in chamber rinses for four experiment durations

		α-HBCD	β-HBCD	γ-HBCD
	<i>Pre experiment dust (ng g⁻¹)</i>	<i>46 ± 18</i>	<i>13 ± 10</i>	<i>50 ± 39</i>
Experiment 1 - 2 hrs	Dust (ng g ⁻¹)	2500	720	3300
	PUF (ng)	65	36	140
	Chamber Rinse (ng)	560	190	970
Experiment 2 - 3 hrs	Dust (ng g ⁻¹)	1400	700	2000
	PUF (ng)	6.9	2.8	10
	Chamber Rinse (ng)	4400	3400	20 000
Experiment 3 - 21 hrs	Dust (ng g ⁻¹)	3200	1700	13 000
	PUF (ng)	56	19	100
	Chamber Rinse (ng)	670	280	1600
Experiment 4 - 48 hrs	Dust (ng g ⁻¹)	23 000	4900	26 000
	PUF (ng)	13	4.1	6.8
	Chamber Rinse (ng)	300	130	410

4.2.2 Interpreting abrasion results in terms of a ‘real world’ scenario.

The abrasion induced in these test chamber experiments is highly intensive, so does not represent realistic abrasion from e.g. 48 hour use of a curtain. However, it is possible to extrapolate these results to reflect day to day use of such a textile. Also, the abrasion resistance of textiles is widely tested in industry with several methods used for this purpose and it was attempted to relate these methods to abrasion of the

HBCD curtain in the chamber experiments. In the industry test methods, abrasion is defined as the physical destruction of fibres, yarns and fabrics resulting from the movement of a textile surface over another surface. It can occur during wear, cleaning, use or washing processes that distort the fabric and cause fibres to be pulled out or remove fibre ends from the surface (Özdil et al., 2012). The measurement of abrasion of textiles is very complex and resistance to abrasion is affected by many factors such as mechanical properties and dimension of the fibres, structure of the yarns, construction of the fabrics and type, fineness, length, thread density, thread interlacing per unit area and amount of finishing material added to fibres, yarns or fabrics (ASTM, 2001, Özdil et al., 2012). Nylon is generally considered to have the highest abrasion resistance, followed by polyester (Özdil et al., 2012), which is the base polymer of the textile in these experiments, investigated further in Chapter 5. ASTM and ISO have several defined methods to quantify abrasion resistance of textiles, which can be divided into two groups. The flat abrasion methods that include the Martindale Tester, or ASTM D4966, and the Uniform Abrasion method, or ASTM D4158, work on the principle of measuring abrasion from flat objects rubbed on to flat materials. Flex or edge abrasion methods include the Oscillatory cylinder method, or ASTM D4157, and subject the material to bending or flexing and may better reflect usage conditions of apparel, furnishings and industry products as generally very little of these products surfaces are flat during use (Özdil et al., 2012).

The Uniform Abrasion method (which can test all types of fabrics) more closely resembles the chamber abrasion experimental design utilised in these textile experiments. In the Uniform method the sample is mounted in a holder and abraded uniformly in all directions in the plane and about every point of the surface of the specimen, where one abrasion cycle is one circular movement or rotation of the instrument (ASTM, 2001). The stirrer bar (abrader) in these chamber generated abrasion experiments spins at 200 revolutions per minute i.e. the equivalent of 200 abrasion cycles a minute in the Uniform Abrasion test, and extrapolating this to the 2 hour abrasion experiment, 24 000 abrasion cycles occur over the experimental test time. As the HBCD mass increment in the dust after the 2 hour abrasion experiment was 1 500 ng Σ HBCDs and the concentration in the original curtain was 43 000 ng g⁻¹ of Σ HBCDs; it can be calculated that the mass of curtain fibres in the dust was almost

35 mg. This method assumes that the HBCD concentration in the textile is homogeneous. A 2 x 2 cm square piece of sample textile was used in the chamber experiment, hence the curtain sample in the abrasion experiment for 2 hours suffered 24 000 abrasion cycles, which abraded 35 mg of fibres, from a 2 x 2 cm square piece of fabric.

These results may also be interpreted in a more realistic time use scenario. As the intended use of the textile studied is as curtains then perhaps 5 to 10 seconds of curtain movement (abrasion) occurs per day. The curtain area to suffer the greatest abrasion would be that in direct contact with a hand that grabs the curtain to pull it open and closed. This would roughly equate to a 4 x 4 cm area, per curtain, and abraded mass per curtain would be 140 mg, contaminating the dust with 5 900 ng of Σ HBCDs. Therefore, two hours of abrasion equates to 720 to 1440 days of curtain use, which abrades 140 mg of fibres per curtain into the dust, contaminating the dust with 5 900 ng of Σ HBCDs over this time period. Loss of 140 mg of fibres over a 2 year period is a realistic figure and this mass (and dust HBCD contamination) would be higher with increased use of the curtain e.g. vacuuming/cleaning the material and with increased fabric age as the textile structure starts to degrade. Estimated use and abraded mass scenarios for each abrasion time frame are listed in Table 4.2.

BFR treated textiles may be used in other products where more extensive daily contact is expected and the results from the HBCD treated curtain experiments can be extrapolated to provide an indication of abrasion from other use scenarios. For instance BFR treated fabrics are used for office chairs and couch coverings and will experience greater use per day than a curtain. An office chair may experience a maximum of 7 hours use a day, with moving on and off and within the chair causing friction and hence abrasion of the material. The average daily time period for watching TV for a UK resident was 4 hours in 2011 (OFcom, 2014), hence a couch in front of a TV set would experience a maximum of 4 hours of abrasion per person per day (in most cases abrasion would be less, depending on how still the occupant is during couch use). The 48 hour chamber abrasion experiment can be related to these scenarios, equating to almost 7 days of office chair use or 12 days of couch use with

each scenario contributing ~14 000 ng of Σ HBCD mass (per 2 x 2 cm abraded area), or 330 mg of fibres to indoor dust.

There are many uncertainties associated with these calculations, with the primary assumption that abrasion from a stirrer bar represents all 'real world' abrasion scenarios. This is not the case as abrasion or general fabric degradation will not be uniform and can occur from wear of the fabric, abuse (punishing environments, excessive contact with other objects), inappropriate application, seam slippage, cleaning and microbial degradation (ACT, 2011). Abrasion will also depend on factors such as the product material (e.g. plastic or fabric), how and how often the product is used, as well as its age and extent to which it is exposed directly to UV light and consequent weathering.

However, results from the various available industry abrasion tests have also shown a lack of consistency in tests with opposing results reported from different instruments (Somogyi Škoc and Pezelj, 2012, ACT, 2011), different laboratories and operators (ASTM, 2001), and even from the same sample with the reliability of the testing process becoming increasingly unreliable as the number of abrasion cycles increases (ACT, 2011). This lack of consistency from industry abrasion test methods makes relating the results from the abrasion chamber experiments to abrasion test measurements very difficult. Overall, abrasion is a problematic process to simulate and describe; however, this study adds to the weight of evidence suggesting that abrasion of BFR-treated fabrics can make a substantial contribution to BFR contamination of indoor dust.

Table 4.2: Estimated ‘real world’ curtain abrasion and subsequent dust contamination scenarios, extrapolated from abrasion experiment results, and other treated fabric scenarios

Experiment Time (Hours)	Abrasion cycles	ΣHBCD mass increment (ng)	Fibre mass in dust (mg per 2 x 2 cm area)	Time of related curtain use (days) – assuming 10 sec use per day
2	24 000	1500	35	720
3	36 000	1000	24	1100
21	250 000	4400	100	7600
48	580 000	14 000	330	14 000
				Time of related <i>office chair</i> use (days)
48	580 000	14 000	330	6.9
				Time of related <i>domestic couch</i> use (days)
48	580 000	14 000	330	12

4.3 Migration of HBCDs *via* direct contact between source and dust

The test chamber experimental design was again modified to investigate migration *via* direct contact between the BFR treated source and dust. A large piece of HBCD treated curtain (3 x 7 cm) was placed in the chamber with a mass of dust (~0.5 g) thinly layered directly on the top surface of the curtain and the chamber was sealed. Fresh textile samples were used for each experiment and samples were kept refrigerated at 4 °C before use. Air flow was excluded from these experiments as covering the curtain surface with dust artificially reduces the emission rate from the source surface, as reported by Schripp et al. (2010), hence emission estimates were not required for this experiment. Also, air flow was excluded to prevent unwanted

disturbance to the dust due to air movement across the sample surface. In a ‘real world’ scenario, air disturbance is likely with air currents across a product surface experiencing diurnal changes, disturbing the dust on textile curtains with movement of the fabric. Despite this, air flow was excluded to study the scenario of highest mass transfer via the direct contact migration pathway i.e. undisturbed dust on a source. The chamber was again kept at room temperature, 22 ± 1 °C, to discourage volatilisation, and to keep the migration via direct contact the primary pathway in this experiment. Figure 4.3 shows a picture of the chamber set up.

Figure 4.3: Chamber experimental configuration for studying direct contact of HBCDs from a treated curtain to dust



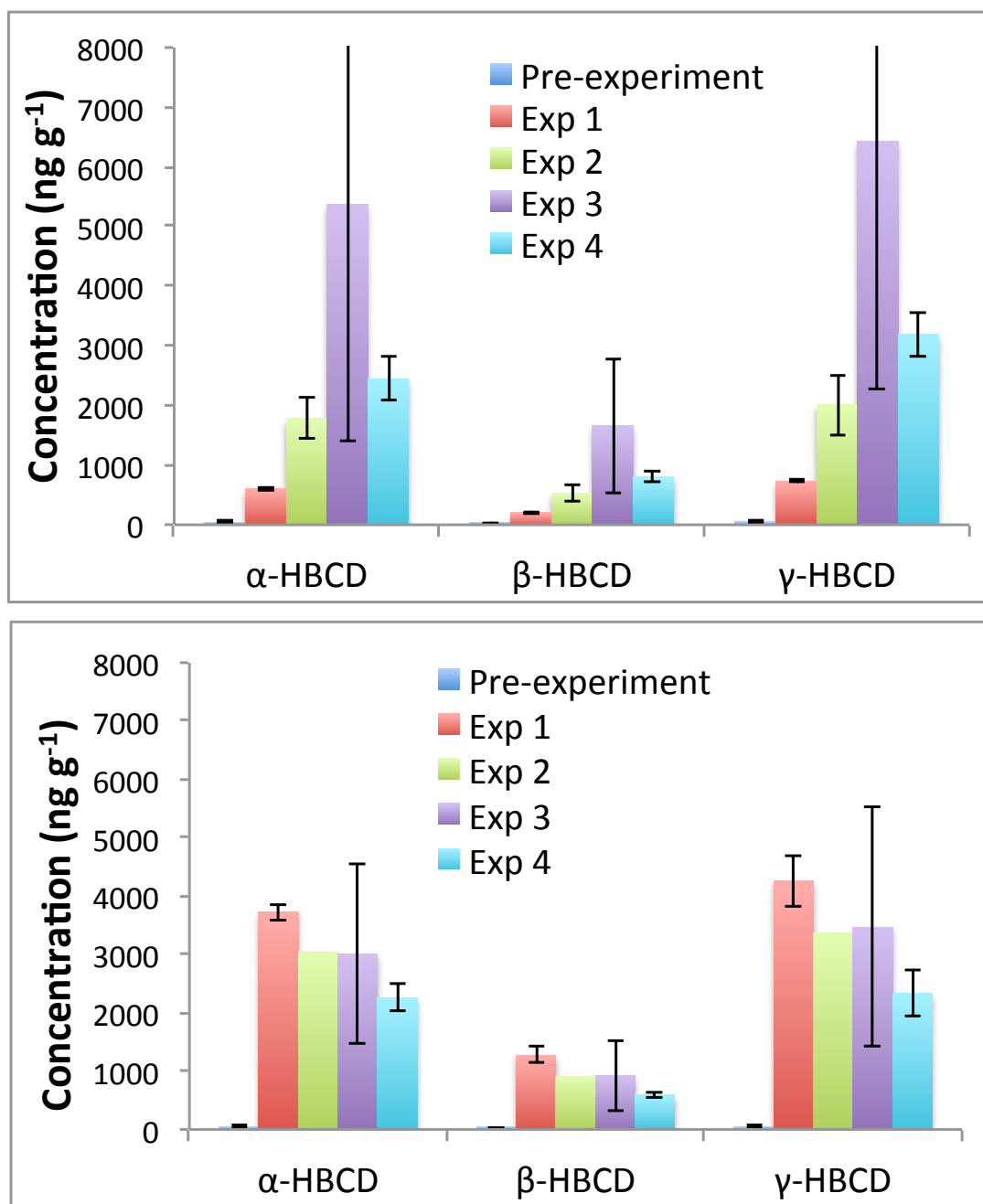
Two different experimental time frames were evaluated; 24 hours (n=4) and 1 week (n=4), and post experiment the dust was collected and vortex mixed before 2 subsamples from each collected dust mass were extracted and analysed for HBCD concentrations. The dust was collected by gently brushing it off the curtain, attempting to avoid removal of textile fibres into the dust. Clausen et al. (2004) investigated the direct transfer of DEHP from treated PVC pieces to dust and suspected that their dust collection process of vacuuming the dust off the source surface abraded PVC particles treated with DEHP into the dust, artificially increasing

DEHP concentrations in the final dust sample. Hence in these experiments, dust collection was as gentle as possible to exclude/minimise any abrasion of fibres into the dust sample. As stated, fresh textile pieces were used for each experiment so any variation in HBCD concentrations between textile pieces (due to heterogeneity of HBCDs throughout the sample) will influence the mass transferred to the dust aliquot. Mean HBCD diastereomer concentrations in the dust (ng g^{-1}) for experiments of the two time periods are listed in Table 4.3. Figure 4.4 plots HBCD concentrations (ng g^{-1}) in the dust in four replicate experiments conducted for: (top) 24 hours and (bottom) 1 week.

Table 4.3: Mean and (min, max) concentrations (ng g^{-1}) of HBCDs in dust from direct contact experiments conducted for 24 hours and 1 week

		α -HBCD	β -HBCD	γ -HBCD	Σ HBCDs
<i>Pre experiment dust (ng g^{-1})</i>		46 ± 18	13 ± 10	50 ± 39	110
24 hours	Experiment 1 (n=2)	600 (580, 630)	200 (190, 210)	730 (730, 740)	1500 (1500, 1600)
	Experiment 2 (n=2)	1800 (1500, 2000)	530 (430, 630)	2000 (1700, 2400)	4300 (3600, 5000)
	Experiment 3 (n=2)	5400 (2600, 8200)	1700 (860, 2500)	6400 (3500, 9400)	14 000 (6900, 20 000)
	Experiment 4 (n=2)	2500 (2200, 2700)	800 (750, 860)	3200 (2900, 3500)	6500 (5900, 7000)
1 week	Experiment 1 (n=2)	3700 (3600, 3800)	1300 (1200, 1400)	4300 (4000, 4600)	9300 (8800, 9800)
	Experiment 2 (n=1)	3000	910	3400	7300
	Experiment 3 (n=2)	3000 (1900, 4100)	920 (500, 1400)	3500 (2000, 4900)	7400 (4400, 10 000)
	Experiment 4 (n=2)	2300 (2100, 2400)	590 (560, 620)	2300 (2100, 2600)	5200 (4700, 5600)

Figure 4.4: Mean concentrations (ng g^{-1}) of HBCDs in dust, pre and post direct contact experiments for (top) 24 hours and (bottom) 1 week exposure. Error bars indicate deviation in repeat analyses



In all repeat experiments, and over both experimental durations, a clear increase in concentrations of HBCDs in dust was observed. There was no substantial difference in measured concentrations after 1 week (5200 to $9300 \text{ ng g}^{-1} \Sigma\text{HBCDs}$), compared to the 24 hour experiments (1500 to $14\ 000 \text{ ng g}^{-1} \Sigma\text{HBCDs}$), with an independent samples T-test returning p values of 0.661 to 0.820 for each diastereomer. Thus this

result suggests that the majority of the mass transfer occurs rapidly and reaches a saturation point during these experimental durations. This transfer is governed by the fugacity of the different phases for HBCDs. The fugacity of a chemical is a measure of its chemical potential in a particular phase (e.g. air, water, solid). When the fugacity of two phases that are in contact are equal, the system is in equilibrium and there is no net mass transfer between phases. However, if the fugacities are unequal, the chemical will transfer from the phase in which its fugacity is higher, to that in which it displays lower fugacity. The difference between the fugacity of the phases in contact is referred to as the fugacity gradient and the stronger the fugacity gradient, the faster the mass transfer between phases (Werth, 2005). Hence the contact between solid phases with a large fugacity gradient will see rapid mass transfer, as observed in these experiments. The fugacity of a chemical in dust is primarily related to the fraction of organic carbon in the dust (Zhang et al., 2009) and as HBCDs are highly hydrophobic they will sorb more strongly to matrices with higher organic carbon content (Abdallah et al., 2012, Yu et al., 2012). Due to this, the fraction of organic carbon will be a limiting factor to total mass uptake. Experimentally, Schripp et al. (2010) have reported a weak correlation between the uptake of di-n-butyl phthalate, DnBP, (another SVOC) and the organic content of the receiving matrix.

An estimated calculation of fugacity capacities (Z) of the dust and the polyester textile can be made to provide an indication of the fugacities of the two matrices and a description of HBCD mass flow. Fugacity capacities are the ratio of the fugacity of a chemical (F) in a matrix and the chemical concentration (C) in that matrix, Equation 4.1.

$$Z \text{ (mol.m}^{-3}\text{.Pa}^{-1}) = C \text{ (mol.m}^{-3}) / F \text{ (Pa)} \quad (4.1)$$

Soil and dust are similar matrices, hence the equations for calculating the fugacity capacity of soil are used here to estimate that for dust (Z_{DUST}). As stated previously, the fugacity of HBCDs in a particular phase will be strongly dependent on its organic carbon content and, as in the mass balance model by Harner et al. (1995), the fugacity capacity of a chemical in organic carbon (Z_{OC}) is calculated as the product of the

organic carbon to water partitioning coefficient (K_{OC}) and the fugacity capacity of water (Z_W) for that chemical, as in Equation 4.2.

$$Z_{OC} = K_{OC} \times Z_W \quad (4.2)$$

The K_{OC} of HBCDs is estimated at 1.25×10^5 (EC, 2011) and Z_W is calculated via Equation 4.3 where H is the Henrys Law constant for HBCDs ($4.7 \text{ Pa}\cdot\text{m}^3\cdot\text{mol}^{-1}$) (EC, 2011).

$$Z_W = 1/H \quad (4.3)$$

Hence the Z_{OC} for HBCDs in organic material is calculated as $2.66 \times 10^4 \text{ mol}\cdot\text{m}^{-3}\cdot\text{Pa}^{-1}$.

According to Harner et al. (1995), the fugacity capacity of the soil or dust is a sum of the chemical fractions in air, water, organic carbon content and mineral content. To simplify these equations and because the fraction of organic carbon (f_{OC}) present will be the most influential factor for these highly hydrophobic compounds, the air, water and mineral contents were assumed constant. Hence a ratio of the products Z_{OC} and f_{OC} for each phase was calculated to provide an indication of the different fugacity capacities of the different phases (dust vs polyester textile).

The mean f_{OC} of the low level dust was measured as 12.7% (results presented in Chapter 7) and as no value was found for the fraction of organic carbon in a polyester textile, the percentage carbon content of the molecule was taken (62% carbon). Using these values provided an estimate of the fugacity capacity of dust (Z_{DUST}) of $3.4 \times 10^3 \text{ mol}\cdot\text{m}^{-3}\cdot\text{Pa}^{-1}$ and the fugacity capacity of polyester (Z_{PE}) of $1.7 \times 10^4 \text{ mol}\cdot\text{m}^{-3}\cdot\text{Pa}^{-1}$. The polyester has a higher estimated fugacity capacity and when multiplied with the large HBCD concentration in the initial product (equation 4.1), a high fugacity is provided for this material. The dust in turn will have a much lower fugacity due to the lower estimated Z_{DUST} value and lower initial HBCD concentrations in the dust. This provides a large fugacity gradient between the two phases and a fast chemical transfer is expected, as experimentally observed. The calculated fugacity capacities and parameters are listed in Table 4.4.

There are many assumptions with these calculations, particularly that the carbon content of polyester can be substituted with organic carbon content of the textile, which is not the case as carbon attached to a polymer backbone will not be as available for HBCD absorption. The dust and polyester are also assumed to be homogeneous in composition, particularly the organic carbon content through the materials. Another assumption is that the air, water and mineral matter fractions will be the same in the two phases, which is not the case, however the high hydrophobicity of the HBCDs dictates that influences from these components will be minimal and the organic carbon will exert the greatest influence. The calculations do however suggest that a large difference in fugacities between the phases exists, thereby accounting for the rapid HBCD mass transfer observed.

Table 4.4: Literature parameters and calculated fugacity capacities (Z) for the HBCD technical formulation in different media

Parameter	Value
Henrys Law constant (Pa.m ³ /mol) (EC, 2011)	4.7
K _{OC} (EC, 2011)	1.25 x 10 ⁵
Fraction organic carbon in dust	0.127
Fraction carbon in polyester	0.624
Z _W (mol.m ⁻³ .Pa ⁻¹)	0.213
Z _{OC} (mol.m ⁻³ .Pa ⁻¹)	2.66 x 10 ⁴
Z _{DUST} (mol.m ⁻³ .Pa ⁻¹)	3.38 x 10 ³
Z _{PE} (mol.m ⁻³ .Pa ⁻¹)	1.66 x 10 ⁴

The variable HBCD concentrations detected in repeat direct contact experiments (almost an order of magnitude variation for the 24 hour experiments) may suggest a heterogeneous distribution of HBCDs through the curtain surface, and thus variable HBCD mass available for uptake by dust. A heterogeneous organic carbon distribution in the dust will also influence the sorptive capacity of the dust and the lower mean HBCD concentration in the dust post experiment 1 for 24 hours may be partly driven by a lower organic carbon content in this dust mass than that used in the other experiments. The organic carbon fraction in the bulk dust was analysed and

showed a heterogeneous content with four replicate analyses determining the fraction of organic carbon to range from 9.8 to 15.4%, described in more detail in Chapter 7. The large variance in the HBCD concentration (and hence high standard deviation) observed through the generated dust from experiment 3 for 24 hours and experiment 3 for 1 week, may also be due to varying organic carbon content in the dust subsample analysed and a heterogeneous distribution of HBCDs throughout the textile, but also may be due to very small fibres from the curtain transferring into the dust sample during the experiment or during dust collection post experiment. The dust was gently brushed off the fabric for collection, however it is possible small fibres may also have been collected from this friable material and these high HBCD concentration fibres, heterogeneously distributed, will influence dust concentrations. This would be realistic in a 'real world' scenario though, with curtain movement causing dust to move/fall off the curtain to the floor, also removing small fibres via abrasion to fall into the floor dust, resulting in a heterogeneous dust sample.

Clausen et al. (2004) and Schripp et al. (2010) investigated the uptake of phthalates (another class of SVOC) to dust via direct contact, successfully replicating this migration pathway in test cell experiments. Schripp et al. (2010) hypothesised that this mass transfer is due to the dust mass being in contact with the boundary layer of the source:air interface (the area immediately adjacent to the source to a point where the flow velocity has reached 'free stream' velocity). Air concentrations of BFRs in the boundary layer will be much higher than in the well-mixed air, providing increased contact and fast uptake into dust, due to the greater gradient between HBCD concentrations in the boundary layer air and the dust. However, Clausen et al. (2004) suggested that the direct contact between the dust and source partially removes the boundary layer, allowing the dust particles to act as an absorbent removing DEHP directly from the source, which again will be reliant on the fugacities of the phases. Clausen et al. (2004) also reported a four times greater concentration of DEHP transferred to dust via direct contact than that emitted to air from the source, again providing evidence that this migration pathway transfers much higher concentrations of SVOCs to dust than via volatilisation before partitioning to dust.

Dust sampled from putative sources in indoor microenvironment studies have also shown elevated concentrations of BFRs in dust in direct contact with putative sources. The study by Harrad et al. (2009a) reported a 23 times higher concentration of Σ HBCDs in dust directly sampled from the back of a TV compared to that sampled from the floor area around the TV ($540 \mu\text{g g}^{-1}$ on the TV compared to $24 \mu\text{g g}^{-1}$ in dust located 1 m from the TV set). This suggests that migration of HBCDs occurred via direct contact of the HBCD treated TV casing to the dust, providing substantially elevated HBCD concentrations to the dust. The fast uptake and high mass of HBCD transferred to dust via this migration pathway show that direct contact with source materials is a potentially important pathway via which BFRs may transfer to indoor dust. Takigami et al. (2008) also reported an increase of BDE-209 in dust sampled directly from the back of TV casings (with components shown to contain BDE-209) as compared to that sampled from the environment around the TV, described further in Chapter 6, showing this pathway is potentially important for other BFRs as well.

4.4 Comparison of HBCD transfer from treated textiles via three different migration pathways

All three hypothesised migration pathways of BFRs to dust were successfully recreated in modified chamber experiments, with HBCDs migrating from a treated textile sample. An order of magnitude difference in HBCD mass transferred to dust was seen between the different pathways with the lowest mass transferred *via* volatilisation with subsequent partitioning to dust (Chapter 3). As expected, highly elevated concentrations of HBCDs were transferred to dust *via* source abrasion. Finally, migration *via* direct contact between BFR source and dust, saw a rapid mass transfer of HBCDs to dust, suggesting this is an important pathway that should not be overlooked. Concentrations of HBCD diastereomers transferred to dust *via* the three different migration pathways in the experiments described in this chapter and Chapter 3 are summarised in Table 4.5.

The large concentration differences for these chamber experiments provides further evidence that migration via different pathways is a contributory factor in the large dust concentration differences reported in the literature in studies of indoor

microenvironments. Of course, differences in putative sources in different microenvironments (i.e. different product matrices, different BFRs, or containing different percentage levels of the same BFR) will be the biggest contributor to variations in BFR concentrations detected, however the different migration pathways will also contribute to the varying concentrations reported. In a ‘real world’ scenario it is likely that a number of migration pathways occur together to varying extents, to contribute to total dust contamination. Moreover, as seen in the abrasion experiments volatilisation of HBCDs may be further encouraged by abrasion. It appears highly plausible therefore, that volatilisation with subsequent partitioning to dust contributes a baseline level of BFRs in dust that may be overlaid to varying degrees by inputs from abraded particles and fibres and transfer from direct contact between dust and putative sources.

Table 4.5: Mean \pm SD concentrations (ng.g⁻¹) of HBCDs in the same starting bulk dust, post experiment, from chamber experiments investigating three different migration pathways using HBCD treated curtains

	α-HBCD	β-HBCD	γ-HBCD
Volatilisation with dust partitioning			
24 hours @ 60 °C (n=4)	180 \pm 52	63 \pm 3.8	370 \pm 85
1 week @ 22 \pm 1 °C (n=3)	160 \pm 100	72 \pm 60	270 \pm 180
Abrasion of fibres directly to dust			
2 hours (n=1)	2500	720	3300
3 hours (n=1)	1400	700	2000
21 hours (n=1)	3200	1700	13 000
48 hours (n=1)	23 000	4900	26 000
Direct transfer from source to dust			
24 hours (n=4)	2600 \pm 2000	800 \pm 620	2900 \pm 2400
1 week (n=4)	3000 \pm 600	930 \pm 280	3400 \pm 790

4.5 Summary/Conclusions

Abrasion of a HBCD treated curtain was successfully replicated in test chamber experiments for the first time with highly elevated HBCD dust concentrations detected in dust post experiment over four different experimental durations. HBCD migration via direct contact between source and dust was also simulated in modified chamber experiments and again showed highly elevated concentrations in dust after both 24 hours and 1 week contact. An attempt to relate these experiments to 'real world' use scenarios was made. The increase in HBCD concentration in dust observed in the shortest abrasion experiment, suggests that general use of a curtain over 2 years (equivalent to 24000 abrasion cycles) will abrade ~35 mg of fibres. This abrasion results in 1500 ng Σ HBCDs transfer from the curtain. Interestingly, these abrasion experiments may also promote volatilisation of HBCDs from the curtain. Experiments studying HBCD transfer as a result of direct contact between the curtain and dust show not only that such transfer is substantial, but that the vast majority of this transfer occurs within the first 24 hours of contact.

All three of the hypothesised migration pathways have been successfully simulated in modified chamber experiments showing migration to dust of HBCDs from a textile treated with the HBCD technical formulation. The ease with which these pathways were simulated in the chamber experiments described here, suggests they all make significant contributions to the observed contamination of indoor dust with BFRs. The extent to which HBCDs were transferred to dust in these experiments varied substantially between the pathways and indicates that the extent to which each pathway occurs in a given microenvironment provides a partial explanation for the widely variable concentrations of BFRs observed in indoor dust.

CHAPTER 5

FORENSIC MICROSCOPY INVESTIGATION OF DUSTs OF ELEVATED BFR CONCENTRATIONS

5.1 Summary

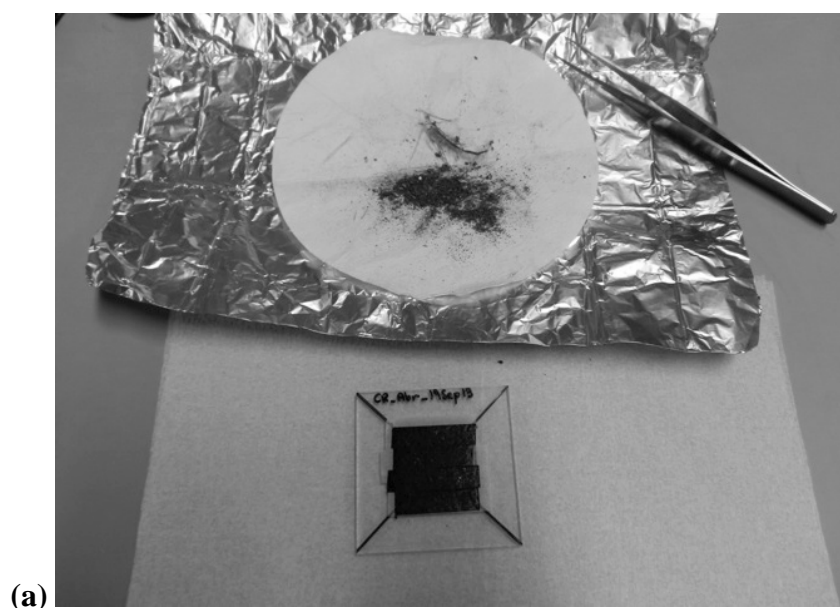
Forensic microscopy techniques such as energy dispersive Micro X-ray fluorescence spectroscopy (Micro XRFS) and scanning electron microscopy with energy dispersive spectroscopy (SEM/EDS) have been utilised previously to provide information on the origins of dust contamination with BFRs (Suzuki et al., 2009, Webster et al., 2009, Ghosal and Wagner, 2013, Wagner et al., 2013). A similar methodology was utilised during this research project to provide further information on migration pathways of BFRs to dust. Dust samples generated from abrasion of a HBCD treated textile curtain were analysed utilising forensic microscopy techniques to show the applicability of these methods to provide information on migration pathways of BFRs to dust. In addition, three archived dust samples, previously sampled from indoor microenvironments in the UK and containing known elevated levels of BFRs, were investigated using the same series of techniques to provide further existing evidence that highly contaminated dusts are likely due to the presence of a small proportion of fibres and/or particles abraded from BFR-treated materials. The following chapter describes the sequence of methods used for this forensic microscopy investigation, results and conclusions from the analysis of the chamber generated dust and ‘real’ dust samples, and the applicability and limitations of these methods for analysing dust highly contaminated with BFRs to provide information on migration pathways.

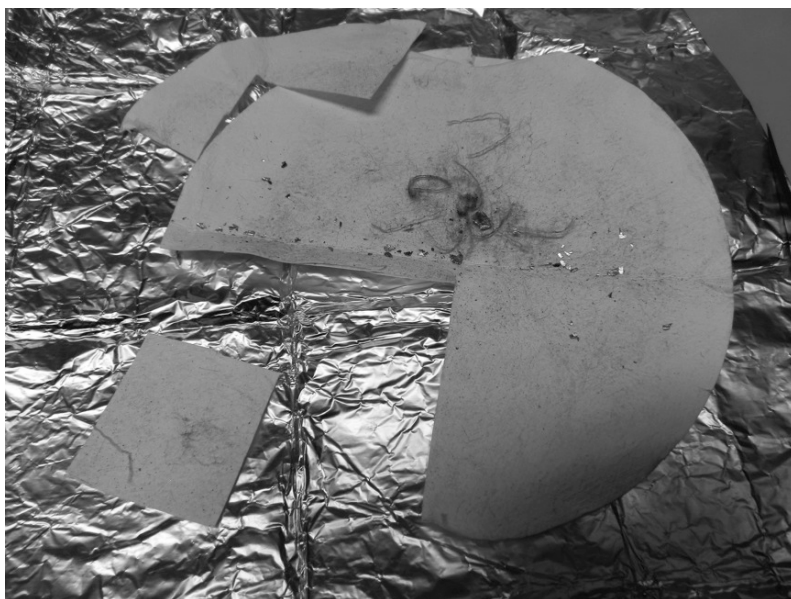
5.2 Forensic Microscopy analysis of chamber generated dust sample

5.2.1 Sample preparation

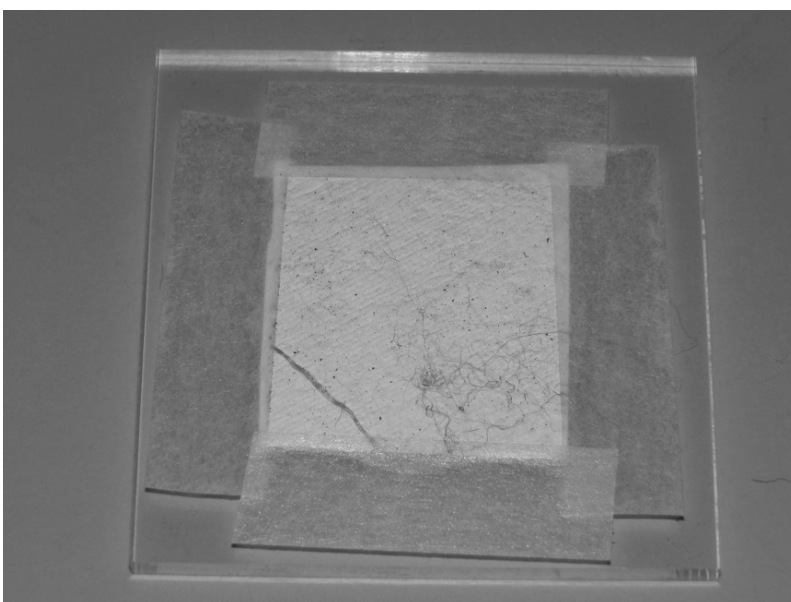
Samples contaminated with abraded fibres from the HBCD treated curtain were prepared in test chamber experiments described previously (Chapter 4, Section 4.2). A sample of the HBCD treated textile curtain was subjected to abrasion in the chamber for 48 hours and fibres were abraded either onto a dust aliquot or onto a clean GFF, with both sample types analysed via a range of forensic microscopy techniques. Fibres were abraded onto a GFF (with no dust) to prepare a batch of abraded, clean fibres, in the event the dust samples were difficult to analyse with the instrumentation. The dust sample (1 mg) was loaded to black carbon tab (following the processes described earlier in Chapter 2) whereas the GFF without dust was cut into a 25 x 25 mm square and stuck to a glass sample plate for Micro XRFS analysis. Figure 5.1 shows photos of this sample preparation.

Figure 5.1: Photographs of sample preparation for Micro XRFS of generated abraded curtain fibre experiments showing (a) fibres in dust for the original sample and loaded onto the black carbon tab (b) abraded fibres on the clean GFF with sample area removed and (c) removed GFF area attached to the glass sample plate





(b)



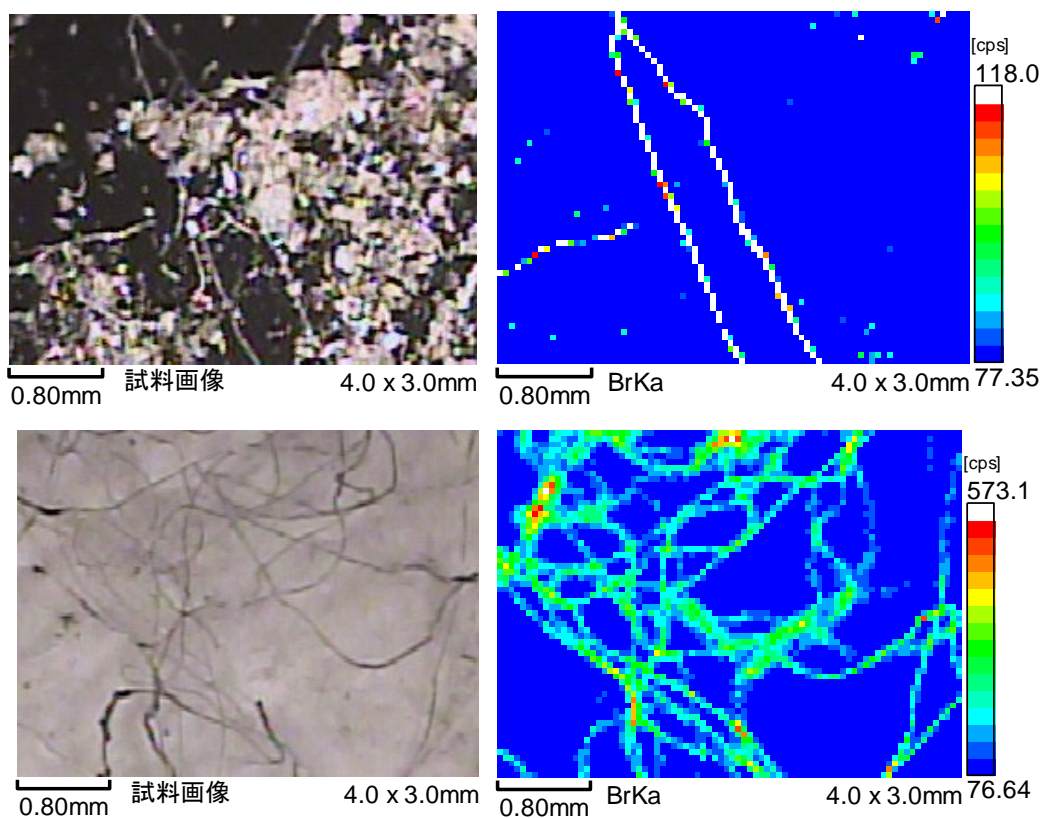
(c)

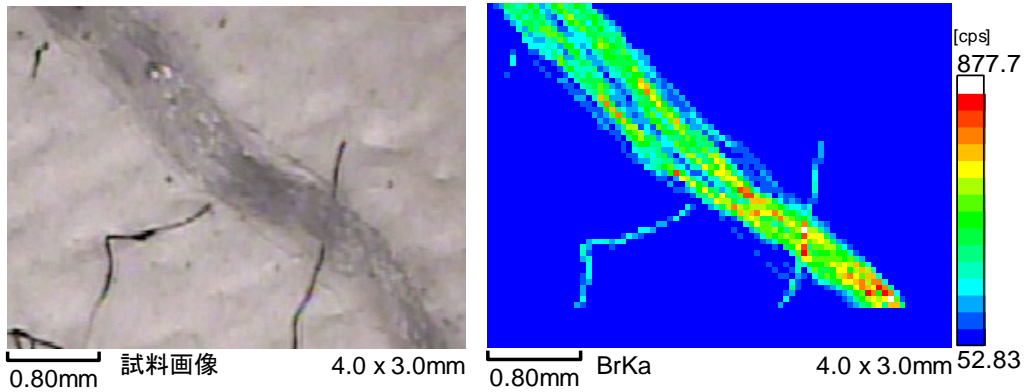
5.2.2 *Micro X-ray Fluorescence Spectroscopy*

The glass sample plates were loaded on to the sample stage in the Micro XRFS for the determination of areas of high bromine content. The faster (0.5 second) scanning mode has lower sensitivity and determining the presence of Br in fibres in the sample was difficult. Therefore these samples were run in 10 second scanning mode to increase sensitivity, over a 4 x 3 mm square area of the sample (equating to a 13 hour analysis time). For both samples, the areas of high Br in the mapping image corresponded to locations of the fibres in the analysed sample. The dust with fibres sample was adhered to the carbon tab and thereby held stationary throughout the

13 hour analysis, providing a clean mapping image. In contrast, where the GFF contained only abraded fibres, the fibres adhered to the GFF by static electricity alone and as a result, the fibres moved inside the Micro XRFS during the course of the experiment, producing a ‘blurred’ mapping image. Captured optical images and bromine mapping images are shown in Figure 5.2.

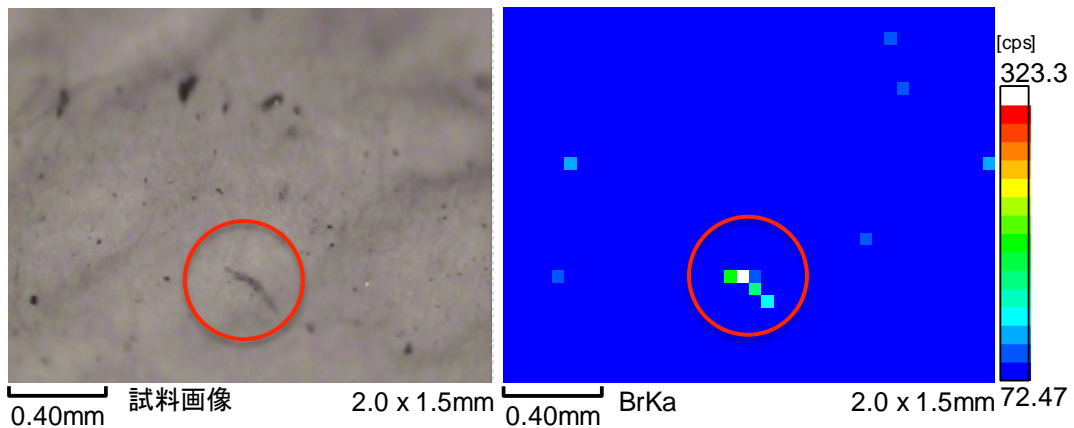
Figure 5.2: Sample areas analysed by Micro XRFS. Optical images on the left are of the 4 x 3 mm sample areas analysed, while images on the right are the corresponding Br mapping images obtained over the 13 hours scan time. Pixels (50 µm square areas) of white, red, yellow and green indicate areas of highest Br content, for (Top) the sample of dust with fibres attached to carbon tab (indicated by the black background) (Middle) area 1 of fibres on the clean GFF and (Bottom) area 2 of fibres on the clean GFF (indicated by the grey background colouring)





Another sample area (2 x 1.5 mm) of the clean GFF, with no larger fibres present, was mapped on the Micro XRFS for 3 hours in 10 second mode to determine if smaller bromine (Br) containing fibres could be located. The smallest located fibre containing a detected Br content was ~ 200 μm in length, suggesting the abrasion process may abrade a range of different fibre sizes into the dust sample. The Micro XRFS optical image and Br mapping images are shown in Figure 5.3.

Figure 5.3: Micro XRFS optical image (Left) of a small fibre on the sample GFF and the corresponding sample Br mapping image (Right), showing higher Br concentrations in the area of this small fibre



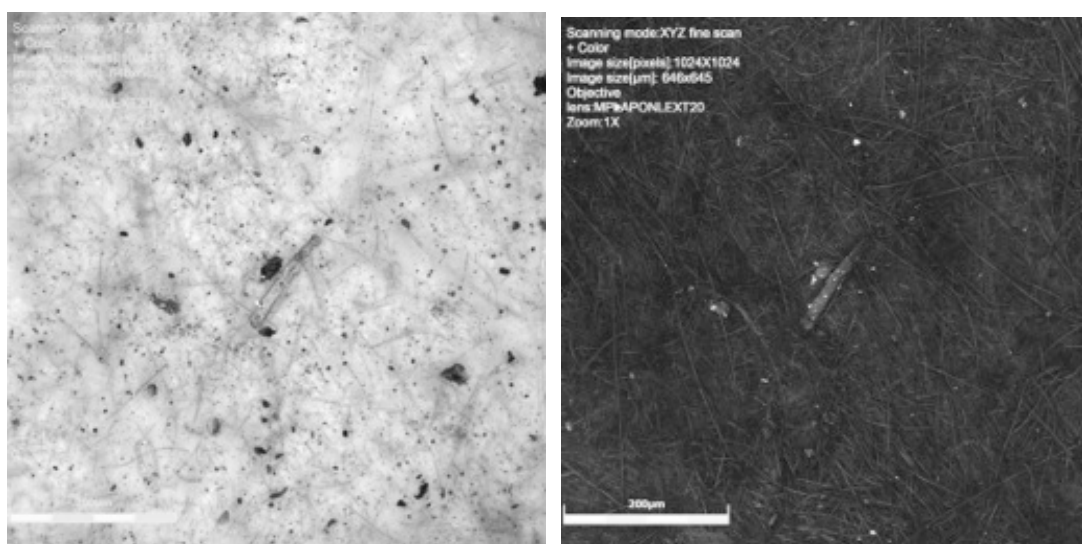
As the incident X-ray excitation beam is a 50 μm square area, the mapping image provides an average of the bromine content in that square area rather than identification of individual bromine rich fragments. Moreover, particles smaller than 50 μm may be missed, creating a selection bias with this method, and requiring

further SEM/EDS analysis for bromine confirmation. However, this method was able to successfully identify fibres of high bromine content in this dust sample.

5.2.3 3D Laser Microscopy

As this sample was known to contain fibres originating from a HBCD treated textile, 3D imaging to determine possible Br sources in the sample areas was not necessary. However the 3D laser microscope was used for the chamber generated samples to again investigate variations in abraded fibre lengths. Sections of the clean GFF, with no larger fibres present, were imaged with the LEXT 3D laser microscope to look at the range of textile fibre sizes present after abrasion and identify possible fragments only observable under microscopy. The smallest fibre identified to possibly originate from the HBCD treated curtain was 130 μm in length and the laser image gave further confidence that the fibre was located on top of the GFF and not a deformation or part of the GFF surface. This again indicates the chamber abrasion method can result in a range of fibres abraded into dust. The optical colour and laser images are shown in Figure 5.4.

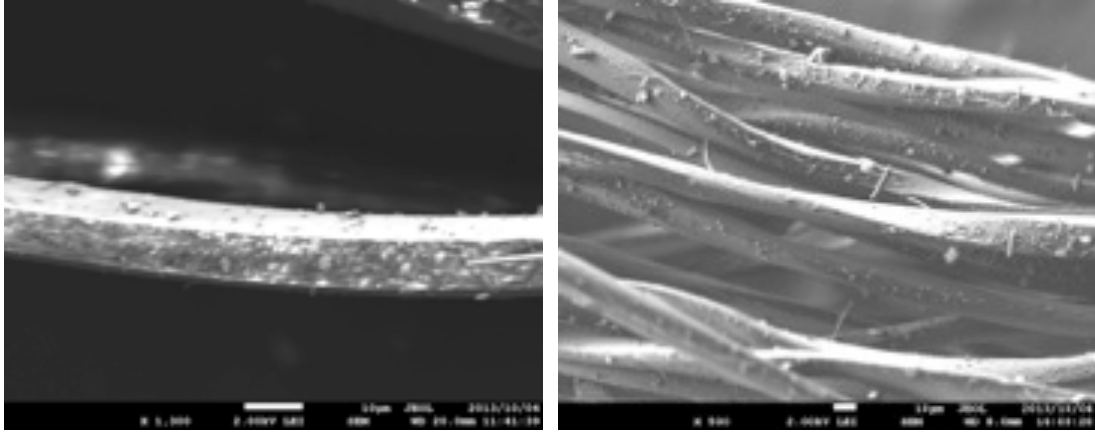
Figure 5.4: (Left) optical and (Right) 3D laser images of GFF containing abraded textile fibres on its surface



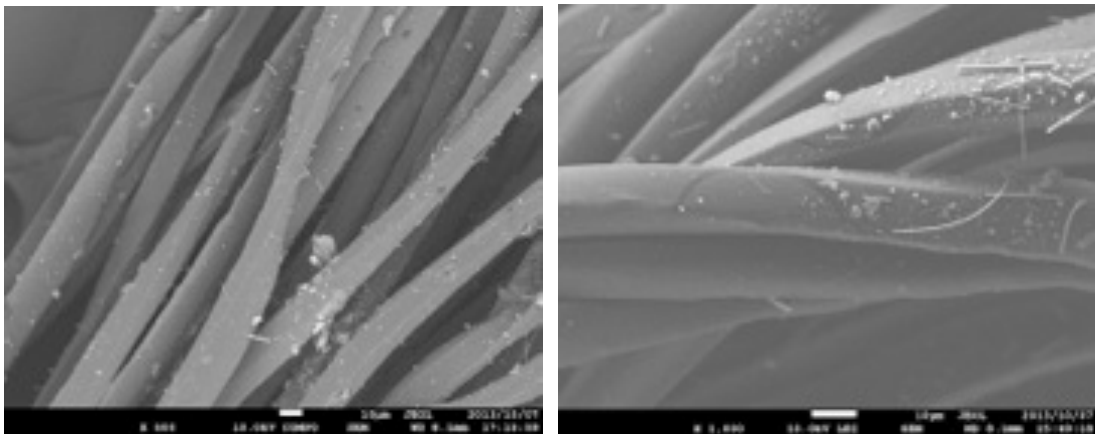
5.2.4 Scanning Emission Microscopy/Energy Dispersive Spectroscopy

After screening with the Micro XRFS, the fibres were investigated with SEM/EDS to confirm the presence of bromine in identified fibres and to image the surface structure. Initial SEM analysis was conducted without coating the sample to not interfere with FTIR analysis. As a result, a charging effect was seen, resulting in difficulty in obtaining a clear image of the fibre surface structure. Charging on the SEM refers to the build up of electrons on the sample surface that interfere with the signal reaching the detector. This effect is usually reduced by coating the sample surface with a conductive material to minimise the negative build up, however if the particles/fibres are to be used in further analyses (as is the case here) they need to remain uncoated to not interfere with subsequent examinations. The charging gave the effect that the fibres were shifting over the sample surface, creating a 'blurry' image. As numerous fibres were generated in the chamber and hence available for further analyses, platinum coating was explored to reduce the charging. The sample was platinum coated for 80 seconds and reanalysed with the SEM, as platinum does not have any spectral peaks that interfere with the elements of interest. Carbon coating, often used for the analysis of metals, was not used on these samples as the polymer backbone of the textile already has a large carbon content hence adding another carbon layer to the sample may mask the other elements in the EDS analysis. Figure 5.5 shows SEM secondary electron images of the fibres with (top) two images before platinum coating the sample surface and (bottom) two images after platinum coating, showing improved image clarity with coating the sample and reducing the charging effects.

Figure 5.5: SEM images of single and intertwined fibres in the analysed sample (Top) before platinum coating the sample surface, showing the effect of charging on image resolution



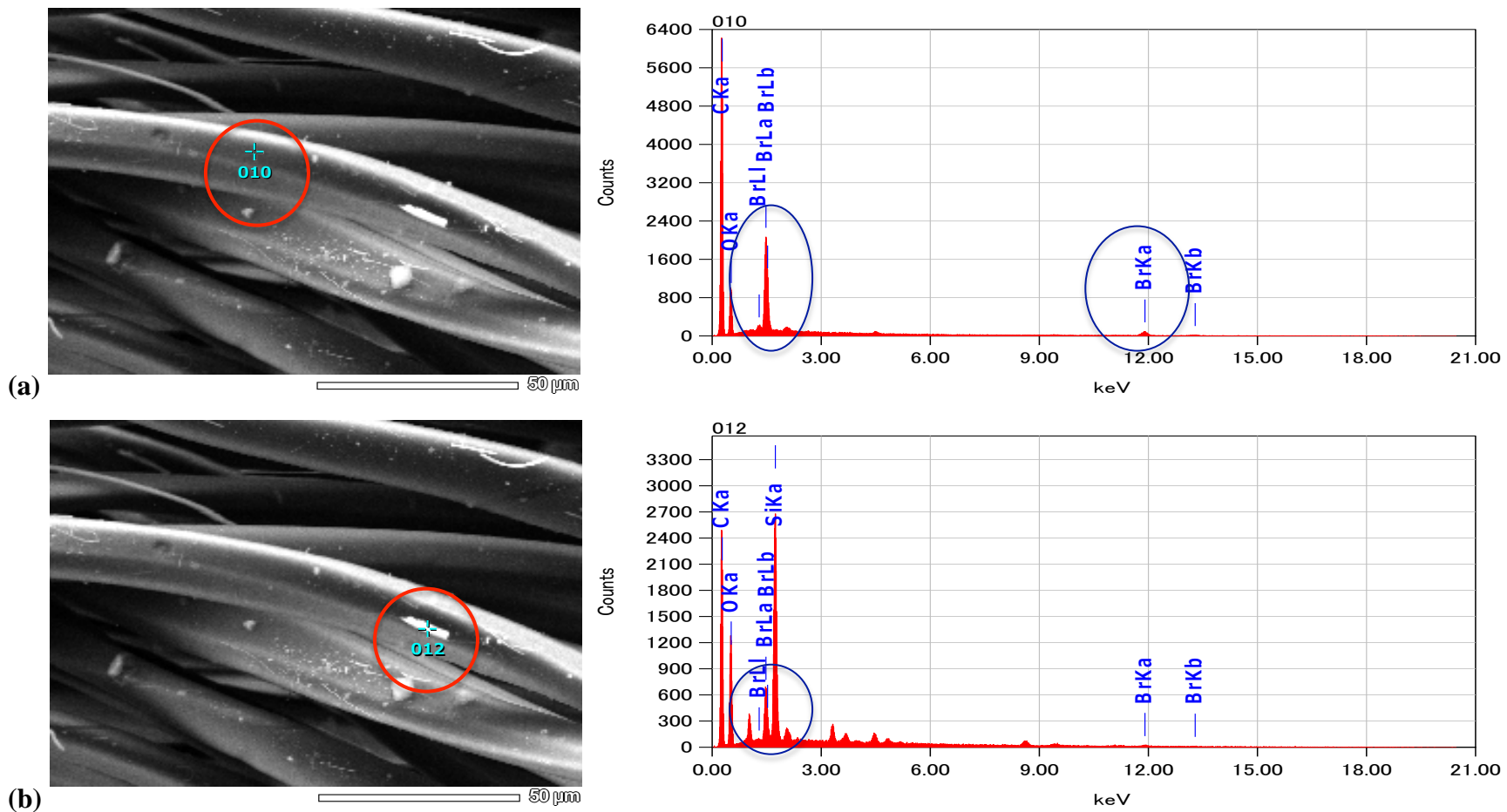
(Bottom) After platinum coating the sample surface, showing the increased resolution

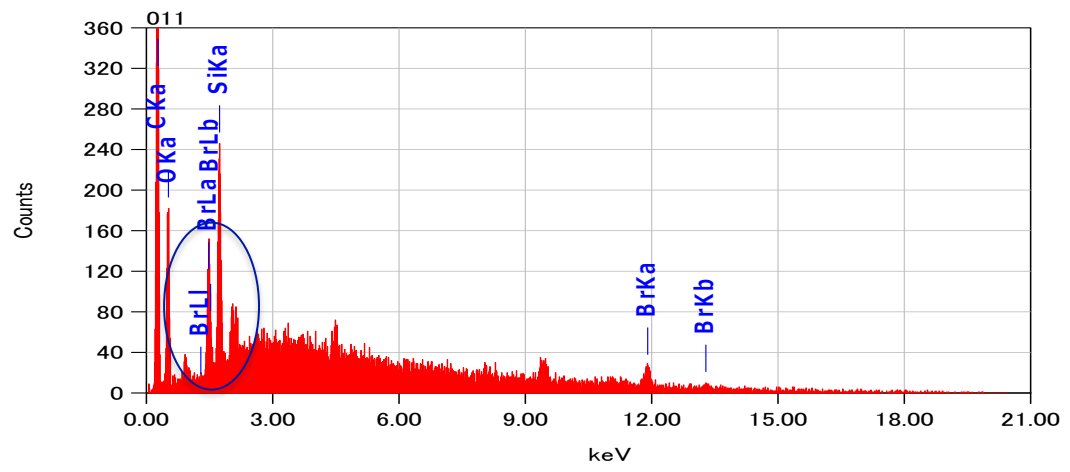
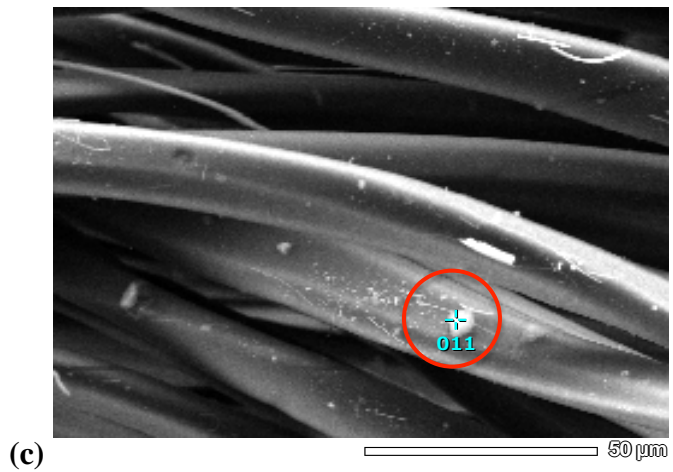


Due to the charging effects and also the uneven topography of the sample surface, the SEM method used in this study is only a screening method as calculated %EDS elemental compositions cannot be relied on as a quantitative measure. The topography of the sample affects measurements, as ideally a flat surface is required to obtain a quantitative result. The dust and fibre sample surface is full of larger particles that the X-rays bounce off, alongside valleys to absorb them before they reach the detector, reducing the signal output and accuracy of the reading. Despite this, the EDS elemental profile still provides confirmatory, qualitative, information on which elements are present in the analysed particle/fibre.

EDS analysis confirmed the presence of Br as the $K\alpha$ and $L\alpha$ lines were both present. The magnified images showed the surface structure of each fibre strand was not smooth, with particles and fine strands observed attached to the fibres. Figure 5.6 (a) shows the collected SEM backscattering image and corresponding EDS elemental profile for point analyses on the fibre, with (b) and (c) depicting the analysis of impurity particles located on the fibre surface. Only very small Br peaks were seen for the analysis of these two impurity particles and the observed Br count is considered likely coming from the underlying fibre. As the SEM was operated at 20 kV, X-rays can penetrate 10 nm into the sample surface i.e. through the particle into the fibre, resulting in generation of Br X-rays and hence the Br count registered. These impurity particles are likely fine dust particles adhered to the fibre surface.

Figure 5.6: SEM backscattering image of a mass of intertwined fibres and corresponding EDS elemental profile from (a) the fibre surface and (b), (c) impurity particles present on the fibre surface





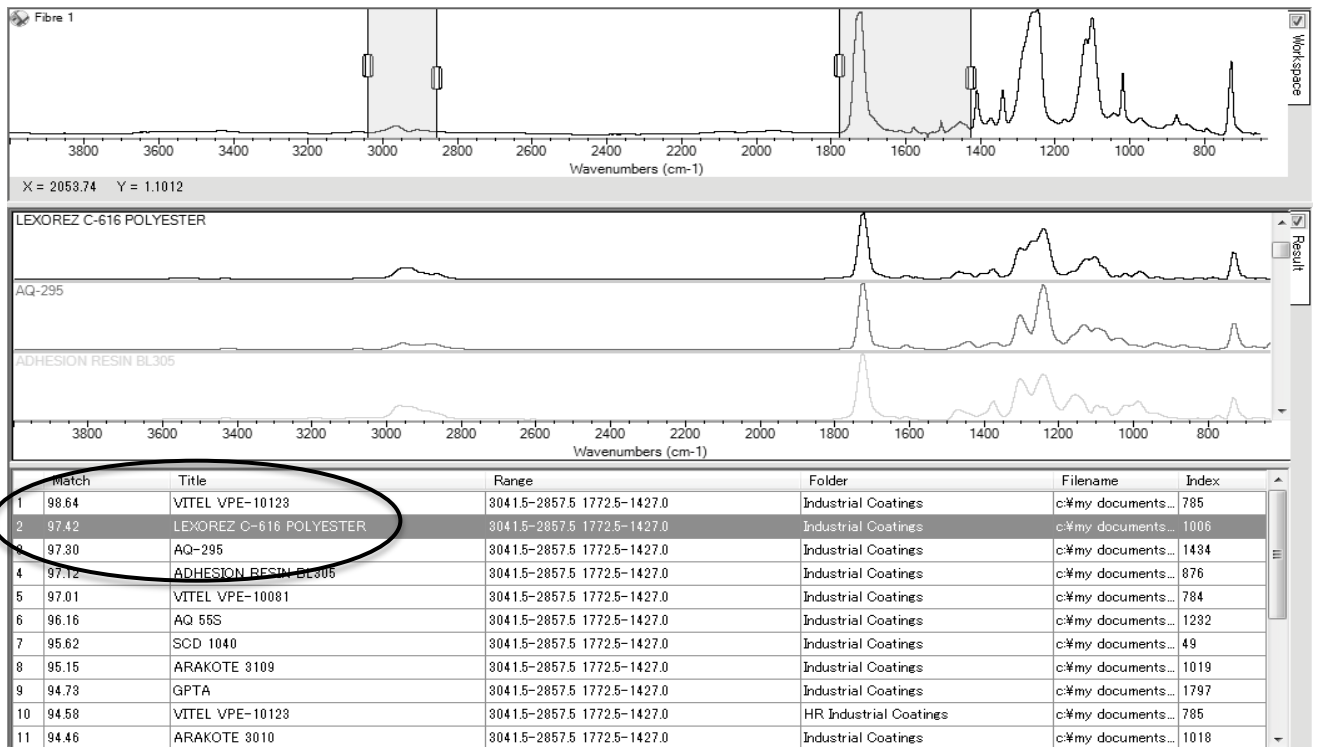
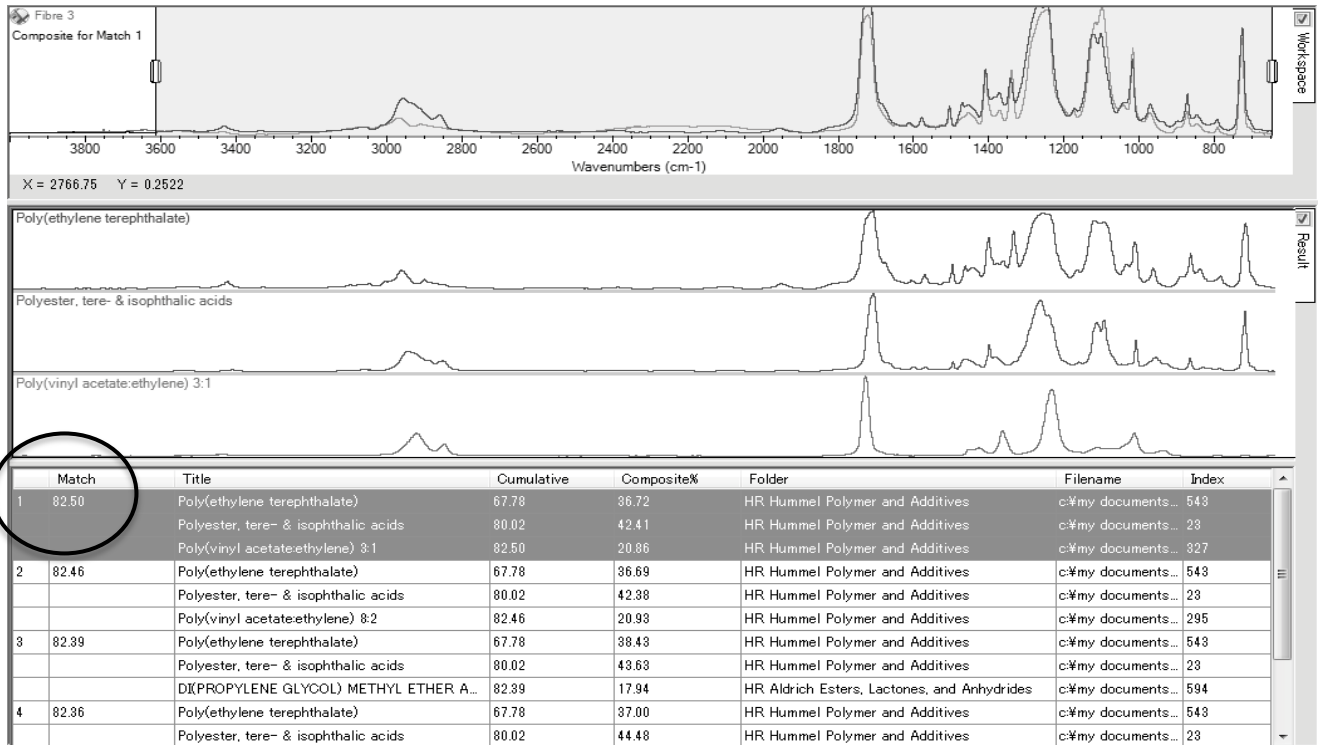
5.2.5 *Fourier Transform Infrared Spectroscopy*

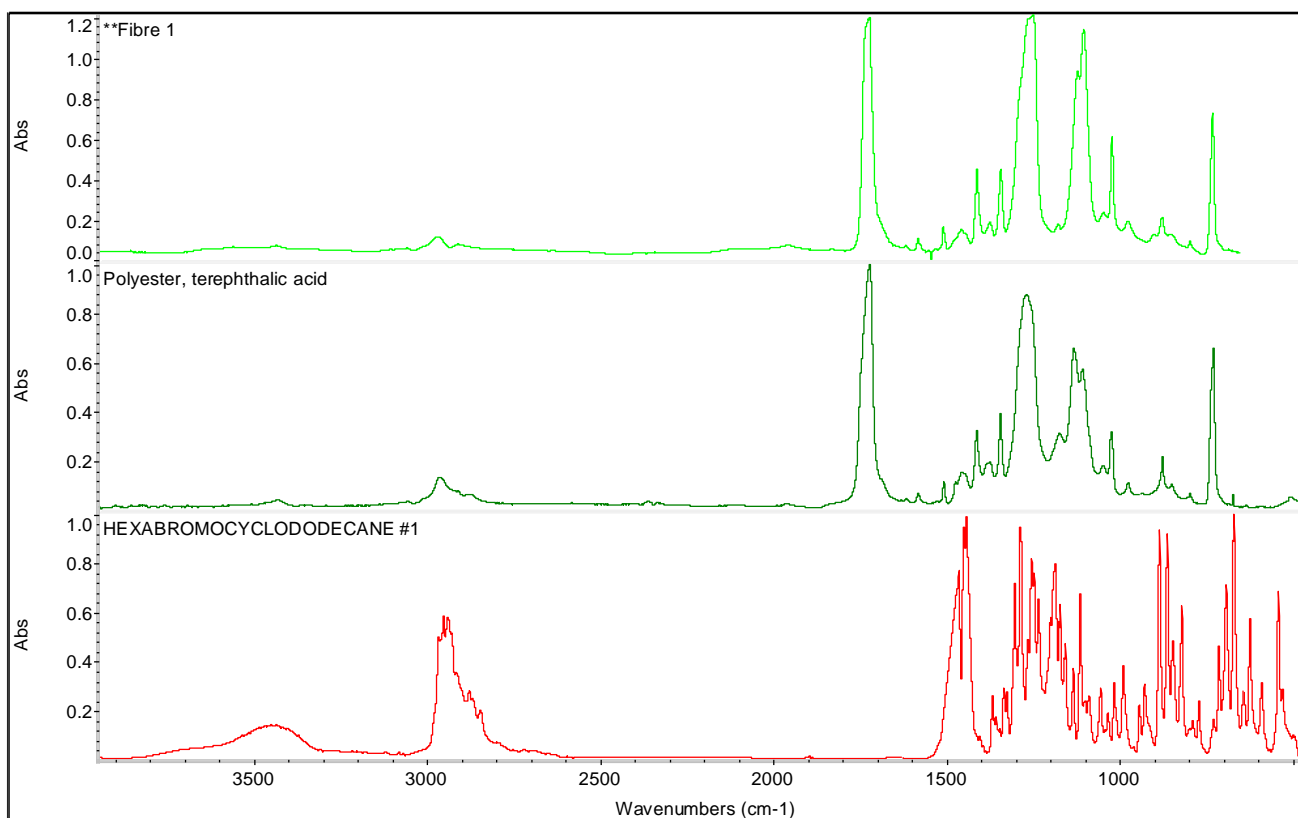
As the fibres analysed with the SEM/EDS had been platinum coated, other fibres from the sample were removed for further, compositional analysis with FTIR spectroscopy. The fibre was isolated from the sample, placed in the diamond compression cell and analysed on the FTIR. Figure 5.7 shows the diamond compression cell and the captured image of the analysed fibre in the cell. Searching the resultant sample spectrum through the software library database found an 83% match for polyester plus other industrial coatings. Peaks of interest in the sample spectrum were searched separately to increase the confidence of the match with the reference spectrum. In particular the strong stretch at $\sim 1700\text{ cm}^{-1}$, representative of a C=O double bond stretch, and weak stretches around 3000 cm^{-1} , representative of alkyl group stretches were searched and returned a 97% match for polyester. As reported previously by Kajiwara et al. (2013) the curtains are known to be HBCD treated textile polyester, showing the FTIR was able to successfully identify the base polymer of these fibres. The HBCD spectrum was not distinguishable however, as the HBCD concentration in the curtain was below the LOD of the FTIR (5% HBCD content). Figure 5.8 presents the library matches for the database search of the entire spectrum and of select absorbance peaks. Figure 5.8 also shows the FTIR spectra of the fibre, alongside reference spectra of the polyester match, and the technical HBCD formulation for comparison.

Figure 5.7: Diamond compression cell used for %Transmission FTIR analysis and captured image of the collected fibre 'squashed' in the cell



Figure 5.8: Returned database spectral searches of (Top) entire sample spectrum showing an 83% match with polyester and other industrial coatings, (Middle) highlighted peaks of interest showing a 97% match with polyester and (Overleaf) comparison of the fibre, polyester reference and HBCD reference spectra





The limits of detection of the FTIR in particular, did not allow confirmation of HBCDs in identified fibres in this sample. However, the presence of Br-rich fibres were confirmed, suggesting the fibres originated from the HBCD treated curtain (particularly as the polyester base polymer was identified) and demonstrated the applicability of these methods for identifying particles/fibres of high Br and high BFR content. To investigate this applicability further, three ‘real’ indoor dust samples were investigated with the same combination of methods, to determine if BFR-containing particles/fibres could be identified in high concentration dust samples.

5.3 Forensic microscopy analysis of archive dust samples

Three dust samples from the Birmingham archive, known to contain elevated concentrations of PBDEs were chosen for forensic microscopy analysis. The samples were prepared similarly to the abrasion generated chamber dust sample where a 1 mg subsample was sprinkled over a 25 x 25 mm area of carbon tab attached to a glass sample plate. Three plates were prepared for each dust sample resulting in a total of 3 mg of each dust analysed. BFR concentrations previously determined in the dust are listed in Table 5.1.

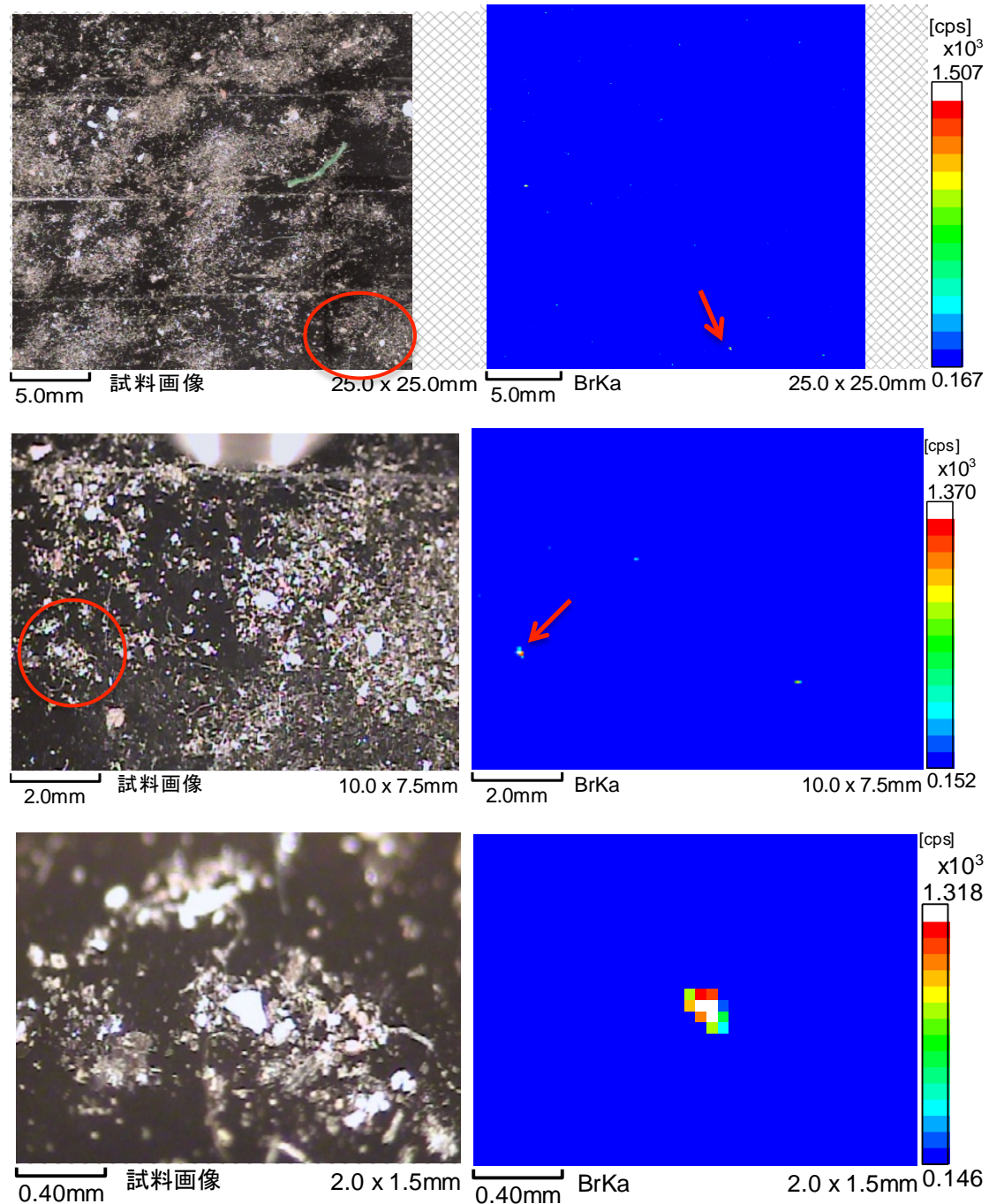
Table 5.1: Concentration (ng.g^{-1}) of HBCDs and BDE-209 in archived dust samples
(Harrad et. al., 2008a, Harrad et. al., 2010b, Harrad et. al., 2008b)

	Concentration in bulk dust (ng g^{-1})			
	α -HBCD	β -HBCD	γ -HBCD	BDE-209
Dust #1	380	340	2 800	1 400 000
Dust #2	280	70	140	280 000
Dust #3	9 900	6 700	72 000	24 000

5.3.1 Micro X-ray Fluorescence Spectroscopy

Bromine mapping of the dust samples was performed in high scanning mode (0.5 seconds) with the entire sample area mapped, before sequentially smaller regions (10 x 7.5 mm and 2 x 1.5 mm) were mapped for a more accurate identification of Br-rich areas. As the BFR concentrations were very high in these samples, areas containing high bromine content were identified in each sub-sample examined (2 to 10 areas per sub-sample) and a more sensitive mapping mode was not required. This is in line with a similar study by Ghosal and Wagner (2013) who used Micro XFRS to map dust samples, identifying ≤ 10 fragments per mg of analysed dust sample. Figure 5.9 shows the process for analysing sequentially smaller sample areas to identify Br-rich areas.

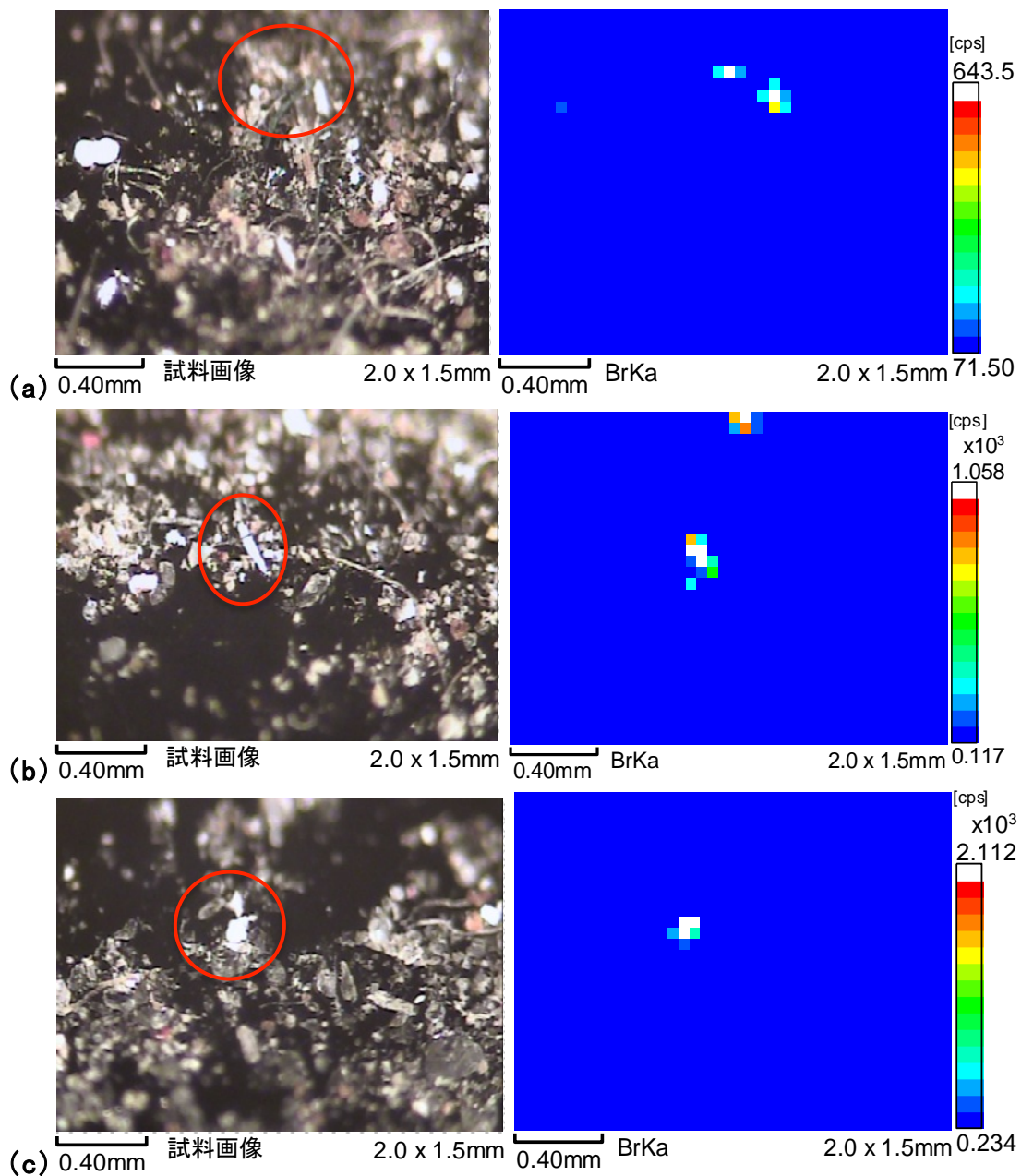
Figure 5.9: An example of the Micro XRF analysis of Dust 2 to identify the location of one high Br content area showing the optical image (left) and corresponding bromine mapping image (right) for a (Top) 25 x 25 mm sample area (Middle) 10 x 7.5 mm area and (Bottom) 2 x 1.5 mm area analysis

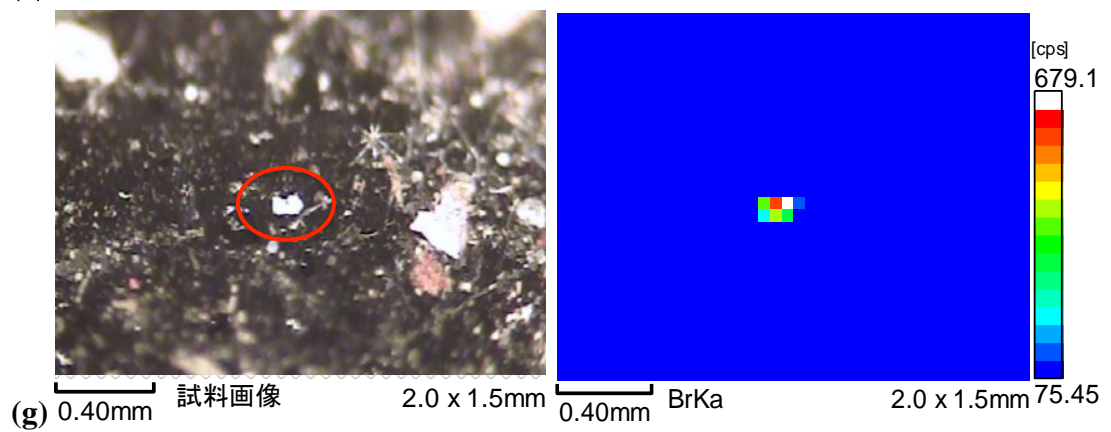
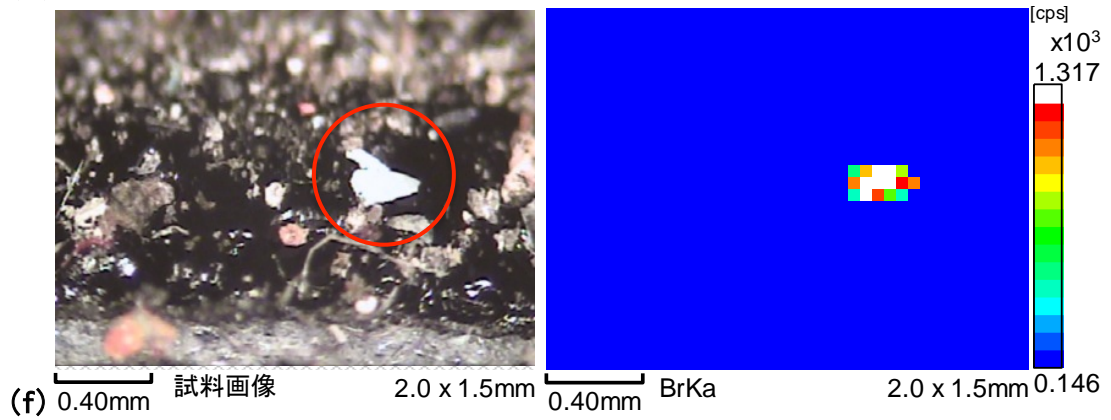
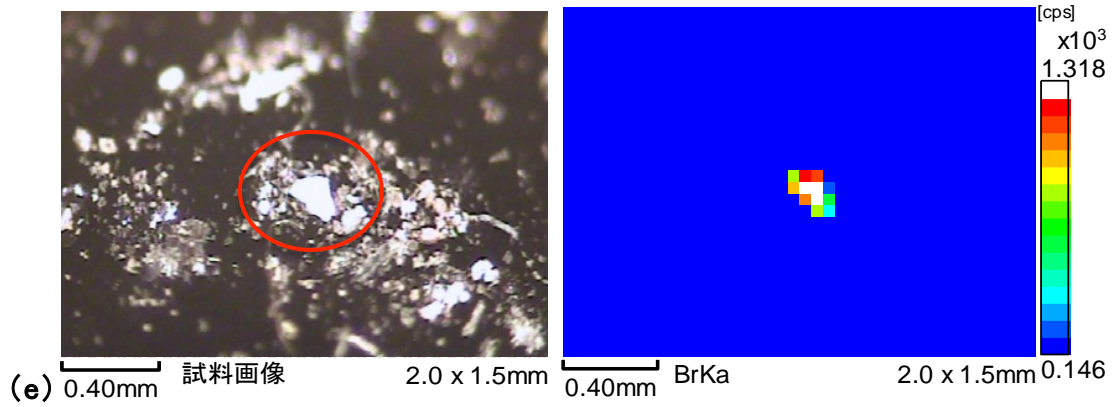
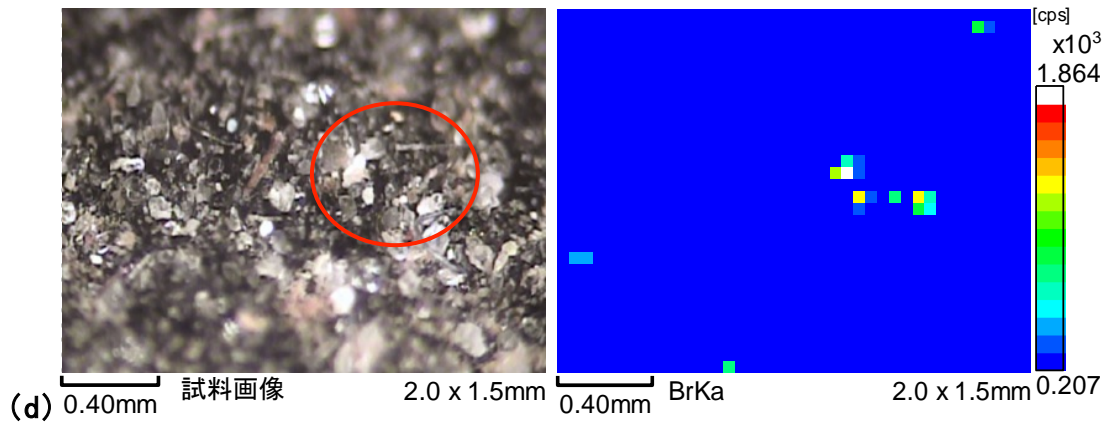


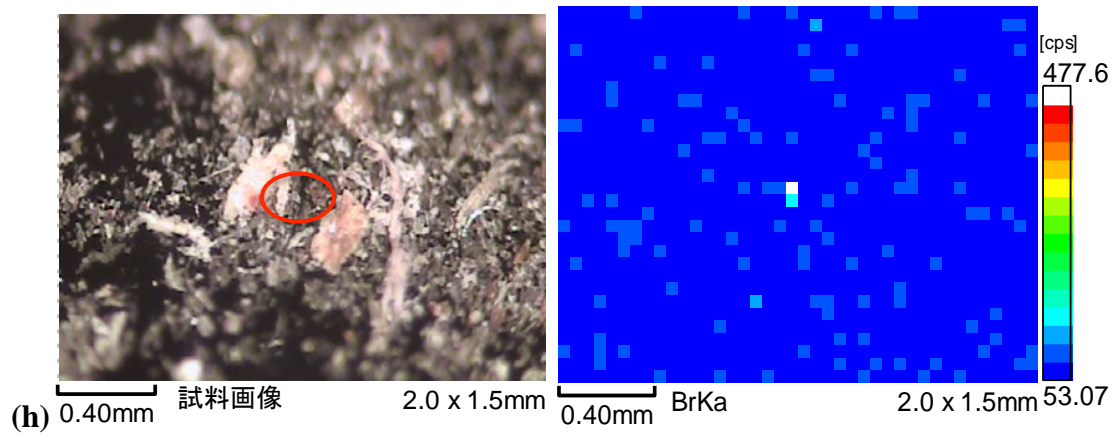
The bromine rich particles identified in these samples ranged in size from 30 to 260 μm in length; however, it is possible larger fragments may have fractured during dust collection preparation techniques (vacuuming, sieving etc) or during application of the dust to the double sided carbon tab. Eight areas of interest were initially

identified for further investigation from the first 1 mg analysis of each archived dust; 4 areas from Dust 1, 3 from Dust 2 and 1 area from Dust 3. Optical and corresponding Br mapped images are provided in Figure 5.10.

Figure 5.10: Micro XRFS analysis of three archived dust samples, with optical images presented on the left and corresponding Br mapped images in the right from Dust 1 (a), (b), (c), (d), Dust 2 (e), (f), (g), and Dust 3 (h)







5.3.2 3D Laser Microscopy

The identified areas of high Br content (2 x 2 mm) were removed from the sample area with a scalpel and tweezers and placed on an aluminium stub for further imaging and analysis. These areas and their suspected Br-rich fragments were imaged with the 3D laser microscope to provide detailed optical and 3D laser images. The length of any suspect Br-rich fragments was also measured with the microscope software. Figure 5.11 illustrates the process for removing areas of interest as well as the OLYMPUS LEXT 3D laser microscope with sample stub in place for analysis.

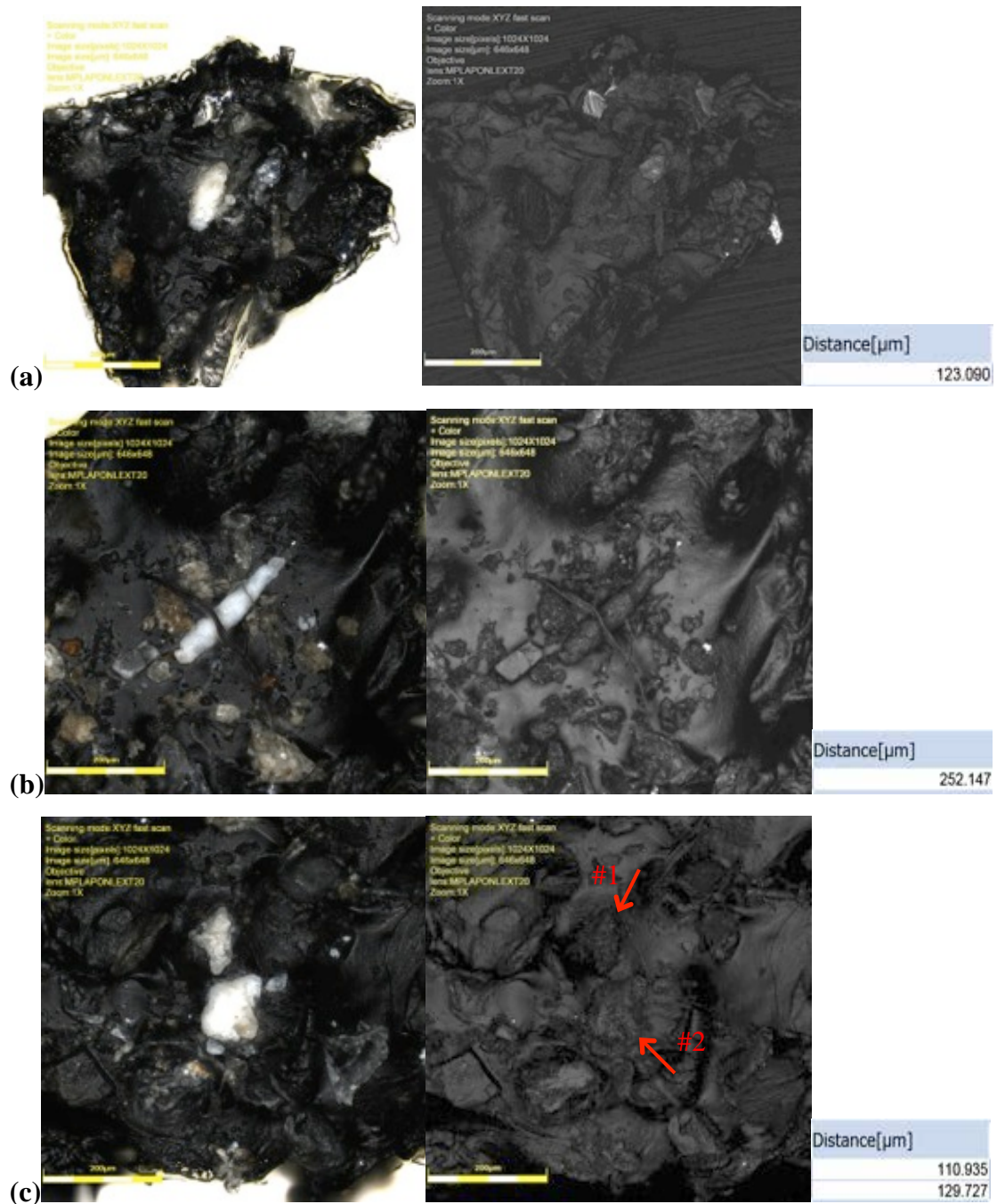
Figure 5.11: Pictures of (Left) microscope used for removing 2 x 2 mm areas of interest from sample to aluminium stub (Right) LEXT 3D laser microscope with sample stub (Bottom) 25 x 25 mm sample with removed region placed on stub

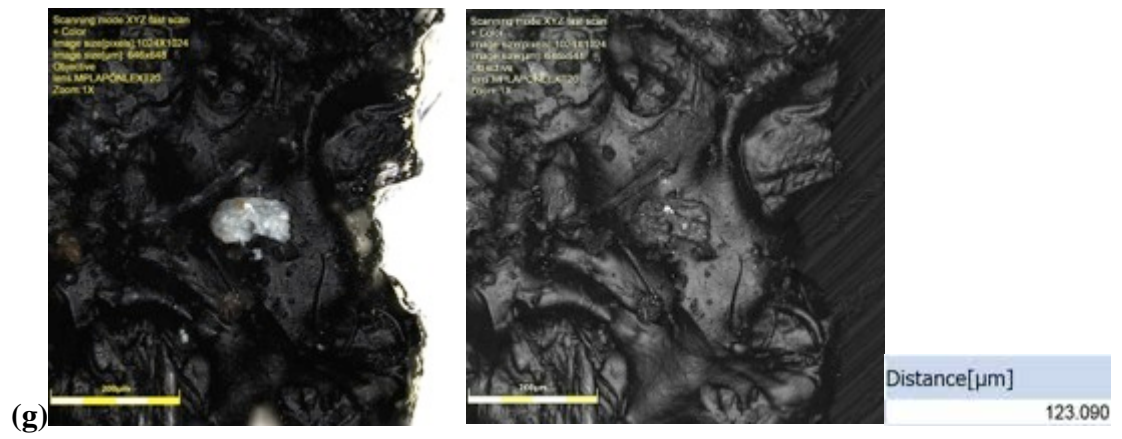
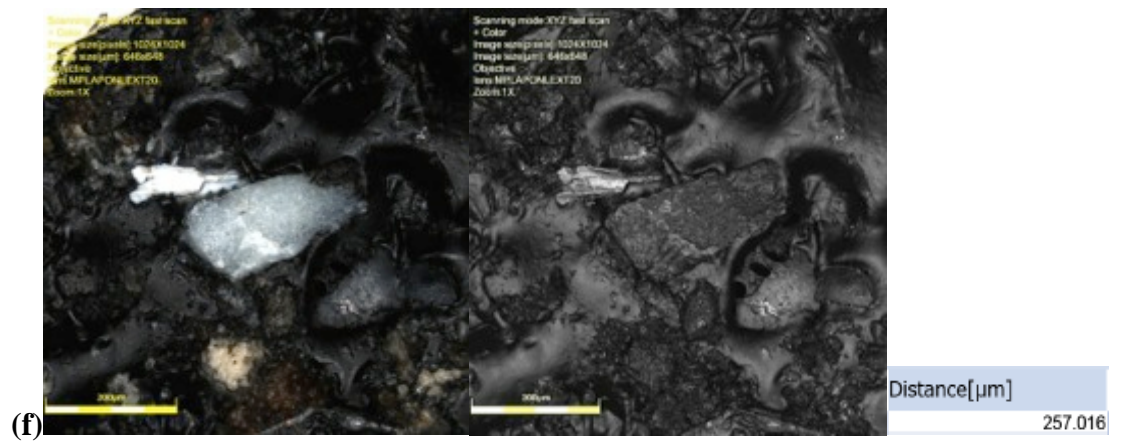
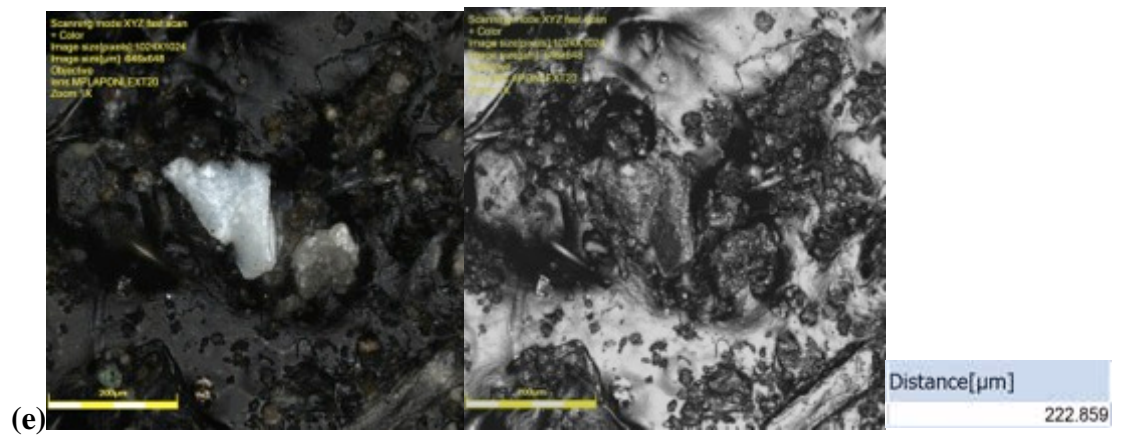
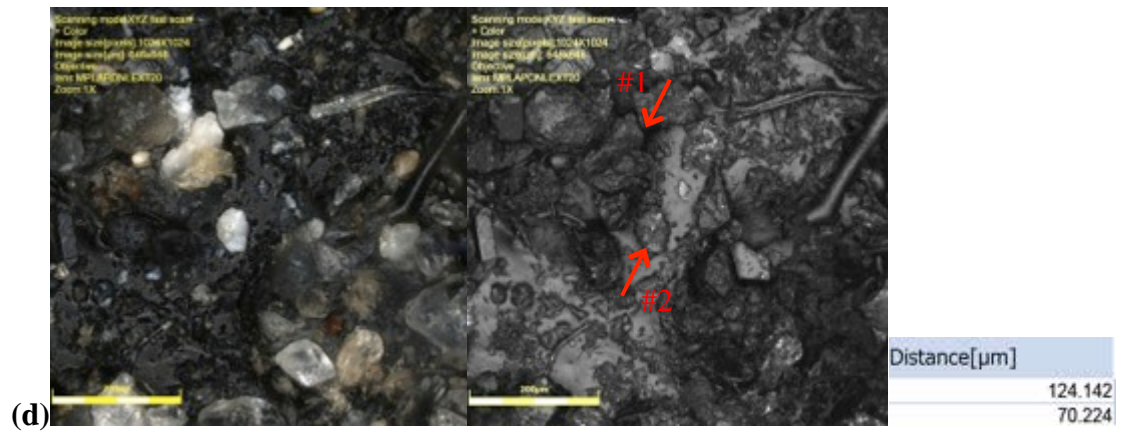


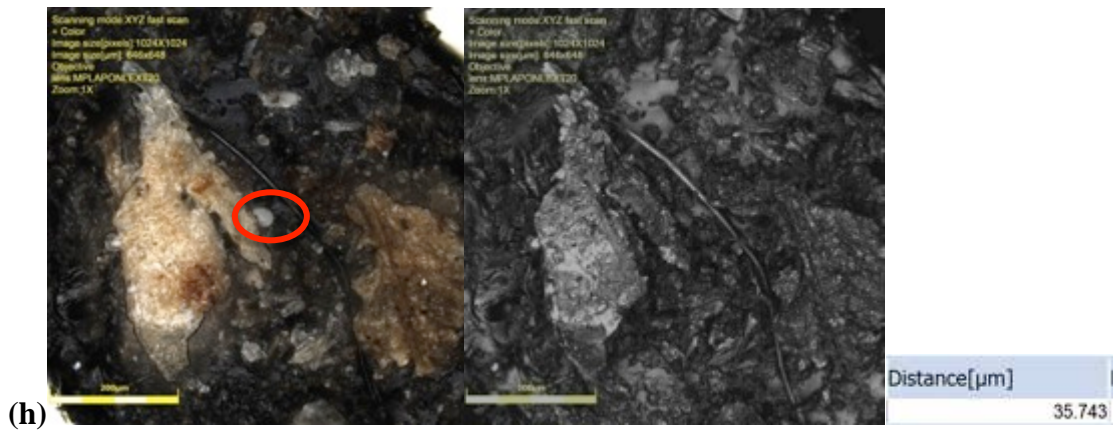
All fragments were visually different from the surrounding dust particles having a white or slightly yellow colouring and sharp edges, suggesting they may be pieces of a fractured polymer rather than typical dust organic matter. Figure 5.12 shows the optical and 3D laser images of the 8 areas of interest removed from the first 1 mg analysis of dust samples 1, 2, and 3. The suspect particle in the last sample area (from Dust 3) was only observed in the 3D microscopy analysis (not on XRFS) due to its

very small size (36 μm) and this method in general helped to locate the possible Br-rich fragments in all sample areas to analyse on the SEM/EDS.

Figure 5.12: (Left) Colour optical and (Right) 3D laser images as well as measured lengths of suspect particles in 8 identified areas of high Br-content. Areas (a), (b), (c), (d) from Dust 1, (e), (f), (g) from Dust 2 and (h) from Dust 3



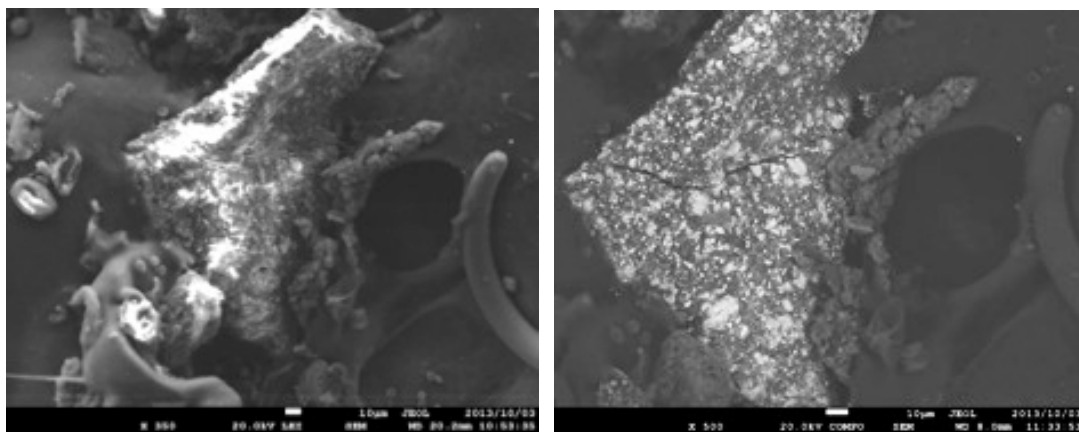




5.3.3 Scanning Emission Microscopy/Energy Dispersive Spectroscopy

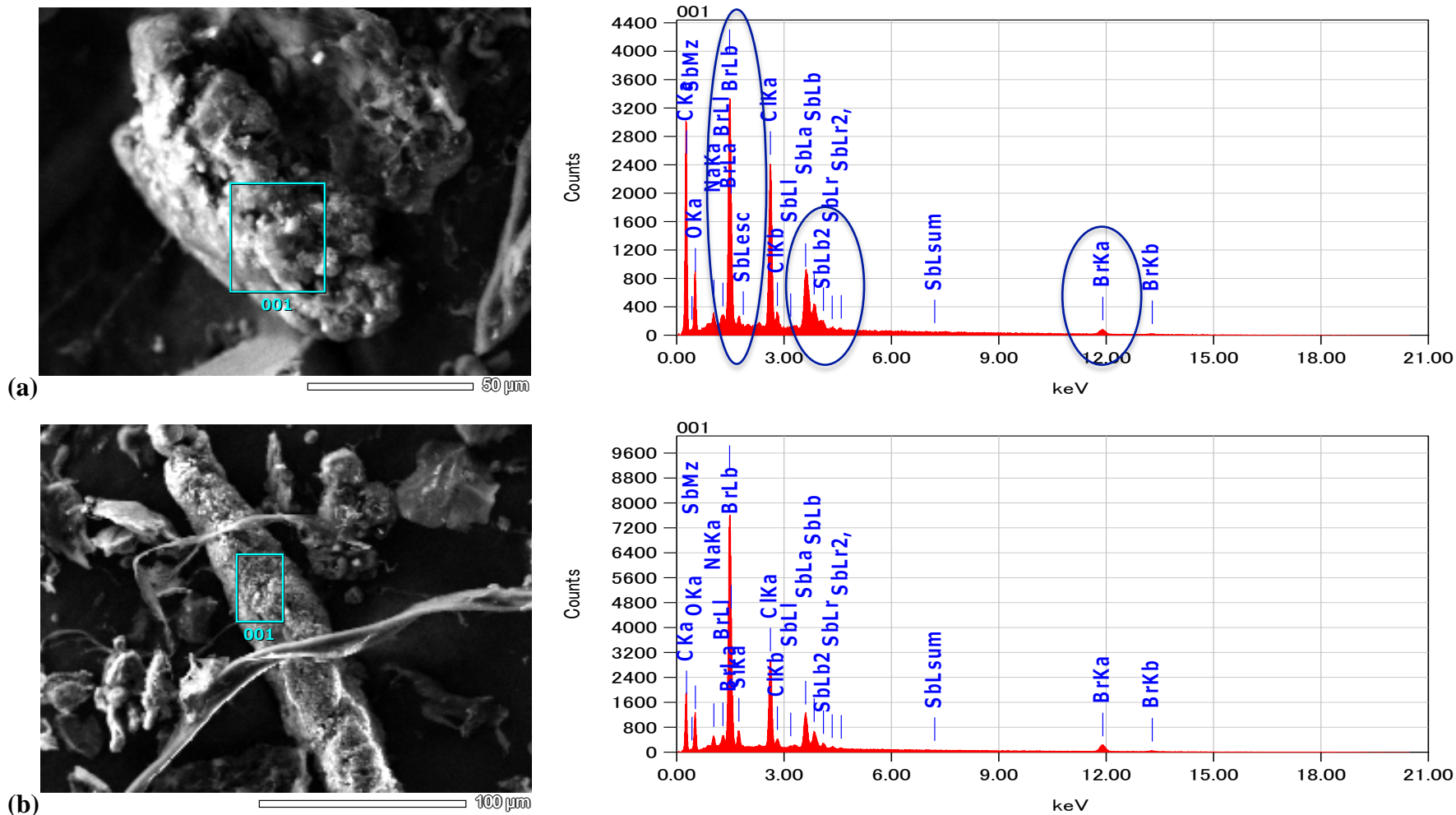
Following the 3D imaging, SEM/EDS analysis was performed on the suspected Br-rich fragments to confirm elemental composition. Images of the particles were captured using both secondary electron and backscattering electron SEM techniques. The backscattering image provided additional information on the distribution of heavier elements over the particle surface as these elements (e.g. bromine and antimony) are located in brighter regions and lighter elements are located in the darker regions. Figure 5.13 shows a comparison of a secondary electron and backscattering image from a Br-rich particle located in Dust 2, showing the difference in captured images between the two techniques. The shine in the image on the left is due to sample charging, as the sample surface had not been coated.

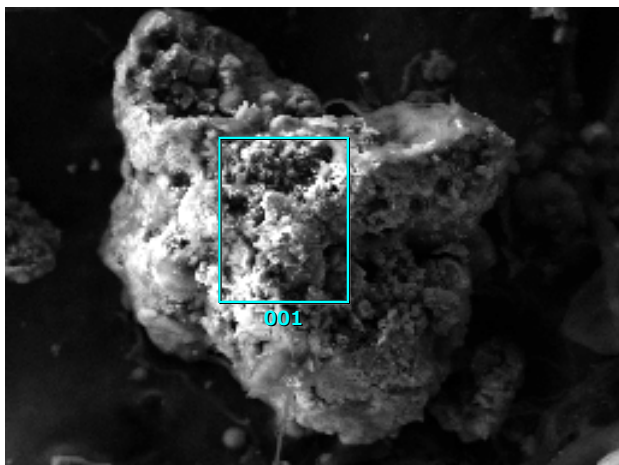
Figure 5.13: (Left) Secondary electron SEM image and (Right) backscattering image, showing the dark and light patches that indicate the presence of lighter and heavier elements respectively



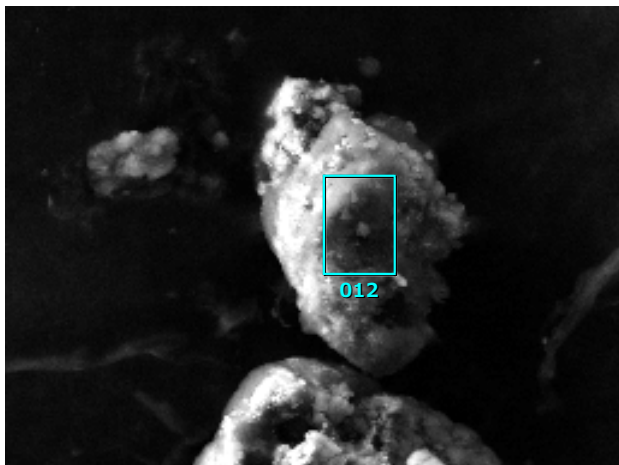
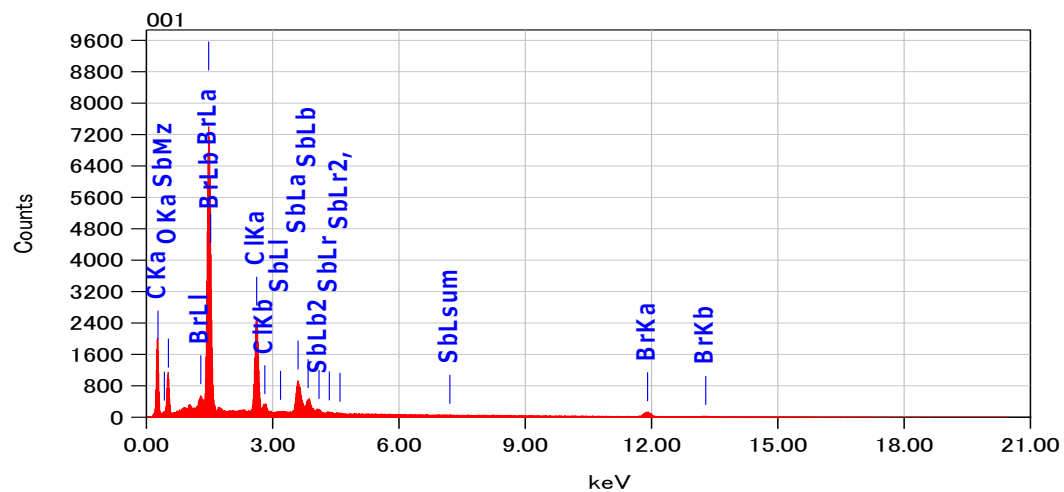
EDS was performed on the particles by scanning the SEM beam across an area defined on the particle surface. The presence of Br and antimony (Sb) were identified in all suspect fragments from the 7 initial areas that were identified in the first 1 mg analysis from Dust 1 and Dust 2. The fragment from Dust 3 was analysed both with and without sample surface coating and is discussed later in this section. Figure 5.14 presents the backscattering electron image and corresponding EDS profile for the fragments isolated from Dust 1 and 2. The samples (except one fragment from Dust 3, described later) were not platinum coated before SEM/EDS to prevent interference with the subsequent FTIR analysis, and as a result there was a charging effect on the images. Due to the charging effect and the uneven topography of the sample surface, quantitative elemental analysis was not possible; rather this SEM method qualitatively identified the presence of these elements. Br and Sb were observed in distinct pockets on each particle surface in a heterogeneous fashion, similar to the study by Wagner et al. (2013) who also observed clear pockets of Br on particle surfaces. Figure 5.15 shows point analyses of dark and light regions over the surface of a particle from Dust 2, with the EDS profile confirming the presence of Br in the light areas only, showing this heterogeneous element distribution.

Figure 5.14: (Left) Backscattering electron images and (Right) corresponding EDS elemental profile, showing the clear presence of Br and Sb (highlighted in (a)), from suspect Br-rich fragments identified in the 7 sample areas removed from the first 1 mg analysis of Dust 1 and Dust 2

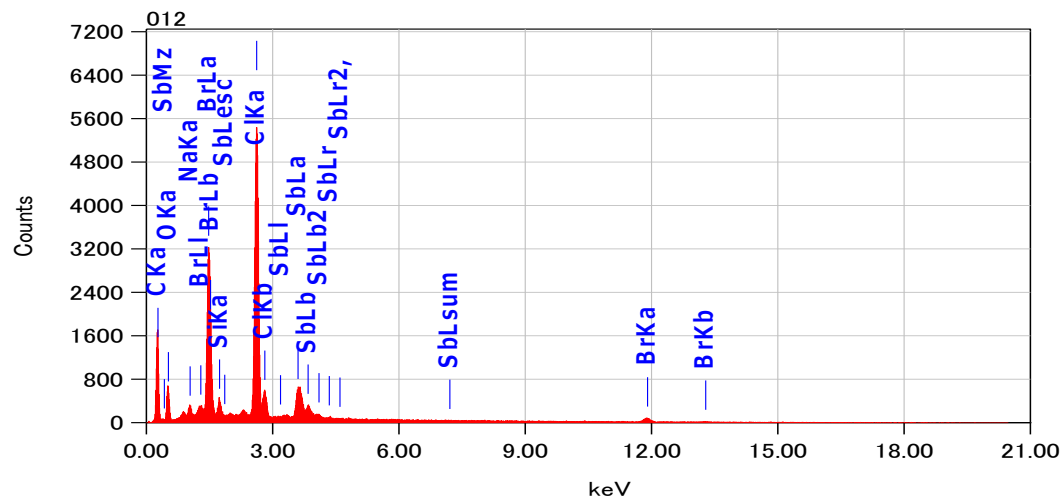


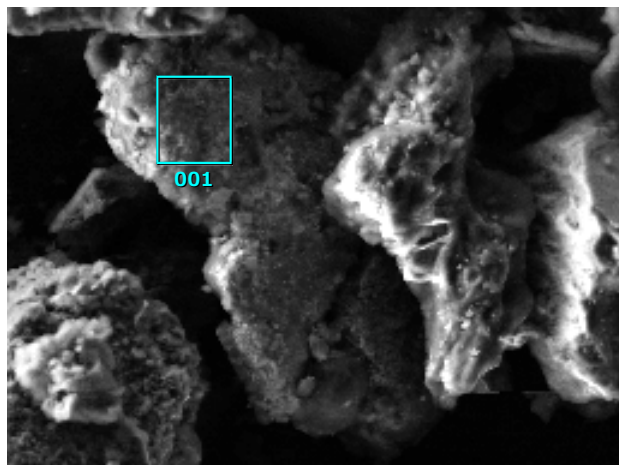


(c)#1



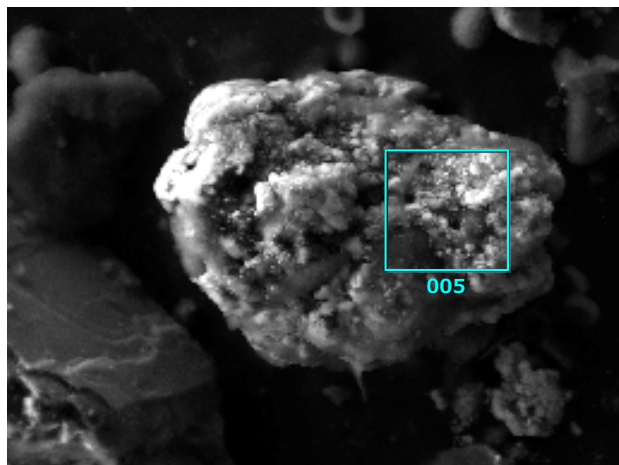
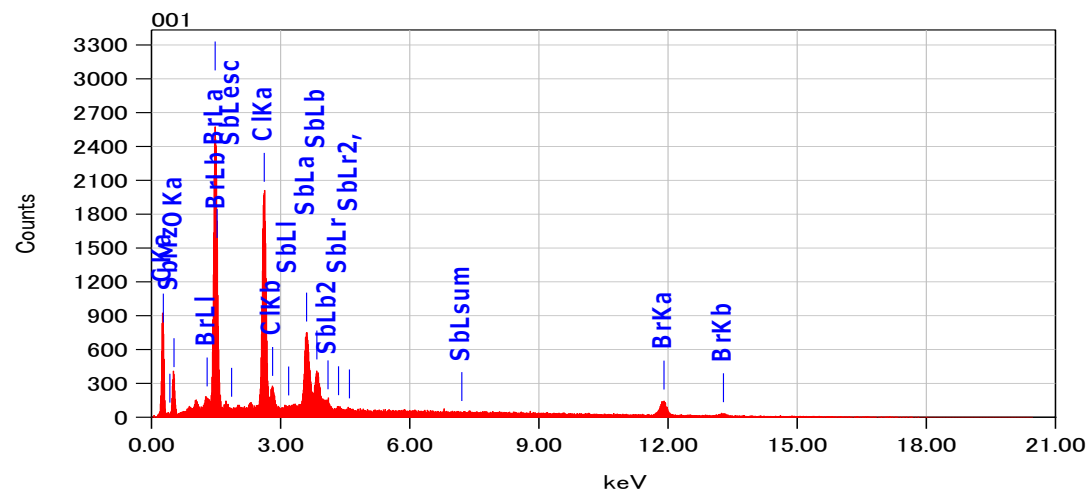
(c)#2





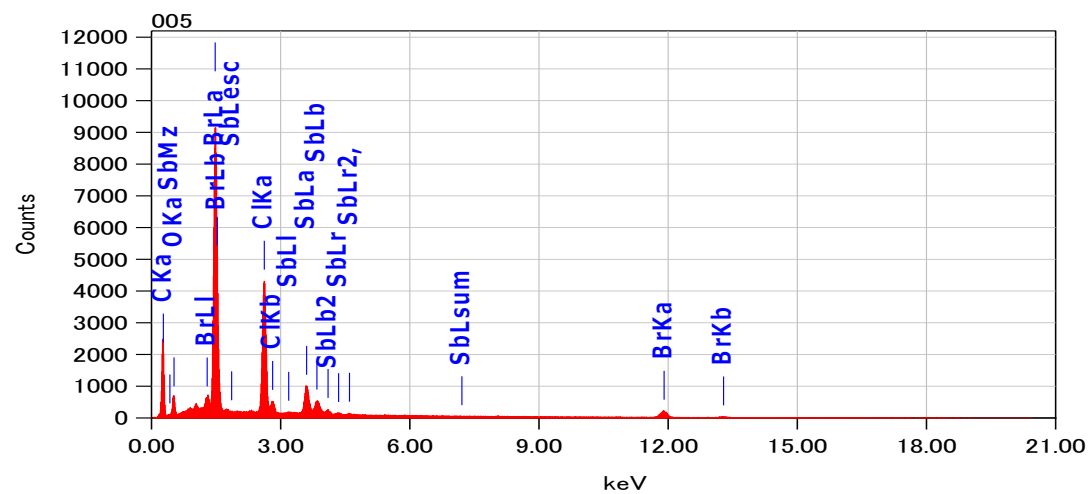
(d)#1

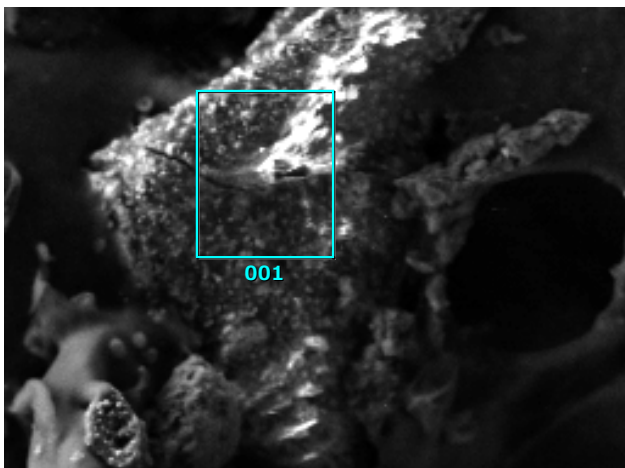
50 μm



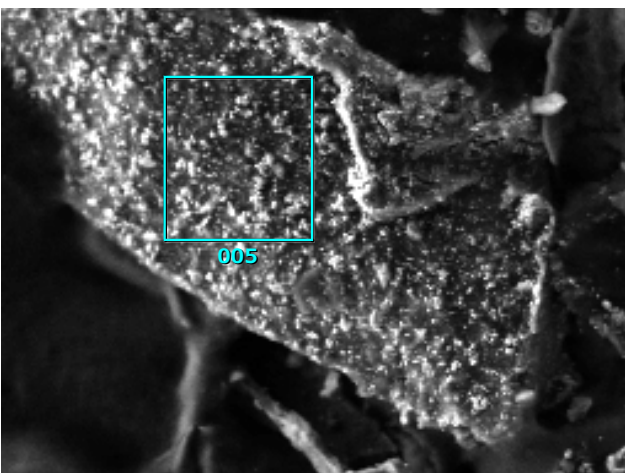
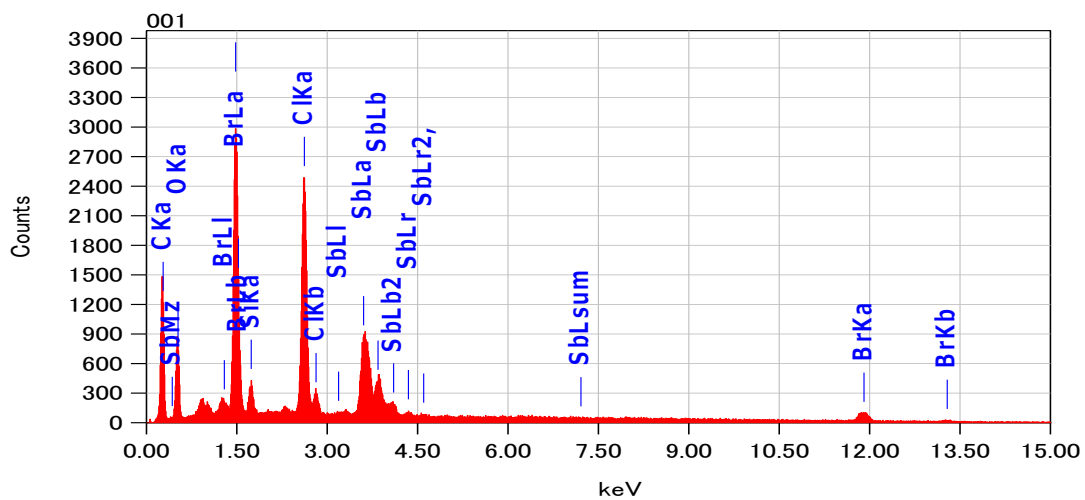
(d)#2

25 μm

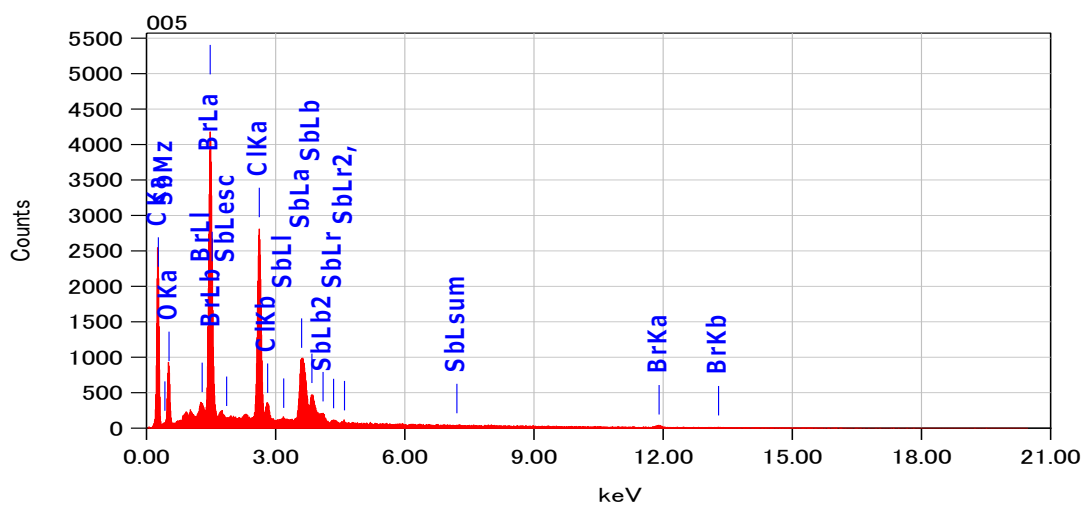




(e) 100 μm



(f) 100 μm



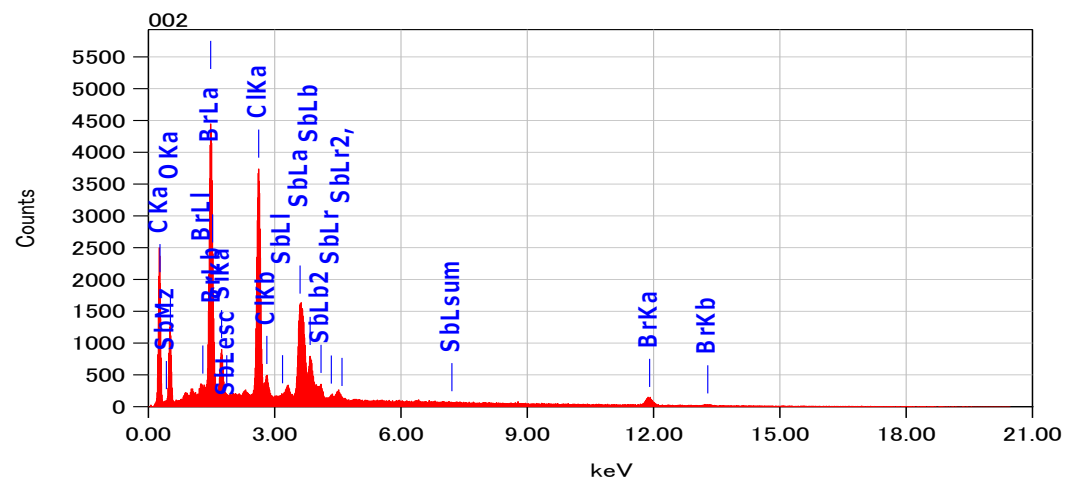
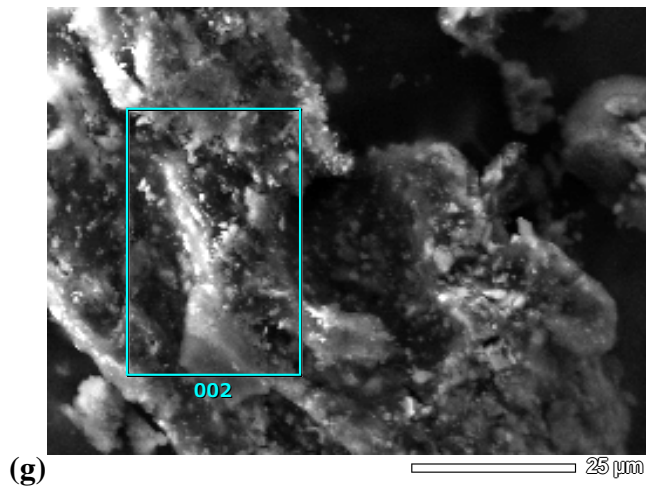
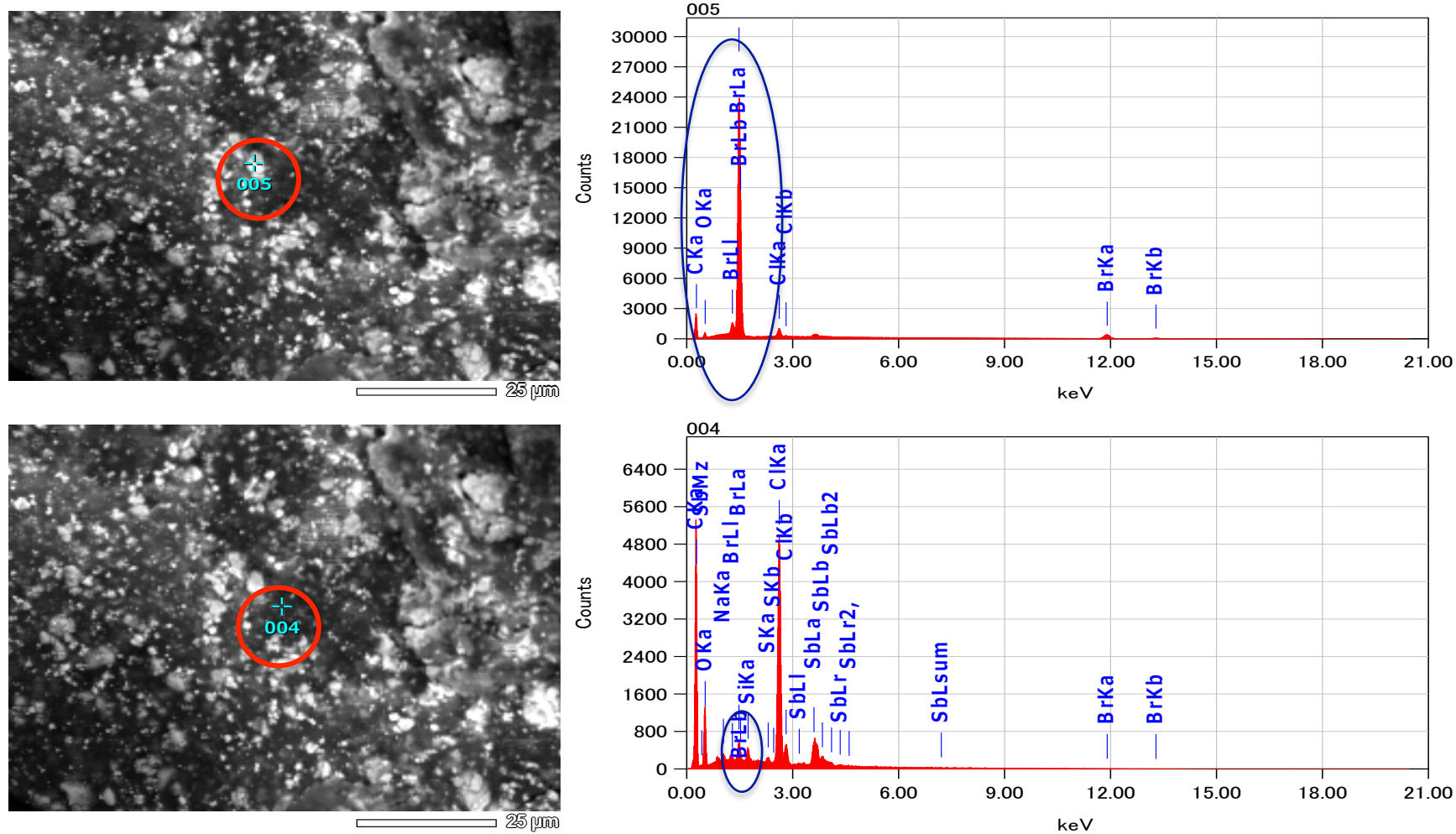
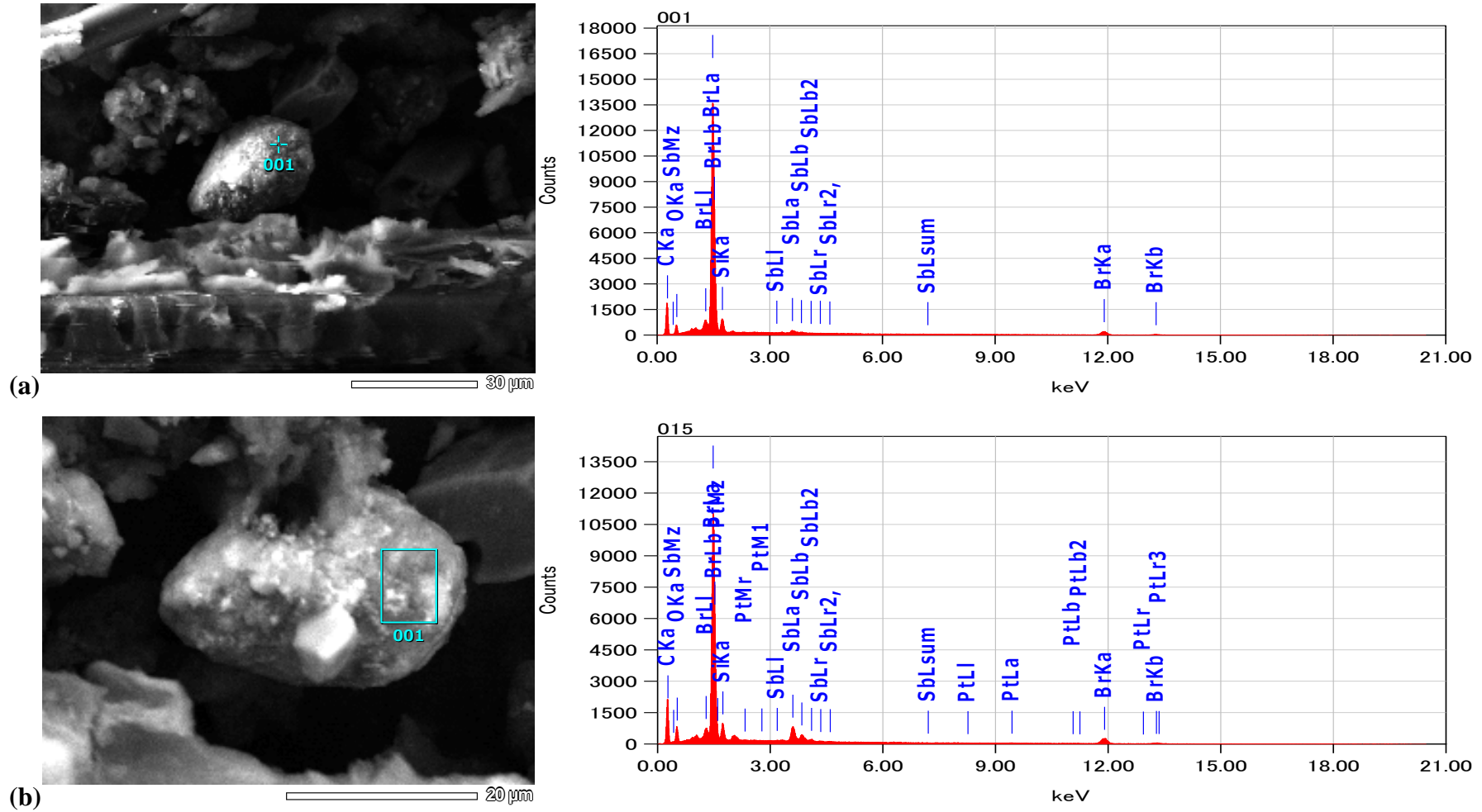


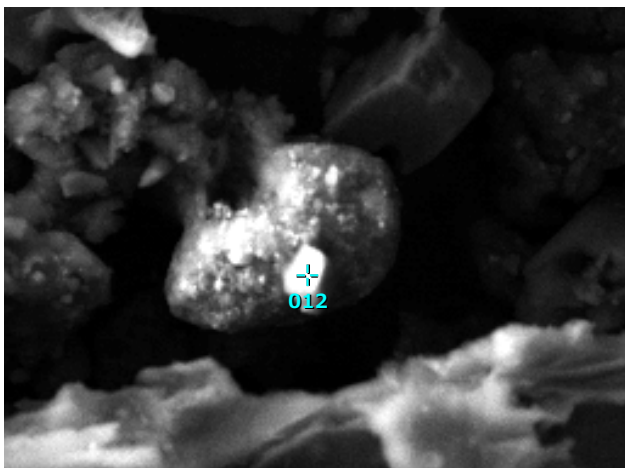
Figure 5.15: (Left) Backscattering electron image and (Right) corresponding EDS point analysis of (top) light and (bottom) dark regions over the surface of a particle isolated from Dust 2 (fragment (g)), showing a heterogeneous bromine distribution



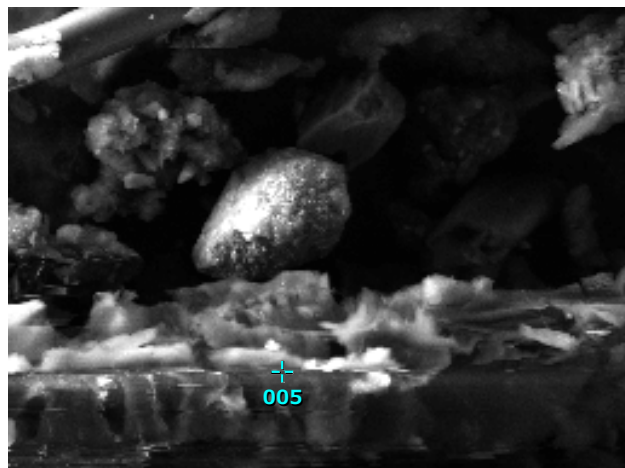
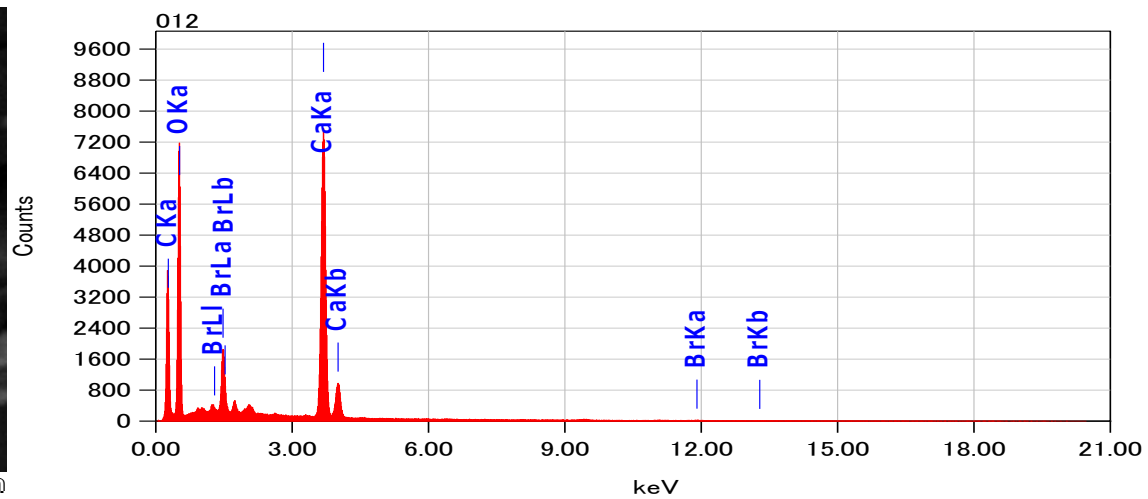
The Br-rich fragment from Dust 3 was very small (36 μm length) and partly hidden under a large piece of organic matter in the dust, yet an elevated bromine content was still detected with the Micro XRFS. Due to the small size of this particle it could not be removed for FTIR analysis so it was analysed twice with SEM/EDS, without coating and after platinum coating for 200 seconds to reduce charging effects. Figure 5.16 shows the backscattering image of the particle and its related EDS elemental profile for both with and without sample surface coating. A similar Br count was seen in the EDS profile before and after coating the sample, however the Sb signal improved after the surface coating was applied. A contaminating particle was observed sitting on the fragment surface, after coating, and EDS analysis of this particle confirmed the presence of calcium and oxygen, suggesting the particle is likely a stray calcium carbonate particle that has shifted and landed on the particle during the instrument obtaining vacuum conditions. The EDS analysis of this particle is also shown in Figure 5.16 and the small bromine signal likely originates from the Br-rich fragment underneath, as the SEM X-rays at 20 kV will be able to penetrate through the small particle into the Br-rich fragment. The large piece of organic material that partially covers the fragment was analysed with EDS, due to curiosity, and the presence of carbon, calcium and various mineral salts (sodium, chlorine, calcium, potassium) was confirmed. This material may be a flake of skin present in the dust sample. The EDS analysis of this organic material is also shown in Figure 5.16.

Figure 5.16: (Left) Backscattering image and (Right) corresponding EDS elemental profile of a small fragment in Dust 3, (a) without coating (b) with Pt coating (c) of contamination particle present on fragment surface and (d) large organic material partially covering the Br-rich fragment

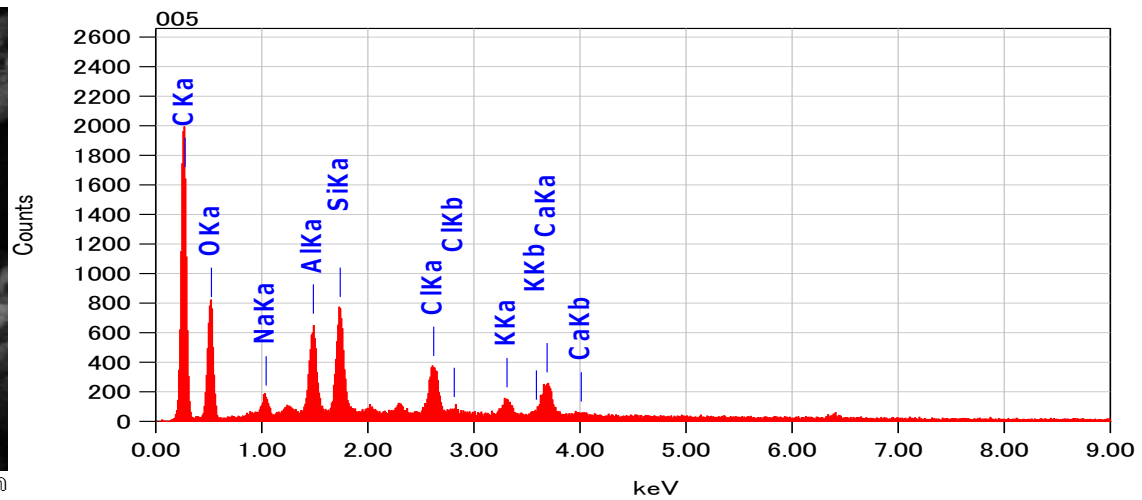




(c)



(d)



The high bromine content areas originally identified with the Micro XRFS, all showed the bromine to be associated with distinct individual particles and a homogeneous bromine distribution over the dust sample was not seen, a result consistent with migration via abrasion, rather than volatilisation and subsequent partitioning to dust.

5.3.4 Fourier Transform Infrared Spectroscopy

After SEM/EDS analysis, these identified individual particles were removed from the sample area with a pair of tweezers for FTIR analysis. All particles identified in all three 1 mg analyses of Dust 3 were $< 50 \mu\text{m}$ in size and too small for removal, thereby preventing further FTIR analysis. Hence in Dust 3, it was only possible to confirm the presence of bromine in the particles.

The initial 7 particles, isolated from the first 1 mg analysis of Dust 1 and 2, were analysed on the FTIR, along with further particles identified in the second and third 1 mg dust samples analysed, to provide information on a total of 8 particles from Dust 1 and 9 particles from Dust 2. All fragments from the same dust sample had very similar spectra, suggesting a common contamination source to that dust. Figure 5.17 presents a comparison of all sample spectra obtained from Dust 1 and 2. Library database searches of the spectra from particles in Dust 1 were obtained to identify closest component matches from the database. Firstly, the entire spectrum was analysed for the top 3 matches in the database that combined, most closely matched the spectrum. An 88% match was returned for the combination of BDE-209, antimony trioxide and an acrylic based industrial coating. To improve the accuracy of the spectral matches, individual peaks and areas of interest in sample spectra were run separately through the software to find the top match in the database for each peak/area. The absorption spectrum in the range of 900 to 1400 cm^{-1} (often due to C-O bond stretches, particularly from ethers) returned a 97% confidence match with BDE-209, while the strong absorption at $\sim 700 \text{ cm}^{-1}$ (possibly from a Sb-O bond stretch) combined with the broad absorption at 3100 - 3500 cm^{-1} (from a Sb=O stretch) returned a 91% match for antimony trioxide. To identify the product polymer, the strong absorbance at $\sim 1750 \text{ cm}^{-1}$ (often from a C=O, or C=N stretch) combined with the absorbance at 2800 - 3000 cm^{-1} (often from various C-H bond stretches) returned a

93% match for a styrene acrylic. Figure 5.18 shows the library database matches for the particles in Dust 1.

The same method was applied for spectra from particles in Dust 2 with a 73% match obtained for the combination of BDE-209, antimony trioxide, and again an acrylic based industrial coating. Once more, comparison of individual peaks/areas resulted in higher confidence level matches with a 92% match for BDE-209, a 90% match for antimony trioxide, and a 95% match for an acrylic copolymer from the strong absorbance at $\sim 1750\text{ cm}^{-1}$ and absorbance at $2800\text{-}3000\text{ cm}^{-1}$. By investigating the spectral peaks/areas separately, the confidence of spectral matches with database spectra was improved greatly. The lower accuracy for the matched total spectrum from Dust 2 is largely due to the presence of the additional broad peak at 1500 cm^{-1} , reducing confidence in the accuracy of the matches. This peak was similar to the broad peak seen in the reference calcium carbonate spectra, suggesting calcium carbonate may have been used as a resin filler in the polymer fragments isolated from Dust 2. Figure 5.20 shows the library database matches for the particles in Dust 2.

The reference spectra for the acrylic copolymer, styrene acrylic and for an acrylonitrile-butadiene-styrene (ABS) copolymer are all similar, and hence are all possible matches for the polymer backbone in these isolated fragments. ABS plastic was compared, as it is commonly flame-retarded with both BDE-209 and antimony trioxide, and it is thus plausible that the fragments may have originated from a source containing BDE-209 treated ABS plastic. The plastic particles may also have suffered some form of degradation due to age, UV or heat exposure that may alter the resultant FTIR spectra, reducing the % match with the reference library spectra, so ABS plastic cannot be ruled out as a possibility. Figure 5.19 shows a comparison of the sample spectrum, BDE-209, antimony trioxide and the ABS copolymer reference spectra for a fragment from Dust 1. Figure 5.21 shows a comparison of the sample spectrum, BDE-209, antimony trioxide, ABS copolymer and calcium carbonate reference spectra for a fragment from Dust 2.

Figure 5.17: FTIR sample spectra from (Top) 8 particles isolated from Dust 1 and (Bottom) 9 particles isolated from Dust 2 with peaks highlighted in the first particle spectra from each dust that represent stretches from the polymer backbone, BDE-209 and antimony trioxide

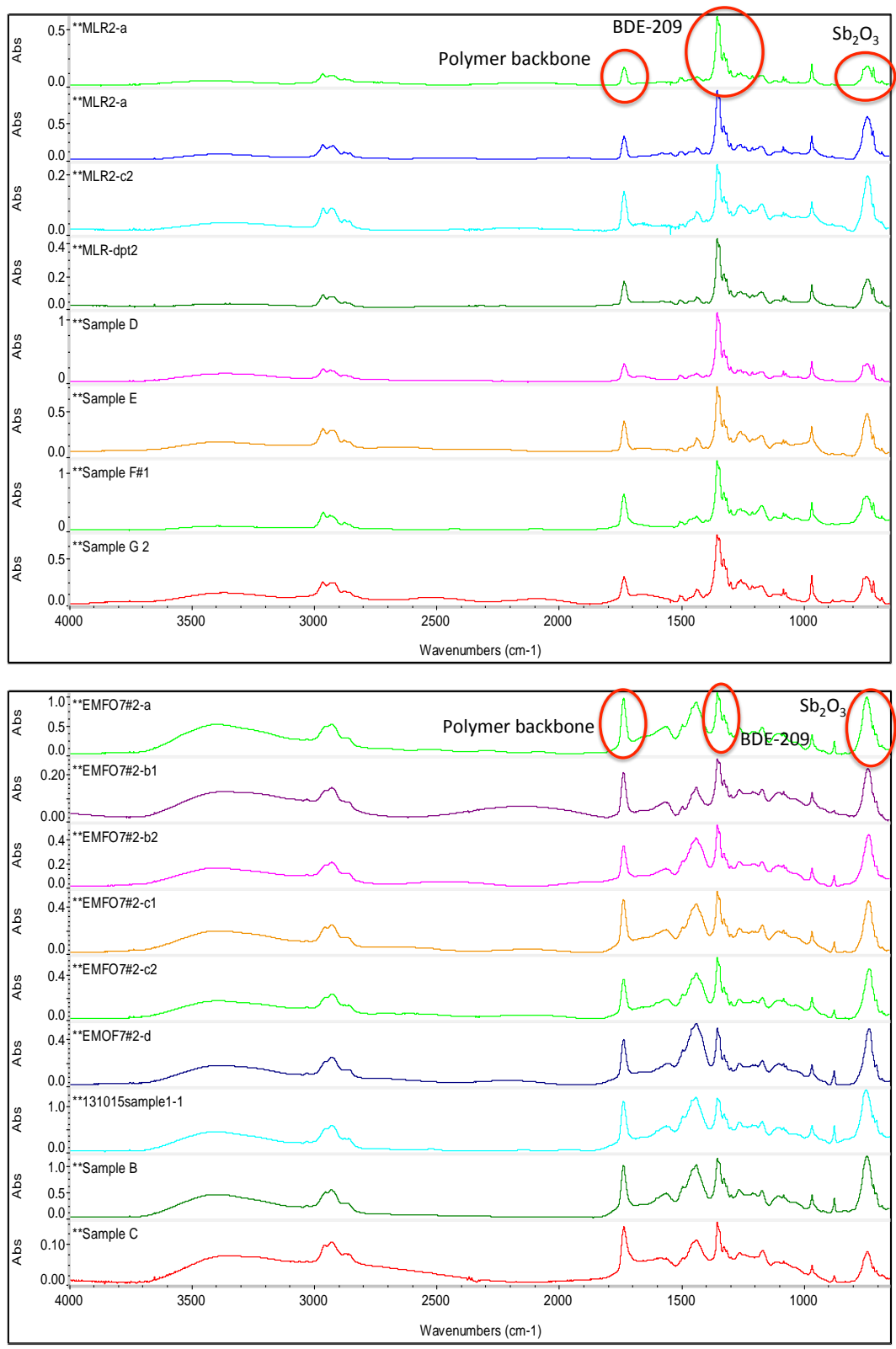
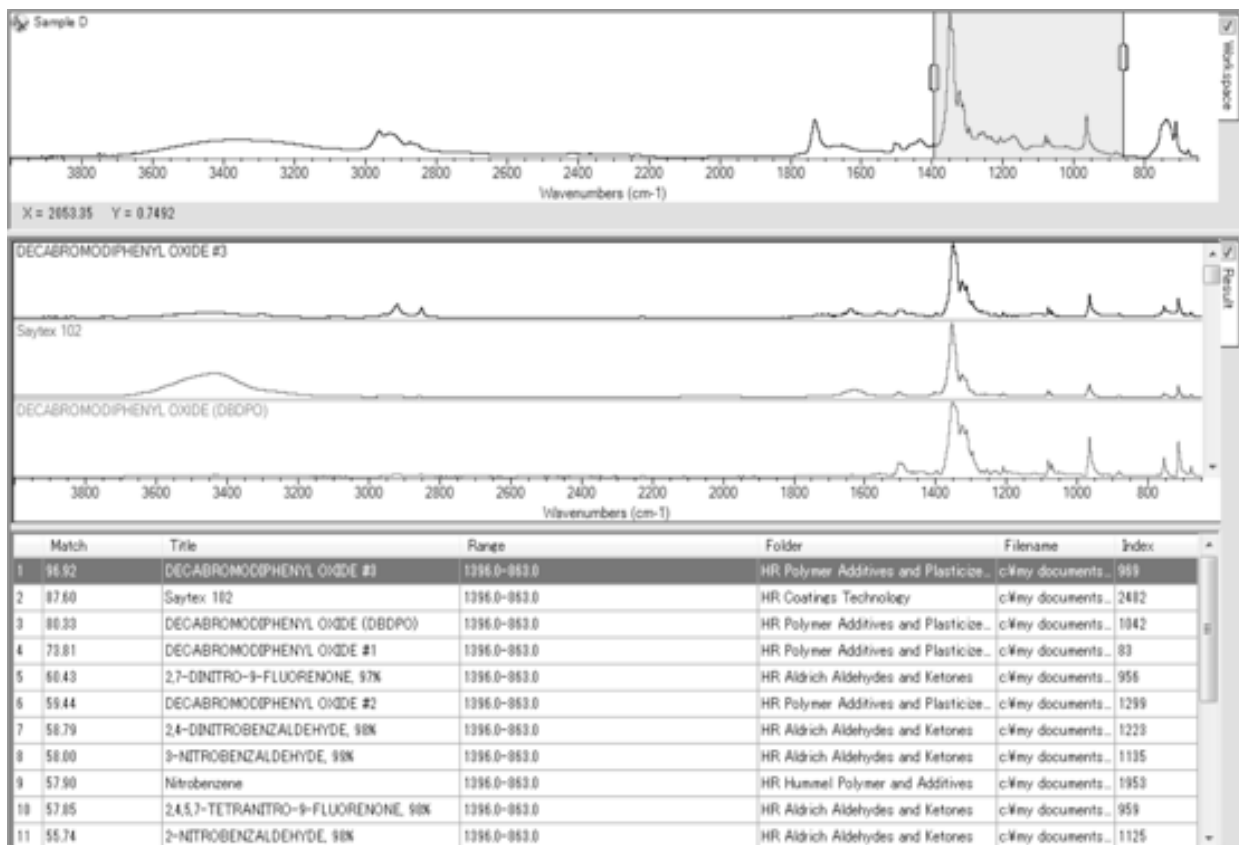
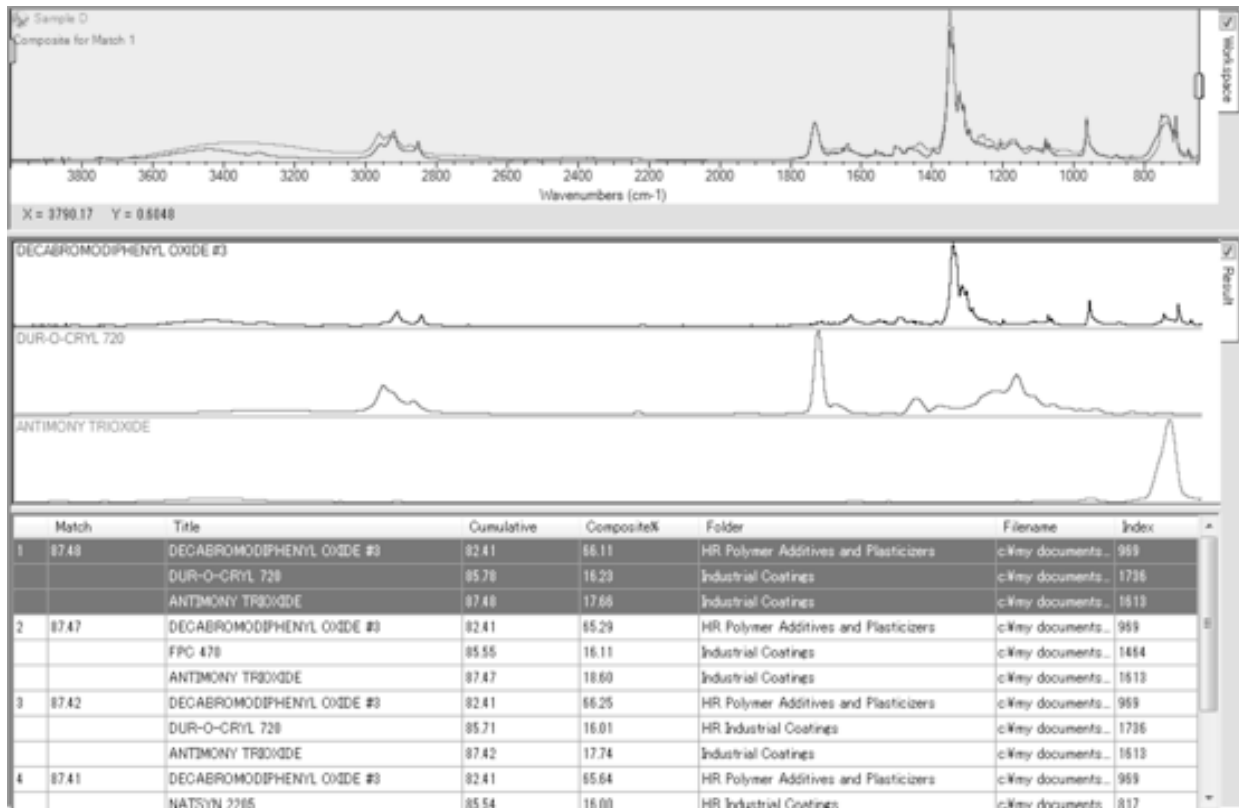


Figure 5.18: Software library database matches for the entire sample spectrum and for peaks of interest to improve match accuracy for Br-rich fragments from Dust 1



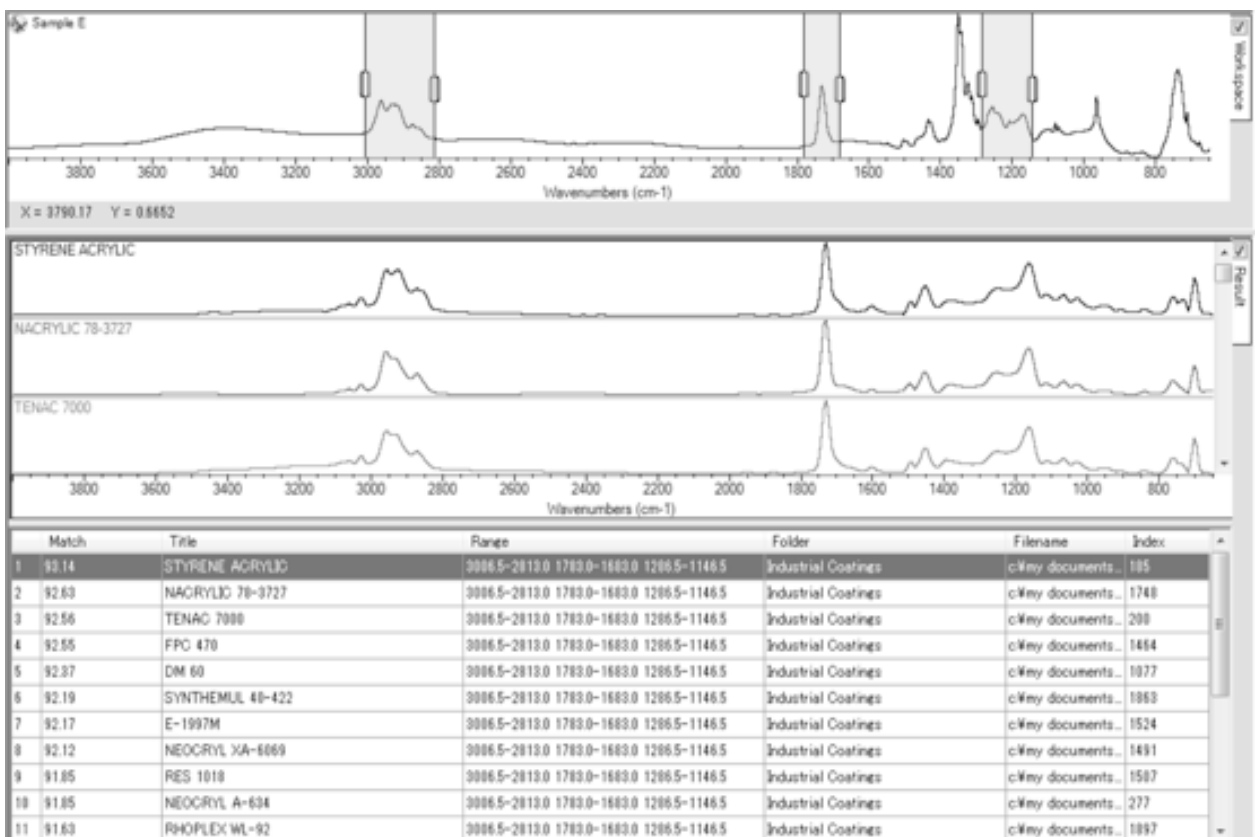
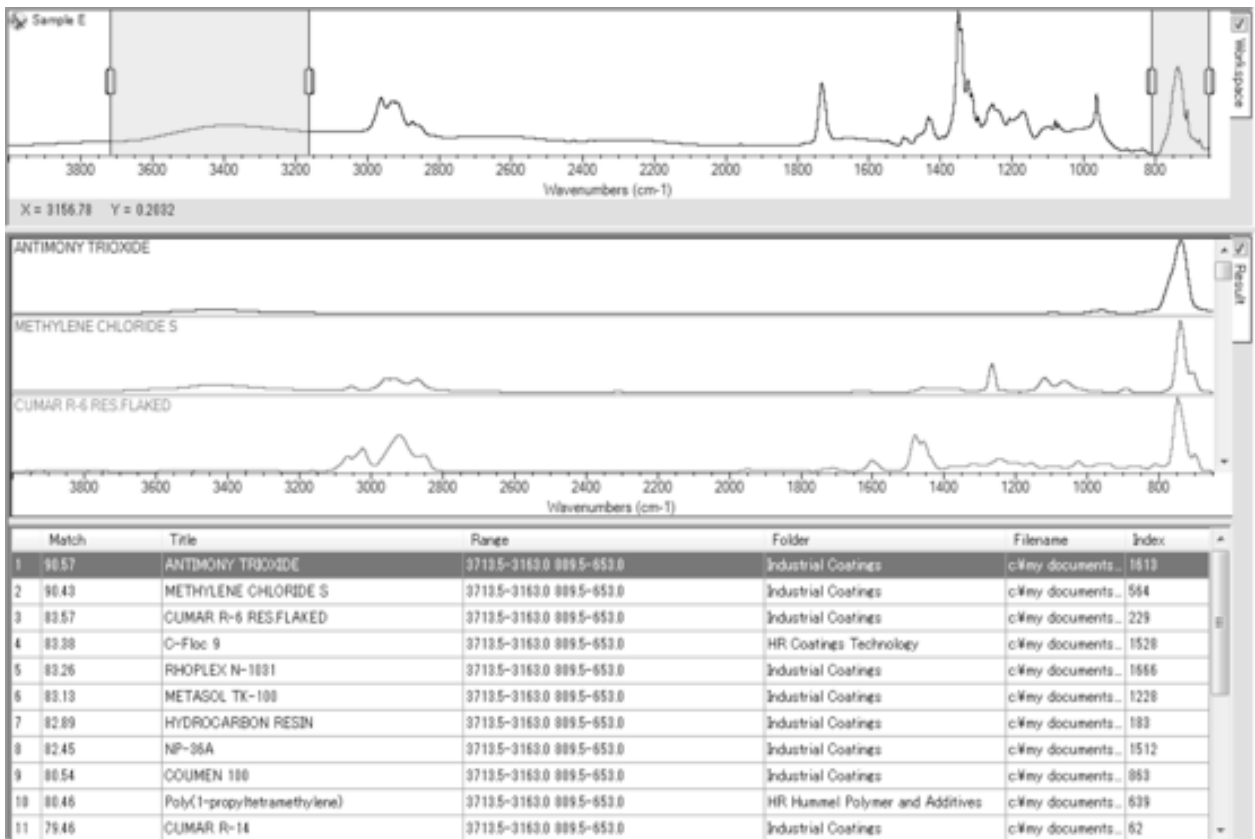


Figure 5.19: Comparison of spectra from a fragment isolated from Dust 1 and reference spectra for BDE-209, antimony trioxide, and ABS copolymer

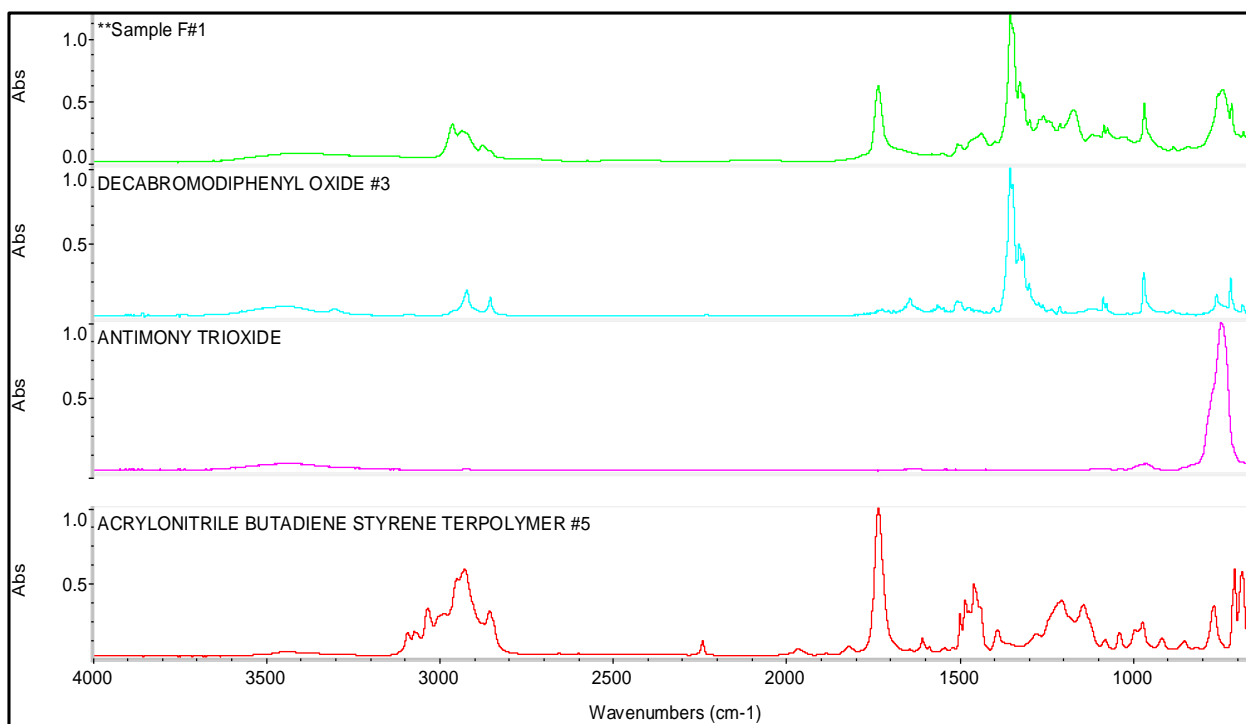
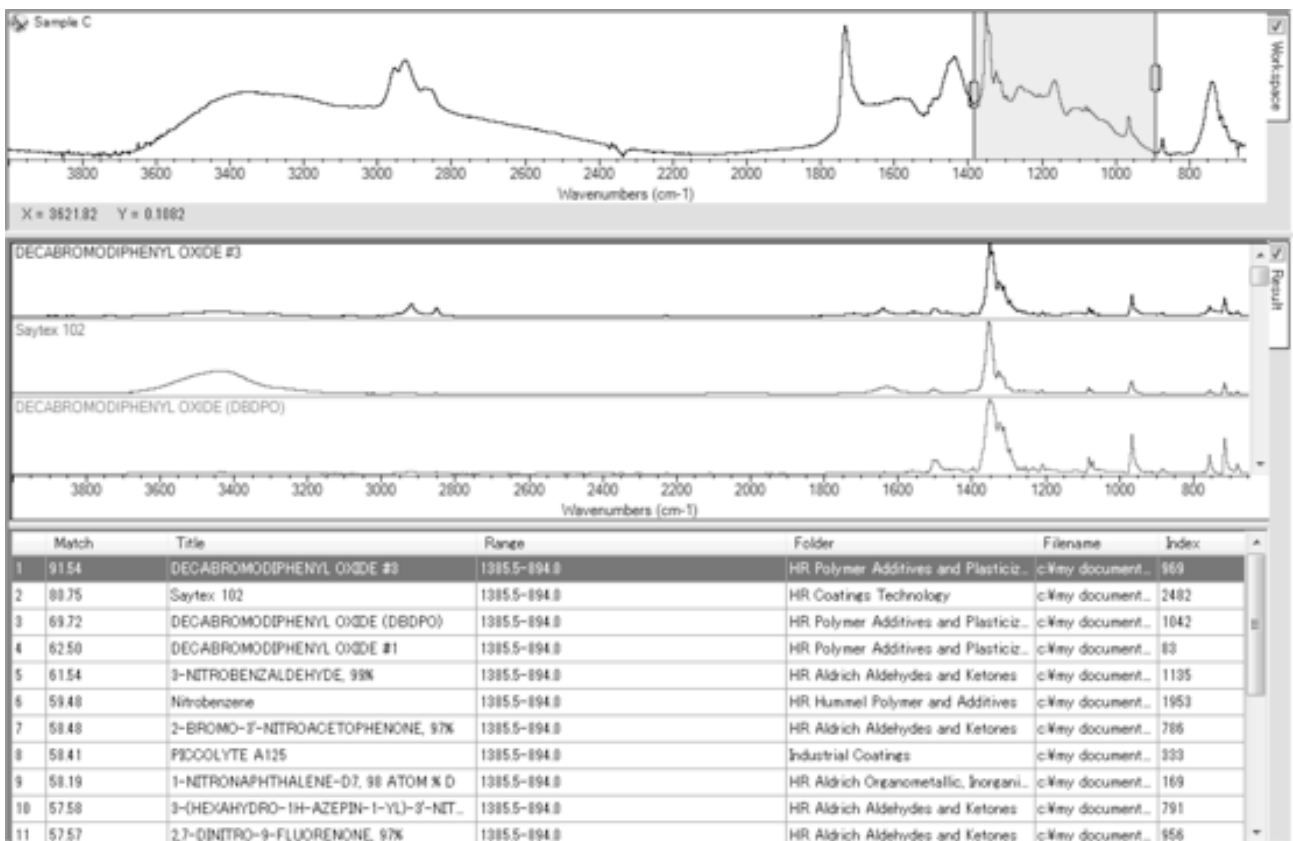
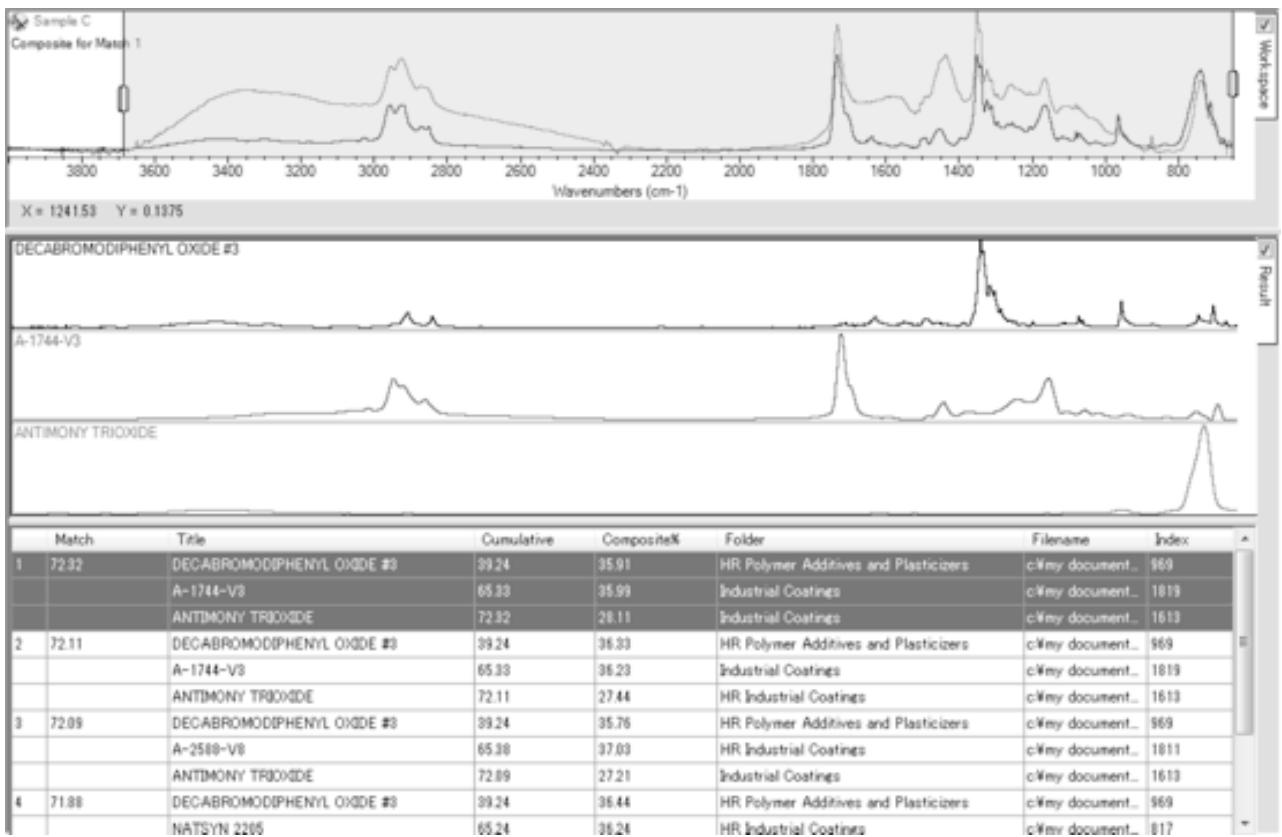


Figure 5.20: Software library database matches for the entire sample spectrum and for peaks of interest to improve match accuracy for Br-rich fragments from Dust 2



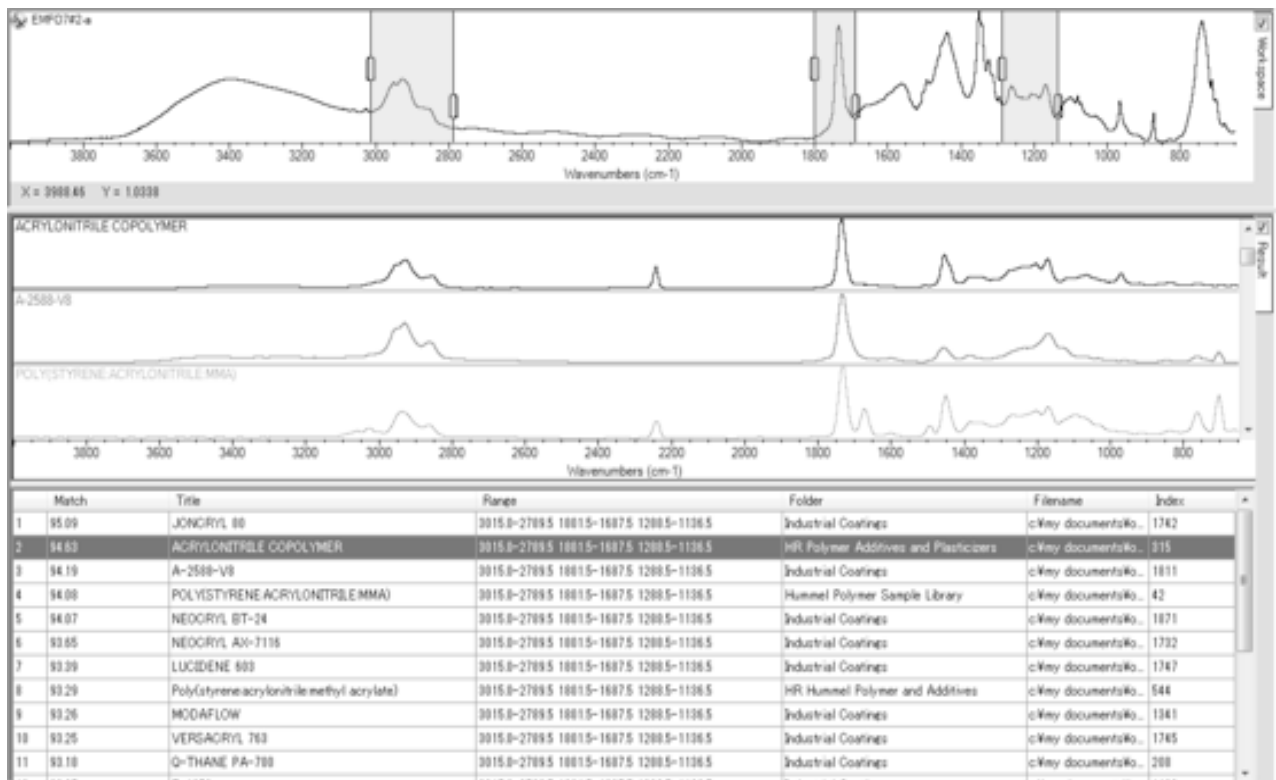
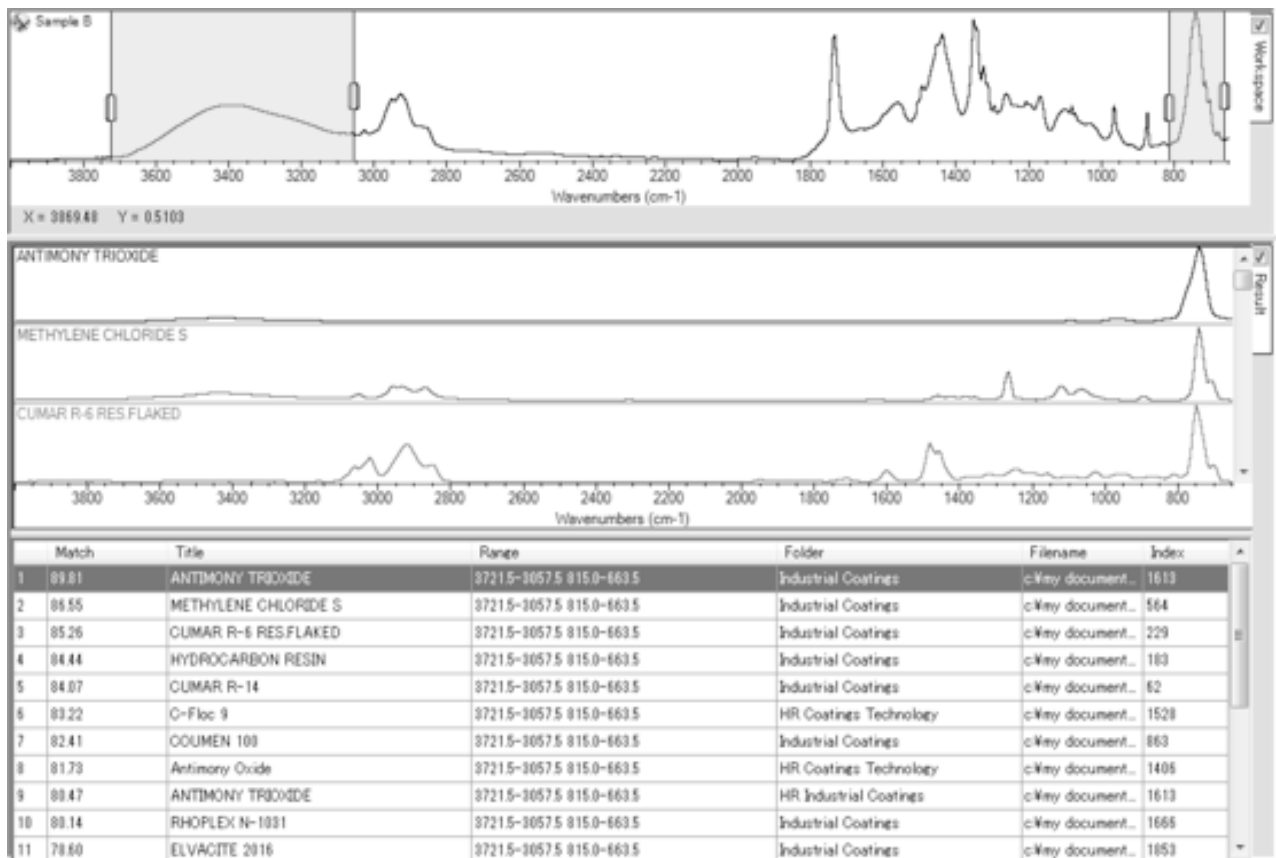
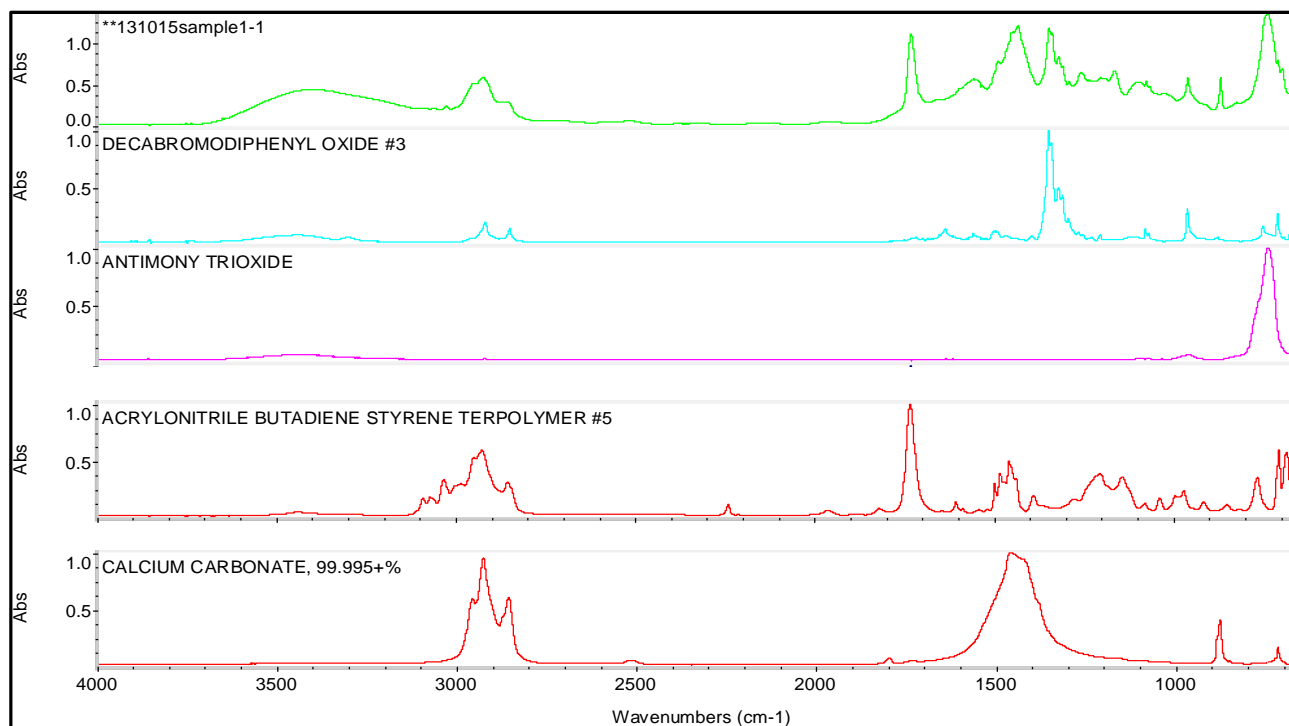


Figure 5.21: Comparison of spectra from a fragment isolated from Dust 2 and reference spectra for BDE-209, antimony trioxide, ABS copolymer and calcium carbonate

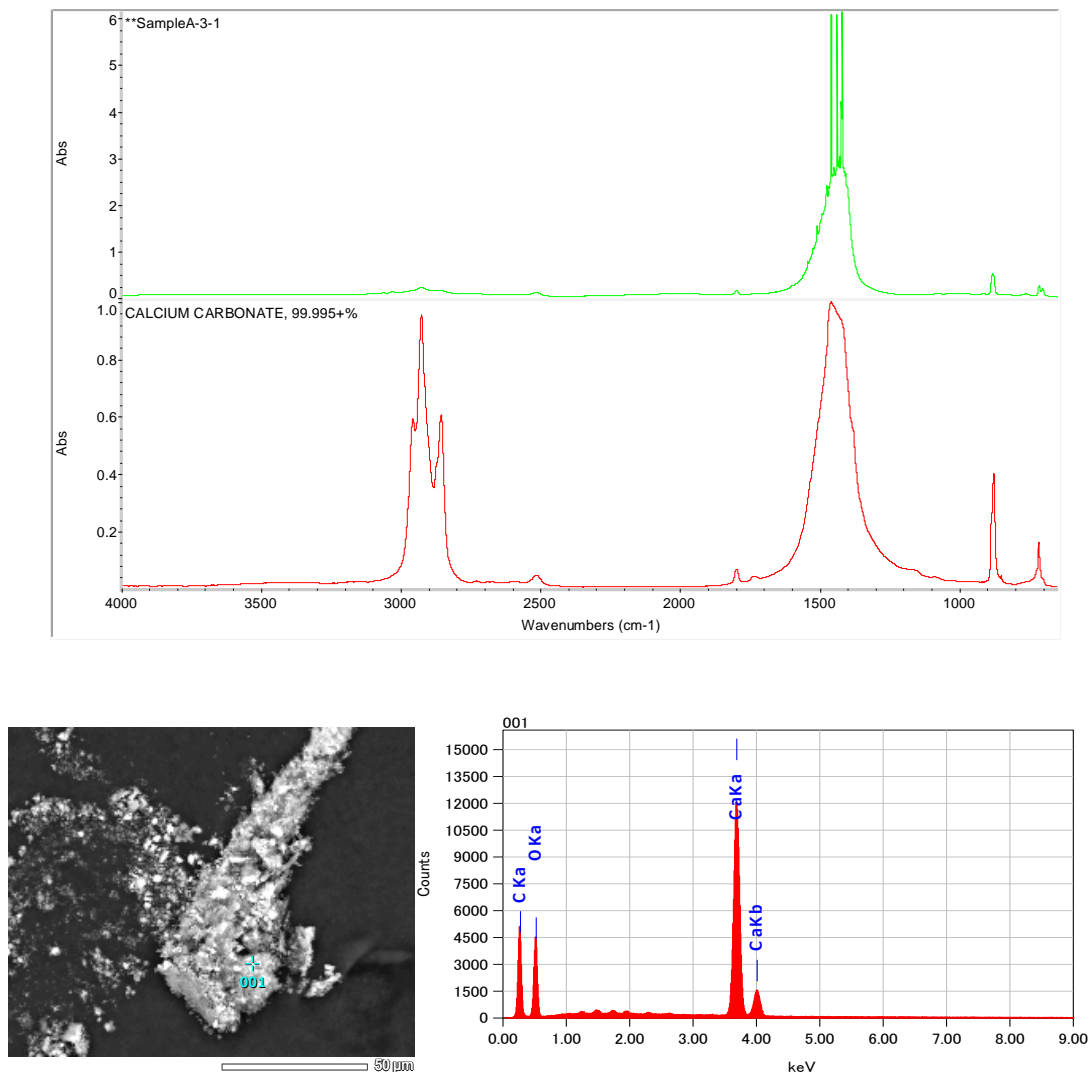


5.3.4.1 Calcium Carbonate

During removal of one Br-rich fragment from Dust 2, the particle fragmented and the smaller fragments were analysed on FTIR separately. One fragment provided a very different spectrum and it was suspected this may be calcium carbonate as the broad strong peak at $\sim 1500\text{ cm}^{-1}$ matched the corresponding peak in the calcium carbonate reference spectrum. The complete sample spectrum of this particle differed to the reference spectrum, as the sample peak at $\sim 3000\text{ cm}^{-1}$ is much smaller than the peak present at $\sim 1500\text{ cm}^{-1}$, whereas the reference spectrum contains peaks of similar height. This isolated particle will not be a pure calcium carbonate particle (other chemicals present) and is likely to contain dust particle impurities on the surface, hence the other chemicals that are present will overlap and interfere with the FTIR spectra collected, resulting in the differences between the sample and reference spectrum for calcium carbonate. For this reason, the FTIR analysis is not a definitive confirmation of identity, but rather provides a plausible chemical match. To gain further confirmation of the particle's composition this fragment was recovered after the FTIR analysis and reanalysed via SEM/EDS to determine elemental composition.

This confirmed the presence of calcium and oxygen, very strongly suggesting this was a calcium carbonate particle and its presence as attached to a Br-rich fragment, further supports the hypothesis that calcium carbonate has been used as a resin filler in the polymer fragments found in Dust 2. This analysis shows how these complementary methods can be utilised to provide information on particle composition. The FTIR particle and reference calcium carbonate spectra as well as the backscattering SEM image and corresponding EDS elemental profile of this particle are presented in Figure 5.22.

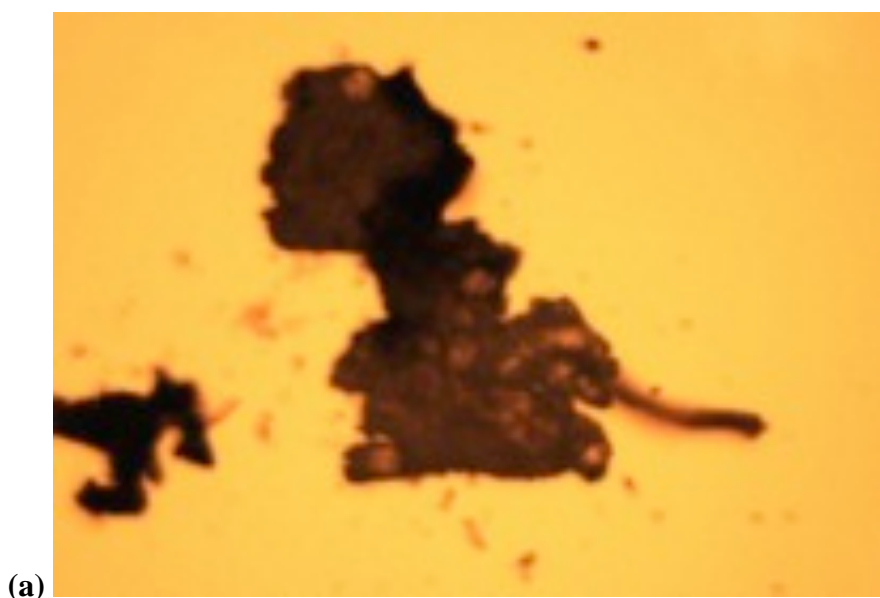
Figure 5.22: (Top) FTIR spectra of fragmented particle and reference calcium carbonate, (Middle) SEM backscattering electron image and (Bottom) corresponding EDS elemental profile obtained post FTIR analysis

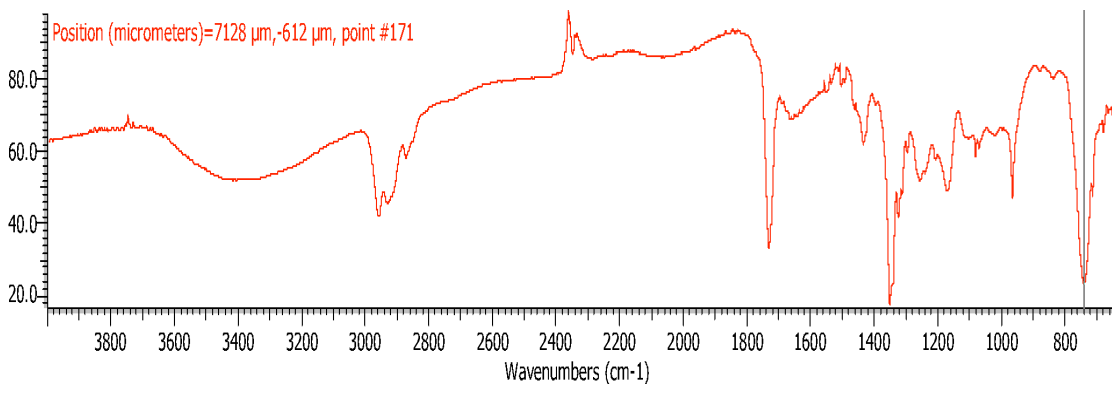
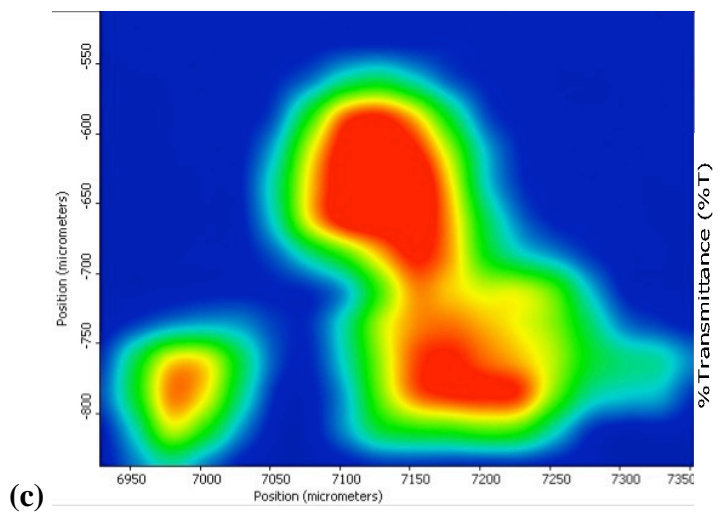
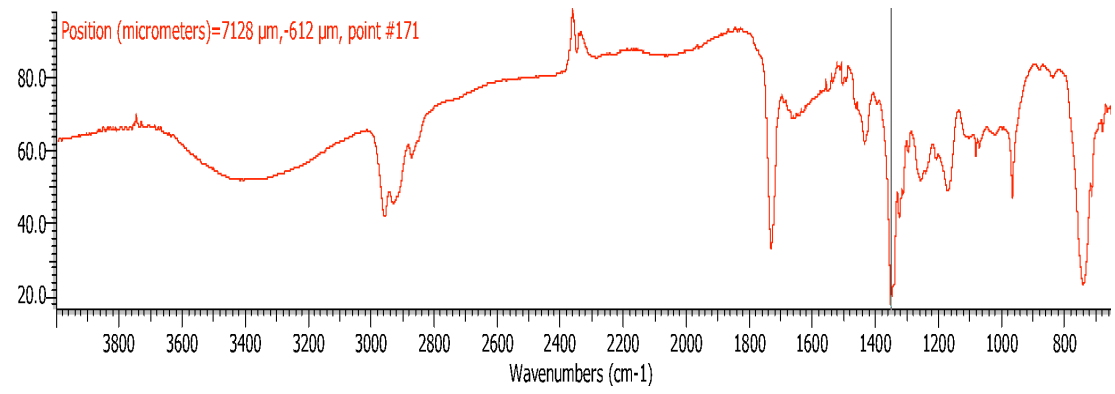
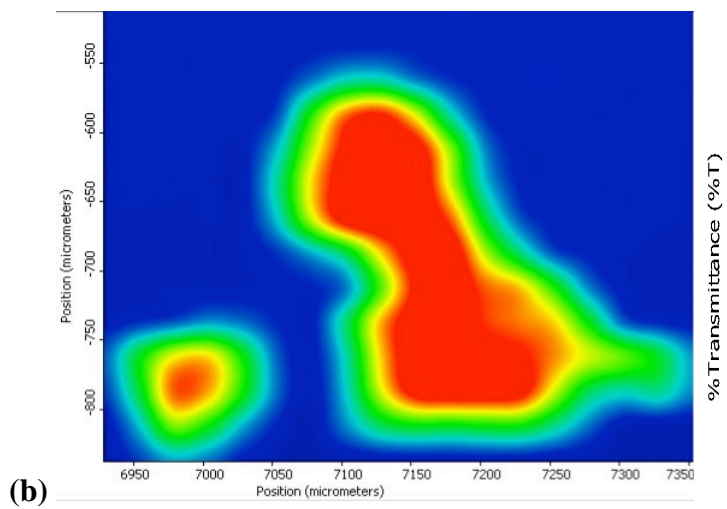


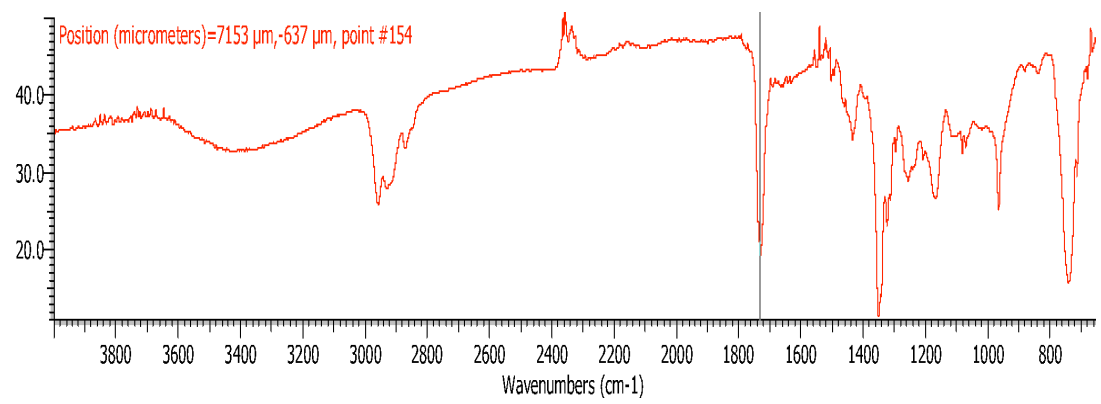
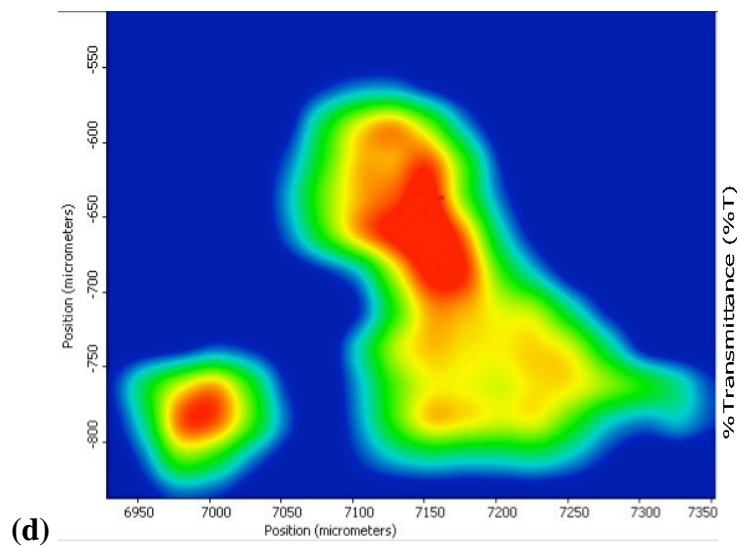
5.3.4.2 FTIR Mapping

The FTIR software provides an option to map the entire sample to provide information on homogeneity of components in the sample. By selecting the appropriate peak in the sample spectra, the mapping image shows the distribution of the compound corresponding to that peak through the sample area. For each particle analysed on the FTIR, the mapping image was produced for the peak corresponding to BDE-209 ($\sim 1350\text{ cm}^{-1}$), antimony trioxide ($\sim 700\text{ cm}^{-1}$) and the polymer backbone ($\sim 1700\text{ cm}^{-1}$). Figure 5.23 below shows (a) the captured image of a particle from Dust 1, as analysed on the FTIR, and the corresponding mapping images for (b) BDE-209, (c) antimony trioxide and (d) the polymer. The mapping images clearly show that all compounds are distributed throughout the particle, although the image cannot distinguish small variations in distribution over the particle surface, and previous SEM analysis has shown a heterogeneous distribution of Br and Sb over the particle surface. This result highlights the biggest limitation with the FTIR method, which is the LOD of the instrument and its inability to distinguish subtle variations in the distribution of target chemicals throughout a particle. This mapping was performed on all particles analysed on FTIR with a homogenous distribution shown for each.

Figures 5.23: (a) Image of particle from Dust 1 in the diamond compression cell, and mapping images of (b) BDE-209 distribution, (c) antimony trioxide distribution and (d) the polymer distribution with the corresponding sample spectra and peak of interest highlighted. Areas of highest to lowest concentration are indicated by red, yellow, green then blue pixels







5.4 Analysis of BFR content in isolated particles

As many BFR containing particles as possible (10 and 15 from Dust 1 and 2 respectively), were collected and combined for determination of BDE-209 content. Table 5.2 lists the BDE-209 content (ng) quantified in the combined particles removed from Dust 1 and 2. On average, the particles removed from Dust 1 were smaller than in Dust 2 and the mean size of identified particles that were measured on the laser microscope from Dust 1 was 110 μm (range 65 to 250 μm) and 150 μm (range 90 to 260 μm) from Dust 2. More particles were successfully removed from Dust 2 and the combination of these factors means that the total particle mass of the particles isolated from Dust 2 was much greater, resulting in the higher BDE-209 content quantified. As with previous studies (Suzuki et al., 2009), an accurate mass measurement could not be determined for the isolated particles, and hence the BDE-209 masses given can only confirm its very strong presence in these particles.

As the mass of the particles could not be determined with available methods, an estimation of mass and hence BFR concentration in the particles was calculated based on the particle average size and the density of ABS plastic (1.04 g cm^{-3}). The particles were assumed to be spherical with the average size of the particle (from each dust) the diameter of the sphere. From this measure and the number of particles removed, the volume of the particles analysed was calculated as $6.97 \times 10^{-6} \text{ cm}^3$ in Dust 1 and $2.65 \times 10^{-5} \text{ cm}^3$ in Dust 2. Using the density of ABS plastic, the mass was then determined as $7.25 \times 10^{-6} \text{ g}$ in Dust 1 and $2.76 \times 10^{-5} \text{ g}$ in Dust 2. Hence, the BDE-209 concentration (using the previously measured content (ng)) was calculated at 69 mg g^{-1} in Dust 1 and 47 mg g^{-1} in Dust 2. The higher BDE-209 concentration determined in the polymer mass isolated from Dust 1, compared to Dust 2, is in keeping with the higher concentration of BDE-209 previously determined in the Dust 1 bulk sample. There are large assumptions with these calculations, which include that the particles are spherical, when in fact this is likely an overestimation of particle volume, and that the BDE-209 content is homogeneously distributed through the particle. It is also assumed that the entire particle is ABS plastic, however ABS has not been confirmed as the polymer backbone and impurities are likely present (such as calcium carbonate) which will affect the final density and hence mass determined. Table 5.2 lists the

particle mean size as well as values used for calculating the BDE-209 concentration ($\text{mg}\cdot\text{g}^{-1}$) in the isolated particles.

Table 5.2: Properties and calculation of estimated BDE-209 concentration in particles isolated from Dust 1 and Dust 2

	Mass of BDE-209 in combined particles (ng)	Mean particle size (range) (μm)	Volume of particles (assuming spherical shape) (cm^3)	Mass of particles (assuming density of $1.04 \text{ g}\cdot\text{cm}^{-3}$) (g)	Concentration of BDE-209 ($\text{mg}\cdot\text{g}^{-1}$)
Dust #1	500	110 (65-250)	6.97×10^{-6}	7.25×10^{-6}	69
Dust #2	1 300	150 (90-260)	2.65×10^{-5}	2.76×10^{-5}	47

5.5 Limitations of the forensic microscopy methods employed

The major limitation of these methods is primarily the high LODs of the instruments, which constrain these analyses to dust with very high concentrations of BFRs. The μRay Micro XRFS used for this analysis detects bromine concentrations $\geq 0.1\%$ in high speed mapping mode (0.5 second dwell time) (Suzuki et al., 2009), and will identify with a high degree of confidence elevated bromine concentrations from fragments $> 50 \mu\text{m}$ in size. This size limitation also means that smaller fragments may not be identified, which introduces a selection bias to this method; hence this instrument is only suitable for identifying Br-rich particles of bromine content $\geq 0.1\%$ and particle length $> 50 \mu\text{m}$. The LOD of the FTIR introduces further limitations to these methods, as the FTIR will only distinguish a BFR spectrum, from the particle/fibre spectrum, if the BFR is present at $> 5\%$, which restricts successful identification of BFRs in contaminated dust samples. This was observed in the analysis of the fibres, generated from artificial abrasion of the HBCD curtain, with HBCDs not identified with FTIR. Particle size is again a consideration for FTIR analysis, as particles are separated from the sample matrix for individual analysis with the diamond collision cell. In this analysis, particles $> 65 \mu\text{m}$ were successfully removed and analysed on the FTIR, with smaller particles (all from Dust 3) unable to be isolated using the present methods. This again created a selection bias in particles

that could be analysed for the presence of BFRs, the resin material and other additives in the particle. The SEM/EDS used in this study, although providing a more specific elemental analysis than the Micro XRFS, only provided a qualitative measure of bromine (and other element) content. The uneven topography of the dust sample makes it difficult for the detector to receive an accurate signal and the charging effect also reduces accuracy of any quantitative measurement. Hence this method can only be used to confirm the presence of certain elements. Furthermore, the SEM spectral lines for bromine and aluminium interfere, and a high bromine content and the presence of the $K\alpha$ bromine line is needed for confirmation. Similarly, the antimony $L\alpha$ and calcium $K\alpha$ lines interfere, providing difficulties in identifying these elements unless one (in this case antimony) is present at a much higher concentration. However, notwithstanding such limitations, the sequence of forensic microscopy methods used in this analysis provided new insights; both into the presence of BFRs in dust and about the origins of BFRs in dust samples containing elevated concentrations of BFRs.

5.6 Summary/Conclusions

The forensic microscopy techniques utilised in this investigation successfully identified fibres of high bromine content throughout a chamber generated dust sample, contaminated with abraded fibres of a HBCD treated textile. The microscopy techniques confirmed that a range of fibre sizes are produced by the chamber generated abrasion method (the smallest detected was $130\ \mu\text{m}$ up to $\sim 1\ \text{cm}$ in length), which is realistic for an indoor textile abrasion scenario. Although the concentration of HBCDs was too low for identification on the FTIR, the polymer backbone of the textile (polyester) was positively identified and the applicability of these methods was demonstrated. The applicability was further demonstrated with the analysis of 'real' indoor dust samples, previously reported to contain elevated concentrations of PBDEs and HBCDs. Bromine rich fragments (2 to 10 per mg dust) were identified in every 1 mg dust sample analysed. Further analysis revealed the fragments to be polymeric in origin and to contain elevated masses of BDE-209, as well as levels of antimony trioxide. Particles from one dust sample contained calcium carbonate, likely used as a resin filler, and bromine and antimony were shown to have a heterogeneous distribution over the particle surface.

This study raises questions about dust sample preparation techniques. Br-rich particles, confirmed to contain BDE-209, of up to 260 μm in size were detected in this study, hence sample preparation techniques that sieve bulk dust samples to a particle size $<250 \mu\text{m}$ may potentially underestimate BFR concentrations in that dust sample. Moreover, the heterogeneity of the distribution of BFR-rich particles in the dust samples studied here, implies obtaining a representative subsample of such dusts for analysis is problematic. The evidence provided by these forensic microscopy methods, suggests strongly that the highly elevated concentrations in these dust samples is due to the presence of such fragments that have arisen via abrasion of friable polymeric material, and hence provides us with further information on to the origins of highly elevated concentrations of BFRs in some dust samples. Although these techniques are limited to the study of dust samples containing very high concentrations of BFRs; in this study they have shown that the abrasion migration pathway is a likely source of the elevated concentrations of BFRs detected in such indoor dust samples.

CHAPTER 6

MIGRATION OF PBDEs FROM PLASTIC TV CASING TO DUST VIA THREE DIFFERENT MIGRATION PATHWAYS

6.1 Summary

The in-house test chamber was utilised to investigate the migration of PBDEs from a sample of plastic TV back casing material, using the previously developed experimental designs. The TV casing was from an inter laboratory study run by the National Institute of Environmental Studies (NIES, Tsukuba, Japan) and contained 9% BDE-209 with lower concentrations of other PBDEs present. As the test chamber experimental designs had previously been optimised to study the migration of HBCDs from fabric to dust, the TV casing provided an opportunity to study the migration of another set of BFRs (the PBDEs), from a different source matrix, via all three migration pathways. The following chapter describes the experiments conducted to investigate PBDE migration to dust via all three mechanisms discussing the migration trends observed.

6.2 InterLab Sample Waste TV backplate Lot No. 01-02

The PBDE treated plastic TV casing was received as small triangular pieces each weighing ~100 mg. The sample was a composite of 50 cathode ray tube (CRT) back casings (high impact polystyrene) that had been melted and remoulded to form the interlab material. Four replicate analyses of the TV casing by NIES, revealed the concentrations of PBDEs in the sample to be as listed in Table 6.1. The higher %RSDs (> 20%) of some of the congeners suggest a degree of inhomogeneity in the distribution of these compounds throughout the TV casing.

Table 6.1: PBDE concentrations ($\mu\text{g g}^{-1}$) and %RSD of 4 analyses of interlab sample Lot No. 01-02 (Plastic TV back casing), as provided by NIES

Analyte	Concentration ($\mu\text{g g}^{-1}$)	%RSD
BDE-47	1.3	15
BDE-85	N/A	N/A
BDE-99	3.2	27
BDE-100	1.1	39
BDE-153	520	26
BDE-154	59	22
BDE-183	3 700	21
BDE-209	90 000	19

* N/A = not analysed

Pieces of this TV casing (3 to 5 depending on the experiment) were used as the BFR source in the developed chamber experiments and results are described in the following sections.

6.3 Migration via volatilisation with subsequent partitioning to dust

The pathway of volatilisation followed by partitioning to dust, was investigated first in the UoB chamber. The chamber experiment was set up as for the HBCD treated curtain investigation (Chapter 3, Section 3.5), with 200 mg of dust on a GFF placed on the chamber floor, air flow attached and PUF plugs connected to collect BFR emissions in exit air. Three pieces of the TV casing were placed on the chamber shelf (situated half way down the chamber) as the BFR source. Figure 6.1 illustrates the chamber configuration, showing the three TV casing pieces situated above the dust aliquot. Two different scenarios were evaluated: (a) 60 °C for 24 hours (n=2) and (b) room temperature (22 ± 1 °C) for 1 week (n=2). The heated chamber scenario was thought a realistic representation of temperatures that an electronic device may reach during operation (Kemmlin et al., 2003). Again the dust, PUFs and chamber inner surface solvent rinses were analysed post experiment for PBDEs. Concentrations of BDE-209 in the dust both pre and post experiment and BDE-209 mass on PUFs and in chamber inner surface solvent rinses are given in Table 6.2.

Figure 6.1: Internal test chamber experiment configuration for investigating migration of PBDEs from TV casing to dust via volatilisation and deposition to dust



Table 6.2: Concentrations of PBDEs (ng g⁻¹) in dust pre and post volatilisation experiments and mass of PBDEs (ng) collected on PUFs and in chamber solvent rinses, from two temperature scenarios

		BDE-47	BDE-85	BDE-99	BDE-100	BDE-153	BDE-154	BDE-183	BDE-209
	<i>Pre experiment (ng g⁻¹)</i>	10 ± 11	2 ± 2	27 ± 31	5 ± 5	6 ± 6	3 ± 3	2 ± 2	230 ± 180
24 Hours at 60 °C									
Experiment 1	Dust (ng g ⁻¹)	<LOQ	<LOQ	1.8	<LOQ	4.1	<LOQ	14	210
	PUF (ng)	<LOQ	<LOQ	<LOQ	<LOQ	<LOQ	<LOQ	<LOQ	<LOQ
	Chamber Rinse (ng)	<LOQ	<LOQ	2.2	<LOQ	3.8	<LOQ	11	270
Experiment 2	Dust (ng g ⁻¹)	<LOQ	<LOQ	2.1	<LOQ	<LOQ	<LOQ	<LOQ	4800
	PUF (ng)	<LOQ	<LOQ	<LOQ	<LOQ	<LOQ	<LOQ	<LOQ	<LOQ
	Chamber Rinse (ng)	<LOQ	<LOQ	<LOQ	<LOQ	1.8	<LOQ	5.6	55
1 week at 22 °C									
Experiment 1	Dust (ng g ⁻¹)	<LOQ	<LOQ	1.5	<LOQ	<LOQ	<LOQ	<LOQ	230
	PUF (ng)	<LOQ	<LOQ	<LOQ	<LOQ	<LOQ	<LOQ	<LOQ	<LOQ
	Chamber Rinse (ng)	<LOQ	<LOQ	<LOQ	<LOQ	<LOQ	<LOQ	6.8	340
Experiment 2	Dust (ng g ⁻¹)	<LOQ	<LOQ	1.5	<LOQ	<LOQ	<LOQ	2.0	120
	PUF (ng)	<LOQ	<LOQ	<LOQ	<LOQ	<LOQ	<LOQ	<LOQ	<LOQ
	Chamber Rinse (ng)	<LOQ	<LOQ	<LOQ	<LOQ	<LOQ	<LOQ	3.7	150

PBDEs were not detected above LOQs on the PUF, at either temperature scenario. Previous chamber experiments that investigated PBDE migration via volatilisation with partitioning to dust from a GFF spiked with 100 ng of analytes (Chapter 3, Section 3.4) saw ~10% of the more volatile BDEs: 47, 99 and 100, transferred to dust. The 100 ng spiked 'source' concentration is about 4 times lower than that present in the plastic TV casing of BDE-47, 99 and 100, hence if the PBDEs in the plastic material are loosely bound to the polymer, a substantial migration to dust should have been observed. An increase in PBDE concentration was not detected in dust or on the PUF, suggesting the PBDEs are more strongly bound to the TV casing than they are to the analyte solvent spike applied to the GFF, and hence less available for migration via this pathway. It should also be noted that the melting and remoulding process used to produce the material tested may also have influenced the strength with which the PBDEs are bound to the polymer.

BDEs-209 and 183 are present in the TV casing at much higher concentrations than the other PBDEs and very small masses of BDE-183 (4 to 11 ng) and of BDE-209 (55 to 340 ng) were detected in all chamber surface rinses. Minor quantities of BDE-153 were detected in chamber rinses from the experiments at 60 °C, and the other PBDEs were not detected. As BDE-183 and 209 have very low estimated vapour pressures they are expected to experience limited volatilisation and a very strong partitioning to particulates/surfaces, hence any volatiles present would almost immediately partition to chamber walls or dust particles, before collection on PUFs. This suggests that volatilisation of BDE-183 and 209 in the chamber environment is limited, and that following volatilisation, these congeners undergo rapid partitioning to chamber surfaces.

Concentrations of BDE-209 detected in dust post-experiment were in 3 out of the 4 experiments, not substantially different to concentrations characterised in the dust pre experiment. This suggests that migration of BDE-209 from the TV casing to dust via volatilisation with subsequent deposition was minimal. However, the second chamber experiment at 24 hours for 60 °C did reveal a noticeable increment in the BDE-209 concentration in the dust post-experiment (4800 ng g⁻¹). While further work would be required to confirm this, the absence of any noticeable increment in the concentration

in dust of any other PBDEs in this experiment, suggests that the higher BDE-209 concentration observed may be attributable to inherent inhomogeneity of BDE-209 in the Belgian dust sample used. No other congeners were detected in dust samples above the pre-characterised concentrations. In conclusion, these chamber experiments suggest that migration of PBDEs from treated plastic TV casing to dust via volatilisation and subsequent deposition is minimal. It is feasible however, that such migration may be substantial from source materials containing elevated concentrations of more volatile PBDEs than present in the material tested here, which was predominantly composed of BDE-209.

6.4 Migration via abrasion of particles directly to dust

Abrasion of fine particles/fibres of the source material that subsequently transfer into dust, was investigated with the same chamber configuration as previously used to investigate the HBCD treated curtains (Chapter 4, Section 4.2). Three pieces of plastic TV casing were used as the BFR source and were placed on the mesh shelf located 3 cm above the dust aliquot on the chamber floor. Abrasion was induced with a magnetic stirrer bar as the abradant and four experiments of different time periods were conducted with the dust analysed for PBDE concentrations. Each experiment was conducted at room temperature and volatile emissions of PBDEs were not monitored, as the results of the experiments described in the previous section showed volatilisation to be negligible. Figure 6.2 shows the abrasion experiment in progress with three pieces of the TV casing and the stirrer bar (abradant) on the mesh shelf.

Figure 6.2: Internal test chamber configuration for investigating migration of PBDEs from plastic to dust via abrasion of fine particles



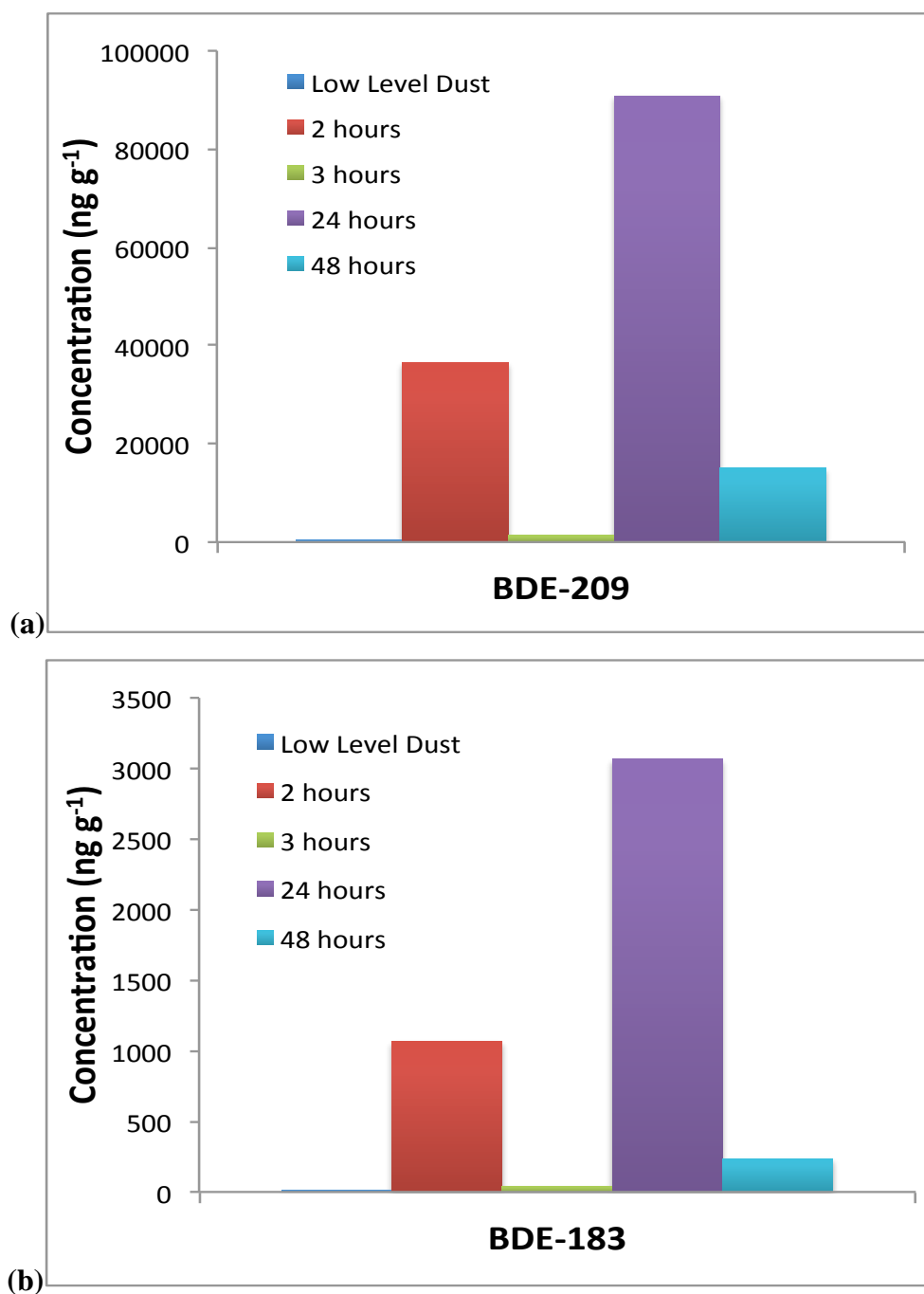
There was a clear increase in concentrations of both BDE-183 and 209 in every dust sample post-experiment, with increases in concentrations of BDEs-153 and 154 in dust also detected in 2 experiments in which the highest concentrations of all PBDEs were observed; indicating the chamber-induced abrasion process is effective for hard plastic matrices as well as textiles. Concentrations of target PBDEs in dust post experiment (ng g^{-1}) are given in Table 6.3.

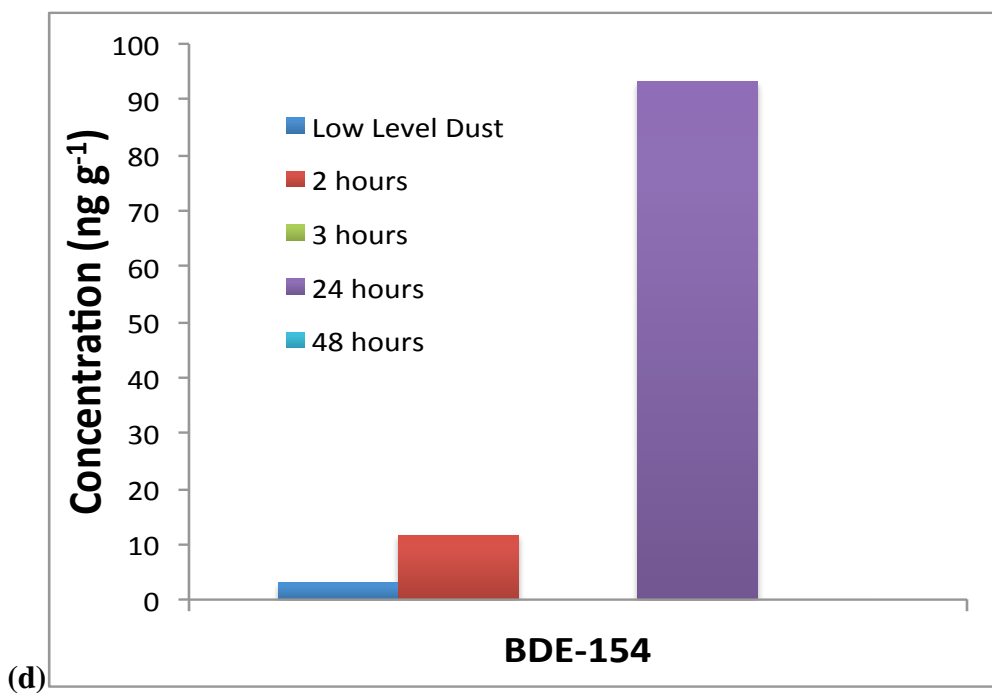
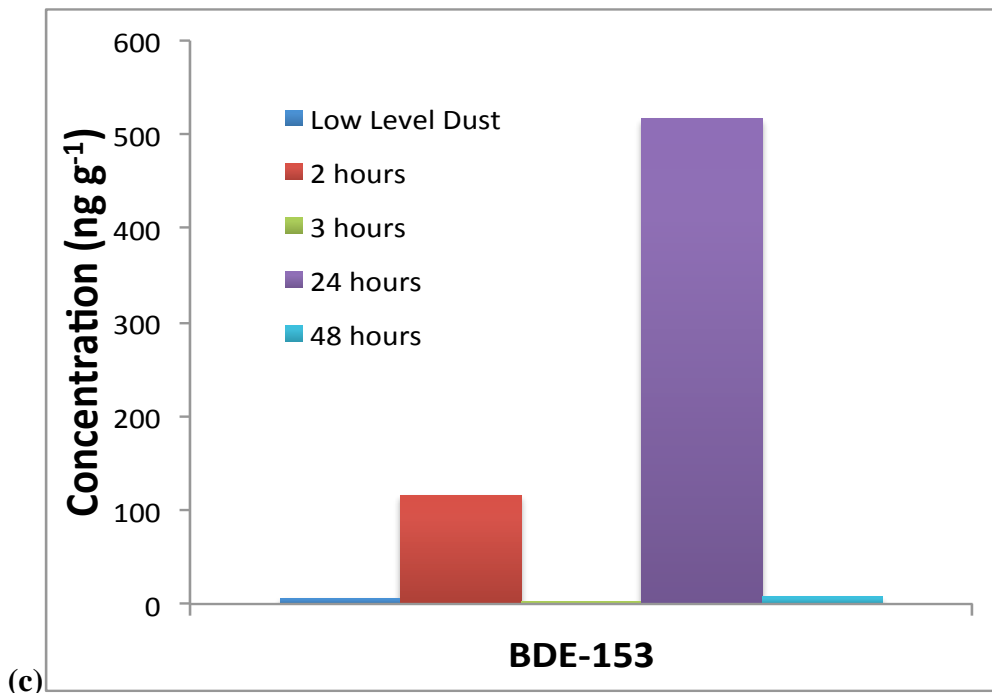
Table 6.3: Concentrations (ng g^{-1}) in dust pre experiment and post experiment for four different abrasion experimental durations

	Belgian Dust (ng g^{-1})	2 hours (ng g^{-1})	3 hours (ng g^{-1})	24 hours (ng g^{-1})	48 hours (ng g^{-1})
BDE-47	10 ± 11	<LOQ	<LOQ	<LOQ	<LOQ
BDE-85	2 ± 2	<LOQ	<LOQ	<LOQ	<LOQ
BDE-99	27 ± 31	3.2	1.9	17	2.5
BDE-100	5 ± 5	<LOQ	<LOQ	<LOQ	<LOQ
BDE-153	6 ± 6	120	<LOQ	520	7.5
BDE-154	3 ± 3	12	<LOQ	93	<LOQ
BDE-183	2 ± 2	1100	41	3100	240
BDE-209	230 ± 180	37 000	1300	91 000	15 000

The abrasion was less consistent for the plastic material and there is no linear correlation ($p = 0.920$ for BDE-209) between dust concentration and abrasion duration. It was particularly difficult to conduct the abrasion for these lighter TV casing pieces in a reproducible fashion, as they had a tendency to ‘flick’ around the chamber. Figure 6.3 plots the concentrations of BDE-209, 183, 153 and 154 in dust pre and post all four abrasion experiments, showing this variation.

Figure 6.3: Concentrations (ng g^{-1}) in dust pre and post abrasion experiments for four experimental durations of (a) BDE-209 (b) BDE-183 (c) BDE-153 (d) BDE-154

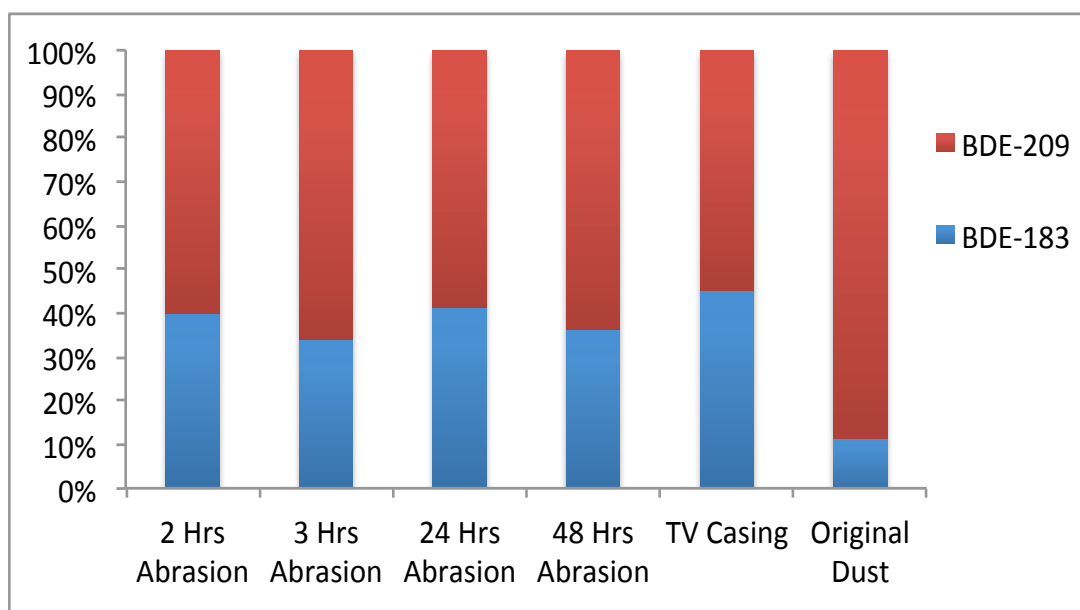




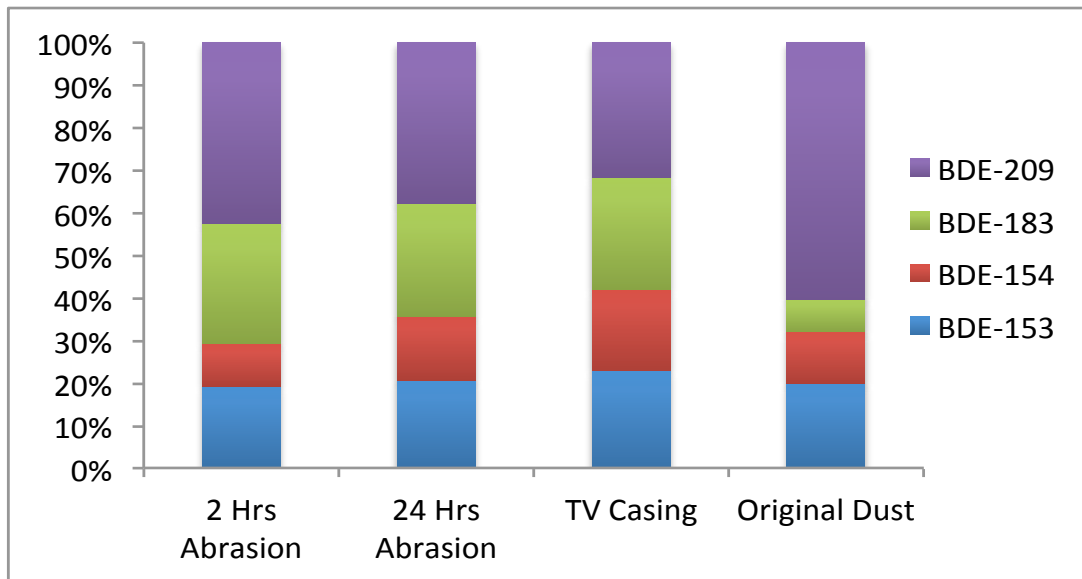
The plots in Figure 6.3, show similar ratios of PBDE congener levels between generated dusts, for all four congeners. To explore this further the concentrations of the congeners were log-transformed to more easily compare the PBDE congener profiles determined in each generated dust sample to that in the original TV casing, and in the original Belgian dust. The log-transformed concentrations were then presented as percentage contributions to the sum of BDEs 183 and 209, or of BDEs 153, 154, 183, and 209 as appropriate. Figure 6.4 (a) compares the relative

contributions of BDE-209 and BDE-183 in each sample, showing a similar ratio in the chamber generated abrasion dust samples to that in the original TV casing, and a different profile to that in the original dust. For the two abrasion experiments where BDE-153 and 154 were detected, relative contributions of all four congeners were compared and Figure 6.4 (b) plots the relative contributions in the chamber generated dust samples, with again a similar profile observed to that present in the TV casing, and a very different profile to that in the original Belgian dust. The similar profiles between generated dusts and the TV casing, and the differing profile to the original dust sample, adds more weight to the conclusion that the chamber dusts have been contaminated with abraded particles of the TV casing. The slight differences in the relative congener contribution is likely the result of inhomogeneity of the congeners through the plastic casing.

Figure 6.4 (a): Relative contributions (%) of BDE-209 and 183 in the four chamber generated abrasion dust samples, the original TV casing and the low level dust pre-experiment, derived from log-normalised concentrations



(b): Relative contributions (%) of BDE-153, 154, 183 and 209 in the 2 hour and 24 hour chamber generated abrasion dust samples, the original TV casing and the low level dust pre-experiment, derived from log-normalised concentrations



As discussed in Chapter 4, the industry methods for measuring abrasion resistance of fabrics often show different results for the same sample and there is often little consistency in the outcome of different tests due to the difficulty of mimicking abrasion in a reproducible fashion, consistent with the results of these experiments. Far fewer industry methods exist for the measurement of abrasion resistance of plastics than textiles. Rather than measuring the number of abrasion cycles to cause breakage of fibres, the mass (mg) abraded from the product /1000 abrasion cycles is assessed for plastics. Commonly, this abrasion is achieved with a Taber abrader in accordance with standards ASTM D1044 or ASTM D4060, which aim to measure a product's resistance to abrasion via rubbing, scraping, or erosion. The general procedure is to weigh the specimen before the test, subject it to a specified number of revolutions or abrasion cycles, and record the mass post experiment (Intertek, 2014).

In the test chamber abrasion experiments described here, the mass abraded from the TV casing in the short time period experiments was too small for an accurate measure of mass loss with available methods. However, an estimated mass can be calculated from the increment in concentrations of BDE-183 and BDE-209 in the dust post-experiment. Tables 6.4 and 6.5 list the parameters used to calculate the mass (mg) abraded from the plastic for each experimental duration, and the estimated abraded

mass (mg) /1000 cycles for BDE-183 and BDE-209 respectively. In the worst-case mass abrasion scenario evaluated here, the plastic TV casing suffered abrasion of 4 µg/1000 abrasion cycles. This method assumes a homogeneous distribution of PBDEs throughout the TV casing, however the %RSDs of ~20% from 4 analyses (Table 6.1) suggests an inhomogeneity throughout the plastic and this would contribute to the different masses calculated from the BDE-183 and BDE-209 concentrations.

To relate these results to a realistic indoor scenario an estimate of possible abrasion time of a TV casing needs to be made. Abrasion can occur from wiping/cleaning the product but it is likely that for TV casing, abrasion would be further encouraged from degradation of the polymer due to high product operating temperatures, or UV degradation if exposed to direct sunlight, hence relating chamber abrasion to a 'real world' scenario is difficult. To compare to a theoretical TV unit, dimensions were taken for the average size TV purchased in 2013 (a 44 cm display screen, with dimensions roughly 60 x 20 x 80 cm H x L x W). Using these TV dimensions, the abrasion area of just the top surface of the TV can be calculated as 4800 cm². The total surface area of the three plastic triangles was 1.9 cm², thus the top surface area of the theoretical TV is 2560 times greater than the plastic pieces in the chamber experiment. For the 2 hour abrasion experiment the calculated mass of TV casing abraded into the dust post experiment (from the transferred BDE-209 concentration) was 0.09 mg which is equivalent to 240 mg of plastic particles abraded from the top surface of the TV casing in our scenario. In the highest abrasion scenario, it was assumed TV abrasion occurred for about 5 seconds a day, which included cleaning (such as wiping) and enhanced polymer degradation leading to increased abrasion. Assuming 5 seconds of use per day, the 2 hour abrasion experiment relates to 1440 days (~4 years) of product use. Hence 4 years of TV use will abrade 240 mg of plastic into house dust, contaminating the dust with 22 000 µg of BDE-209, or 5400 µg of BDE-209 contamination per year, just considering the top surface of the unit. The side and rear panels of the unit will contribute further abraded particles although the mass abraded is expected to be less as the top surface will suffer larger polymer structure degradation from direct sunlight and escaping heat generated during operation. Other product uses of BFR treated plastics (such as computer keyboards)

that have higher user contact time periods would be expected to suffer even more extensive abrasion.

Table 6.4: Calculated BDE-183 abrasion mass (mg), relation to abrasion test standards and estimated 'real world' TV casing abrasion

Experiment Time (Hours)	Abrasion cycles	BDE-183 mass increment (ng)	Particle mass in dust (mg)	Abraded mass (mg) / 1000 abrasion cycles	Time of related TV use (days) – assuming 5 sec use/day
2	24 000	240	0.066	2.3×10^{-3}	1400
3	36 000	9.4	0.0024	6.7×10^{-5}	2200
24	290 000	640	0.17	6.0×10^{-4}	17 000
48	580 000	60	0.016	2.8×10^{-5}	35 000

Table 6.5: Calculated BDE-209 abrasion mass (mg), relation to abrasion test standards and estimated 'real world' TV casing abrasion

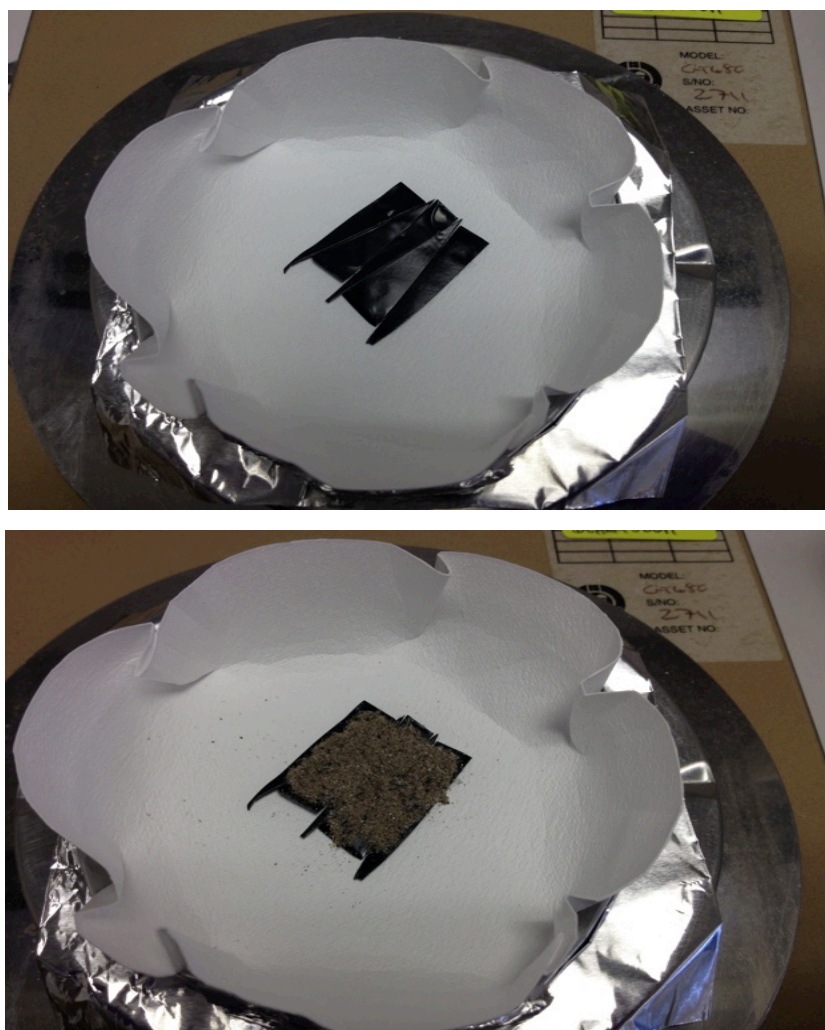
Experiment Time (Hours)	Abrasion cycles	BDE-209 mass increment (ng)	Particle mass in dust (mg)	Abraded mass (mg) / 1000 abrasion cycles	Time of related TV use (days) – assuming 5 sec use/day
2	24 000	8 400	0.093	3.9×10^{-3}	1400
3	36 000	310	0.0034	9.4×10^{-5}	2200
24	290 000	19 000	0.21	7.3×10^{-4}	17 000
48	580 000	3 700	0.041	7.1×10^{-5}	35 000

The migration of PBDEs to dust via abrasion, particularly the less volatile congeners, was simulated successfully in the test chamber experiments. The experimental configuration previously shown to work for treated textiles was shown to also work for treated plastic materials. Substantial masses of BDE- 209 and 183 were transferred to dust via this migration pathway and the ease with which this was generated presents abrasion as a highly plausible pathway for describing the migration of low-volatility analytes to dust.

6.5 Migration via direct contact between source and dust

The transfer of BFRs *via* direct contact between source and dust was investigated with the TV casing in a similar chamber experiment to that employed to examine HBCD transfer to dust from HBCD treated curtains (Chapter 4, Section 4.3). As the TV casing pieces were small, 5 triangular pieces were positioned next to each other (on a piece of tape) providing a square surface area of 2.5 x 2.5 cm. This square was then placed on a GFF on the chamber shelf (now positioned half way down the chamber) and 0.15 g of dust layered evenly over the top surface of the plastic. Figure 6.5 shows a picture of the TV casing 'square' before and after dust application.

Figure 6.5: Experimental configuration used to investigate migration of PBDEs from plastic to dust via direct contact between source and dust, showing (Top) five plastic pieces positioned together and (Bottom) dust layered on the top surface of the source



The average (n=2) BDE-209 concentration transferred to dust after the two different exposure durations show a higher average mass transferred after a week, than after 24 hours (4900 vs 820 ng g⁻¹ for 1 week and 24 hour experiments respectively). An independent samples T-test did not reveal a significant difference between results, with p values of 0.215 to 0.425 for BDE-154, 183 and 209. However, only two experiments were conducted at each exposure period, with a large variation between replicate experiments, hence this result is treated with caution and a trend cannot be concluded. The results do suggest that the uptake of PBDEs from plastic casing may take longer than 24 hours to reach a saturation point, likely due to a stronger binding to the plastic (than the binding of HBCDs to textile fibres) or to the lower volatility of BDE-209 and BDE-183 slowing the migration. The physical processes for migration of SVOCs between source and dust from direct contact is not completely understood however Schripp et al. (2010) suggested SVOCs are transferred due to contact of the dust with the boundary layer directly above the source. Compounds with lower vapour pressures will have lower concentrations present in this layer (and a slower release into the layer to replace mass absorbed to dust) hence lower concentrations are available for uptake over time. However, the transfer may occur via direct uptake from immediate contact between dust particles and the source as Clausen et al. (2004) has suggested that the dust may partly remove this boundary layer allowing direct source-dust contact. In such a scenario, stronger binding of the BFRs to the polymer (as opposed to the curtain fabric) is likely the cause of the slower uptake to the dust of BDE-209 and 183. Table 6.6 and Figure 6.6 present the PBDE concentrations transferred to dust post experiment.

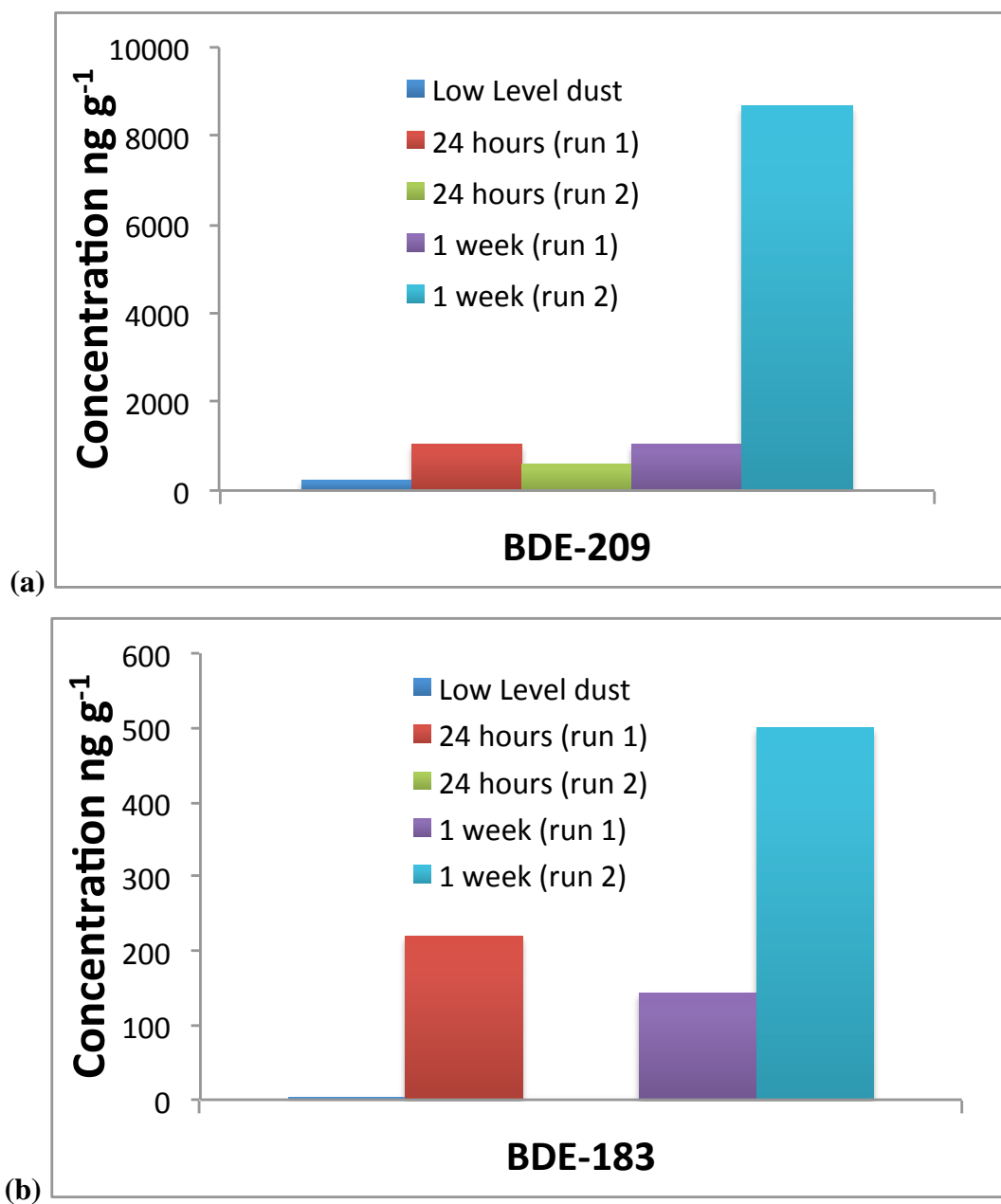
Due to the smaller dust mass available from the smaller scale TV casing experiments only one analysis from each dust mass collected was afforded, so BFR variation through the dust sample was not investigated. The replicate experiments for each exposure duration, show large variations in PBDE mass transferred to dust, which may be due to an inhomogeneity of PBDE concentrations across the source surface; perhaps a result of the melting and remoulding process for formation of the sample, or because the dust aliquots exposed may have different organic carbon contents. As mentioned previously in the discussion of the HBCD treated curtains (Chapter 4), BFRs are hydrophobic, and will thus have a stronger uptake to dusts with a higher organic carbon content (Abdallah et al., 2012, Yu et al., 2012). Moreover, the fugacity

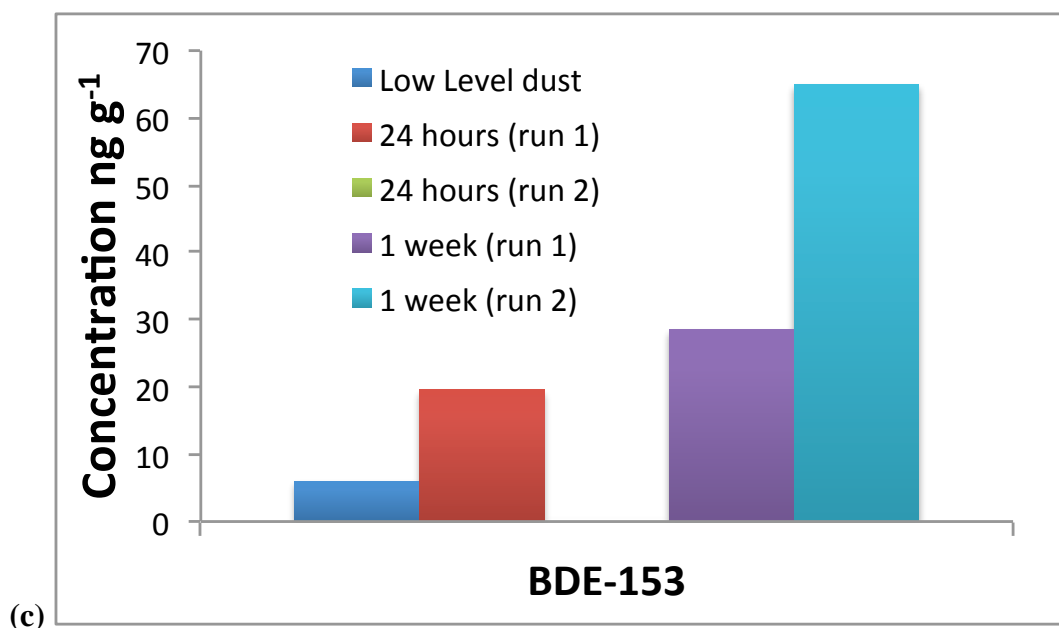
capacity of the dust is dependent on the fraction of organic carbon. Despite some differences with the equivalent experiments for transfer of HBCDs from a treated curtain; PBDE uptake to dust via direct contact is shown here to be a rapid process with substantial mass transfer occurring in just the first 24 hours of exposure. The rapid uptake via direct source-dust contact from both fabrics and polymers observed here, suggests it is largely independent of the source matrix.

Table 6.6: Mean \pm SD concentrations (ng g^{-1}) of PBDEs in dust pre experiment and maximum and minimum concentrations (ng g^{-1}) in dust post direct contact experiment for 24 hours and 1 week exposure ($n=2$)

	Pre experiment (ng g^{-1})	24 hours (ng g^{-1})	1 week (ng g^{-1})
BDE-47	10 ± 11	<4.5	<4.5
BDE-85	2 ± 2	<0.8	<0.8
BDE-99	27 ± 31	<0.8	<0.8
BDE-100	5 ± 5	<0.7	<0.7
BDE-153	6 ± 6	(<1.3, 20)	(29, 65)
BDE-154	3 ± 3	<1.8	<1.8
BDE-183	2 ± 2	(<1.0, 220)	(140, 500)
BDE-209	230 ± 180	(590, 1000)	(1000, 8700)

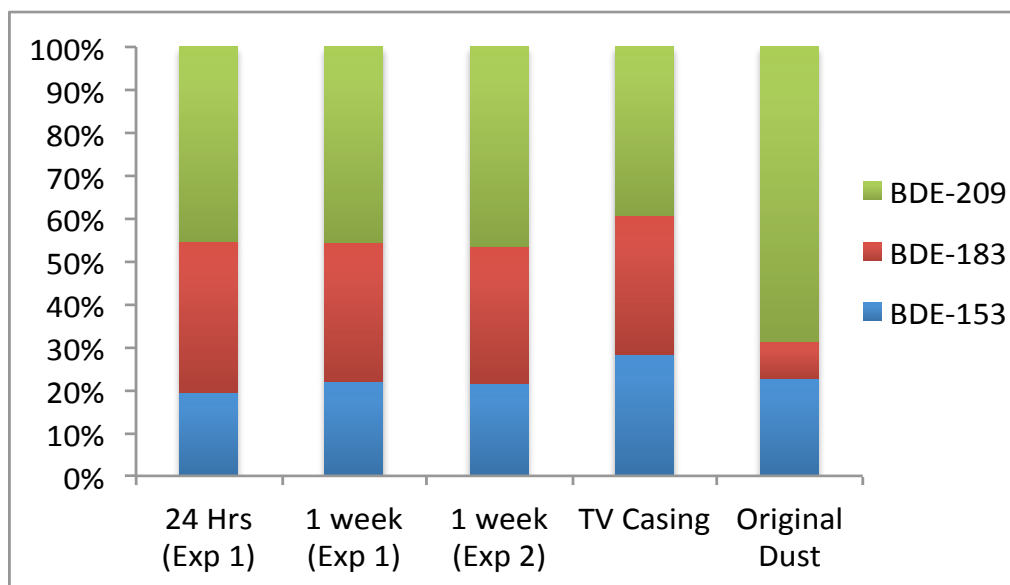
Figure 6.6: Concentrations (ng g^{-1}) of (a) BDE-209, (b) BDE-183 and (c) BDE-153 in dust pre and post partitioning via direct contact experiments





The PBDE congener pattern in the dust post experiment was compared to that present in the TV casing and in the original Belgian dust. To facilitate comparison, concentrations of the congeners in the dust were log-transformed and presented as percentage contribution profiles in Figure 6.7. Due to the lower concentrations in the second 24 hour experiment, only BDE-209 was detected, hence this experiment is not included in this comparison. A very similar congener profile is seen in both the dust post-experiment and the TV casing, that is very different to that observed in the dust at the start of each experiment. The similar profile between post-experiment dust and the TV casing, again adds more weight to the conclusion that the post-experiment dust is contaminated via direct uptake from the TV casing. The comparable congener profiles in dust and putative source, also suggests the transfer is not driven by volatilisation into the surface boundary layer, as if this was the case, one would expect a congener profile in the dust that would be comparatively enriched in the more volatile congeners like BDE-153 compared to BDE-209. The slight differences between the congener profile in the post-experiment dust samples and the TV casing is likely attributable to an inhomogeneous distribution of the PBDEs in the casing.

Figure 6.7: Relative contributions (%) of BDE-153, 183 and 209 in three chamber generated abrasion dust samples, the original TV casing and the low level dust pre-experiment, derived from log-normalised concentrations



Only a few studies have investigated BFR concentrations in dust samples removed from putative sources in indoor microenvironment studies. Prominent amongst these, the study by Takigami et al. (2008) reported elevated concentrations of BDE-209 in dust sampled directly from the back casings of various TVs compared to that in the surrounding floor dust. The components of the TV were also analysed for PBDEs, with BDE-209 the dominant congener in the rear plastic cabinets of the TVs and in all dust samples. As the congener profile in the dust sampled from the TV was similar to that in the TV components it was strongly suggested that extensive PBDE transfer occurred directly from the components in the TV casing to the dust, a similar finding to that seen in these chamber experiments. The rapid uptake and high PBDE masses transferred to dust that were observed in the experiments in this chapter further confirm that direct contact between dust and source materials is a potentially important pathway of BFR migration to dust, particularly for low volatility BFRs such as BDE-209.

6.6 Summary/Conclusions

The previously developed chamber experimental designs were applied to study the migration of PBDEs to dust from a PBDE treated plastic TV casing. This BFR source

provided the opportunity to investigate the source-to-dust migration behaviour of less volatile BFRs in chamber experiments. Results show that the migration of BDE-209 to dust in indoor microenvironments is strongly influenced by the abrasion and direct contact, between source and dust, migration pathways. In contrast, volatilisation with subsequent partitioning to dust appears to exert little influence over mass transfer. This result is expected as the very low vapour pressure of BDE-209 implies it will undergo minimal volatilisation. The abrasion chamber configuration was successful in abrading a plastic matrix containing BFRs, with elevated concentrations of PBDEs detected in dust after as little as 2 hours of abrasion. The direct contact experiments again transferred highly elevated concentrations to dust and the majority of the uptake was achieved in the first 24 hours of exposure. This suggests the plastic and fabric source matrices had little influence on the uptake (at least in these specific cases) and the fugacity of both source matrices is sufficiently high to promote fast mass transfer. The results also suggest that physical properties of the receiving dust (such as the fraction of organic carbon) have a greater influence on mass transfer than the source matrix material.

In a ‘real world’ scenario, migration of BDE-209 to dust is likely due to a combination of the three migration pathways outlined in this study. Dust samples containing highly elevated concentrations of involatile BFRs like BDE-209, likely contain a significant number of abraded particles/fibres. By comparison, the evidence presented here, suggests that the lower “background” contamination with BDE-209 seen in the majority of dust samples, arises principally due to direct source:dust contact, with an additional (likely less substantial) contribution from BFR volatilisation from source followed by deposition to dust. Where abrasion occurs, it is overlaid on top of this background contamination.

CHAPTER 7

BIOACCESSIBILITY STUDY OF HBCDs FROM DUST CONTAMINATED VIA DIFFERENT MIGRATION PATHWAYS

7.1 Summary

Bioavailability and bioaccessibility are useful tools to assess the potential risk of BFRs from human exposure via ingestion. Oral bioavailability refers to the fraction of a chemical ingested that reaches the central (blood) compartment of the gastrointestinal tract and hence enters the circulatory system of the organism. Bioavailability is difficult to assess with *in vitro* methods and the bioaccessibility of a chemical is assessed instead. The bioaccessibility refers to the fraction that is *available* for absorption into the circulatory system, i.e. the fraction that initially enters the gastrointestinal tract (Cave et al., 2010). The total fraction that is bioaccessible will not necessarily enter the circulation system (i.e. be bioavailable) however it provides a good indication of the potential risk from exposure for the organism.

A study was conducted in collaboration with the University of Reading to assess the human bioaccessibility of dust contaminated with HBCDs via different migration pathways. The previously developed chamber experimental designs were utilised to generate dust samples contaminated with HBCDs emitted from a HBCD treated curtain in two distinct ways. These were: (a) volatilisation with subsequent deposition to dust particles, and (b) abrasion of textile fibres directly to dust. The generated dust samples were exposed to an *in vitro* bioaccessibility model developed by the University of Reading (Tilston et al., 2011). Specifically, this model is a colon extended physiologically based extraction test (CE-PBET), which mimics the processes a digested dust sample would experience on passing through the stomach, small intestines and colon in the human body. Monitoring the partitioning of HBCDs into the small intestine, colon and residue pellet provides a measure of the bioaccessibility of the compound, i.e. the fraction of the total compound introduced

into the gastrointestinal tract that dissolves and is therefore available for absorption into the body. The CE-PBET method aims to model human exposure to pollutants from direct ingestion as a result of hand to mouth activity (Tilston et al., 2011). Similar *in vitro* models have been used in the past, but have predominantly focused on the bioaccessibility of trace elements in soil.

Dust samples contaminated via the two migration pathways were exposed to the bioaccessibility methodology to determine if the bioaccessibility of HBCDs from dust is dependent on the migration pathway. For dust contaminated via volatilisation, it was hypothesised that HBCDs will be loosely bound to particles and hence readily available for absorption into the body. In contrast, for dust contaminated via abrasion it was hypothesised that the incorporation of HBCDs into the source fibres present in the dust would make them less bioaccessible. This is due in part to the possibly stronger binding between HBCDs and the source material fibres, but also because the highly elevated HBCD concentrations on such fibres may place a solubility limitation on HBCD absorption into gut fluid.

The methodology for bioaccessibility testing is described in more detail in the following chapter, with a discussion of the results and their implications for human exposure to dust contaminated via different migration pathways.

7.2 Dust Characterisation

A previously characterised dust sample containing low concentrations of HBCDs (Belgian dust, Section 2.1.7) was used for the generation of dust samples contaminated via different migration pathways. The bulk dust (already sieved to <500 µm) was sieved further to <250 µm before use, as larger particles were considered less relevant for assessing bioaccessibility from dust ingested by hand to mouth contact, as they will adhere to a lower extent to hands. There are limited studies on the adherence of dust particles to hands; however, USEPA models for measuring the bioavailability of chemicals in soils, a matrix of similar composition to dust, specify a particle size cut off <250 µm (USEPA 2005, USEPA 2003). Moreover, the USEPA's Integrated Exposure Uptake Biokinetic (IEUBK) model specifies that it is "critical to

sieve soil samples to $<250\ \mu\text{m}$ to more closely represent the size of soil particles that would be expected to adhere to children's hands" (USEPA, 1999).

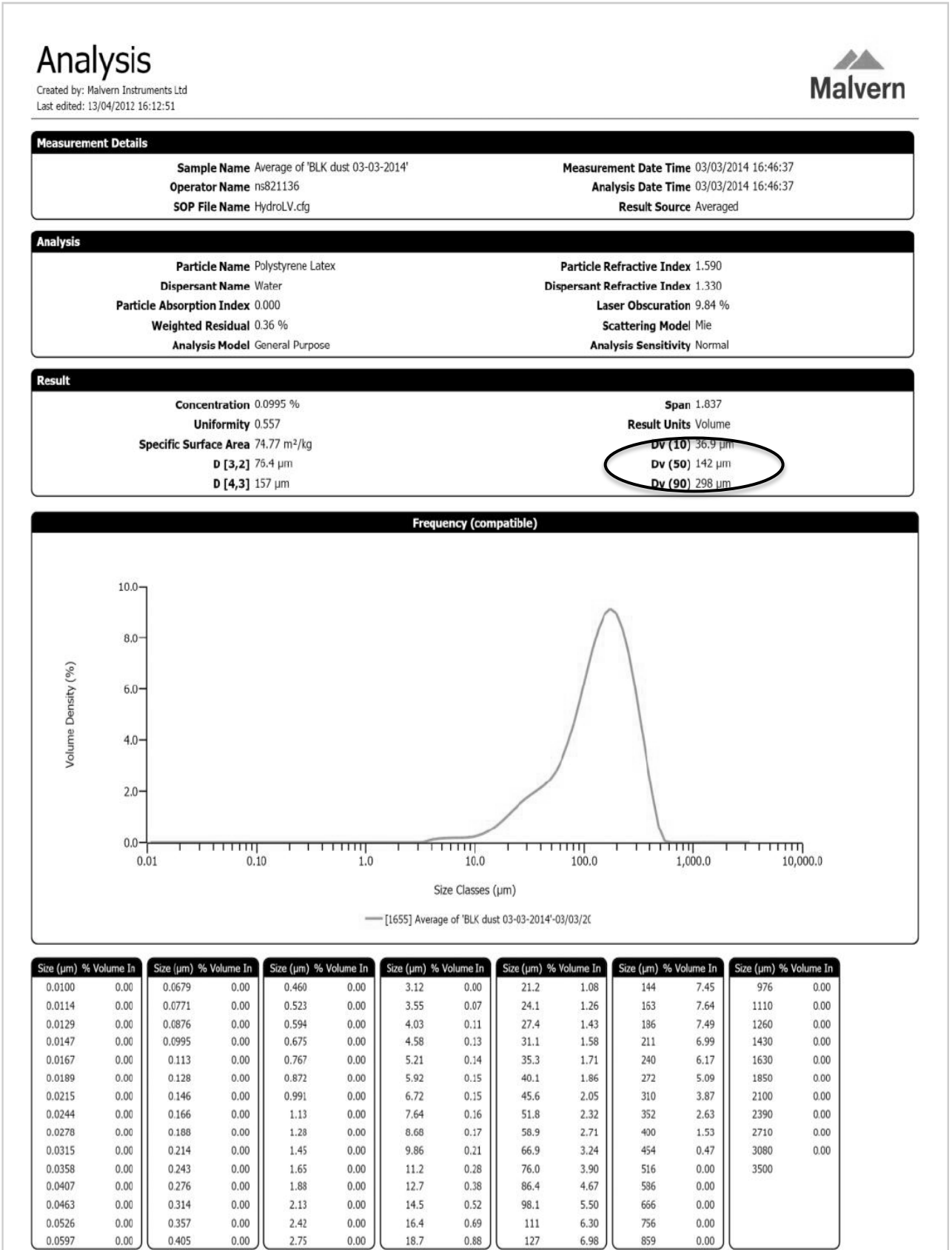
The few reported studies that have investigated adherence of particles of different size ranges to hands experimentally, have mostly investigated adherence of soil particles. Duggan and Inskip (1985) investigated four soil particle size ranges by rubbing 20 mg of a size fraction between thumb and forefinger, and weighing the dust mass adhered to the hand. From the observed results, it was stated: "if the hand-mouth route is the important one for children, then there would be some merit in analyzing only those particles of diameter less than, say, $200\ \mu\text{m}$." The authors concluded that application of a $200\ \mu\text{m}$ particle size limit would capture 95% of the mass adhering to hands (Duggan and Inskip, 1985). Yamamoto et al. (2006) also investigated soil particle size ranges, adhering to children's hands ($n=9$, mean age of 4 years) in a nursery. There was a 6-fold difference in the mode particle size determined on the hands with the maximum particle size observed ranging up to $300\ \mu\text{m}$. Que Hee et al. (1985) investigated dust particle adherence to hands for different size fractions, up to $246\ \mu\text{m}$; with an equal mass adhered to the palm for all particle size ranges ($<246\ \mu\text{m}$). These studies are all consistent with the cut off size of $<250\ \mu\text{m}$ chosen for study in these bioaccessibility experiments, and provides reasonable assurance that this is the size range that would adhere to palms and hence be available for ingestion via hand to mouth contact. The particle size distribution in this dust sample and the fraction of organic carbon in the low level Belgian dust were also determined at the University of Reading for comparison, from small sample sets of replicate analyses ($n=4$ to 5).

7.2.1 Particle size distribution

A sample of the Belgian dust was analysed at the University of Reading to determine the particle size distribution. Between 0.1 to 0.5 g of the dust bulk was analysed 5 times using a Coulter fluid module LS230. The Coulter fluid module uses laser diffraction to measure particle size in a suspension. A chamber containing the suspended particles is irradiated with light from a laser and the scattering of the light is detected by a photo detector array, and converted into a particle size distribution

plot. The mode particle size was determined as 142 μm with a size range of 3.55 to 454 μm . Figure 7.1 shows the results of the analysis.

Figure 7.1: Particle size distribution analysis results and plot for low level Belgian dust



7.2.2 Fraction of organic carbon

The percentage carbon and nitrogen content of the dust sample was also determined at the University of Reading, with flash dynamic combustion using a CE-Elantech Flash 2000. Dynamic combustion consists of complete combustion of a sample to measure the elemental gases produced and thus calculating elemental content. 10 mg replicates of the dust were analysed; aspartic acid was analysed as a control, and an in-house prepared QC soil sample analysed for testing instrument performance. Table 7.1 lists mean, standard deviation and RSD values for 7 replicate analyses of aspartic acid, 3 analyses of QC soil and the 4 analyses of the Belgian dust sample used in this project. The low RSD values in Table 7.1 for measurements of carbon and nitrogen (0.6 and 1.7%) in aspartic acid, show the instrument meets QC criteria for repeatability. The larger RSD values (~20%) for the Belgian dust sample is thus indicative of heterogeneous distribution of these elements in this dust. This is further confirmed by the fact that the QC soil (a matrix similar to dust) returned a RSD of 4% for three analyses of the carbon content.

Table 7.1: Mean, SD and RSD of %Nitrogen and %Carbon contents in instrument QC samples and the low level Belgian dust.

	Aspartic Acid (n=7)			QC Soil (n=3)			Belgian Dust (n=4)		
	Mean	SD	RSD	Mean	SD	RSD	Mean	SD	RSD
Nitrogen	10.4	0.2	1.7	0.3	0.1	17.1	1.7	0.3	20.6
Carbon	36.0	0.2	0.6	3.6	0.1	3.6	12.7	2.5	19.6

7.3 Chamber generation of dust samples

The in-house test chamber was utilised, with the previously developed chamber experimental methods, to generate dust samples contaminated with HBCDs from the HBCD treated textile curtain. Five samples containing HBCDs incorporated via volatilisation and subsequent partitioning to dust, and five samples contaminated with HBCDs via source abrasion were generated. As shown in the previous chamber experiments with this HBCD treated textile (Chapters 3 and 4) for experiments of a similar time period, migration via the volatilisation pathway results in lower HBCD mass transfer to dust than via the abrasion pathway. However, dust samples

containing similar concentrations of HBCDs (within an order of magnitude) were required for this study, to minimise any influence on bioaccessibility due to differences in HBCD concentration. To achieve this, HBCD mass transfer via the volatilisation pathway was enhanced through longer chamber experimental times and by deploying above ambient chamber temperatures to facilitate volatilisation. Moreover, to reduce the total HBCD concentration in dust samples generated via abrasion; a small aliquot of the chamber generated dust sample was mixed with another aliquot of Belgian dust to ‘dilute’ the HBCD concentration in the dust sample used for bioaccessibility testing.

7.3.1 Volatilisation with partitioning to dust particles

The chamber experiments for generating dust contaminated with HBCDs via volatilisation with subsequent partitioning to dust, were configured as previously described with chamber experiments conducted for 1 week, heated to 35 °C in a hot water bath. A 4 x 4 cm textile sample was used as the HBCD source. Air flow was not attached to this chamber and it was sealed from the outside environment for the duration of the experiment to retain all volatilised analytes inside the chamber and encourage partitioning of volatiles to dust particles. The above-ambient temperature (35 °C) was chosen as a realistic ‘highest volatilisation case’ scenario for curtains in an indoor environment, representing temperatures that a curtain in direct sunlight may reach on a warmer day in summer. In order to provide adequate dust for three repeats of the bioaccessibility method from the same dust, 1.2 g of the Belgian dust was placed on the chamber floor. Post-experiment, the dust was homogenised by vortexing, and two subsamples (0.05 g each) extracted and analysed for HBCDs. The remainder of the dust sample was exposed in the bioaccessibility model.

7.3.2 Abrasion of textile fibres to dust

The chamber generation of dusts contaminated via abrasion was configured as previously described, with a 2 x 2 cm square of the HBCD treated textile subjected to stirrer bar abrasion. The experiments were conducted for 24 hours at room temperature, with 0.5 g of dust placed on the chamber floor. Post experiment, dust samples were homogenised by thorough vortex mixing, and one 0.05 g aliquot analysed for HBCDs. After determining HBCD concentrations, the dust was further

diluted with the addition of an aliquot of the Belgian dust to reduce the HBCD concentration in the final sample to within an order of magnitude of that in the volatilisation pathway experiments. For the five abrasion dust samples prepared, 0.03-0.4 g of the initial dust was diluted to 1.2 g total mass, thoroughly mixed by vortexing, and three subsamples (0.05 g) extracted and analysed for HBCDs. The remainder of the dust sample was exposed to the bioaccessibility methodology.

7.3.3 Concentration in generated dust samples

Two to three subsamples of the chamber generated contaminated dusts were analysed to determine HBCD concentrations present in the dust and to gain a measure of the homogeneity of the distribution of HBCD mass throughout the dust. It was hypothesised that dust contaminated via the volatilisation pathway would have a more homogeneous distribution of HBCD through the dust sample than dust contaminated via the abrasion pathway, with HBCD contamination in the latter being more heterogeneous owing to the presence of HBCD treated textile fibres. Table 7.2 lists concentrations of HBCDs determined in the dusts generated via the volatilisation pathway, while Table 7.3 lists concentrations in both the initial sample generated via abrasion, as well as those in the ‘diluted’ dust used in the bioaccessibility experiments.

Table 7.2: Concentration of HBCDs (ng g⁻¹) in replicate analyses of dust samples contaminated via migration of HBCDs via volatilisation with subsequent partitioning to dust

		α-HBCD	β-HBCD	γ-HBCD
Volatilisation #1	Analysis 1	190	74	280
Volatilisation #2	Analysis 1	4500	1600	5900
	Analysis 2	400	130	500
Volatilisation #3	Analysis 1	1200	400	1500
	Analysis 2	940	300	1200
Volatilisation #4	Analysis 1	5200	1800	6700
	Analysis 2	3000	940	3900
Volatilisation #5	Analysis 1	820	280	1100
	Analysis 2	450	170	1200

Table 7.3: Concentration of HBCDs (ng g^{-1}) in the initial dust samples contaminated via abrasion of textile fibres and replicate analyses of the final dust sample after dilution with low level dust

		α -HBCD	β -HBCD	γ -HBCD
<i>Abrasion #1</i>	<i>Initial Analysis</i>	870	360	2500
Diluted Abrasion #1	Analysis 1	470	170	840
	Analysis 2	290	96	410
	Analysis 3	570	350	4100
<i>Abrasion #2</i>	<i>Initial Analysis</i>	7700	2500	12 000
Diluted Abrasion #2	Analysis 1	3600	1100	5000
	Analysis 2	610	220	840
	Analysis 3	320	100	400
<i>Abrasion #3</i>	<i>Initial Analysis</i>	21 000	6600	30 000
Diluted Abrasion #3	Analysis 1	6800	2300	10 000
	Analysis 2	430	140	570
<i>Abrasion #4</i>	<i>Initial Analysis</i>	29 000	9800	47 000
Diluted Abrasion #4	Analysis 1	700	200	850
	Analysis 2	1100	500	2600
	Analysis 3	250	90	310
<i>Abrasion #5</i>	<i>Initial Analysis</i>	24 000	7800	38 000
Diluted Abrasion #5	Analysis 1	3100	830	3300
	Analysis 2	230	72	280
	Analysis 3	450	160	610

All dusts generated by the abrasion method show large variations in repeat analyses with an order of magnitude concentration range seen in all cases. The variation in the abrasion-generated dusts was expected, as the HBCDs were suspected to be primarily associated with abraded textile fibres in the dust. Hence the concentration in any subsample analysed will depend strongly on the mass of fibres present. The volatilisation with subsequent partitioning to dust pathway has been suggested to result in a more uniform or homogeneous BFR distribution through dust (Webster et al., 2009, Suzuki et al., 2009). Consequently, a more homogenous HBCD distribution was expected for dusts generated via this pathway. In general, these dust samples did

display smaller concentration variations, although duplicate analyses of the Volatilisation #2 dust reveals an order of magnitude difference in concentration between the two sub-samples. Such heterogeneity of HBCD content of the dusts tested was therefore taken into account in subsequent bioaccessibility testing.

An Independent Samples T-test was performed with SPSS to determine if a significant difference exists between concentrations in the volatilisation generated dusts and the abrasion generated dusts. There was no significant difference ($p > 0.05$) in determined concentrations in the two dust types and the mean and standard deviation of the concentrations from the two different dust types and the results of the T-test are presented in Table 7.4. This shows that we achieved our objective of generating dusts via both volatilisation and abrasion pathways that contained similar concentrations of HBCDs. This is crucial, as it means that any difference in HBCD bioaccessibility between the two dust types is unlikely to be attributable to concentration differences.

Table 7.4: Results of Independent Samples T-test for comparison of HBCD concentrations determined in volatilisation generated (n=9) and abrasion generated dusts (n=14)

Group Statistics				T-test results			
		Mean	Standard Deviation		Degrees of Freedom	t-value	p-value
α -HBCD	<i>Volatilisation</i>	1900	1900	<i>Equal variances</i>	21	0.623	0.550
	<i>Abrasion</i>	1400	1900				
β -HBCD	<i>Volatilisation</i>	630	640	<i>Equal variances</i>	21	0.619	0.543
	<i>Abrasion</i>	460	630				
γ -HBCD	<i>Volatilisation</i>	2500	2400	<i>Equal variances</i>	21	0.281	0.782
	<i>Abrasion</i>	2200	2800				

7.4 Bioaccessibility method

7.4.1 Method description

The prepared dusts were subjected to the colon extended physiologically based extraction test (CE-PBET) method. The CE-PBET method consists of sample incubation in modelled stomach, small intestine and colon medium solutions, as previously reported for polyaromatic hydrocarbons (PAHs) by Tilston et al. (2011) and for BFRs by Abdallah et al. (2012). By measuring the concentrations of HBCDs in the different compartments, the bioaccessibility of the target contaminants from the sample can be calculated.

7.4.2 Chemicals

All solvents used during this extraction and clean up in this study were of analytical grade from Merck (Darmstadt, Germany). Silica gel (40 µm pore size) was purchased from J.T.Baker (Avantor Performance Materials B.V, The Netherlands) and anhydrous sodium sulfate and concentrated sulfuric acid were purchased from Merck (Darmstadt, Germany). Analytical grade inorganic salts were obtained from Fisher Scientific (Loughborough, U.K.) and organic components and laboratory sand were purchased from Sigma-Aldrich (Gillingham, U.K.). Empty polypropylene filtration tubes (3 mL) and SPE cartridges were obtained from Sigma-Aldrich (Gillingham, U.K.).

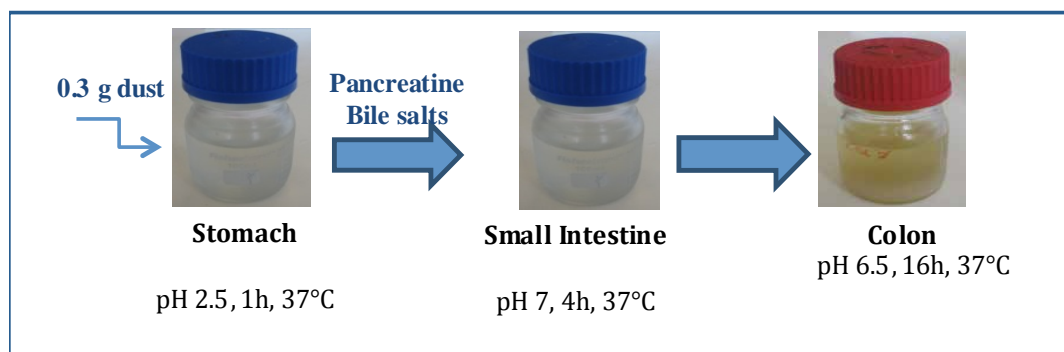
7.4.3 Methodology

The bioaccessibility method (or gastro-intestinal extraction) consists of a series of continuous incubations in a modelled stomach, small intestine and then colon solutions, maintained at 37 °C to mimic human body temperature. The experimental method is depicted in Figure 7.2 and the ingredients used to prepare the gastro-intestinal solutions are listed in Table 7.5.

Table 7.5: Ingredients in each solution media to model the different compartments of the gastrointestinal tract.

	Ingredient	Amount added
Stomach (pH 2.5)	Sodium malate	0.5 g
	Sodium citrate	0.5 g
	Lactic acid	0.42 mL
	Acetic acid	0.5 mL
	Pepsin	1.25 g
Small Intestine (pH 7) (added to stomach medium)	Pancreatine	1.78 g
	Bile salts	0.5 g
Colon (pH 6.5)	CaCl ₂	0.15 g
	KH ₂ PO ₄	0.5 g
	K ₂ HPO ₄	0.5 g
	NaCl	6.1 g
	MgSO ₄ .7H ₂ O	1.25 g
	KCl	4.5 g
	FeSO ₄	0.005 g
	NaHCO ₃	1.5 g
	Bile salts	0.4 g
	Mucin	5 g
	Haemin	0.05 g
	Cysteine HCl	0.8 g
Dietary components (for a fed-state medium)	Starch	5 g
	Pectin	2 g
	Yeast extract	4.46 g
	Peptone	3.3 g
	Tryptone	5 g
	Inulin	1 g
	Xylan	2 g
	Casein	3 g
	Arabinogalactan	2 g
	Guar gum	1 g

Figure 7.2: Illustration of the bioaccessibility methodology



Representation of the worst case scenario (maximum bioaccessibility), was conducted with the model in a 'fed state'. Previous studies have shown that the increased concentration of bile salts and organic ingredients from the food present in the "fed state" promotes the release of hydrophobic compounds from the matrix into the gastrointestinal fluids, thus increasing bioaccessibility (Hack and Selenka, 1996, Rostami and Juhasz, 2011, Yu et al. , 2011).

The following samples were exposed to the bioaccessibility model: triplicate 0.3 g aliquots of each of the generated dust samples, low level Belgian dust, laboratory sand as a method blank, and SRM 2585 (organics in dust) for QC purposes. HBCD concentrations in each compartment were determined for each sample tested to calculate the bioaccessibility.

7.4.4 Stomach/small intestine

A 50 mL bottle containing the stomach medium was pre warmed for 30 minutes to 37 °C before addition of the 0.3 g dust sample. The sample solution was incubated with automatic agitation for 1 hour in a hot water bath at 37 °C. The sample solution was then converted to the small intestine model with the addition of 1 mL of pancreatin (0.04 mg mL^{-1}) and 1 mL of bile salts (0.14 mg mL^{-1}) followed by a pH increase from 2.5 to 7 through addition of saturated NaHSO_4 . Again the sample solution was incubated with agitation for 4 hours at 37 °C. The solution was centrifuged at 3500 rpm and 20 °C for 20 minutes and the supernatant removed for extraction and analysis (labelled the 'small intestine' sample). The residue pellet was retained for the next stage.

7.4.5 Colon and Residue

The isolated sample pellet was introduced into a 50 mL bottle containing the prepared colon solution. The sample was incubated for 16 hours in a shaking hot water bath at 37 °C. After the incubation, the sample solution was centrifuged for 20 minutes at 3500 rpm and 20 °C. The sample supernatant was removed for separate extraction and analysis (labelled the 'colon' sample). The separated residue pellet was also collected for extraction and analysis (labelled the 'residue' sample). This residue pellet represents the non-bioaccessible fraction of the sample.

50 mL of each gastrointestinal solution was used in order to obtain a solid:liquid (S:L) ratio with the dust matrix of 1:160. Lower S:L ratios have been associated with lower bioaccessibility values due to the phenomenon of contaminant saturation reported by Van de Wiele et al. (2007). In a similar study, Yu et al. (2011) assessed the bioaccessibility of PBDEs from indoor dust, and suggested an optimum S:L ratio of between 1:150 and 1:250.

7.4.6 Extraction and Clean up

The small intestine, colon and residue samples obtained from each 0.3 g dust sample exposed in the bioaccessibility methodology were extracted and purified by colleagues at Reading University with methods previously established for the analysis of PCBs and PBDEs by Bordajandi et. al. (2008). Each sample was fortified with 4 ng each of ¹³C-labelled α-, β-, and γ-HBCD. The supernatants ('small intestine' and 'colon' samples) were extracted via a single liquid-liquid extraction with the addition of 30 mL of acetone-hexane (1:1 v/v), followed by incubation of the sample in a water bath for 1 hour at 37 °C with peristaltic movement, followed by ultrasound for 30 minutes. The hexane layer was removed and evaporated to 1 mL under a steady stream of nitrogen. The residue pellet was similarly extracted with 30 mL of acetone-hexane (1:1 v/v) prior to sample incubation for 1 hour at 37 °C, followed by ultrasound for 30 minutes, before the hexane layer was removed and concentrated to 1 mL. Sample clean up was performed with 0.5 mL of concentrated sulfuric acid, added to sample vials, and vortex mixing for 1 minute. The hexane (top) layer was removed for acid silica clean up. Empty solid phase extraction (SPE) cartridges were prepared for use by addition of 1 g of acidified silica (44% w/w), then 0.5 g of

anhydrous sodium sulfate. The acid silica was prepared following a previously reported method by Ali et al. (2011) where 50 g of silica gel was washed with 80 mL of *n*-hexane before sonication in an ultrasonic bath for 30 minutes. The silica was heated to 160 °C overnight, then after cooling to room temperature, 22 mL of concentrated sulfuric acid (98%) was slowly added under continuous stirring. HBCDs were eluted from the prepared SPE columns with 15 mL of *n*-hexane followed by 3 mL of DCM.

Samples were transported to the University of Birmingham for analysis after evaporation to dryness under a gentle stream of nitrogen. Samples were reconstituted to 200 μ L with 4 ng of d₁₈- γ -HBCD in HPLC grade methanol, used as a recovery standard for internal standard recovery determination. Samples were analysed with LC-MS/MS using the previously described instrumental methods (Chapter 2).

7.4.7 Bioaccessibility calculation

The HBCD mass (ng) determined from the LC-MS/MS analysis of each compartment (the small intestine, colon and residue) was divided by the initial mass (g) of the dust or blank sand exposed to the methodology. This provided a HBCD concentration (ng g⁻¹) in each compartment of the model, and allowed the bioaccessibility to be calculated. In the previous study of HBCDs in dust (Abdallah et. al., 2012), bioaccessibility was calculated as the percentage concentration found in the gastrointestinal tract solutions compared to the concentration in the original dust sample. The samples generated for this experiment were shown to be extremely heterogeneous (Section 7.1.3) with up to an order of magnitude difference between replicate analyses of the same dust sample. An appropriate single measure of the concentration in the original dust therefore could not be determined, so the bioaccessibility was calculated as the sum of the HBCD concentration from the supernatants of the small intestine and colon compartments, divided by the sum of the concentrations in the two supernatants and the residue pellet, equation 7.1.

$$\text{Bioaccessibility}(\%) = \frac{\text{Concentration in small intestine + colon}}{\text{Concentration in small intestine + colon + residue}} \quad (7.1)$$

7.5 Results

7.5.1 Method Blanks

Three 0.3 g replicates of laboratory-grade sand were run through the CE-PBET model as a method blank. The results showed concentrations of HBCDs to be close to or <LOQ in two samples, with the remaining sample displaying only low concentrations. Concentrations of HBCDs in the three different model compartments, for the three sand replicates, are listed in Table 7.6.

Table 7.6: HBCD concentrations (ng g⁻¹) in method compartments from three replicates of bioaccessibility test of laboratory sand, used as a method blank.

		α-HBCD	β-HBCD	γ-HBCD
Sand #1	Small Intestine	<LOQ	<LOQ	5.1
	Colon	<LOQ	<LOQ	<LOQ
	Residue	<LOQ	<LOQ	4.6
Sand #2	Small Intestine	<LOQ	<LOQ	<LOQ
	Colon	<LOQ	<LOQ	7.1
	Residue	<LOQ	<LOQ	5.6
Sand #3	Small Intestine	3.4	<LOQ	23
	Colon	<LOQ	<LOQ	4.3
	Residue	12	<LOQ	140

The method blanks were deemed acceptable. Analysis blanks for the University of Birmingham methodology were prepared with six replicates of 20 mL of hexane fortified with 4 ng of HBCD internal standards, before evaporation and reconstitution with recovery standards, following the same methodology as the samples. HBCD concentrations in these blanks were all <LOQ.

7.5.2 HBCD concentrations in compartments of bioaccessibility assay using SRM 2585 dust as the test sample

Three aliquots (0.3 g) of the SRM 2585 (organics in indoor dust) was subjected to the bioaccessibility test method as another QC check. Table 7.7 lists the HBCD concentration (ng g⁻¹) returned in each compartment with the reported indicative values (Keller et al., 2007). Elevated concentrations were determined in each analysis

of the SRM, particularly in the residue pellet, that exceeded the indicative concentrations reported for this SRM. The high concentrations in the residue may be due to contamination. However, as reported above, substantial HBCD concentrations were not detected in either the method or analysis blanks.

Table 7.7: Indicative concentrations (ng g⁻¹) of HBCDs in SRM 2585 and HBCD concentrations in each compartment from the bioaccessibility study for three replicate analyses of the SRM.

		α-HBCD	β-HBCD	γ-HBCD
SRM - Indicative values		<i>19 ± 3.7</i>	<i>4.3 ± 1.1</i>	<i>120 ± 22</i>
SRM #1	Small Intestine	1.0	<LOQ	10
	Colon	6.4	2.2	33
	<i>Residue</i>	<i>110</i>	<i>47</i>	<i>530</i>
	Bioaccessibility (%) *	6.3	4.6	7.5
SRM #2	Small Intestine	2.5	1.2	16
	Colon	4.1	1.4	23
	<i>Residue</i>	<i>32</i>	<i>13</i>	<i>300</i>
	Bioaccessibility (%) *	17	17	12
SRM #3	Small Intestine	2.3	0.2	22
	Colon	4.3	1.7	28
	<i>Residue</i>	<i>230</i>	<i>90</i>	<i>830</i>
	Bioaccessibility (%) *	2.8	2.0	5.7

* Bioaccessibility calculated with equation 7.1

To investigate further the elevated concentrations in the SRM bioaccessibility test samples, an aliquot of the SRM used at the University of Reading (UoR) was obtained and analysed to check against that used at the University of Birmingham (UoB). Two aliquots of the UoR dust and an aliquot of the UoB dust were analysed and the results are listed in Table 7.8. The concentrations determined are consistent with previously reported indicative HBCD values in the SRM, showing that the issue is not related to inhomogeneity of HBCD concentrations in the SRM.

Table 7.8: Concentrations (ng g^{-1}) of HBCDs in SRM 2585 used at (a) the University of Reading and (b) the University of Birmingham

	α -HBCD	β -HBCD	γ -HBCD
<i>SRM - Indicative values</i>	19 ± 3.7	4.3 ± 1.1	120 ± 22
UoR SRM #1	21	6.2	130
UoR SRM #2	24	7.7	96
UoB SRM	18	5.3	110

The SRM was subjected again to bioaccessibility testing, to investigate further the elevated concentrations seen in the first analysis. The repeat analysis had concentrations more consistent with the indicative values, and concentrations and calculated bioaccessibilities are listed in Table 7.9. The results suggest the first analysis may have suffered some laboratory contamination issues. As substantial HBCD concentrations are frequently detected in UK dust, it is possible that dust contamination occurred during analysis of the first batch of SRM aliquots subjected to bioaccessibility testing.

Table 7.9: HBCD concentrations (ng g^{-1}) in each compartment from the experiment repeat of the bioaccessibility study for three SRM replicate analyses.

		α -HBCD	β -HBCD	γ -HBCD
<i>SRM - Indicative values</i>		19 ± 3.7	4.3 ± 1.1	120 ± 22
SRM #1	Small Intestine	<LOQ	<LOQ	2.2
	Colon	<LOQ	<LOQ	4.2
	<i>Residue</i>	17	5.5	68
	Bioaccessibility (%)	0	0	8.6
SRM #2	Small Intestine	<LOQ	<LOQ	3.6
	Colon	<LOQ	<LOQ	3.3
	<i>Residue</i>	21	7.3	170
	Bioaccessibility (%)	0	0	4.0
SRM #3	Small Intestine	<LOQ	<LOQ	2.4
	Colon	<LOQ	<LOQ	2.8
	<i>Residue</i>	45	14	260
	Bioaccessibility (%)	0	0	2.0

The chamber generated dust samples were also exposed to the bioaccessibility method and extracted and cleaned-up at Reading around the same time as the first set of SRM dust. There is thus the possibility of contamination in these samples, although no evidence of this was seen in the method blanks run at the same time.

7.5.3 *HBCD concentrations in compartments of bioaccessibility assay for a low-HBCD dust sample*

The low level Belgian dust was also subjected (0.3 g) to bioaccessibility testing and concentrations in the compartments of the assays were compared to those previously measured in the dust bulk. Total concentrations obtained from analysis one, were in line with concentrations previously characterised in the dust; however, analyses two and three showed elevated concentrations. Table 7.10 lists the HBCD concentration (ng g^{-1}) in each compartment and the pre-characterised dust concentrations. The lack of consistency in the results again suggests the last two analyses may have been impacted by a degree of contamination.

Table 7.10: Indicative concentrations (ng g^{-1}) of HBCD in low level Belgian dust and HBCD concentrations in each compartment from the bioaccessibility study for three replicate analyses.

		α -HBCD	β -HBCD	γ -HBCD
<i>Pre-characterised Dust</i>		46 ± 18	13 ± 10	50 ± 39
Belgian Dust #1	Small Intestine	4.6	1.5	15
	Colon	12	3.3	87
	<i>Residue</i>	35	12	95
	Bioaccessibility (%)	32	29	52
Belgian Dust #2	Small Intestine	8.5	4.6	38
	Colon	440	110	5900
	<i>Residue</i>	61	24	350
	Bioaccessibility (%)	88	83	94
Belgian Dust #3	Small Intestine	2.8	1.0	8.3
	Colon	7.3	4.0	21
	<i>Residue</i>	190	110	1100
	Bioaccessibility (%)	5.0	4.3	2.6

Following these initial data, replicates of the Belgian dust were exposed to the bioaccessibility methodology again. Analysis of this second batch revealed total concentrations more consistent with the previously characterised dust concentrations and reproducible bioaccessibilities, Table 7.11, suggesting the first batch may have again suffered some laboratory contamination issues. As highlighted above, while the method blanks run at the same time revealed no contamination issues; the chamber generated dust samples were exposed to the bioaccessibility method and extracted and cleaned-up at Reading around the same time as the first set of Belgian dusts, and one cannot therefore exclude the possibility of contamination in these samples.

Table 7.11: HBCD concentrations (ng g⁻¹) in each compartment from experiment repeat of bioaccessibility test of Belgian dust analyses

		α -HBCD	β -HBCD	γ -HBCD
<i>Pre-characterised</i>		46 ± 18	13 ± 10	50 ± 39
Belgian Dust #1	Small Intestine	3.7	1.5	18
	Colon	1.7	<LOQ	1.4
	<i>Residue</i>	46	7.2	71
	Bioaccessibility (%)	11	18	21
Belgian Dust #2	Small Intestine	2.6	<LOQ	3.9
	Colon	2.7	0.5	1.8
	<i>Residue</i>	29	4.8	29
	Bioaccessibility (%)	16	10	17
Belgian Dust #3	Small Intestine	3.3	1.1	8.2
	Colon	4.2	0.6	7.3
	<i>Residue</i>	52	8.1	78
	Bioaccessibility (%)	15	18	17

7.5.4 HBCD concentrations in compartments of bioaccessibility assay of generated dusts and calculated bioaccessibility for each dust analysis

The five chamber generated dusts contaminated with HBCDs via volatilisation with subsequent partitioning to dust and the five dusts contaminated via abrasion of HBCD treated curtain fibres were all run through the bioaccessibility methodology in

triplicate. The concentrations in each method compartment and the calculated bioaccessibility for each volatilisation dust are listed in Tables 7.12 and for the abrasion dusts listed in Tables 7.13. There was a large variation in total concentrations returned from repeat assays of three of the abrasion dusts (#3, 4 and 5) and in one of the volatilisation dusts (#4), with up to an order of magnitude difference in total concentration. This is not so surprising, as the abrasion dusts displayed a large heterogeneity in the HBCD concentration through the dust samples. However, volatilisation dust #4 did not display a large concentration difference between duplicate analyses of the generated dust sample, further emphasising that more extensive dust analyses are required to provide an indication of HBCD homogeneity. The large concentration differences also give further credence to the choice of calculating the bioaccessibility from the total concentration seen in each analysis, rather than an average concentration determined in the dust before testing.

In general, the samples contain much higher concentrations in the residue compartment, suggesting ingested HBCDs are more likely to stay bound to dust and pass through the digestive system without being absorbed. However, a few samples show higher concentrations in the small intestine supernatant phase (assays of volatilisation #4 and abrasion #3). This may be due to inadequate removal from the supernatant of the dust under test, or to overloading of the system due to elevated concentrations. There is also the possibility of laboratory contamination as the first analyses of the SRM and Belgian dust samples indicated a contamination issue. Two samples from the volatilisation dusts, both the small intestine samples from assay 3 of volatilisation #3 and #4, had very low internal standard recoveries for each diastereomer (between 0.3 and 4%) and these samples were rejected as they failed to meet QA/QC criteria for acceptable IS recoveries.

Tables 7.12: Concentrations (ng g^{-1}) previously determined in the generated dust samples and concentrations (ng g^{-1}) and calculated bioaccessibilities for dust samples generated via volatilisation with partitioning of HBCDs.

Volatilisation #1		α -HBCD	β -HBCD	γ -HBCD
<i>Predetermined Concentration (ng g^{-1})</i>		190	74	280
Assay 1	Small Intestine	3.1	1.0	5.0
	Colon	4.1	1.1	9.3
	Residue	92	41	510
	<i>Total Concentration</i>	99	43	520
	Bioaccessibility (%)	7.3	4.8	2.7
Assay 2	Small Intestine	3.2	1.1	4.2
	Colon	6.3	2.1	18
	Residue	60	19	140
	<i>Total Concentration</i>	70	22	160
	Bioaccessibility (%)	14	15	14
Assay 3	Small Intestine	4.5	1.6	17
	Colon	42	10	420
	Residue	90	37	370
	<i>Total Concentration</i>	140	49	810
	Bioaccessibility (%)	34	24	54
Mean (n=3)	Small Intestine	3.6 \pm 0.8	1.2 \pm 0.3	8.7 \pm 7.1
	Colon	17 \pm 21	4.5 \pm 5.1	150 \pm 240
	Residue	81 \pm 18	32 \pm 12	340 \pm 190
	<i>Mean Total Concentration</i>	100 \pm 33	38 \pm 14	500 \pm 320
	Mean Bioaccessibility (%)	18 \pm 14	15 \pm 9.7	24 \pm 27

Volatilisation #2		α -HBCD	β -HBCD	γ -HBCD
<i>Predetermined Concentration (ng g^{-1})</i>		400, 4500	130, 1600	500, 5900
Assay 1	Small Intestine	99	54	630
	Colon	6.1	2.1	19
	Residue	73	16	120
	<i>Total Concentration</i>	180	72	780

	Bioaccessibility (%)	59	78	84
Assay 2	Small Intestine	48	24	290
	Colon	3.4	0.6	5.8
	Residue	78	19	220
	<i>Total Concentration</i>	<i>130</i>	<i>43</i>	<i>510</i>
	Bioaccessibility (%)	40	56	58
Assay 3	Small Intestine	54	31	360
	Colon	8.8	3.1	39
	Residue	160	56	330
	<i>Total Concentration</i>	<i>230</i>	<i>90</i>	<i>720</i>
	Bioaccessibility (%)	28	38	55
Mean (n=3)	Small Intestine	67 ± 28	36 ± 16	430 ± 180
	Colon	6.1 ± 2.7	1.9 ± 1.3	21 ± 17
	Residue	100 ± 50	30 ± 22	220 ± 100
	<i>Mean Total Concentration</i>	<i>180 ± 48</i>	<i>68 ± 23</i>	<i>55 ± 140</i>
	Mean Bioaccessibility (%)	42 ± 16	57 ± 20	66 ± 16

The small intestine sample in the third analysis of dust ‘Volatilisation #3’ returned a very low internal standard recovery for all HBCD diastereomers (0.3 to 4%) hence was rejected based on a failure to meet QA/QC criteria. Therefore, assay number 3 was removed and bioaccessibility was only assessed from two replicate analyses of ‘Volatilisation #3’ dust.

Volatilisation #3		α-HBCD	β-HBCD	γ-HBCD
<i>Predetermined Concentration (ng g⁻¹)</i>		<i>940, 1200</i>	<i>300, 400</i>	<i>1200, 1500</i>
Assay 1	Small Intestine	19	4.2	28
	Colon	4.7	1.1	4.8
	Residue	130	47	300
	<i>Total Concentration</i>	<i>160</i>	<i>52</i>	<i>340</i>
	Bioaccessibility (%)	15	10	10
Assay 2	Small Intestine	17	8.2	67
	Colon	4.8	1.3	5.4
	Residue	310	110	550

	<i>Total Concentration</i>	330	120	620
	Bioaccessibility (%)	6.6	8.0	12
Assay 3	<i>Small Intestine*</i>	-	-	-
	<i>Colon</i>	10	3.4	38
	<i>Residue</i>	310	98	390
Mean (n=2)	Small Intestine	18	6.2	48
	Colon	4.7	1.2	5.1
	Residue	220	78	420
	<i>Mean Total Concentration</i>	240	86	480
	Mean Bioaccessibility (%)	11	9.0	11

* sample failed QA/QC due to unsatisfactory IS recoveries

The small intestine sample in the third analysis of dust ‘Volatilisation #4’ returned a very low internal standard recovery for all HBCD diastereomers (0.3 to 3%) hence was rejected based on a failure to meet QA/QC criteria. Therefore, assay number 3 was removed and bioaccessibility was only assessed from two replicate analyses of ‘Volatilisation #4’ dust.

Volatilisation #4		α-HBCD	β-HBCD	γ-HBCD
<i>Predetermined Concentration (ng g⁻¹)</i>		3000, 5200	940, 1800	3900, 6700
Assay 1	Small Intestine	12	2.6	11
	Colon	8.9	3.5	42
	Residue	240	72	510
	<i>Total Concentration</i>	260	78	560
	Bioaccessibility (%)	8.0	7.8	9.4
Assay 2	Small Intestine	370	250	2700
	Colon	5.8	1.6	14
	Residue	650	290	980
	<i>Total Concentration</i>	1000	540	3700
	Bioaccessibility (%)	37	46	73
Assay 3	<i>Small Intestine *</i>	-	-	-
	<i>Colon</i>	5.0	1.4	12
	<i>Residue</i>	310	120	780

Mean (n=2)	Small Intestine	190	130	1300
	Colon	7.4	2.5	28
	Residue	450	180	740
	<i>Mean Total Concentration</i>	<i>650</i>	<i>310</i>	<i>2100</i>
	Mean Bioaccessibility (%)	22	27	41

* sample failed QA/QC due to unsatisfactory IS recoveries

Volatilisation #5		α-HBCD	β-HBCD	γ-HBCD
<i>Predetermined Concentration (ng g⁻¹)</i>		<i>450, 820</i>	<i>170, 280</i>	<i>1100, 1200</i>
Assay 1	Small Intestine	27	6.0	37
	Colon	6.0	2.3	14
	Residue	200	64	330
	<i>Total Concentration</i>	<i>240</i>	<i>72</i>	<i>380</i>
	Bioaccessibility (%)	14	11	14
Assay 2	Small Intestine	14	4.4	27
	Colon	14	3.8	56
	Residue	100	37	300
	<i>Total Concentration</i>	<i>130</i>	<i>45</i>	<i>380</i>
	Bioaccessibility (%)	22	18	22
Assay 3	Small Intestine	12	4.5	29
	Colon	4.6	1.7	11
	Residue	77	22	290
	<i>Total Concentration</i>	<i>93</i>	<i>28</i>	<i>330</i>
	Bioaccessibility (%)	17	22	12
Mean (n=3)	Small Intestine	17 ± 8.0	5.0 ± 0.9	31 ± 5.4
	Colon	8.1 ± 4.9	2.6 ± 1.1	27 ± 25
	Residue	130 ± 67	41 ± 21	300 ± 20
	<i>Mean Total Concentration</i>	<i>150 ± 74</i>	<i>48 ± 22</i>	<i>360 ± 29</i>
	Mean Bioaccessibility (%)	18 ± 3.9	17 ± 5.5	16 ± 5.1

Tables 7.13: Concentrations (ng g⁻¹) and calculated bioaccessibility for extraction of generated dust samples contaminated via the abrasion of HBCD treated textile fibres.

Abrasion #1		α -HBCD	β -HBCD	γ -HBCD
<i>Predetermined Concentration (ng g⁻¹)</i>		290, 570	96, 350	410, 4100
Assay 1	Small Intestine	11	3.5	12
	Colon	4.0	1.6	8.4
	Residue	140	110	5100
	<i>Total Concentration</i>	160	120	5100
	Bioaccessibility (%)	10	4.4	0.4
Assay 2	Small Intestine	6.9	1.4	7.3
	Colon	6.2	1.1	5.0
	Residue	100	32	190
	<i>Total Concentration</i>	120	35	200
	Bioaccessibility (%)	11	7.3	6.2
Assay 3	Small Intestine	7.3	1.9	6.4
	Colon	4.2	1.6	9.3
	Residue	70	32	210
	<i>Total Concentration</i>	82	35	220
	Bioaccessibility (%)	14	10	7.1
Mean (n=3)	Small Intestine	8.5 ± 2.5	2.3 ± 1.1	8.4 ± 2.8
	Colon	4.8 ± 1.2	1.4 ± 0.3	7.6 ± 2.3
	Residue	110 ± 37	58 ± 45	1800 ± 2800
	<i>Mean Total Concentration</i>	120 ± 39	62 ± 47	1900 ± 2800
	Mean Bioaccessibility (%)	12 ± 2.3	7.2 ± 2.8	4.6 ± 3.6

Abrasion #2		α -HBCD	β -HBCD	γ -HBCD
<i>Predetermined Concentration (ng g⁻¹)</i>		320, 3600	100, 1100	400, 5000
Assay 1	Small Intestine	6.9	1.6	8.7
	Colon	5.5	1.0	5.8
	Residue	140	46	170
	<i>Total Concentration</i>	150	49	190
	Bioaccessibility (%)	8.3	5.3	7.8

Assay 2	Small Intestine	19	3.6	7.5
	Colon	7.6	1.8	12
	Residue	140	61	520
	<i>Total Concentration</i>	<i>170</i>	<i>66</i>	<i>540</i>
	Bioaccessibility (%)	16	8.2	3.7
Assay 3	Small Intestine	27	13	300
	Colon	11	5.3	66
	Residue	70	31	500
	<i>Total Concentration</i>	<i>110</i>	<i>50</i>	<i>850</i>
	Bioaccessibility (%)	35	37	42
Mean (n=3)	Small Intestine	17 ± 10	6.1 ± 6.2	100 ± 170
	Colon	8.1 ± 2.9	2.7 ± 2.3	28 ± 33
	Residue	120 ± 39	46 ± 15	390 ± 190
	<i>Mean Total Concentration</i>	<i>140 ± 29</i>	<i>55 ± 9.6</i>	<i>530 ± 330</i>
	Mean Bioaccessibility (%)	20 ± 14	17 ± 18	18 ± 21

Abrasion #3		α-HBCD	β-HBCD	γ-HBCD
<i>Predetermined Concentration (ng g⁻¹)</i>		<i>430, 6800</i>	<i>140, 2300</i>	<i>570, 10 000</i>
Assay 1	Small Intestine	24	6.2	53
	Colon	6.4	2.2	7.8
	Residue	240	110	440
	<i>Total Concentration</i>	<i>270</i>	<i>120</i>	<i>500</i>
	Bioaccessibility (%)	11	7.3	12
Assay 2	Small Intestine	50	23	180
	Colon	14	6.1	87
	Residue	190	86	1000
	<i>Total Concentration</i>	<i>250</i>	<i>120</i>	<i>1300</i>
	Bioaccessibility (%)	26	25	21
Assay 3	Small Intestine	300	210	2100
	Colon	58	45	430
	Residue	420	290	3100
	<i>Total Concentration</i>	<i>780</i>	<i>540</i>	<i>5600</i>

	Bioaccessibility (%)	46	47	44
Mean (n=3)	Small Intestine	130 ± 160	80 ± 110	770 ± 1100
	Colon	26 ± 28	18 ± 24	180 ± 230
	Residue	280 ± 120	160 ± 110	1500 ± 1400
	<i>Mean Total Concentration</i>	<i>430 ± 300</i>	<i>260 ± 250</i>	<i>2500 ± 2800</i>
	Mean Bioaccessibility (%)	28 ± 18	27 ± 20	26 ± 17

Abrasion #4		α-HBCD	β-HBCD	γ-HBCD
<i>Predetermined Concentration (ng g⁻¹)</i>		<i>250, 1100</i>	<i>90, 500</i>	<i>310, 2600</i>
Assay 1	Small Intestine	32	21	260
	Colon	18	10	96
	Residue	410	240	2500
	<i>Total Concentration</i>	<i>460</i>	<i>270</i>	<i>2900</i>
	Bioaccessibility (%)	11	11	13
Assay 2	Small Intestine	17	5.3	37
	Colon	5.0	1.1	7.4
	Residue	86	31	160
	<i>Total Concentration</i>	<i>110</i>	<i>38</i>	<i>210</i>
	Bioaccessibility (%)	21	17	21
Assay 3	Small Intestine	15	4.8	26
	Colon	5.5	1.6	6.4
	Residue	130	49	230
	<i>Total Concentration</i>	<i>150</i>	<i>56</i>	<i>260</i>
	Bioaccessibility (%)	14	12	12
Mean (n=3)	Small Intestine	22 ± 9.3	10 ± 9.1	110 ± 130
	Colon	10 ± 7.4	4.2 ± 4.8	37 ± 52
	Residue	210 ± 180	110 ± 120	960 ± 1300
	<i>Mean Total Concentration</i>	<i>240 ± 190</i>	<i>120 ± 130</i>	<i>1100 ± 1500</i>
	Mean Bioaccessibility (%)	15 ± 4.9	13 ± 3.4	15 ± 5.2

Abrasion #5	α-HBCD	β-HBCD	γ-HBCD
<i>Predetermined Concentration (ng g⁻¹)</i>	<i>230, 3100</i>	<i>72, 830</i>	<i>280, 3300</i>

Assay 1	Small Intestine	6.9	2.5	13
	Colon	14	6.7	22
	Residue	1000	720	8400
	<i>Total Concentration</i>	<i>1100</i>	<i>730</i>	<i>8400</i>
	Bioaccessibility (%)	2.0	1.3	0.4
Assay 2	Small Intestine	9.0	2.9	9.1
	Colon	9.3	2.3	10
	Residue	190	79	390
	<i>Total Concentration</i>	<i>210</i>	<i>84</i>	<i>410</i>
	Bioaccessibility (%)	8.9	6.1	4.7
Assay 3	Small Intestine	13	3.0	11
	Colon	6.4	1.9	19
	Residue	180	69	310
	<i>Total Concentration</i>	<i>200</i>	<i>74</i>	<i>340</i>
	Bioaccessibility (%)	10	6.7	8.6
Mean (n=3)	Small Intestine	10 ± 3.1	2.8 ± 0.3	11 ± 2.2
	Colon	10 ± 4.0	36 ± 2.7	17 ± 6.3
	Residue	470 ± 500	290 ± 370	3000 ± 4600
	<i>Mean Total Concentration</i>	<i>490 ± 500</i>	<i>300 ± 380</i>	<i>3100 ± 4600</i>
	Mean Bioaccessibility (%)	6.8 ± 4.2	4.7 ± 3.0	4.6 ± 4.1

Given the observed heterogeneity in HBCD concentrations in the dust samples before bioaccessibility testing, any significant difference in total HBCD concentrations in the bioaccessibility experiments for each dust type was also tested. As before, this was conducted to check that any differences in bioaccessibility between the two dust types, was not due to differences in HBCD concentrations alone. An Independent Samples T-test was conducted with the total concentration determined in each bioaccessibility assay (i.e. the sum of that determined in each compartment) as input for the volatilisation generated dusts compared to the abrasion generated dusts. There was no significant difference ($p > 0.05$) between the dust types. The mean and standard deviation of the concentrations from the two dust types and the results of the T-test are presented in Table 7.14. As there was no significant difference between concentrations predetermined in the dust samples (Section 7.3.3) or in the total

concentrations seen in each bioaccessibility assay, we were confident that a comparison of bioaccessibility between dust types would not be unduly influenced by differences in concentration alone.

Table 7.14: Results of Independent Samples T-test for comparison of total HBCD concentration determined in each bioaccessibility assay, from volatilisation generated (n=13) and abrasion generated dusts (n=15)

Group Statistics				T-test results			
		Mean	Standard Deviation		Degrees of Freedom	t-value	p-value
α -HBCD	<i>Volatilisation</i>	240	250	<i>Equal variances</i>	26	0.477	0.637
	<i>Abrasion</i>	290	280				
β -HBCD	<i>Volatilisation</i>	96	140	<i>Equal variances</i>	26	0.928	0.362
	<i>Abrasion</i>	160	210				
γ -HBCD	<i>Volatilisation</i>	750	900	<i>Equal variances</i>	26	1.405	0.171
	<i>Abrasion</i>	1800	2600				

7.5.5 Bioaccessibility comparison between generated dust samples

Mean bioaccessibilities for individual diastereomers were higher in the volatilisation dusts (23 to 32%) than in the abrasion dusts (14 to 16%), however there was also substantial variation between samples, and between replicate assays of the same sample. An Independent Samples T-test was conducted on the calculated bioaccessibilities and the mean and standard deviation of the bioaccessibilities from the two different dust types and the results of the T-test are listed in Table 7.15. There was no significant difference ($p > 0.05$) for bioaccessibility values obtained for the α - or β -HBCD diastereomers between dust types, but a significant difference was observed for the γ -HBCD isomer ($p = 0.032$). From these results, the hypothesis that a significant difference exists in the bioaccessibility of HBCDs from dusts contaminated via two different pathways was not shown in this experiment for α - or β -HBCD. However, there were indications of a significant difference for γ -HBCD. It is noted that only a small dataset was analysed in this study (n=13 or 15 for volatilisation and abrasion dusts respectively) hence these results only provide a first

indication as to bioaccessibilities of HBCDs in different dust types and more replicate analyses are required.

Table 7.15: Calculated values from an Independent Samples T-test of bioaccessibilities determined in dust contaminated post volatilisation of HBCDs (n=13) and via abrasion (n=15) of textile fibres

Data set comparisons				Student t-test results			
		Mean	Standard Deviation		Degrees of Freedom	t-value	p-value
α -HBCD	<i>Volatilisation</i>	23	16	<i>Equal variances</i>	26	1.34	0.191
	<i>Abrasion</i>	16	12				
β -HBCD	<i>Volatilisation</i>	26	22	<i>Equal variances</i>	26	1.83	0.079
	<i>Abrasion</i>	14	13				
γ -HBCD	<i>Volatilisation</i>	32	28	<i>Equal variances</i>	26	2.27	0.032
	<i>Abrasion</i>	14	13				

Yu et al. (2013b) investigated the bioaccessibility of PBDEs from dust and observed a significant negative correlation between dust particle size and PBDE bioaccessibility. Smaller particles are thought to have a larger surface contact area relative to their size, promoting interactions between bile salts and PBDEs in the dust particle. Smaller particles are also thought to contain a higher mineral content, which have a weaker capacity to bind PBDEs hence the PBDEs are more easily released under the action of bile salts. In the present study, lower mean bioaccessibilities were determined in the abrasion dusts, although the differences were only significant for γ -HBCD. However, in the abrasion dusts, HBCD bioaccessibilities may in part be influenced by the HBCDs being confined to larger particles/fibres abraded from the source, than to the smaller dust particles that HBCDs partition to post volatilisation. The larger particles/fibres will have a smaller contact surface area normalised to size and hence provide proportionally fewer active sites for interaction with the GIT solution. This, combined with a potentially stronger binding of HBCDs to particles/fibres of a certain than to other dust particle surfaces, (such as smaller particles with a high mineral content) may explain the lower mean bioaccessibilities seen for the abrasion generated dusts.

A similar mean bioaccessibility was observed for all three diastereomers from the abrasion dusts, whereas a higher mean bioaccessibility for the γ -HBCD diastereomer (than for α - or β -HBCD) was observed in the volatilisation dusts. This difference was not significant however ($p = 0.321$ and $p = 0.536$ for γ -HBCD comparison with α - and β -HBCD respectively). γ -HBCD has a higher K_{OW} and lower water solubility than either α - or β -HBCD so in theory it should experience a stronger binding to the dust/residue pellet and be less available for uptake into the GIT solutions. Therefore, significantly lower concentrations are expected in GIT solutions however this was not seen in the current study. The model used in this study simulates a ‘fed state’ of the digestive system and the addition of the food components may encourage the partitioning of the more hydrophobic γ -HBCD to the GIT solution and the organic matter associated with the food components, resulting in a higher bioaccessibility for this diastereomer. The study by Abdallah et al. (2012) reported a reverse trend with greater mean bioaccessibilities for the α - and β -HBCDs than the γ -HBCD (92, 80 and 72% for α -, β - and γ -HBCD respectively), yet this earlier study was conducted with an ‘unfed state’ model, hence the addition of food components may result in the preferential uptake of γ -HBCD into the GIT solutions and the reversed pattern seen in the present study.

The study by Abdallah et al. (2012) is the only other study to date to have investigated the bioaccessibility of HBCDs from dust, with repeated analyses of one bulk house dust sample investigated using a similar CE-PBET method. The dust sample was shown to have a more homogeneous HBCD concentration (RSD < 5% for 10 replicate analyses) than the dusts in the present study, and consistent bioaccessibility values were reported for three replicate assays of this dust sample (92 ± 4.2 , 80 ± 3.8 and $72 \pm 2.7\%$ for α -, β - and γ -HBCD respectively). Likewise, in the present study, more consistent bioaccessibility values were observed for the triplicate assays of the “naturally contaminated” low level Belgian dust (14 ± 2.6 , 15 ± 5.6 , $18 \pm 2.3\%$ for α -, β - and γ -HBCD respectively). We therefore hypothesise that the highly variable bioaccessibility values obtained for the chamber generated dusts in this study stems from an inhomogeneous distribution of HBCD concentrations throughout these samples.

7.5.6 Influence of HBCD concentration in dust on bioaccessibility

Previous bioaccessibility studies of PBDEs in dust (Abdallah et al., 2012, Lepom et al., 2010, Yu et al., 2012) have reported a consistent PBDE bioaccessible fraction between studies, regardless of the dust concentration (27-66% for tri-heptaBDEs and 14% for BDE-209), hence the vast differences in bioaccessibilities in the present study (0.4 to 84% for γ -HBCD alone) were surprising. The low water solubility of HBCD suggests that an aqueous solubility saturation point may exist, above which additional concentrations added to the system will not partition to the GIT solution, or be bioaccessible. We therefore tested this hypothesis by examining the relationship between bioaccessibility and the total concentration determined for each diastereomer (i.e. the sum of the concentrations detected in the small intestine, colon and residue). As it was also hypothesised that the contamination pathway (abrasion or volatilisation) exerts an influence on bioaccessibility, we regressed the data for the volatilisation and abrasion dust data sets separately. Figures 7.3 and 7.4 present the plots and the associated p-values obtained for a linear regression of bioaccessibility against total concentration for each diastereomer for the volatilisation and abrasion dusts respectively. Significant correlations were not observed ($p > 0.05$) for the α - or β -HBCD diastereomers for either dust type; however a significant correlation was observed for γ -HBCD for the volatilisation dusts ($p = 0.045$). The volatilisation data set was reanalysed with the outlier sample for which the concentration was 3700 ng g^{-1} removed to determine if this sample was driving the correlation; however an even stronger correlation ($p = 0.017$) was seen with the outlier removed, illustrated in Figure 7.3. The abrasion data set for γ -HBCD, showing no significant correlation ($p = 0.962$), was reanalysed with the high concentration outliers (above 1000 ng g^{-1}) removed, and a significant correlation was observed ($p = 0.045$), Figure 7.4. A significant correlation was still not observed when the outlier was removed from the volatilisation dusts for α - or β -HBCD ($p = 0.451$, $p = 0.118$ respectively) or when the higher concentration outliers for the abrasion dusts were removed ($p = 0.571$, $p = 0.532$ for α - and β -HBCD respectively).

Only small data sets are regressed in this analysis ($n \leq 15$) and more replicate analyses are needed to determine if this relationship is reproducible. The α - and β -HBCDs in

the volatilisation dusts are present at lower concentrations than γ -HBCD, and a smaller concentration range is compared, thus a larger range of concentrations may in fact show a correlation between concentration and bioaccessibility for these diastereomers and should also be investigated in further research studies. Although as discussed earlier in this chapter, some evidence of contamination in occasional QA/QC samples was evident; no evidence of contamination was present in method blanks, careful scrutiny of these data removed two suspect data points, and the observed pattern in the data is inconsistent with the random nature of the blank contamination. We therefore believe that we have accounted adequately for any potential contamination issues.

The results from the regression analysis provide an initial indication that at lower concentrations in dust, the bioaccessibility of γ -HBCD increases linearly with concentration, yet a critical saturation point in the GIT solution is reached, at a concentration in dust of $\sim 1000 \text{ ng g}^{-1}$ for γ -HBCD. Beyond this concentration, bioaccessibility does not increase. We examined this further by calculating for each sample the concentrations of γ -HBCD that would be achieved if all that present in the dust dissolved in the 50 mL small intestine and colon solutions. The calculated concentrations of γ -HBCD in the small intestine and colon solutions ranged from 0 to $3.1 \mu\text{g L}^{-1}$ except for the outlier volatilisation dust and the abrasion dust with the second highest total sample concentration; for which concentrations in the small intestine solutions were 16 and $13 \mu\text{g L}^{-1}$ respectively. For comparison, the reported water solubility of γ -HBCD is $2.1 \mu\text{g L}^{-1}$ (EC, 2011). This is consistent with the hypothesis that above this concentration, bioaccessibility would plateau owing to solubility limitations.

In contrast, a similar relationship between concentration in dust and bioaccessibility was not observed for α - or β -HBCD for either the volatilisation or abrasion dust samples. The absence of evidence of a solubility limit value beyond which bioaccessibility does not increase, is consistent with the fact that the maximum concentrations in the small intestine and colon solutions of these diastereomers were – at 1.3 and $2.2 \mu\text{g L}^{-1}$ for α - and β -HBCD respectively – both well below their respective reported water solubilities of 49 and $15 \mu\text{g L}^{-1}$ (Canada, 2011). In contrast,

the absence of a positive linear relationship between concentration and bioaccessibility for α - and β -HBCD is not explicable at the current time, and further detailed research is required to provide insights into why these diastereomers behave differently to γ -HBCD. Such research should investigate a wider range of concentrations to both confirm our observed relationship between bioaccessibility and concentration for γ -HBCD and to determine if a correlation with α - and β -HBCD exists. The influence of dust particle size on bioaccessibility of HBCDs should be examined, and a wider range of flame retardants examined.

Figure 7.3: Concentration vs bioaccessibility (%) for α - and β -HBCDs (left and right top respectively) in dusts contaminated via volatilisation with subsequent partitioning to dust and associated correlation p -values, and γ -HBCD with and without the data point at 3700 $\text{ng}\cdot\text{g}^{-1}$ (left and right bottom respectively)

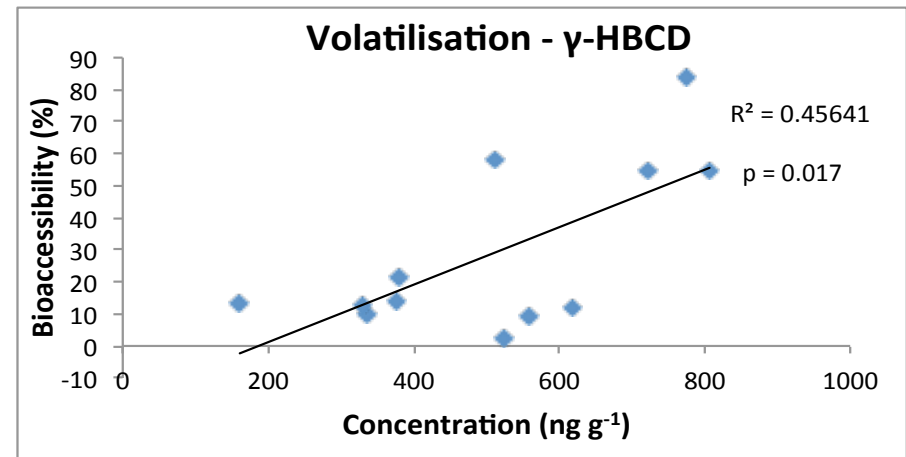
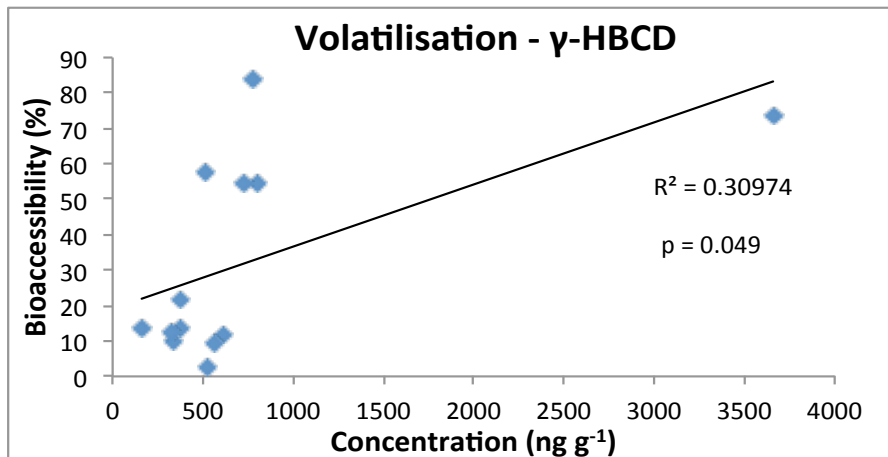
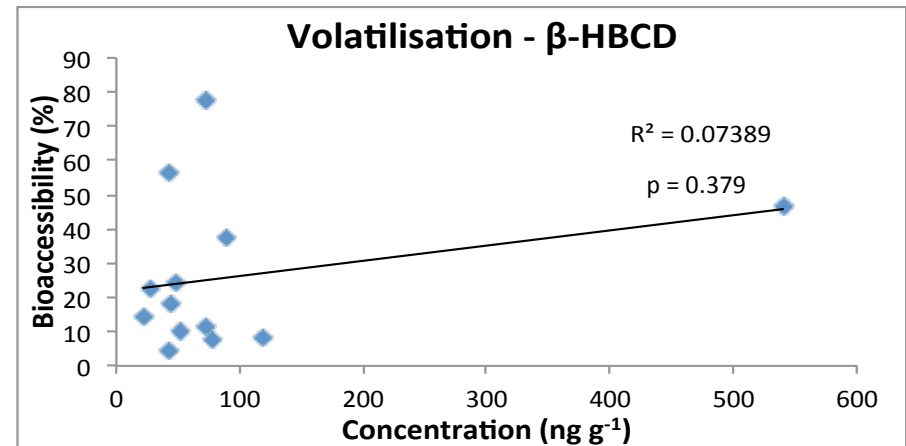
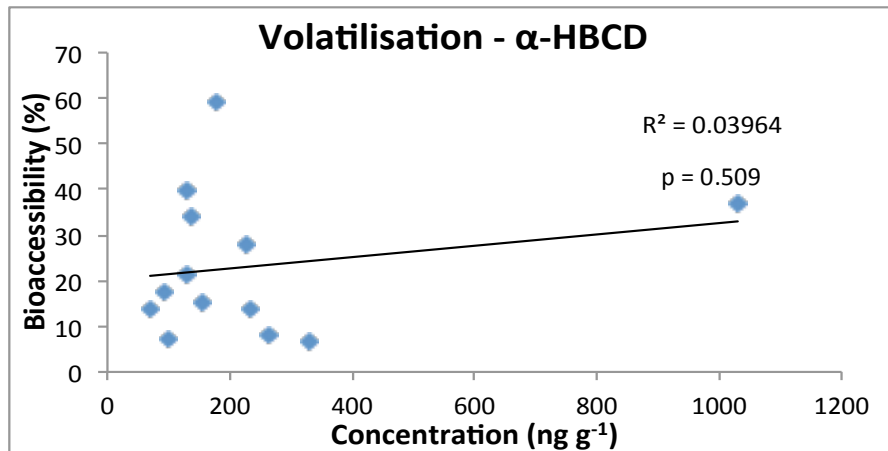
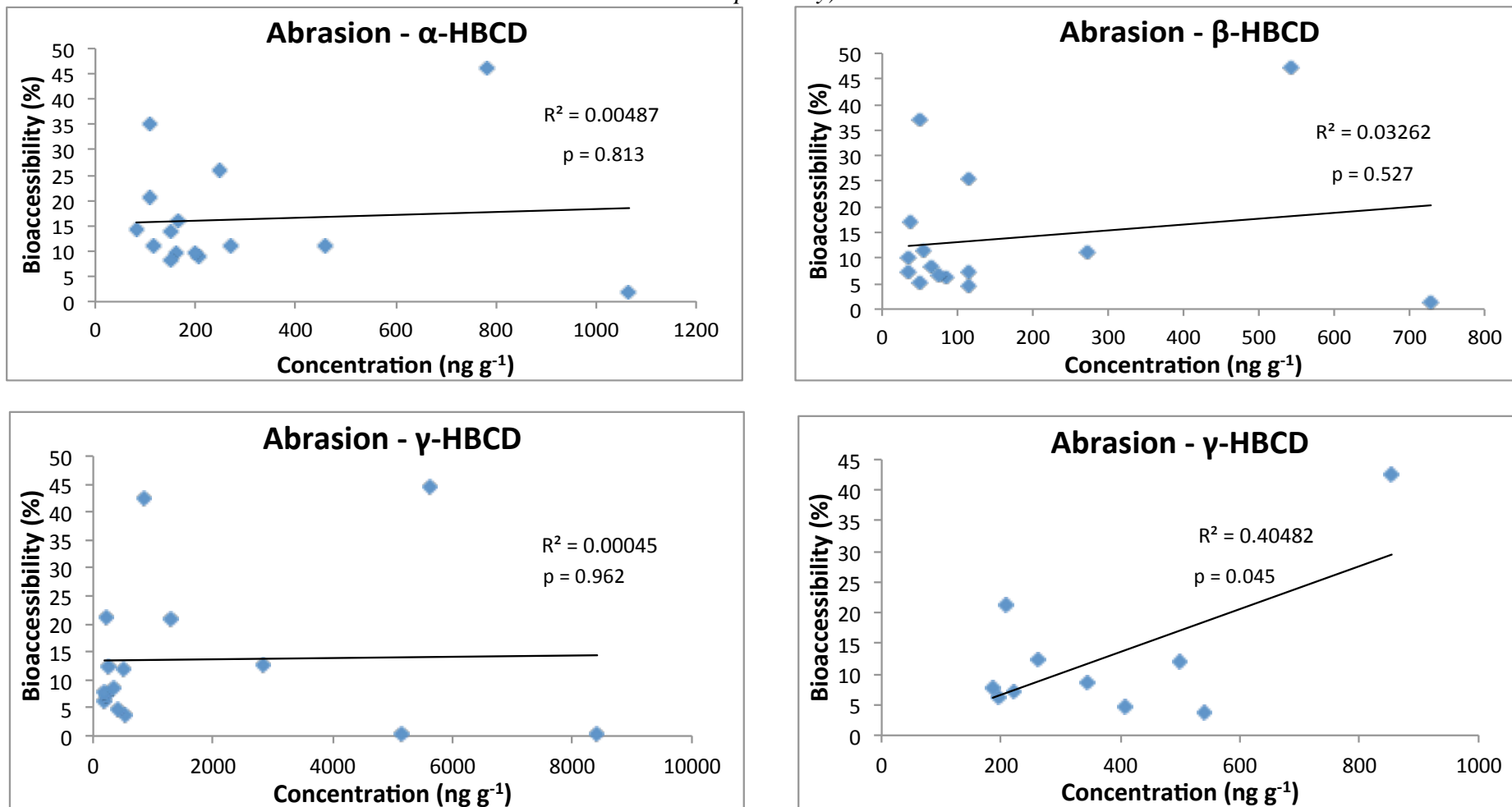


Figure 7.4: Concentration vs bioaccessibility (%) for α - and β -HBCDs (left and right top respectively) in dusts contaminated via abrasion of fibres to dust and associated correlation p -values, and γ -HBCD with and without the data points above 2000 $\text{ng}\cdot\text{g}^{-1}$ (left and right bottom respectively)



The current study has provided several insights into areas of future research for assessing the bioaccessibility of HBCDs (and other flame retardants) from dust. To summarise, replicate analyses of the current study are required to confirm the reproducibility of the concentration vs bioaccessibility correlation for γ -HBCD. A more extensive range of concentrations should be investigated to identify the concentration range the γ -HBCD correlation covers and to determine if a correlation exists for α - and β -HBCD. The study should also be repeated with a homogenous dust sample to investigate the reproducibility of the calculated bioaccessibilities.

Another interesting extension of this study would be to investigate a range of different flame retardants to assess variations in bioaccessibilities for dust contaminated via different migration pathways of chemicals with differing physicochemical properties. How different flame retarded product matrices influence the mass of flame retardant that is released into the GIT solution (and hence are bioaccessible) is another interesting avenue to investigate, which would shed light on the extent to which the processes used to incorporate the flame retardant into the product, can influence FR bioaccessibility. These processes include incorporation into a back coating; mixing into the molten polymer; dipping the final product into the flame retardant; as well as if the flame retardant is incorporated into the product in a reactive or additive fashion.

7.6 Summary/Conclusions

This study is the first to test the hypothesis that the migration pathway influences bioaccessibility. Although the average mean calculated bioaccessibilities of γ -HBCD from abrasion contaminated dusts were significantly lower ($p < 0.05$) than those in volatilisation contaminated dusts; a significant difference was not seen for either α - or β -HBCD. Also tested, was the hypothesis that bioaccessibility is influenced by the HBCD concentration in the dust sample. The hypothesis was tested with a regression analysis and although a correlation between bioaccessibility and concentration was not seen for α - or β -HBCD, a significant ($p < 0.05$) correlation was seen for γ -HBCD in both dust types. This correlation was only seen below 1000 ng g^{-1} for γ -HBCD suggesting that the bioaccessibility increased linearly with concentration until 1000 ng g^{-1} above which concentration the bioaccessibility plateaus. Above 1000

ng g⁻¹, the concentration in the GIT solutions (particularly the small intestine) exceeded the aqueous solubility of γ -HBCD (2 $\mu\text{g L}^{-1}$). This trend was not seen for α - or β -HBCD; however, due to the small sample size more replicate analyses and more intensive investigation are needed.

It is important to note that more data are required to confirm the observed relationship for γ -HBCD, and also the apparent absence of a similar relationship for α - and β -HBCDs. Moreover, the results from the current study were obtained under only one specific BFR usage scenario, HBCDs present in a treated textile; and more research is needed to assess the behaviour of different BFRs and the influence of different source materials. The current study also highlights the difficulty of replicating the complex processes that exist in the gastrointestinal system, in an *in vitro* model. Given the observed substantial differences in bioaccessibility of HBCDs determined previously by Abdallah et al. (2012) using a similar *in vitro* model, but in an “unfed state” as opposed to the “fed state” examined here; the influence of such model parameters needs to be examined more closely to determine their influence on bioaccessibility.

In conclusion, the results from this study suggest that current exposure estimates of HBCDs to humans from ingested dust may overestimate the risk associated with exposure via ingestion, if 100% uptake is assumed. Importantly - while more research is needed to confirm this - there are indications that bioaccessibility may be less efficient from samples containing elevated concentrations of BFRs as bioaccessibility values for HBCD diastereomers in individual samples in this study ranged from 2.7 to 84% for the volatilisation dusts and 0.4 to 47% for the abrasion generated dusts.

CHAPTER 8

SUMMARY AND CONCLUSIONS

Brominated flame retardants (BFRs) have been manufactured and in use since the 1970s (ATSDR, 2004a) with polybrominated diphenyl ethers (PBDEs) and hexabromocyclododecanes (HBCDs) two of the most widely produced BFRs. Due to their extensive range of indoor uses they are ubiquitous in indoor air and dust. Consequently, as humans spend up to 95% of their time in indoor environments (Palm Cousins, 2012) there is the opportunity for continuous exposure and consequent potential health risks. Emission to indoor air occurs via volatilisation from products containing BFRs (Kemmlein et al., 2003). BFR concentrations detected in indoor air are elevated compared to that in outdoor air, hence inhalation is an appreciable human exposure pathway. Moreover, concentrations of BFRs in indoor dust vastly exceed those in comparable outdoor matrices (e.g. soil). Dust has been demonstrated to constitute an important vector of human exposure route to PBDEs and HBCDs, especially for toddlers (Jones-Otazo et al., 2005, Abdallah et al., 2008a). Despite the greater importance of dust contamination in the context of human exposure to BFRs however, the mechanisms via which BFRs transfer from source materials to dust have hitherto been subject to only limited study.

The aims of this research were thus to investigate pathways via which BFRs transfer from sources to indoor dust and evaluate the bioaccessibility from dust of BFRs originating via different transfer mechanisms. The three principal pathways via which BFRs are hypothesised to migrate from sources to dust, are: (a) volatilisation from sources with subsequent partitioning to dust, (b) abrasion of particles or fibres of treated products which deposit directly to dust, and (c) migration via direct source-dust contact. The main achievements and outcomes of this project are summarised below.

8.1 Development of a test chamber and experimental designs to simulate migration of BFRs to dust

A stainless steel test chamber was designed and built to assess the migration of BFRs from sources to dust. The experimental designs were optimised to successfully replicate BFR transfer to dust via all three migration pathways mentioned above and inherent problems associated with the analysis of SVOCs in test chambers were explored. The lower vapour pressures of BFRs, mean they undergo preferential partitioning to particles and surfaces. Consequently, substantial losses from sorption to chamber walls, and the polypropylene tubing connecting the chamber exit air line to the collection PUF, were observed. Investigations were thus conducted to minimise this cause of analyte loss. Shortening the length of the tubing used for the exit air train substantially increased the analyte fraction detected on the collection PUFs with maximum increases from 1.2 to 28% for γ -HBCD and 8.4 to 51% for BDE-100. Different methods were explored to reduce losses or recover analytes sorbed to inner chamber stainless steel surfaces such as: heating the chamber post experiment, using a glass rather than a stainless steel chamber, and coating internal chamber surfaces with polytetrafluoroethylene (PTFE). Despite these efforts, complete analyte recovery was not achieved and a substantial loss (up to 60% for BDE-47) of the more volatile congeners was observed in all optimisation experiments. Emissions through volatilisation were compared to that predicted from physicochemical data for individual PBDE congeners and HBCD diastereomers. A significant positive linear relationship ($p = 0.003$) was seen between volatilised mass and vapour pressure, along with a significant negative linear relationship ($p = 0.013$) between volatilised mass and K_{OA} . Even though there is uncertainty in the reported physicochemical data for BFRs, their volatilisation in the chamber experiments was adequately described by such properties.

Due to the lower vapour pressures of BFRs, longer experimental times are expected for the attainment of steady state conditions in a test chamber compared to those required for VOCs; as both the slower release rate from the source and substantial partitioning to surfaces of BFRs impedes the attainment of steady state. This was investigated for HBCDs and PBDEs, via a chamber experiment studying their volatilisation at 60°C. After 4 days, the emission of HBCDs and PBDEs (assessed by

the BFR mass determined on the collection PUF every 24 hours) reduced to levels near method LOQs. These preliminary experiments suggest that more than 4 days is required (and even longer still for experiments at room temperature), before steady state conditions are attained. However, longer experimental durations are practically challenging. Despite these limitations, the developed experimental designs were shown to be fit-for-purpose.

8.2 Migration of BFRs to dust via three migration pathways from treated consumer products

8.2.1 Partitioning to dust post volatilisation

The transfer of BFRs from a treated product through volatilisation with subsequent partitioning to dust, was successfully generated in the test chamber for a textile treated with the HBCD technical formulation (4% Σ HBCD content). Concentrations in dust substantially increased after experiments at both elevated temperatures (60 °C) and at room temperature (22 °C). The average concentration of Σ HBCDs in the dust pre-experiment was 110 ng g⁻¹ while those post- experiment were respectively 610 ng g⁻¹ and 500 ng g⁻¹ for experiments conducted at 24 hours at 60 °C and 1 week at room temperature. A comparison study was conducted using a commercially-available emission chamber (designed primarily for emission measurements of VOCs) to investigate the migration of HBCDs via volatilisation from a treated textile followed by deposition to dust. Again there was a clear increase in the dust concentrations post experiment (to 760 ng Σ HBCD g⁻¹). However, a greater variation in replicate experiments was observed with the commercial chamber. This was suspected to arise because the configuration of the commercial chamber induced abrasion of small fibres from the source which were subsequently transferred to dust. The results of this comparison provided insights into the importance of experimental design for chamber experiments and further emphasised that the in-house chamber was fit-for-purpose for the investigation of migration of HBCDs to dust, via volatilisation and subsequent deposition.

These volatilisation experiments were repeated with the in-house chamber using as the source, a plastic TV casing sample, previously determined to contain PBDEs,

specifically 9% BDE-209. Experiments were conducted at 60 °C and room temperature (22 °C), however an increase in dust concentrations of any PBDE congener was not seen for either scenario. These data highlight that migration of BFRs to dust via partitioning post volatilisation is related to the vapour pressure of the chemical, and as BDE-209 has an extremely low vapour pressure, significant migration of this congener via this pathway was not observed. However, migration of other PBDE congeners (with higher vapour pressures) that were present in the TV casing was also not observed; possibly indicating strong incorporation within the plastic matrix and hence limited volatilisation. In summary, the extent to which BFRs transfer from source to dust via volatilisation followed by deposition to dust, will vary substantially depending on the physicochemical properties of the BFR, as well as the nature of the source matrix.

8.2.2 Abrasion of particles or fibres to dust

The in-house test chamber was further modified to successfully generate abrasion of particles/fibres from both a HBCD treated textile and a PBDE treated plastic source material. After experimental duration of only 2 hours, substantial elevation in concentrations of HBCDs and PBDEs were detected in dust samples. Abrasion of the HBCD treated textile generated visible fibres in the dust, with concentrations of Σ HBCDs in the dust post experiment, ranging from 4,100 to 54,000 ng g⁻¹ for four experimental durations of between 2 and 48 hours. A significant correlation ($p < 0.05$) was observed between the duration of abrasion and the post-experiment BFR concentration in the dust. Under a realistic curtain use scenario, it was estimated that ~18 mg of curtain fibres would abrade annually from everyday use of this curtain, transferring 3,000 ng Σ HBCDs per year to dust.

Abrasion of the PBDE-treated TV casing led to visible polymer particles in the chamber dust post experiment. This resulted in highly elevated PBDE concentrations - between 1,300 and 91,000 ng g⁻¹ BDE-209 - in dust for four different abrasion durations. Abrasion of the TV casing was more variable than abrasion of the curtain and no correlation between abrasion duration and post-experiment concentration of PBDE was observed. Under a realistic TV use scenario, an estimated 60 mg of plastic casing was abraded annually, transferring 5,400 μ g BDE-209 per year to dust from

this specific source. BDEs-153, 154 and 183 were also detected in the dust post abrasion experiments. The relative abundance of these and of BDE-209 in the TV casing, as well as the dust pre- and post-experiment was compared. There was a clear match between the congener pattern in the TV casing and the dust post-experiment, that differed from that in the dust, pre-experiment. This provided further evidence that abraded particles of the TV casing were the source of the elevated PBDE concentrations in the dust post-experiment. The abrasion migration pathway was shown to contribute greater BFR concentrations to dust than the partitioning post volatilisation pathway. It was also demonstrated to be independent of the physicochemical properties of the BFR, depending rather on the physical properties of the source matrix.

8.2.3 Uptake to dust via direct contact between source and dust

Transfer of BFRs to dust from direct contact between source and dust was successfully replicated in the in-house chamber; from both an HBCD treated textile curtain and a PBDE treated plastic TV casing. In these experiments, the dust was exposed for either 24 hours or 1 week. For both treated product types, elevated concentrations of BFRs were transferred to the dust over both exposure durations. The results indicate that the majority of uptake (for both matrices) occurred in the first 24 hours of contact, after which further uptake to the dust was minimal. Experiments with the HBCD treated textile saw similar concentrations transferred during exposure for 24 hours and 1 week with average Σ HBCD concentrations in dust of 6,600 and 7,300 ng g⁻¹ observed for 24 hours and 1 week respectively. However, there was substantial variation in concentrations recorded in replicate experiments. Such variation in transfer via this pathway is likely a result of the measured heterogeneous distribution of organic carbon in the dust sample and the hypothesised heterogeneity of HBCDs in the treated textile.

Experiments using the TV casing as a source of PBDEs, recorded average concentrations in dust after 24 hours and 1 week of exposure of respectively 590 and 8,700 ng g⁻¹ for BDE-209, 140 and 500 ng g⁻¹ for BDE-183 and 20 and 60 ng g⁻¹ for BDE-153. Lower concentrations of all congeners were detected after 24 hours than 1 week, suggesting that a saturation point is reached after 24 hours for PBDEs from this

plastic material. A comparison of the congener profile in the dust, post experiment, saw a pattern similar to that in the original TV casing but different to that in the dust pre-experiment. This congener pattern match suggests that PBDE migration in this experiment occurred through direct uptake by the dust, rather than volatilisation into a boundary layer at the source:air interface, as volatilisation would favour those congeners with higher vapour pressures. In summary, these results suggest migration via direct contact between source and dust is an important pathway, especially for low volatility compounds like BDE-209. As with abrasion, migration via this pathway appeared independent of the physicochemical properties of the BFR, and more influenced by properties of the dust such as its organic carbon content.

8.3 Forensic Microscopy investigation of BFR containing dust samples

Forensic microscopy using a variety of instrumental techniques was used to provide additional insights into how BFRs are incorporated into dust. Energy dispersive micro X-ray fluorescence spectroscopy (Micro XRFS), scanning electron microscopy with energy dispersive spectroscopy (SEM/EDS), 3D laser microscopy and Fourier transform infrared spectroscopy (FTIR) were utilised along with LC-MS/MS for confirmatory analysis. Using these techniques in sequence, their applicability was successfully demonstrated. Chamber-generated dusts containing abraded HBCD treated textile fibres were analysed and fibres of high bromine content positively identified. Archived indoor dust samples, sampled from 'real' indoor microenvironments, were examined and shown to contain fragmented particles that presented a strong FTIR match to an acrylic polymer, and contained an extremely high content of BDE-209. Thus it was deemed highly likely that these archived dusts were contaminated via abrasion of a plastic consumer product that had been treated with BDE-209, thereby providing further evidence to support the hypothesis that the abrasion migration pathway is a highly plausible explanation for the highly elevated concentrations of BFRs observed in some dust samples.

8.4 *In vitro* bioaccessibility study

A colon extended physiologically based extraction test (CE-PBET) was utilised to investigate the bioaccessibility of HBCDs incorporated into dust via two migration pathways. The hypothesis that the bioaccessibility of BFRs is lower for BFRs incorporated into particles or fibres abraded from a treated product into dust, than for BFRs partitioned to dust particles post volatilisation was investigated. The average bioaccessibilities of each diastereomer were lower for the abrasion dusts and a significant difference between dust types was seen for γ -HBCD ($p = 0.032$), however a statistically significant difference ($p > 0.05$) was not seen for α - or β -HBCD. The variability of the calculated bioaccessibilities led to the additional hypothesis that the highly variable bioaccessibilities stem from an inhomogeneous distribution of HBCD concentration throughout the samples. A regression analysis was conducted and a significant positive correlation between bioaccessibility and concentration was seen for γ -HBCD for dust concentrations $< 1000 \text{ ng g}^{-1}$ in both the volatilisation and abrasion dusts ($p = 0.017$ and 0.045 respectively). This result suggested that bioaccessibility increased linearly with concentration up to a concentration of $\sim 1000 \text{ ng g}^{-1}$ where the bioaccessibility plateaus, consistent with the system reaching a solubility limitation. A significant correlation was not seen for α - or β -HBCD for either dust type. However, this was a small study size and further analyses are required to investigate this further.

8.5 Research gaps and future areas of research

The work presented in this thesis makes a valuable contribution to our understanding of the mechanisms via which BFRs transfer from sources to dust. However, there remain gaps in knowledge that need to be addressed. These include:

- 1) Further investigation into minimising sink effects and the conditions required for the attainment of steady state conditions inside test chambers.
- 2) Evaluation of the behaviour in chamber experiments of different flame retardants, particularly those with different physicochemical properties such as vapour pressure. This will provide an assessment of the relative contribution

of each migration pathway to indoor dust contamination for these chemicals. Flame retardants that are incorporated via the reactive (as opposed to additive) reaction process need also to be assessed.

- 3) Investigating how different source materials influence the atmospheric release of flame retardants. For example, determining if rigid polymers such as those used in electronics housing retain flame retardants more strongly than textiles.
- 4) Investigating more appropriate subsampling methods to reduce the influence of possible BFR heterogeneity throughout a sample. These should include: testing larger samples, a greater number of samples, more thorough homogenisation of test samples, and representative subsampling e.g. sampling each corner as well as the middle of the test piece.
- 5) Relating data from a chamber experiment back to an indoor microenvironment scenario, via an appropriate modelling study. Also, investigating factors that influence an indoor environment which are not included in a chamber scenario but likely affect transfer to dust, such as:
 - a. Human and pet activities contributing to dust and particle resuspension
 - b. Diurnal variation in air temperature and air change rate
 - c. Seasonal variations
 - d. Cleaning behaviours that effect periodic dust removal
- 5) Determining if the forensic microscopy techniques in this investigation can be used for the analysis of flame retardants that are not brominated, e.g. chlorinated or phosphorus containing compounds, such as TCPP and TDCPP.
- 6) More detailed bioaccessibility studies are required to both confirm the observed relationship between concentration in dust and bioaccessibility for γ -HBCD, and if proven, to establish whether similar relationships exist for other BFRs.

REFERENCES

- Abdallah, M.A.-E. and Harrad, S. (2014) Polybrominated diphenyl ethers in UK human milk: Implications for infant exposure and relationship to external exposure, *Environment International*, **63**, 130-136.
- Abdallah, M.A.-E., Harrad, S. and Covaci, A. (2008a) Hexabromocyclododecanes and Tetrabromobisphenol-A in Indoor Air and Dust in Birmingham, UK: Implications for Human Exposure, *Environmental Science & Technology*, **42**, 18, 6855-6861.
- Abdallah, M.A.-E., Harrad, S. and Covaci, A. (2009) Isotope Dilution Method for Determination of Polybrominated Diphenyl Ethers Using Liquid Chromatography Coupled to Negative Ionization Atmospheric Pressure Photoionization Tandem Mass Spectrometry: Validation and Application to House Dust, *Analytical Chemistry*, **81**, 17, 7460-7467.
- Abdallah, M.A.-E., Ibarra, C., Neels, H., Harrad, S. and Covaci, A. (2008b) Comparative evaluation of liquid chromatography-mass spectrometry versus gas chromatography-mass spectrometry for the determination of hexabromocyclododecanes and their degradation products in indoor dust, *Journal of Chromatography A*, **1190**, 1-2, 333-341.
- Abdallah, M.A.E., Tilston, E., Harrad, S. and Collins, C. (2012) *In vitro* assessment of the bioaccessibility of brominated flame retardants in indoor dust using a colon extended model of the human gastrointestinal tract, *Journal of Environmental Monitoring*, **14**, 3276-3283.
- ACT. Association for Contract Textiles. (2011) Abrasion Resistance: Considerations for Textile Specifiers (online). Available from: http://www.contracttextiles.org/uploads/images/banners/pdf/white_paper_synopsis_060211.pdf (Accessed 14 March 2014).
- Ali, N., Harrad, S., Muenhor, D., Neels, H. and Covaci, A. (2011) Analytical characteristics and determination of major novel brominated flame retardants (NBFRs) in indoor dust, *Analytical and Bioanalytical Chemistry*, **400**, 9, 3073-3083.
- Allen, J.G., McClean, M.D., Stapleton, H.M., Nelson, J.W. and Webster, T.F. (2007) Personal Exposure to Polybrominated Diphenyl Ethers (PBDEs) in Residential Indoor Air, *Environmental Science & Technology*, **41**, 13, 4574-4579.
- Allen, J.G., McClean, M.D., Stapleton, H.M. and Webster, T.F. (2008a) Critical factors in assessing exposure to PBDEs via house dust, *Environment International*, **34**, 8, 1085-1091.
- Allen, J.G., McClean, M.D., Stapleton, H.M. and Webster, T.F. (2008b) Linking PBDEs in House Dust to Consumer Products using X-ray Fluorescence, *Environmental Science & Technology*, **42**, 11, 4222-4228.
- Allen, J.G., Stapleton, H.M., Vallarino, J., McNeely, E., McClean, M.D., Harrad, S.J., Rauert, C.B. and Spengler, J.D. (2013) Exposure to flame retardant chemicals on commercial airplanes, *Environmental Health*, **12**, 17.
- Ambidge, P.F., Cox, E.A., Creaser, C.S., Greenberg, M., Gem, M.G.d.M., Gilbert, J., Jones, P.W., Kibblewhite, M.G., Levey, J., Lisseter, S.G., Meredith, T.J., Smith, L., Smith, P., Startin, J.R., Stenhouse, I. and Whitworth, M. (1990) Acceptance criteria for analytical data on polychlorinated dibenzo-p-dioxins and polychlorinated dibenzofurans, *Chemosphere*, **21**, 8, 999-1006.

- Andersson, Ö. and Blomkvist, G. (1981) Polybrominated aromatic pollutants found in fish in Sweden, *Chemosphere*, **10**, 9, 1051-1060.
- ASTM. (2001) American Society for Testing and Materials: ASTM D4158-01. Standard Guide for Abrasion Resistance of Textile Fabrics (Uniform Abrasion).
- ATSDR. Agency for Toxic Substances and Disease Registry. (2004a) Public Health Statement - Polybrominated Diphenyl Ethers (online). Available from: <http://www.atsdr.cdc.gov/ToxProfiles/tp68-pbde-c1-b.pdf> (Accessed 14 January 2014).
- ATSDR. Agency for Toxic Substances and Disease Registry. (2004b) Toxicological Profile for Polybrominated Biphenyls and Polybrominated Diphenyl Ethers (PBBs and PBDEs), September 2004 (online). Available from: <http://www.atsdr.cdc.gov/ToxProfiles/tp68.pdf> (Accessed 14 January 2014).
- Bahn, A.K., Mills, J.L., Snyder, P.J., Gann, P.H., Houten, L., Bialik, O., Hollmann, L. and Utiger, R.D. (1980) Hypothyroidism in Workers Exposed to Polybrominated Biphenyls, *New England Journal of Medicine*, **302**, 1, 31-33.
- Bakó-Biró, Z., Wargocki, P., Weschler, C.J. and Fanger, P.O. (2004) Effects of pollution from personal computers on perceived air quality, SBS symptoms and productivity in offices, *Indoor Air*, **14**, 3, 178-187.
- Batterman, S.A., Chernyak, S., Jia, C., Godwin, C. and Charles, S. (2009) Concentrations and Emissions of Polybrominated Diphenyl Ethers from U.S. Houses and Garages, *Environmental Science & Technology*, **43**, 8, 2693-2700.
- Björklund, J., Tollbäck, P. and Östman, C. (2003) Mass spectrometric characteristics of decabromodiphenyl ether and the application of isotopic dilution in the electron capture negative ionization mode for the analysis of polybrominated diphenyl ethers, *Journal of Mass Spectrometry*, **38**, 4, 394-400.
- Bläuenstein, M. (2007) Modeling the Environmental Fate of Polybrominated Diphenyl Ethers in Lake Thun, *Diploma Thesis at Institute for Chemical and Bioengineering, ETH, Zurich, Switzerland*
- Boon, J.P., Lewis, W.E., Tjoen-A-Choy, M.R., Allchin, C.R., Law, R.J., de Boer, J., ten Hallers-Tjabbes, C.C. and Zegers, B.N. (2002) Levels of Polybrominated Diphenyl Ether (PBDE) Flame Retardants in Animals Representing Different Trophic Levels of the North Sea Food Web, *Environmental Science & Technology*, **36**, 19, 4025-4032.
- Bordajandi, L.R., Abad, E. and González, M.J. (2008) Occurrence of PCBs, PCDD/Fs, PBDEs and DDTs in Spanish breast milk: Enantiomeric fraction of chiral PCBs, *Chemosphere*, **70**, 4, 567-575.
- Braekevelt, E., Tittlemier, S.A. and Tomy, G.T. (2003) Direct measurement of octanol-water partition coefficients of some environmentally relevant brominated diphenyl ether congeners, *Chemosphere*, **51**, 7, 563-567.
- BSEF. Bromine Science and Environmental Forum. (2012) Fast Facts on Fire Safety and Flame Retardants (online). Available from: <http://www.bsef.com/index.php?mact=MediaRoom,cntnt01,details,0&cntnt01documentid=621&cntnt01dateformat=%A %d %B %Y&cntnt01returnid=153> (Accessed 14 January 2014).
- Budakowski, W. and Tomy, G. (2003) Congener-specific analysis of hexabromocyclododecane by high-performance liquid chromatography/electrospray tandem mass spectrometry, *Rapid Communications in Mass Spectrometry*, **17**, 13, 1399-1404.

- Butt, C.M., Diamond, M.L., Truong, J., Ikonomou, M.G. and ter Schure, A.F.H. (2004) Spatial Distribution of Polybrominated Diphenyl Ethers in Southern Ontario As Measured in Indoor and Outdoor Window Organic Films, *Environmental Science & Technology*, **38**, 3, 724-731.
- Cao, Z.-G., Yu, G., Chen, Y.-S., Cao, Q.-M., Fiedler, H., Deng, S.-B., Huang, J. and Wang, B. (2012) Particle size: A missing factor in risk assessment of human exposure to toxic chemicals in settled indoor dust, *Environment International*, **49**, 24-30.
- Carlsson, H., Nilsson, U. and Östman, C. (2000) Video Display Units: An Emission Source of the Contact Allergenic Flame Retardant Triphenyl Phosphate in the Indoor Environment, *Environmental Science & Technology*, **34**, 18, 3885-3889.
- Cave, M., Wragg, J., Harrison, I., Vane, C.H., Van de Wiele, T., de Groeve, E., Nathanail, C.P., Ashmore, M., Thomas, R., Robinson, J. and Daly, P. (2010) Comparison of batch mode and dynamic physiologically based bioaccessibility tests for PAHs in soil samples, *Environmental Science & Technology*, **44**, 2654-2660.
- Cetin, B. and Odabasi, M. (2005) Measurement of Henry's law constants of seven polybrominated diphenyl ether (PBDE) congeners as a function of temperature, *Atmospheric Environment*, **39**, 29, 5273-5280.
- Cetin, B. and Odabasi, M. (2007) Particle-Phase Dry Deposition and Air-Soil Gas-Exchange of Polybrominated Diphenyl Ethers (PBDEs) in Izmir, Turkey, *Environmental Science & Technology*, **41**, 14, 4986-4992.
- Chao, H.-R., Wang, S.-L., Lee, W.-J., Wang, Y.-F. and Pöpke, O. (2007) Levels of polybrominated diphenyl ethers (PBDEs) in breast milk from central Taiwan and their relation to infant birth outcome and maternal menstruation effects, *Environment International*, **33**, 2, 239-245.
- ChemSpider. (2014) CSID:9938313. Available from: <http://www.chemspider.com/Chemical-Structure.9938313.html> (Accessed May 15, 2014).
- Chen, L., Mai, B., Xu, Z., Peng, X., Han, J., Ran, Y., Sheng, G. and Fu, J. (2008) In- and outdoor sources of polybrominated diphenyl ethers and their human inhalation exposure in Guangzhou, China, *Atmospheric Environment*, **42**, 1, 78-86.
- Chevrier, J., Harley, K.G., Bradman, A., Gharbi, M., Sjodin, A., and Eskenazi, B. (2010) Polybrominated diphenyl ether (PBDE) flame retardants and thyroid hormone during pregnancy, *Environmental Health Perspectives*, **118**, 1444-1449.
- Clausen, P.A., Hansen, V., Gunnarsen, L., Afshari, A. and Wolkoff, P. (2004) Emission of Di-2-ethylhexyl Phthalate from PVC Flooring into Air and Uptake in Dust: Emission and Sorption Experiments in FLEC and CLIMPAQ, *Environmental Science & Technology*, **38**, 9, 2531-2537.
- Clausen, P.A. and Kofoed-Sørensen, V. (2009) Sampling and Analysis of SVOCs and POMs in Indoor Air, Chapter 2, In: Salthammer, T. and Uhde, E. (eds) *Organic Indoor Air Pollutants: Occurrence, Measurement, Evaluation*, Weinheim, WILEY, 19-45.
- Clausen, P.A., Liu, Z., Kofoed-Sørensen, V., Little, J. and Wolkoff, P. (2012) Influence of Temperature on the Emission of Di-(2-ethylhexyl)phthalate (DEHP) from PVC Flooring in the Emission Cell FLEC, *Environmental Science & Technology*, **46**, 2, 909-915.

- Clausen, P.A., Liu, Z., Xu, Y., Kofoed-Sørensen, V. and Little, J.C. (2010) Influence of air flow rate on emission of DEHP from vinyl flooring in the emission cell FLEC: Measurements and CFD simulation, *Atmospheric Environment*, **44**, 23, 2760-2766.
- Covaci, A., Harrad, S., Abdallah, M.A.E., Ali, N., Law, R.J., Herzke, D. and de Wit, C.A. (2011) Novel brominated flame retardants: A review of their analysis, environmental fate and behaviour, *Environment International*, **37**, 2, 532-556.
- Covaci, A., Voorspoels, S., Ramos, L., Neels, H. and Blust, R. (2007) Recent developments in the analysis of brominated flame retardants and brominated natural compounds, *Journal of Chromatography A*, **1153**, 1-2, 145-171.
- D'Hollander, W., Roosens, L., Covaci, A., Cornelis, C., Reynders, H., Campenhout, K.V., Voogt, P.d. and Bervoets, L. (2010) Brominated flame retardants and perfluorinated compounds in indoor dust from homes and offices in Flanders, Belgium, *Chemosphere*, **81**, 4, 478-487.
- de Wit, C.A. (2002) An overview of brominated flame retardants in the environment, *Chemosphere*, **46**, 5, 583-624.
- de Wit, C.A., Björklund, J.A. and Thuresson, K. (2012) Tri-decabrominated diphenyl ethers and hexabromocyclododecane in indoor air and dust from Stockholm microenvironments 2: Indoor sources and human exposure, *Environment International*, **39**, 1, 141-147.
- Debrauwer, L., Riu, A., Jouahri, M., Rathahao, E., Jouanin, I., Antignac, J.-P., Cariou, R., Le Bizec, B. and Zalko, D. (2005) Probing new approaches using atmospheric pressure photo ionization for the analysis of brominated flame retardants and their related degradation products by liquid chromatography-mass spectrometry, *Journal of Chromatography A*, **1082**, 1, 98-109.
- Destailats, H., Maddalena, R.L., Singer, B.C., Hodgson, A.T. and McKone, T.E. (2008) Indoor pollutants emitted by office equipment: A review of reported data and information needs, *Atmospheric Environment*, **42**, 7, 1371-1388.
- Dinn, P.M., Johannessen, S.C., Ross, P.S., Macdonald, R.W., Whiticar, M.J., Lowe, C.J. and van Roodselaar, A. (2012) PBDE and PCB accumulation in benthos near marine wastewater outfalls: The role of sediment organic carbon, *Environmental Pollution*, **171**, 241-248.
- Duggan, M.J. and Inskip, M.J. (1985) Childhood exposure to lead in surface dust and soil: A community health problem., *Public Health Review*, **13**, 1-54.
- Environment Canada. (2006) Canadian Environmental Protection Act, 1999. Ecological Screening Assessment Report on Polybrominated Diphenyl Ethers (PBDEs). Available from: https://www.ec.gc.ca/lcpe-cepa/documents/substances/pbde/sar_pbde-eng.pdf (Accessed July 2014).
- Environment Canada. (2011) Screening Assessment Report on Hexabromocyclododecane, Chemical Abstracts Service Registry Number 3194-55-6. November 2011 (online). Available from: <http://www.ec.gc.ca/ese-ees/7882C148-8AE4-4BA4-8555-668C49F91500/HBCD - FSAR - EN.pdf> (Accessed February 2014).
- ECHA European Chemicals Association. (2008) Risk Assessment: Hexabromocyclododecane (online). Available from: http://echa.europa.eu/documents/10162/6434698/orats_final_rar_hexabromocyclododecane_en.pdf (Accessed May 2014).
- ECHA European Chemicals Association. (2012) Member State Committee: Support document for identification of bis(pentabromophenyl) ether as a substance of very high concern because of its PBT/vPvB properties (online). Available

- from: <http://echa.europa.eu/documents/10162/1f83d2de-8eaf-405a-90a1-a9e2d0651459> (Accessed May 2014).
- EFRA. European Flame Retardants Association. (2007) Flame Retardants. Frequently Asked Questions (online). Available from: http://www.flameretardants-online.com/images/userdata/pdf/168_DE.pdf (Accessed 14 January 2014).
- EFRA. European Flame Retardants Association. (2014) The Reality / Statistics (online). Available from: http://www.cefic-efra.com/index.php?option=com_content&view=article&id=331&Itemid=252&lang=en (Accessed 14 January 2014).
- Eguchi, A., Isobe, T., Ramu, K., Tue, N.M., Sudaryanto, A., Devanathan, G., Viet, P.H., Tana, R.S., Takahashi, S., Subramanian, A. and Tanabe, S. (2013) Soil contamination by brominated flame retardants in open waste dumping sites in Asian developing countries, *Chemosphere*, **90**, 9, 2365-2371.
- Eskenazi, B., Chevrier, J., Rauch, S.A., Kogut, K., Harley, K.G., Johnson, C., Trujillo, C., Sjodin, A., and Bradman, A. (2013) In utero and childhood polybrominated diphenyl ether (PBDE) exposures and neurodevelopment in the CHAMACOS study, *Environmental Health Perspectives*, **121**, 257-262.
- European Commission Directive 2002/657/EC of 12 August 2002, The performance of analytical methods and the interpretation of results, *Official Journal of the European Communities*, L 221, 17.8.2002
- Frederiksen, M., Vorkamp, K., Thomsen, M. and Knudsen, L.E. (2009) Human internal and external exposure to PBDEs – A review of levels and sources, *International Journal of Hygiene and Environmental Health*, **212**, 2, 109-134.
- FSA. UK Food Standards Agency. (2006) Brominated Chemicals: UK Dietary Intakes (online). Available from: multimedia.food.gov.uk/multimedia/pdfs/fsis1006.pdf (Accessed April 2014)
- Fu, J. and Suuberg, M. (2011) Vapor Pressure of Solid Polybrominated Diphenyl Ethers Determined via Knudson Effusion Method, *Environmental Toxicology and Chemistry*, **30**, 10, 2216-2219.
- Fulong, C.R.P. and Espino, M.P.B. (2013) Decabromodiphenyl ether in indoor dust from different microenvironments in a university in the Philippines, *Chemosphere*, **90**, 1, 42-48.
- Gao, S., Wang, J., Yu, Z., Guo, Q., Sheng, G. and Fu, J. (2011) Hexabromocyclododecanes in Surface Soils from E-Waste Recycling Areas and Industrial Areas in South China: Concentrations, Diastereoisomer- and Enantiomer-Specific Profiles, and Inventory, *Environmental Science & Technology*, **45**, 6, 2093-2099.
- Gascon, M., Vrijheid, M., Martinez, D., Forn, J., Grimalt, J.O., Torrent, M., and Sunyer, J. (2011) Effects of pre and postnatal exposure to low levels of polybromodiphenyl ethers on neurodevelopment and thyroid hormone levels at 4 years of age, *Environment International* **37**, 605-611.
- Gaylor, M.O., Harvey, E. and Hale, R.C. (2013) Polybrominated Diphenyl Ether (PBDE) Accumulation by Earthworms (*Eisenia fetida*) Exposed to Biosolids-, Polyurethane Foam Microparticle-, and Penta-BDE-Amended Soils, *Environmental Science & Technology*, **47**, 23, 13831-13839.
- Gevao, B., Al-Bahloul, M., Al-Ghadban, A.N., Ali, L., Al-Omar, A., Helaleh, M., Al-Matrouk, K. and Zafar, J. (2006) Polybrominated diphenyl ethers in indoor air in Kuwait: Implications for human exposure, *Atmospheric Environment*, **40**, 8, 1419-1426.

- Ghosal, S. and Wagner, J. (2013) Correlated Raman micro-spectroscopy and scanning electron microscopy analyses of flame retardants in environmental samples: a micro-analytical tool for probing chemical composition, origin and spatial distribution, *Analyst*, **138**, 13, 3836-3844.
- Goss, K.-U., Arp, H.P.H., Bronner, G. and Niederer, C. (2008) Partition Behavior of Hexachlorocyclohexane Isomers, *Journal of Chemical & Engineering Data*, **53**, 3, 750-754.
- Hack, A. and Selenka, F. (1996) Mobilization of PAH and PCB from contaminated soil using a digestive tract model, *Toxicology Letters*, **88**, 1-3, 199-210.
- Hardell, L., Lindstrom, G. and van Bavel, B. (1998) Concentrations of the flame retardant 2,2',4,4'-tetrabrominated diphenyl ether in human adipose tissue in Swedish persons and the risk for non-Hogkin's lymphoma., *Oncology Research*, **10**, 8, 429-432.
- Hardy, M.L. (2002) A comparison of the properties of the major commercial PBDPO/PBDE product to those of major PBB and PCB products, *Chemosphere*, **46**, 5, 717-728.
- Hardy, M.L. (2004) A comparison of the fish bioconcentration factors for brominated flame retardants with their nonbrominated analogues, *Environmental Toxicology and Chemistry*, **23**, 3, 656-661.
- Harner, T., Mackay, D. and Jones, K.C. (1995) Model of the Long-Term Exchange of PCBs between Soil and the Atmosphere in the Southern U.K., *Environmental Science & Technology*, **29**, 1200-1209.
- Harner, T. and Shoeib, M. (2002) Measurements of Octanol-Air Partition Coefficients (K_{OA}) for Polybrominated Diphenyl Ethers (PBDEs): Predicting Partitioning in the Environment, *Journal of Chemical & Engineering Data*, **47**, 2, 228-232.
- Harrad, S. and Abdallah, M.A.-E. (2008) Calibration of two passive air sampler configurations for monitoring concentrations of hexabromocyclododecanes in indoor air, *Journal of Environmental Monitoring*, **10**, 4, 527-531.
- Harrad, S. and Abdallah, M.A.-E. (2011) Brominated flame retardants in dust from UK cars - Within-vehicle spatial variability, evidence for degradation and exposure implications, *Chemosphere*, **82**, 9, 1240-1245.
- Harrad, S., Abdallah, M.A.-E. and Covaci, A. (2009a) Causes of variability in concentrations and diastereomer patterns of hexabromocyclododecanes in indoor dust, *Environment International*, **35**, 3, 573-579.
- Harrad, S., Abdallah, M.A.-E., Rose, N.L., Turner, S.D. and Davidson, T.A. (2009b) Current-Use Brominated Flame Retardants in Water, Sediment, and Fish from English Lakes, *Environmental Science & Technology*, **43**, 24, 9077-9083.
- Harrad, S., de Wit, C.A., Abdallah, M.A.-E., Bergh, C., Björklund, J.A., Covaci, A., Darnerud, P.O., de Boer, J., Diamond, M., Huber, S., Leonards, P., Mandalakis, M., Östman, C., Haug, L.S., Thomsen, C. and Webster, T.F. (2010a) Indoor Contamination with Hexabromocyclododecanes, Polybrominated Diphenyl Ethers, and Perfluoroalkyl Compounds: An Important Exposure Pathway for People?, *Environmental Science & Technology*, **44**, 9, 3221-3231.
- Harrad, S., Goosey, E., Desborough, J., Abdallah, M.A.-E., Roosens, L. and Covaci, A. (2010b) Dust from U.K. Primary School Classrooms and Daycare Centers: The Significance of Dust As a Pathway of Exposure of Young U.K. Children to Brominated Flame Retardants and Polychlorinated Biphenyls, *Environmental Science & Technology*, **44**, 11, 4198-4202.

- Harrad, S., Hazrati, S. and Ibarra, C. (2006) Concentrations of Polychlorinated Biphenyls in Indoor Air and Polybrominated Diphenyl Ethers in Indoor Air and Dust in Birmingham, United Kingdom: Implications for Human Exposure, *Environmental Science & Technology*, **40**, 15, 4633-4638.
- Harrad, S. and Hunter, S. (2006) Concentrations of Polybrominated Diphenyl Ethers in Air and Soil on a Rural-Urban Transect Across a Major UK Conurbation, *Environmental Science & Technology*, **40**, 15, 4548-4553.
- Harrad, S., Ibarra, C., Abdallah, M.A.-E., Boon, R., Neels, H. and Covaci, A. (2008a) Concentrations of brominated flame retardants in dust from United Kingdom cars, homes, and offices: Causes of variability and implications for human exposure, *Environment International*, **34**, 8, 1170-1175.
- Harrad, S., Ibarra, C., Diamond, M., Melymuk, L., Robson, M., Douwes, J., Roosens, L., Dirtu, A.C. and Covaci, A. (2008b) Polybrominated diphenyl ethers in domestic indoor dust from Canada, New Zealand, United Kingdom and United States, *Environment International*, **34**, 2, 232-238.
- Harrad, S., Wijesekera, R., Hunter, S., Halliwell, C. and Baker, R. (2004) Preliminary Assessment of U.K. Human Dietary and Inhalation Exposure to Polybrominated Diphenyl Ethers, *Environmental Science & Technology*, **38**, 8, 2345-2350.
- Haukås, M., Hylland, K., Nygård, T., Berge, J.A. and Mariussen, E. (2010) Diastereomer-specific bioaccumulation of hexabromocyclododecane (HBCD) in a coastal food web, Western Norway, *Science of The Total Environment*, **408**, 23, 5910-5916.
- Hazrati, S. and Harrad, S. (2006) Causes of Variability in Concentrations of Polychlorinated Biphenyls and Polybrominated Diphenyl Ethers in Indoor air, *Environmental Science & Technology*, **40**, 24, 7584-7589.
- He, M.-J., Luo, X.-J., Yu, L.-H., Wu, J.-P., Chen, S.-J. and Mai, B.-X. (2013) Diastereoisomer and enantiomer-specific profiles of hexabromocyclododecane and tetrabromobisphenol A in an aquatic environment in a highly industrialized area, South China: Vertical profile, phase partition, and bioaccumulation, *Environmental Pollution*, **179**, 105-110.
- Hearn, L.K., Hawker, D.W., Toms, L.-M.L. and Mueller, J.F. (2013) Assessing exposure to polybrominated diphenyl ethers (PBDEs) for workers in the vicinity of a large recycling facility, *Ecotoxicology and Environmental Safety*, **92**, 222-228.
- Heeb, N.V., Bernd Schweizer, W., Mattrel, P., Haag, R., Gerecke, A.C., Schmid, P., Zennegg, M. and Vonmont, H. (2008) Regio- and stereoselective isomerization of hexabromocyclododecanes (HBCDs): Kinetics and mechanism of γ - to α -HBCD isomerization, *Chemosphere*, **73**, 8, 1201-1210.
- Herbstman, J.B., Sjodin, A., Jones, R., Kurzon, M., Lederman, S.A., Rauh, V.A., Needham, L.L., Wang, R., and Perera, F.P. (2008) Prenatal exposure to PBDEs and neurodevelopment, *Epidemiology*, **19**, S348.
- Hoffman, K., Adgent, M., Goldman, B.D., Sjodin, A., and Daniels, J.L. (2012) Lactational exposure to polybrominated diphenyl ethers and its relation to social and emotional development among toddlers, *Environmental Health Perspectives*, **120**, 1438-1442.
- Ilyas, M., Sudaryanto, A., Setiawan, I.E., Riyadi, A.S., Isobe, T., Ogawa, S., Takahashi, S. and Tanabe, S. (2011) Characterization of polychlorinated

- biphenyls and brominated flame retardants in surface soils from Surabaya, Indonesia, *Chemosphere*, **83**, 6, 783-791.
- Ilyas, M., Sudaryanto, A., Setiawan, I.E., Riyadi, A.S., Isobe, T. and Tanabe, S. (2013) Characterization of polychlorinated biphenyls and brominated flame retardants in sludge, sediment and fish from municipal dumpsite at Surabaya, Indonesia, *Chemosphere*, **93**, 8, 1500-1510.
- Intertek. Intertek Group plc. (2014) Taber Abrasion ASTM D1044 (Haze), ASTM D4060 (Weight Loss) (online). Available from <http://www.intertek.com/polymers/testlopedia/taber-abrasion/> (Accessed 20 March 2014).
- ISO/TC92. Fire Safety Secretariat. Fire safety in ISO - Information about ISO/TC 92 (online). Available from: http://www.sp.se/sv/units/fire/Documents/BR/ISO_TC_92_Information_Sheet.pdf (Accessed 14 January 2014).
- Jones-Otazo, H.A., Clarke, J.P., Diamond, M.L., Archbold, J.A., Ferguson, G., Harner, T., Richardson, G.M., Ryan, J.J. and Wilford, B. (2005) Is House Dust the Missing Exposure Pathway for PBDEs? An Analysis of the Urban Fate and Human Exposure to PBDEs, *Environmental Science & Technology*, **39**, 14, 5121-5130.
- Julander, A., Karlsson, M., Hagström, K., Ohlson, C.G., Engwall, M., Bryngelsson, I.L., Westberg, H. and van Bavel, B. (2005) Polybrominated diphenyl ethers—plasma levels and thyroid status of workers at an electronic recycling facility, *Int Arch Occup Environ Health*, **78**, 7, 584-592.
- Kajiwara, N., Desborough, J., Harrad, S. and Takigami, H. (2013) Photolysis of brominated flame retardants in textiles exposed to natural sunlight, *Environmental Science: Processes & Impacts*, **15**, 3, 653-660.
- Kajiwara, N. and Takigami, H. (2013) Emission behavior of hexabromocyclododecanes and polybrominated diphenyl ethers from flame-retardant-treated textiles, *Environmental Science: Processes & Impacts*, **15**, 10, 1957-1963.
- Kakimoto, K., Nagayoshi, H., Takagi, S., Akutsu, K., Konishi, Y., Kajimura, K., Hayakawa, K. and Toriba, A. (2014) Inhalation and dietary exposure to Dechlorane Plus and polybrominated diphenyl ethers in Osaka, Japan, *Ecotoxicology and Environmental Safety*, **99**, 69-73.
- Kang, Y., Wang, H.S., Cheung, K.C. and Wong, M.H. (2011) Polybrominated diphenyl ethers (PBDEs) in indoor dust and human hair, *Atmospheric Environment*, **45**, 14, 2386-2393.
- Karlsson, M., Julander, A., van Bavel, B. and Hardell, L. (2007) Levels of brominated flame retardants in blood in relation to levels in household air and dust, *Environment International*, **33**, 1, 62-69.
- Katsumata, H., Murakami, S., Kato, S., Hoshino, K. and Ataka, Y. (2008) Measurement of semi-volatile organic compounds emitted from various types of indoor materials by thermal desorption test chamber method, *Building and Environment*, **43**, 3, 378-383.
- Kefeni, K.K. and Okonkwo, J.O. (2012) Analysis of major congeners of polybromobiphenyls and polybromodiphenyl ethers in office dust using high resolution gas chromatography, mass spectrometry, *Chemosphere*, **87**, 9, 1070-1075.
- Keller, J.M., Stapleton, H.M., Heltsley, R., Peck, A., Kucklick, J.R., Schantz, M.M. and Wise, S.A. (2007) Standard reference materials available from the

- National Institute of Standards and Technology for the analysis of brominated flame retardants. *Poster presented at BFR 2007* The Netherlands: Amsterdam.
- Kelly, B.C., Ikonomou, M.G., Blair, J.D., Morin, A.E. and Gobas, F.A.P.C. (2007) Food Web Specific Biomagnification of Persistent Organic Pollutants, *Science*, **317**, 5835, 236-239.
- Kemmlin, S., Hahn, O. and Jann, O. (2003) Emissions of organophosphate and brominated flame retardants from selected consumer products and building materials, *Atmospheric Environment*, **37**, 39-40, 5485-5493.
- Koppen, R., Becker, R., Jung, C. and Nehls, I. (2008) On the thermally induced isomerisation of hexabromocyclododecane stereoisomers, *Chemosphere*, **71**, 4, 656-662.
- Kupper, T., de Alencastro, L.F., Gatsigazi, R., Furrer, R., Grandjean, D. and Tarradellas, J. (2008) Concentrations and specific loads of brominated flame retardants in sewage sludge, *Chemosphere*, **71**, 6, 1173-1180.
- Kuramochi, H., Maeda, K. and Kawamoto, K. (2004) Physicochemical properties of selected polybrominated diphenylethers and comparison with some brominated aromatics and PCDDs, *Organohalogen Compounds*, **66**, 2420-2425.
- Kuramochi, H. and Sakai, S. (2013) Measurement of vapor pressures of some PBDEs and HBCD diastereoisomers. *Poster presented at BFR 2013* USA: San Francisco.
- La Guardia, M.J., Hale, R.C. and Harvey, E. (2006) Detailed Polybrominated Diphenyl Ether (PBDE) Congener Composition of the Widely Used Penta-, Octa-, and Deca-PBDE Technical Flame-retardant Mixtures, *Environmental Science & Technology*, **40**, 20, 6247-6254.
- Lagalante, A. and Oswald, T. (2008) Analysis of polybrominated diphenyl ethers (PBDEs) by liquid chromatography with negative-ion atmospheric pressure photoionization tandem mass spectrometry (LC/NI-APPI/MS/MS): application to house dust, *Analytical and Bioanalytical Chemistry*, **391**, 6, 2249-2256.
- Lagalante, A.F., Oswald, T.D. and Calvosa, F.C. (2009) Polybrominated diphenyl ether (PBDE) levels in dust from previously owned automobiles at United States dealerships, *Environment International*, **35**, 3, 539-544.
- Law, K., Halldorson, T., Danell, R., Stern, G., Gewurtz, S., Alae, M., Marvin, C., Whittle, M. and Tomy, G. (2006) Bioaccumulation and trophic transfer of some brominated flame retardants in a Lake Winnipeg (Canada) food web, *Environmental Toxicology and Chemistry*, **25**, 8, 2177-2186.
- Law, R.J., Kohler, M., Heeb, N.V., Gerecke, A.C., Schmid, P., Voorspoels, S., Covaci, A., Becher, G., JanAk, K. and Thomsen, C. (2005) Hexabromocyclododecane Challenges Scientists and Regulators, *Environmental Science & Technology*, **39**, 13, 281A-287A.
- Lepom, P., Berndt, M., Duffek, A. and Warmbrunn-Suckrom, E. (2010) Oral Bioaccessibility of PBDEs in Dust Using an In Vitro Gastrointestinal Model, *5th International Symposium on Brominated Flame Retardants, BFR 2010, Kyoto, Japan*.
- Liu, C., Liu, Z., Little, J.C. and Zhang, Y. (2013) Convenient, Rapid and Accurate Measurement of SVOC Emission Characteristics in Experimental Chambers, *PLoS ONE*, **8**, 8, e72445.
- Lorber, M. (2008) Exposure of Americans to polybrominated diphenyl ethers, *Journal of Exposure Science and Environmental Epidemiology*, **18**, 1, 2-19.

- Luo, Q., Wong, M., Wang, Z. and Cai, Z. (2013) Polybrominated diphenyl ethers in combusted residues and soils from an open burning site of electronic wastes, *Environ Earth Sci*, **69**, 8, 2633-2641.
- Luo, Y., Luo, X.-J., Lin, Z., Chen, S.-J., Liu, J., Mai, B.-X. and Yang, Z.-Y. (2009) Polybrominated diphenyl ethers in road and farmland soils from an e-waste recycling region in Southern China: Concentrations, source profiles, and potential dispersion and deposition, *Science of The Total Environment*, **407**, 3, 1105-1113.
- Mandalakis, M., Atsarou, V. and Stephanou, E.G. (2008) Airborne PBDEs in specialized occupational settings, houses and outdoor urban areas in Greece, *Environmental Pollution*, **155**, 2, 375-382.
- Mandalakis, M., Besis, A. and Stephanou, E.G. (2009) Particle-size distribution and gas/particle partitioning of atmospheric polybrominated diphenyl ethers in urban areas of Greece, *Environmental Pollution*, **157**, 4, 1227-1233.
- Marvin, C.H., Tomy, G.T., Armitage, J.M., Arnot, J.A., McCarty, L., Covaci, A. and Palace, V. (2011) Hexabromocyclododecane: Current Understanding of Chemistry, Environmental Fate and Toxicology and Implications for Global Management, *Environmental Science & Technology*, **45**, 20, 8613-8623.
- Meeker, J.D., Johnson, P.I., Camann, D. and Hauser, R. (2009) Polybrominated diphenyl ether (PBDE) concentrations in house dust are related to hormone levels in men, *Science of The Total Environment*, **407**, 10, 3425-3429.
- Muenhor, D. and Harrad, S. (2012) Within-room and within-building temporal and spatial variations in concentrations of polybrominated diphenyl ethers (PBDEs) in indoor dust, *Environment International*, **47**, 23-27.
- NFPA. National Fire Protection Association. (2013) Michael J Karter Jr., Fire loss in the United States during 2012. USA, September 2013 (online). Available from: http://www.nfpa.org/~media/files/research/nfpa_reports/overall_fire_statistics/osfireloss.pdf (Accessed 14 January 2014).
- Ni, Y., Kumagai, K. and Yanagisawa, Y. (2007) Measuring emissions of organophosphate flame retardants using a passive flux sampler, *Atmospheric Environment*, **41**, 15, 3235-3240.
- NRC (2000) The National Research Council, *Hexabromocyclododecane In: Toxicological Risks of Selected Flame-Retardant Chemicals*, Washington D.C, The National Academies Press, 53-71.
- Ofcom (2014) Independent regulator and competition authority for the UK communication industries (online). Available from: <http://stakeholders.ofcom.org.uk/market-data-research/market-data/communications-market-reports/cmr12/tv-audio-visual/uk-2.42/> (Accessed April 2014).
- Oros, D.R., Hoover, D., Rodigari, F., Crane, D. and Sericano, J. (2004) Levels and Distribution of Polybrominated Diphenyl Ethers in Water, Surface Sediments, and Bivalves from the San Francisco Estuary, *Environmental Science & Technology*, **39**, 1, 33-41.
- Özdil, N., Özçelik Kayseri, G. and Süpüren Mengüç, G. (2012) Analysis of Abrasion Characteristics in Textiles, *Abrasion Resistance of Materials*, Dr Marcin Adamiak (Ed.), ISBN: 978-953-51-0300-4, InTech. Available from: <http://www.intechopen.com/books/abrasion-resistance-of-materials/analysis-of-abrasion-characteristics-in-textiles> (accessed 14 March 2014).
- Palm, A. (2001) The environmental fate of polybrominated diphenyl ethers in the centre of Stockholm-assessment using a multi-media fugacity model. IVL

- Rapport/report B 1400., . M.S. Thesis, IVL Swedish Environmental Research Institute Ltd. .
- Palm, A., Cousins, I.T., Mackay, D., Tysklind, M., Metcalfe, C. and Alaee, M. (2002) Assessing the environmental fate of chemicals of emerging concern: a case study of the polybrominated diphenyl ethers, *Environmental Pollution*, **117**, 2, 195-213.
- Palm Cousins, A. (2012) The effect of the indoor environment on the fate of organic chemicals in the urban landscape, *Science of The Total Environment*, **438**, 233-241.
- Que Hee, S.S., Peace, B., Clark, C.S., Boyle, J.R., Bornschein, R.L. and Hammond, P.B. (1985) Evolution of efficient methods to sample lead sources, such as house dust and hand dust, in the homes of children., *Environmental Research*, **38**, 77-95.
- Raff, J.D. and Hites, R.A. (2006) Gas-Phase Reactions of Brominated Diphenyl Ethers with OH Radicals, *The Journal of Physical Chemistry A*, **110**, 37, 10783-10792.
- Rawn, D.F.K., Gaertner, D.W., Weber, D., Curran, I.H.A., Cooke, G.M. and Goodyer, C.G. (2014) Hexabromocyclododecane concentrations in Canadian human fetal liver and placental tissues, *Science of The Total Environment*, **468–469**, 622-629.
- Riu, A., Zalko, D. and Debrauwer, L. (2006) Study of polybrominated diphenyl ethers using both positive and negative atmospheric pressure photoionization and tandem mass spectrometry, *Rapid Communications in Mass Spectrometry*, **20**, 14, 2133-2142.
- Robson, M., Melymuk, L., Bradley, L., Treen, B. and Backus, S. (2013) Wet deposition of brominated flame retardants to the Great Lakes basin – Status and trends, *Environmental Pollution*, **182**, 299-306.
- Rostami, I. and Juhasz, A.L. (2011) Assessment of Persistent Organic Pollutant (POP) Bioavailability and Bioaccessibility for Human Health Exposure Assessment: A Critical Review, *Critical Reviews in Environmental Science and Technology*, **41**, 623-656.
- Salthammer, T., Fuhrmann, F. and Uhde, E. (2003) Flame retardants in the indoor environment – Part II: release of VOCs (triethylphosphate and halogenated degradation products) from polyurethane, *Indoor Air*, **13**, 1, 49-52.
- Santín, G., Barón, E., Eljarrat, E. and Barceló, D. (2013) Emerging and historical halogenated flame retardants in fish samples from Iberian rivers, *Journal of Hazardous Materials*, **263**, Part 1, 116-121.
- Schripp, T., Fauck, C. and Salthammer, T. (2010) Chamber studies on mass-transfer of di(2-ethylhexyl)phthalate (DEHP) and di-n-butylphthalate (DnBP) from emission sources into house dust, *Atmospheric Environment*, **44**, 24, 2840-2845.
- She, J., Petreas, M., Winkler, J., Visita, P., McKinney, M. and Kopec, D. (2002) PBDEs in the San Francisco Bay Area: measurements in harbor seal blubber and human breast adipose tissue, *Chemosphere*, **46**, 5, 697-707.
- She, Y.-Z., Wu, J.-P., Zhang, Y., Peng, Y., Mo, L., Luo, X.-J. and Mai, B.-X. (2013) Bioaccumulation of polybrominated diphenyl ethers and several alternative halogenated flame retardants in a small herbivorous food chain, *Environmental Pollution*, **174**, 164-170.
- Sjödin, A., Hagmar, L., Klasson-Wehler, E., Björk, J. and Bergman, Å. (2000) Influence of the consumption of fatty Baltic Sea fish on plasma levels of

- halogenated environmental contaminants in Latvian and Swedish men., *Environmental Health Perspectives*, **108**, 1035-1041.
- Somogyi Škoc, M. and Pezelj, E. (2012) Abrasion Resistance of High Performance Fabrics, *Abrasion Resistance of Materials*, Dr Marcin Adamiak (Ed.), ISBN: 978-953-51-0300-4, InTech. Available from: <http://www.intechopen.com/books/abrasion-resistance-of-materials/abrasion-resistance-of-high-performance-fabrics> (accessed 14 March 2014).
- Sørmo, E.G., Salmer, M.P., Jenssen, B.M., Hop, H., Bæk, K., Kovacs, K.M., Lydersen, C., Falk-Petersen, S., Gabrielsen, G.W., Lie, E. and Skaare, J.U. (2006) Biomagnification of polybrominated diphenyl ether and hexabromocyclododecane flame retardants in the polar bear food chain in Svalbard, Norway, *Environmental Toxicology and Chemistry*, **25**, 9, 2502-2511.
- Stapleton, H., Harner, T., Shoeib, M., Keller, J., Schantz, M., Leigh, S. and Wise, S. (2006) Determination of polybrominated diphenyl ethers in indoor dust standard reference materials, *Analytical and Bioanalytical Chemistry*, **384**, 3, 791-800.
- Stapleton, H.M., Allen, J.G., Kelly, S.M., Konstantinov, A., Klosterhaus, S., Watkins, D., McClean, M.D. and Webster, T.F. (2008) Alternate and New Brominated Flame Retardants Detected in U.S. House Dust, *Environmental Science & Technology*, **42**, 18, 6910-6916.
- Stapleton, H.M., Eagle, S., Sjödin, A. and Webster, T.F. (2012) Serum PBDEs in a North Carolina Toddler Cohort: Associations with Handwipes, House Dust, and Socioeconomic Variables, *Environmental Health Perspectives*, **120**, 7, 1049-1054.
- Strandberg, B., Dodder, N.G., Basu, I. and Hites, R.A. (2001) Concentrations and Spatial Variations of Polybrominated Diphenyl Ethers and Other Organohalogen Compounds in Great Lakes Air, *Environmental Science & Technology*, **35**, 6, 1078-1083.
- Suzuki, G., Kida, A., Sakai, S.-i. and Takigami, H. (2009) Existence State of Bromine as an Indicator of the Source of Brominated Flame Retardants in Indoor Dust, *Environmental Science & Technology*, **43**, 5, 1437-1442.
- Takigami, H., Suzuki, G., Hirai, Y., Ishikawa, Y., Sunami, M. and Sakai, S.-i. (2009) Flame retardants in indoor dust and air of a hotel in Japan, *Environment International*, **35**, 4, 688-693.
- Takigami, H., Suzuki, G., Hirai, Y. and Sakai, S.-i. (2008) Transfer of brominated flame retardants from components into dust inside television cabinets, *Chemosphere*, **73**, 2, 161-169.
- Tan, J., Cheng, S.M., Loganath, A., Chong, Y.S. and Obbard, J.P. (2007) Polybrominated diphenyl ethers in house dust in Singapore, *Chemosphere*, **66**, 6, 985-992.
- Tang, Z., Huang, Q., Cheng, J., Yang, Y., Yang, J., Guo, W., Nie, Z., Zeng, N. and Jin, L. (2014) Polybrominated Diphenyl Ethers in Soils, Sediments, and Human Hair in a Plastic Waste Recycling Area: A Neglected Heavily Polluted Area, *Environmental Science & Technology*, **48**, 3, 1508-1516.
- Thuresson, K., Björklund, J.A. and de Wit, C.A. (2012) Tri-decabrominated diphenyl ethers and hexabromocyclododecane in indoor air and dust from Stockholm microenvironments 1: Levels and profiles, *Science of The Total Environment*, **414**, 713-721.

- Tian, S., Zhu, L., Bian, J. and Fang, S. (2012) Bioaccumulation and Metabolism of Polybrominated Diphenyl Ethers in Carp (*Cyprinus carpio*) in a Water/Sediment Microcosm: Important Role of Particulate Matter Exposure, *Environmental Science & Technology*, **46**, 5, 2951-2958.
- Tilston, E.L., Gibson, G.R. and Collins, C.D. (2011) Colon Extended Physiologically Based Extraction Test (CE-PBET) Increases Bioaccessibility of Soil-Bound PAH, *Environmental Science & Technology*, **45**, 12, 5301-5308.
- Tittlemier, S.A., Halldorson, T., Stern, G.A. and Tomy, G.T. (2002) Vapor pressures, aqueous solubilities, and Henry's law constants of some brominated flame retardants, *Environmental Toxicology and Chemistry*, **21**, 9, 1804-1810.
- Tomko, G. and McDonald, K.M. (2013) Environmental fate of hexabromocyclododecane from a new Canadian electronic recycling facility, *Journal of Environmental Management*, **114**, 324-327.
- Tomy, G.T., Budakowski, W., Halldorson, T., Whittle, D.M., Keir, M.J., Marvin, C., MacInnis, G. and Alae, M. (2004) Biomagnification of α - and γ -Hexabromocyclododecane Isomers in a Lake Ontario Food Web, *Environmental Science & Technology*, **38**, 8, 2298-2303.
- Uhde, E. and Salthammer, T. (2006) Influence of molecular parameters on the sink effect in test chambers, *Indoor Air*, **16**, 2, 158-165.
- UNEP Stockholm Convention on POPs. (2009) Decisions SC-4/14 and SC-4/18 (online). Available from: <http://chm.pops.int/Convention/ConferenceofthePartiesCOP/COPDecisions/tabid/208/Default.aspx>. (Accessed December 2013).
- UNEP. Stockholm Convention on POPs. (2010) POPRC-5/6: Hexabromocyclododecane (online). Available from: <http://chm.pops.int/TheConvention/POPsReviewCommittee/Meetings/POPRC5/POPRC5ReportandDecisions/tabid/719/Default.aspx>. (Accessed April 2014).
- UNEP. Stockholm Convention of POPs. (2011) Report of the persistent organic pollutants review committee on the work of its seventh meeting (online). Available from: <http://saferinsulation.org/wp-content/uploads/2013/07/HBCD-Risk-Mgt-Evaluation-UNEP-POPS-POPRC.7-19-Add.1.English.pdf> (Accessed April 2014).
- UNEP. Stockholm Convention on POPs. (2013) SC-6/13: Listing of hexabromocyclododecane (online). Available from: <https://treaties.un.org/doc/Publication/CN/2013/CN.934.2013-Eng.pdf> (Accessed December 2013).
- USEPA. US Environmental Protection Agency. (1999) Short Sheet: IEUBK Model Soil/Dust Ingestion Rates; EPA 540-F-00-007, OSWER 9285.7-33; Office of Solid Waste and Emergency Response: Washington, DC.
- USEPA. US Environmental Protection Agency. (2003) Superfund Lead-Contaminated Residential Sites Handbook; Final; OSWER 9285.7-50; Office of Solid Waste and Emergency Response, Lead Sites Workgroup: Washington, DC.
- USEPA. US Environmental Protection Agency. (2005) Estimation of Relative Bioavailability of Arsenic in Soil and Soil-Like Materials by in Vivo and in Vitro Methods; USEPA Review Draft; Region 8: Denver, CO.
- USEPA. US Environmental Protection Agency. (2007) Toxicological Review of 2,2',4,4'-Tetrabromodiphenyl Ether (BDE-47) (online). Available from: <http://www.epa.gov/iris/toxreviews/1010tr.pdf> (Accessed April 2014)

- USEPA. US Environmental Protection Agency. (2008a) Supporting Documents for Initial Risk-Based Prioritization of High Production Volume Chemicals (online). Available from: <http://www.epa.gov/hpvis/rbp/HBCD.3194556.Web.SupportDocs.31408.pdf> (Accessed 14 January 2014).
- USEPA. US Environmental Protection Agency. (2008b) Toxicological Review of 2,2',4,4'-Tetrabromodiphenyl ether (BDE-47) (online). Available from: <http://www.epa.gov/iris/toxreviews/1010tr.pdf> (Accessed May 2014).
- USEPA. US Environmental Protection Agency. (2008c) Toxicological Review of 2,2',4,4',5-Pentabromodiphenyl ether (BDE-99) (online). Available from: <http://www.epa.gov/iris/toxreviews/1008tr.pdf> (Accessed May 2014).
- USEPA. US Environmental Protection Agency. (2008d) Toxicological Review of 2,2',4,4',5,5'-Hexabromodiphenyl ether (BDE-153) (online). Available from: <http://www.epa.gov/iris/toxreviews/1009tr.pdf> (Accessed May 2014).
- USEPA. US Environmental Protection Agency. (2008e) Toxicological Review of Decabromodiphenyl ether (BDE-209) (online). Available from: <http://www.epa.gov/iris/toxreviews/0035tr.pdf> (Accessed May 2014).
- USEPA. US Environmental Protection Agency. (2009) Polybrominated Dipheyl Ethers (PBDEs) Action Plan (online). Available from: http://www.epa.gov/oppt/existingchemicals/pubs/actionplans/pbdes_ap_2009_1230_final.pdf (Accessed 14 January 2014).
- USEPA. US Environmental Protection Agency. (2010a) An exposure assessment of polybrominated diphenyl ethers (online). Available from: the National Technical Information Service, Springfield, VA, and online at <http://www.epa.gov/ncea>. (Accessed November 2013).
- USEPA. US Environmental Protection Agency. (2010b) Hexabromocyclododecane (HBCD) Action Plan (online). Available from: http://www.epa.gov/oppt/existingchemicals/pubs/actionplans/RIN2070-AZ10_HBCD_action_plan_Final_2010-08-09.pdf (Accessed January 2014).
- USEPA. (2011) Exposure Factors Handbook: Chapter 16-Activity Factors. U.S. Environment Protection Agency. November 2011. Available from: <http://www.epa.gov/ncea/efh/pdfs/efh-chapter16.pdf> (Accessed July 2014).
- USEPA. US Environmental Protection Agency. (2012a) Octabromodiphenyl ether (CASRN 32536-52-0) (online). Available from: <http://www.epa.gov/iris/subst/0180.htm> (Accessed May 2014).
- USEPA. US Environmental Protection Agency. (2012b) Pentabromodiphenyl ether (CASRN 32534-81-9) (online). Available from: <http://www.epa.gov/iris/subst/0184.htm> (Accessed May 2014).
- USEPA. US Environmental Protection Agency. (2012c) Technical Fast Sheet - Polybrominated Diphenyl Ethers (PBDEs) and Polybrominated Biphenyls (PBBs) (online). Available from: http://www.epa.gov/fedfac/pdf/technical_fact_sheet_pbde_pbb.pdf (Accessed 14 January 2014).
- USEPA. US Environmental Protection Agency. (2014) Particulate matter (PM) (online). Available from: <http://www.epa.gov/airquality/particulatematter/> (Accessed July 2014).
- Van Ael, E., Covaci, A., Das, K., Lepoint, G., Blust, R. and Bervoets, L. (2013) Factors Influencing the Bioaccumulation of Persistent Organic Pollutants in Food Webs of the Scheldt Estuary, *Environmental Science & Technology*, **47**, 19, 11221-11231.

- Van de Wiele, T.R., Oomen, A.G., Wragg, J., Cave, M., Minekus, M., Hack, A., Cornelis, C., Rempelberg, C.J., De Zwart, L.L. and Klinck, B. (2007) Comparison of five in vitro digestion models to in vivo experimental results: lead bioaccessibility in the human gastrointestinal tract., *Journal of Environmental Science and Health Part A*, **42**, 1203-1211.
- Wagner, J., Ghosal, S., Whitehead, T. and Metayer, C. (2013) Morphology, spatial distribution, and concentration of flame retardants in consumer products and environmental dusts using scanning electron microscopy and Raman microspectroscopy, *Environment International*, **59**, 16-26.
- Wang, X.-p., Sheng, J.-j., Gong, P., Xue, Y.-g., Yao, T.-d. and Jones, K.C. (2012) Persistent organic pollutants in the Tibetan surface soil: Spatial distribution, air-soil exchange and implications for global cycling, *Environmental Pollution*, **170**, 145-151.
- Wania, F. and Dugani, C.B. (2003) Assessing the long-range transport potential of polybrominated diphenyl ethers: A comparison of four multimedia models, *Environmental Toxicology and Chemistry*, **22**, 6, 1252-1261.
- Wania, F., Lei, Y.D. and Harner, T. (2002) Estimating Octanol-Air Partition Coefficients of Nonpolar Semivolatile Organic Compounds from Gas Chromatographic Retention Times, *Analytical Chemistry*, **74**, 14, 3476-3483.
- Watkins, D.J., McClean, M.D., Fraser, A.J., Weinberg, J., Stapleton, H.M., Sjödin, A. and Webster, T.F. (2011) Impact of Dust from Multiple Microenvironments and Diet on PentaBDE Body Burden, *Environmental Science & Technology*, **46**, 2, 1192-1200.
- Webster, E., Hughes, L. and D, M. (2006) PBDE loadings in agricultural soils in Ontario: modelling chemical fate in biosolids-amended soils., *Report to the Ontario Ministry of the Environment*, Canadian Environmental Modelling Centre, Trent University, Peterborough, Ontario, Canada.
- Webster, T.F., Harrad, S., Millette, J.R., Holbrook, R.D., Davis, J.M., Stapleton, H.M., Allen, J.G., McClean, M.D., Ibarra, C., Abdallah, M.A.-E. and Covaci, A. (2009) Identifying Transfer Mechanisms and Sources of Decabromodiphenyl Ether (BDE 209) in Indoor Environments Using Environmental Forensic Microscopy, *Environmental Science & Technology*, **43**, 9, 3067-3072.
- Weil, E.D. and Levchik, S.V. (2007) Flame Retardants for Polystyrenes in Commercial Use or Development, *Journal of Fire Sciences*, **25**, 3, 241-265.
- Werth, C.J. (2005) Environmental Impact Assessment of Recycled Wastes on Surface and Ground Waters, In: Kassim, T. A. (ed) *Handbook of Environmental Chemistry*, Vol. 3, Berlin, SPRINGER.
- Weschler, C.J. and Nazaroff, W.W. (2010) SVOC partitioning between the gas phase and settled dust indoors, *Atmospheric Environment*, **44**, 30, 3609-3620.
- WHO. World Health Organisation. (2011) Burn Prevention - Success Stories and Lessons Learned Online (online). Available from: http://whqlibdoc.who.int/publications/2011/9789241501187_eng.pdf (Accessed 14 January 2014).
- Wilford, B.H., Harner, T., Zhu, J., Shoeib, M. and Jones, K.C. (2004) Passive Sampling Survey of Polybrominated Diphenyl Ether Flame Retardants in Indoor and Outdoor Air in Ottawa, Canada: Implications for Sources and Exposure, *Environmental Science & Technology*, **38**, 20, 5312-5318.

- Wilford, B.H., Thomas, G.O., Alcock, R.E., Jones, K.C. and Anderson, D.R. (2003) Poyurethane Foam as a Source of PBDEs to the Environment, *Organohalogen Compounds*, **61**, 219-222.
- Wilford, B.H., Thomas, G.O., Jones, K.C., Davison, B. and Hurst, D.K. (2008) Decabromodiphenyl ether (deca-BDE) commercial mixture components, and other PBDEs, in airborne particles at a UK site, *Environment International*, **34**, 3, 412-419.
- Wu, N., Herrmann, T., Paepke, O., Tickner, J., Hale, R., Harvey, E., La Guardia, M., McClean, M.D. and Webster, T.F. (2007) Human Exposure to PBDEs: Associations of PBDE Body Burdens with Food Consumption and House Dust Concentrations, *Environmental Science & Technology*, **41**, 5, 1584-1589.
- Wurl, O., Lam, P.K.S. and Obbard, J.P. (2006) Occurrence and distribution of polybrominated diphenyl ethers (PBDEs) in the dissolved and suspended phases of the sea-surface microlayer and seawater in Hong Kong, China, *Chemosphere*, **65**, 9, 1660-1666.
- Xu, Y., Liu, Z., Park, J., Clausen, P.A., Benning, J.L. and Little, J.C. (2012) Measuring and Predicting the Emission Rate of Phthalate Plasticizer from Vinyl Flooring in a Specially-Designed Chamber, *Environmental Science & Technology*, **46**, 22, 12534-12541.
- Yamada-Okabe, T., Sakai, H., Kashima, Y. and Yamada-Okabe, H. (2005) Modulation at a cellular level of the thyroid hormone receptor-mediated gene expression by 1,2,5,6,9,10-hexabromocyclododecane (HBCD), 4,4'-diiodobiphenyl (DIB), and nitrofen (NIP), *Toxicology Letters*, **155**, 1, 127-133.
- Yamamoto, N., Takahashi, Y., Yoshinaga, J., Tanaka, A. and Shibata, Y. (2006) Size distributions of soil particles adhered to children's hands., *Archive of Environmental Contamination and Toxicology*, **51**, 157-163.
- Yang, M., Hong-Liang, J., Wan-Li, M., Hong, Q., Song, C. and Yi-Fan, L. (2012) Levels, compositions, and gas-particle partitioning of polybrominated diphenyl ethers and dechlorane plus in air in a Chinese northeastern city, *Atmospheric Environment*, **55**, 73-79.
- Yang, M., Qi, H., Jia, H.-L., Ren, N.-Q., Ding, Y.-S., Ma, W.-L., Liu, L.-Y., Hung, H., Sverko, E. and Li, Y.-F. (2013) Polybrominated Diphenyl Ethers in Air across China: Levels, Compositions, and Gas-Particle Partitioning, *Environmental Science & Technology*, **47**, 15, 8978-8984.
- Yu, L., Luo, X., Zheng, X., Zeng, Y., Chen, D., Wu, J. and Mai, B. (2013a) Occurrence and biomagnification of organohalogen pollutants in two terrestrial predatory food chains, *Chemosphere*, **93**, 3, 506-511.
- Yu, Y., Pang, Y., Zhang, X., Li, C., Yu, Z. and Fu, J. (2011) Optimization of an in vitro method to measure the bioaccessibility of polybrominated diphenyl ethers in dust using response surface methodology, *Journal of Environmental Sciences*, **23**, 10, 1738-1746.
- Yu, Y., Yang, D., Wang, X., Huang, N., Zhang, X., Zhang, D. and Fu, J. (2013b) Factors influencing on the bioaccessibility of polybrominated diphenyl ethers in size-specific dust from air conditioner filters, *Chemosphere*, **93**, 10, 2603-2611.
- Yu, Y.-X., Pang, Y.-P., Li, C., Li, J.-L., Zhang, X.-Y., Yu, Z.-Q., Feng, J.-L., Wu, M.-H., Sheng, G.-Y. and Fu, J.-M. (2012) Concentrations and seasonal variations of polybrominated diphenyl ethers (PBDEs) in in- and out-house dust and human daily intake via dust ingestion corrected with bioaccessibility of PBDEs, *Environment International*, **42**, 124-131.

- Zeng, Y.-H., Yu, L.-H., Luo, X.-J., Chen, S.-J., Wu, J.-P. and Mai, B.-X. (2013) Tissue accumulation and species-specific metabolism of technical pentabrominated diphenyl ether (DE-71) in two predator fish, *Environmental Toxicology and Chemistry*, **32**, 4, 757-763.
- Zhang, B.-Z., Zhang, K., Li, S.-M., Wong, C.S. and Zeng, E.Y. (2012) Size-Dependent Dry Deposition of Airborne Polybrominated Diphenyl Ethers in Urban Guangzhou, China, *Environmental Science & Technology*, **46**, 13, 7207-7214.
- Zhang, X., Diamond, M.L., Ibarra, C. and Harrad, S. (2009) Multimedia Modeling of Polybrominated Diphenyl Ether Emissions and Fate Indoors, *Environmental Science & Technology*, **43**, 8, 2845-2850.
- Zhang, X., Diamond, M.L., Robson, M. and Harrad, S. (2011) Sources, Emissions, and Fate of Polybrominated Diphenyl Ethers and Polychlorinated Biphenyls Indoors in Toronto, Canada, *Environmental Science & Technology*, **45**, 8, 3268-3274.
- Zhang, Y., Fu, S., Liu, X., Li, Z. and Dong, Y. (2013a) Polybrominated diphenyl ethers in soil from three typical industrial areas in Beijing, China, *Journal of Environmental Sciences*, **25**, 12, 2443-2450.
- Zhang, Y., Sun, H., Liu, F., Dai, Y., Qin, X., Ruan, Y., Zhao, L. and Gan, Z. (2013b) Hexabromocyclododecanes in limnic and marine organisms and terrestrial plants from Tianjin, China: Diastereomer- and enantiomer-specific profiles, biomagnification, and human exposure, *Chemosphere*, **93**, 8, 1561-1568.

APPENDIX A:

PUBLICATIONS

- Allen, J., Stapleton, H., Vallarino, J., McNeely, E., McClean, M., Harrad, S., **Rauert, C.**, and Spengler, J. “Exposure to flame retardant chemicals on commercial airplanes.” *Environmental Health*, **12**: 17 (2013)
- **Rauert, C.**, Lazarov, B., Harrad, S., Covaci, A., Stranger, M., “A review of chamber experiments for determining specific emission rates and investigating migration pathways of flame retardants.” *Atmospheric Environment*, **82**: 44-55 (2014)
- **Rauert, C.**, Harrad, S., Suzuki, G., Takigami, H., Uchida, N., Takata, K., “Test Chamber and Forensic Microscopy Investigation of the Transfer of Brominated Flame Retardants into Indoor Dust via Abrasion of Source Materials.” *Science of the Total Environment*, **493**: 639-648 (2014)
- **Rauert, C.**, Harrad, S., Stranger, M., Lazarov, B., “Test Chamber Investigation of the Volatilisation from Source Materials of Brominated Flame Retardants and their Subsequent Deposition to Indoor Dust.” *Indoor Air*, In publication (2014).

CONFERENCE PRESENTATIONS

- **Rauert, C.**, Harrad, S., “How do Brominated Flame Retardants migrate from treated products into indoor dust?” *2nd UK and Ireland Exposure Science Meeting*, Manchester **UK** (2014) – *Oral presentation*
- **Rauert, C.**, Harrad, S., Stranger, M., Lazarov, B., “How do BFRs migrate from treated products into indoor dust?” *International Symposium on Halogenated Persistent Organic Pollutants (Dioxins 2013)*, Daegu, **South Korea** (2013) – *Oral presentation*
- **Rauert, C.**, Harrad, S., Stranger, M., Lazarov, B., “How do BFRs migrate from products into indoor dust?” *7th Network Conference on Persistent Organic Pollutants (POPs 2013)*, Birmingham, **UK**, (2013) – *Oral presentation*

- **Rauert, C.**, Harrad, S., Takigami, H., Suzuki, G., “Microscopic investigations of indoor dust contamination with Brominated Flame Retardants.” *2nd UK and Ireland Exposure Science Meeting*, Manchester, **UK** (2014) – **Poster presentation**
- **Rauert, C.**, Harrad, S., Stranger, M., Lazarov, B., “A review of chamber experiments for determining emission factors and investigating migration pathways of flame retardants.” *International Symposium on Halogenated Persistent Organic Pollutants (Dioxins 2013)*, Daegu, **South Korea** (2013) – **Poster presentation**
- **Rauert, C.**, Harrad, S., Stranger, M., Lazarov, B., “Emission test cell investigations of Brominated Flame Retardants (BFRs).” *International Symposium on Brominated Flame Retardants (BFR 2013)*, San Francisco, **USA** (2013) – **Poster presentation**
- **Rauert, C.**, Harrad, S. “Micro-emission chamber investigations of Brominated Flame Retardants (BFRs).” *International Symposium on Halogenated Persistent Organic Pollutants (Dioxins 2012)*, Cairns, **Australia** (2012) – **Poster presentation**